UNIVERSITY OF CALIFORNIA,
IRVINE

Engineering Virus-Mimicking Protein Nanoparticles for Cancer Immunotherapy

DISSERTATION

submitted in partial satisfaction of the requirements
for the degree of

DOCTOR OF PHILOSOPHY

in Chemical and Biochemical Engineering

by

Nicholas Molino

Dissertation Committee:
Associate Professor Szu-Wen Wang, Chair
Professor Nancy A. Da Silva
Associate Professor Edward L. Nelson

2015

DEDICATION

To

My grandfather Michael Mizenko, who passed during my pursuit

My family, Andrea Molino, Mark Molino, and Robynn Molino, and my other, Tonika Lam, for unwavering emotional and professional support

Those who assured me the path to high level academic achievement and graduate success would be too arduous

May I never be complete. May I never be content. May I never be perfect.

TABLE OF CONTENTS

LIST OF ABBREVIATIONS

AA	Amino acid
Abs	Absorbance
AF	Alexa Fluor
AF488	Alexa Fluor 488
AF532	Alexa Fluor 532
AF-E2	E2 nanoparticle with AF488 conjugated internally
APC	Antigen presenting cell
BMDC	Bone marrow-derived dendritic cell
BMDM	Bone marrow-derived macrophage
BMPH	(N-β-maleimidopropionic acid hydrazide)
CD	Cluster of differentiation (if followed by #; *e.g.*, CD8) OR circular dichroism
CFSE	Carboxy fluorescein succinimidyl ester
CpG	Nonmethylated single-stranded DNA with repeating CG motifs
CpG-E2	E2 nanoparticles with covalently encapsulated CpG 1826 (Mouse Type B)
CpG-gp-E2	E2 nanoparticles with encapsulated CpG and surface displayed $gp100_{25\text{-}33}$
CpG-PEG-E2	E2 nanoparticle with surface conjugated CpG 1826 via a 2000 Da PEG linker
CpG-S-E2	E2 nanoparticles with encapsulated CpG and surface displayed SIINFEKL
CTL	CD8+ cytotoxic T lymphocyte
CYS-PEG-E2	E2 nanoparticle with L-cysteine surface displayed via 2000 Da PEG
D381C	E2 nanoparticle with an internal point mutation to cysteine at AA 381
DAMP	Danger-associated molecular pattern
DC	Dendritic cell

dLN	Draining lymph nodes
DLS	Dynamic light scattering
DNA	Deoxyribonucleic acid
E2	E2 catalytic subunit of the pyruvate dehydrogenase enzyme complex
E279C	E2 nanoparticle with an external point mutation to cysteine at AA 279
E2-WT	E2 nanoparticle with the native sequence from *Bacillus stearothermophilus*
EA	Erythrocyte
ELISA	Enzyme-linked immunosorbent assay
ELISpot	Enzyme-linked immunospot assay
ESI-MS	Electrospray ionization mass spectrometry
FACS	Fluorescence assisted cell sorting
FBS	Fetal bovine serum
FITC	Fluorescein isothiocyanate
FoxP3	Forkhead box P3 transcription factor
FPLC	Fast protein liquid chromatography
gp100	Premelanasome protein; an overexpressed melanoma tumor antigen
$gp100_{25\text{-}33}$	KVPRNQDWL immunodominant MHC I-restricted epitope from gp100
gp-E2	E2 nanoparticle with surface displayed $gp100_{25\text{-}33}$ peptides
HIV	Human immunodeficiency virus
HMDM	Human monocyte-derived macrophages
HPLC	High performance liquid chromatography
iDC	Immature dendritic cell
IFN-γ	Interferon gamma

Ig	Immunoglobulin
LAL	Limulus amebocyte lysate
LN	Lymph node
LPS	Lipopolysaccharide
MΦ	Macrophage
mal-PEG	Maleimide-PEG linker
MFI	Mean fluorescence index
MHC	Major histocompatibility complex
Mo	Monocyte
mPEG-E2	E2 nanoparticle with surface conjugated 2000 Da methyl-PEG
mPEG-NHS	2000 Da methy-PEG-(N-hydroxy succinimide) linker
NHS	N-hydroxy succinimide OR normal human serum (Chapter 4 only)
NK	Natural killer cell
OVA	Chicken ovalbumin
PAMP	Pathogen-associated molecular pattern
PBMC	Peripheral blood mononuclear cells
PD-1	Programmed cell death 1 receptor
PEG	Poly(ethylene glycol)
PHA	Phytohaemagglutinin
PI	Proliferation index
PLGA	Poly(lactic-co-glycolic acid)
PRR	Pattern recognition receptor
RME	Receptor-mediated endocytosis

RNA	Ribonucleic acid
RT	Room temperature
S-E2	E2 nanoparticle with surface displayed SIINFEKL peptides
SC	Subcutaneous
S.D.	Standard deviation
S.E.M.	Standard error of the mean
SDS-PAGE	Sodium dodecyl sulfate polyacrylamide gel electrophoresis
SIINFEKL	MHC I-restricted epitope from the chicken ovalbumin protein (AA 257-264)
SMCC	Succinimidyl trans-4-(maleimidylmethyl)cyclohexane-1-Carboxylate
TAA	Tumor-associated antigen
TCR	T cell receptor
TEM	Transmission electron microscopy
TLR	Toll-like receptor
VLP	Virus-like particle
WT	Wild-type

LIST OF FIGURES

LIST OF TABLES

ACKNOWLEDGMENTS

First I would like to thank my advisor, Dr. Szu Wang, for her support and continual guidance in my professional and academic development over the years, particularly the early years where my naivety and lack of experience were probably large tests of her patience. Thank you for taking a chance on me. I genuinely enjoyed my research.

My research was funded by the National Institutes of Health (R21 EB010161 and R21 EB017995) and the University of California Cancer Research Coordinating Committee.

I would like to thank my other committee members, Dr. Nancy Da Silva and Dr. Edward Nelson, for constructive feedback and helping to direct my research efforts and agreeing to evaluate my competency to enter the world as a PhD scientist.

I would like to thank all of my collaborators, including Dr. Edward Nelson, Dr. Amanda Anderson, Dr. Jo Anne Tucker, and Dr. Deborah Fraser, for their invaluable advice, direction, help on experiments, and contributions to publishing high quality research,

I would like to acknowledge everyone who allowed my use of their facilities/equipment and for providing materials, training, and advice, including Dr. Nancy Da Silva, Dr. Jin Wook Choi, Javier Cardenas, Dr. Esser-Kahn, Dr. Wendy Liu, Dr. Paolo Casali, Dr. Tonika Lam, Dr. Zhenming Xu, Dr. Nilabh Shahstri, Dr. Craig Walsh, Dr. Andrea Tenner, and Dr. Sergey Ryazantsev at UCLA.

I would like to acknowledge some of the core facilities here at UCI and the informative individuals who maintain those facilities and help troubleshoot our issues, including Dr. John Greaves and Beniam Berhane in the Mass Spectrometry Facility and Dr. Wytze van der Weer, previous director of the Laser Spectroscopy Facility.

I would like to acknowledge all of my lab mates, past and present, for useful discussions and assistance, and for maintaining the Wang Lab as a comfortable, friendly, and fun place to work every day.

I need to thank all my friends that I have made here in Southern California, for maintaining my sanity and providing an unforgettable experience. Thank you, Tonika, for supporting me and being my companion on many adventures. I would also like to acknowledge all of my awesome and supportive lifelong east coast friends with whom I remain close.

Finally, I will thank my family; My mother, Andrea Molino, and her best friend, Michael Popson; My father, Mark Molino, and stepmother, Mary Molino; My sister, Robynn Molino, brother-in-law, Jeff Markus, and nephew and niece, Izzy Markus and Maxine Markus, for all of their unconditional love and support. This would not be possible without this group of amazing people.

DECLARATION REGARDING THE AUTHORSHIP OF WORK THAT APPEARS IN THIS DISSERTATION

All experiments were designed and conducted by Nicholas Molino, under the guidance of Dr. Szu-Wen Wang, with the exception of contributions from the following individuals:

CHAPTER 4

Design, cloning, and purification of E2 mutants	Kateryna Bilotkach
Design of PEGylation protocol	Kateryna Bilotkach
Figure 4.6B	Dr. Deborah Fraser

Nicholas Molino

570-582-5077
Brooklyn, NY
nmolino44@gmail.com

OBJECTIVE

- Apply my expertise in biotechnology to support the efforts of emerging healthcare related technologies

EDUCATION

University of California Irvine | Ph.D., Chemical Engineering **2015**
- M.S. in Chemical and Biochemical Engineering
- GPA: 3.92

University of Pittsburgh | BS, Bioengineering **2009**
- Minors: Industrial Engineering, Chemistry

WORK AND LEADERSHIP EXPERIENCE

University of California Irvine, Department of Chemical Engineering **Irvine, CA**
Graduate Student Researcher and Teaching Assistant 2009-Present

- Thesis work in Szu Wang's lab developed viral-mimicking nanoparticles as platforms for cancer immunotherapy
- Directly aided in the preparation of 2 successful grant proposals (NIH R21 and University of California CRCC)
- Initiated 2 collaborations and acted as liaison between our laboratory and experts in oncology and immunology

McGowan Institute of Regenerative Medicine **Pittsburgh, PA**
Undergraduate Student Researcher 2007-2009

- Work in Marina Kameneva's lab studied drag-reducing polymer effects on blood and the immune system
- Initiated collaboration with a clinical research laboratory in the pathology department at UPMC

University of California San Diego, Department of Bioengineering **La Jolla, CA**
NSF Student Researcher 2008-2008

- Elected to the competitive NSF REU program in bioengineering, reserved for highly capable student scientists
- Worked in Geert Schmid-Schönbein's lab studied the gastrointestinal effects of ischemic shock in animals

HONORS AND AWARDS

- Recipient of 2013 UCI Travel Grant Award

MENTORSHIP OPPORTUNITIES

- Trained 6 students in laboratory techniques, research problem solving, and experimental design at UCI
- Teaching Assistant to Chemical Engineering Senior Laboratory and Heat Transfer courses at UCI
- Undergraduate Teaching Assistant to Bioengineering Methods Laboratory course at Pittsburgh

SKILLS, KNOWLEDGE, AND INTERESTS

- SOFTWARE: Microsoft Office, Adobe Products, GraphPad Prism, HTML (some), MATLAB (some)
- PRACTICAL: Advanced Mathematical and Quantitative Analysis, Excellent Written and Oral Communication and Presentation Skills, Superior Critical Thinking and Problem Solving Abilities, Resourceful
- SCIENTIFIC: Biotechnology, Nanotech, Immunology, Proteins, Virus-like particles, Drug Delivery, Vaccines
- RESEARCH: Immune Assays (ELISA, ELISpot, T cell proliferation/lysis), Flow Cytometry, Protein Engineering (Cloning, Expression, Purification, Characterization, Chemical Functionalization), Mammalian and Bacterial Cell Culture, Animal Work, Organ and Primary Cell Isolation
- INTERESTS: Traveling, Hiking, College Sports, Skiing, Adult Softball, Surfing, Homebrewing

PUBLICATIONS

- Molino, N.M., Wang, S.W., Caged Protein Nanoparticles for Drug Delivery, Current Opinion in Biotechnology, 2014, 28, 75-82
- Molino, N.M., Anderson, A.K.L., Nelson, E.L., Wang, S.W., Biomimetic Protein Nanoparticles Facilitate Enhanced Dendritic Cell Activation and Cross-Presentation, ACS Nano, 2013, 7(11), 9743-9752
- Molino, N.M., Bilotkach, K., Fraser, D.A., Ren, D.R., Wang, S.W., Complement Activation and Cell Uptake Responses Toward Polymer-Functionalized Protein Nanocapsules, Biomacromolecules, 2012, 13(4), 974-981

PRESENTATIONS

- Molino, N.M., Nelson, E.L., Wang, S.W., Biomimetic Protein Nanoparticles for Modulation of Immune Response Towards Cancer, 2015 International Conference on Materials for Advanced Technologies
- Molino, N.M., Nelson, E.L., Wang, S.W., Biomimetic Protein Nanoparticles for Modulation of Immune Response Towards Cancer, 2015 Physical Virology Gordon Research Conference
- Molino, N.M., Anderson, A.K.L., Nelson, E.L., Wang S.W., Protein Nanoparticles Facilitate Enhanced Dendritic Cell Activation and Cross-Presentation, 2013 UCI Immunology Fair
- Molino, N.M., Anderson, A.K.L., Nelson, E.L., Wang S.W., Protein Nanoparticles Facilitate Enhanced Dendritic Cell Activation and Cross-Presentation, 2013 Cancer Nanotechnology Gordon Research Conference
- Molino, N.M., Bilotkach, K., Fraser, D.A., Ren, D.R., Wang, S.W., Complement Activation and Cell Uptake Responses Toward Polymer-Functionalized Protein Nanocapsules, 2012
- Molino, N.M., Ren, D.R., Wang, S.W., Display of Targeting Peptides on a Properly Assembled Protein Nanoparticle, 2011 ACS National Meeting
- Molino, N.M., Chang, M., Schmid-Schönbein, G., Pancreatic Serine Protease Activity and Histology in the Rat Intestinal Wall Following Ischemia/Reperfusion, 2008 BMES National Meeting

ABSTRACT OF THE DISSERTATION

Engineering Virus-Mimicking Protein Nanoparticles for Cancer Immunotherapy

By

Nicholas Molino

Doctor of Philosophy in Chemical and Biochemical Engineering

University of California, Irvine, 2015

Professor Szu-Wen Wang, Chair

The immune system represents a powerful resource for the eradication of cancer. To harness the full potential of this sophisticated network to overcome the low immunogenicity of tumor cells, a sufficiently strong cytotoxic CD8 T cell (CTL)-mediated adaptive immune response is required, which is partly orchestrated by the professional antigen presenting cells of the innate immune system, most notably the dendritic cell (DC). Protein nanoparticles represent a potentially exceptional vaccination platform for cancer, as they have the ability to mimic viral infections, which are known potent inducers of CTL immunity.

We have been exploring the E2 protein nanoparticle as a delivery platform for antigens and immune-stimulating compounds. The E2 nanoparticle was successfully packaged internally with endolysosomal-releasable immune-activating DNA (CpG) and surface functionalized with MHC I-restricted peptide epitopes. The virus-mimicking nanoparticle induced DC activation at a 25-fold lower concentration compared to free CpG and induced a 3-fold increase in cross-presentation of attached epitopes, compared to free

forms of peptides or activators. Furthermore, we demonstrated that co-delivery of melanoma-associated epitopes and immune-activating CpG with E2 enhanced antigen specific CTL proliferation index by 1.5-fold with a concomitant 5-fold increase in IFN-γ cytokine secretion, compared to unbound peptide and CpG. Remarkably, a single immunization with the multifunctional E2 nanoparticle increased the frequency of melanoma-specific CTL *in vivo* (120-fold increase in the lymph node and 30-fold increase in the spleen) and the CTL generated showed approximately three times the lytic capacity toward a gp100-expressing melanoma cell line, compared to unbound peptide and CpG immunization.

We were also able to tune cellular and immunological interactions toward the E2 nanoparticle with surface display of poly(ethylene glycol) polymers, where PEGylation through various methods (native surface amines or a recombinantly introduced cysteine) was shown to decrease cell uptake by greater than 50% of both mouse and human cell lines. PEGylation was also shown to mediate moderate increases in complement activation (~35% C5a production, compared to a known activator), a humoral innate immune mechanism, whereas E2 itself did not cause complement activation. Surface display of CpG on PEGylated E2 nanoparticles was shown to specifically increase cellular uptake by antigen presenting cells.

Fluorescently-labelled E2 was shown to preferentially drain to the lymph nodes after subcutaneous administration, and surface PEGylation allowed further diffusion to more distal locations and blood draining organs. In contrast, surface display of CpG caused increased proximal lymph node accumulation, and demonstrated superior retention, with ~ 10-fold increase in LN fluorescence after 48 hours over the other nanoparticles. Within

the lymph nodes, ~50% of the nanoparticles were associated with antigen presenting cells, including dendritic cells.

Altogether, our results demonstrate the potential of the E2 protein nanoparticle as a versatile virus-mimicking immunomodulatory cancer vaccine platform. We have developed a nanoparticle biomaterial for DC-targeting, lymph node retention, and superior induction of CTL-mediated responses against cancer.

CHAPTER 1

BACKGROUND: CANCER IMMUNOTHERAPY, NANO-DELIVERY PLATFORMS, AND THE E2 PROTEIN NANOPARTICLE

Portions of this chapter have been slightly modified and published as: Molino NM, Wang SW: Caged protein nanoparticles for drug delivery. *Curr Opin Biotechnol* 2014, 28:75-82

1.1 Cancer and the Immune System

1.1.1 Cancer Immunoediting—Brief History and Overview

Evidence has long indicated that an individual's own immune system is capable of recognizing and destroying tumor cells. In fact, the notion of cellular-mediated suppression of neoplasia was first proposed in 1909 by Paul Ehrlich [1]. This idea, however, was not generally well accepted and there was not much in the way of experimental evidence to support these claims, primarily due to lack of understanding of the immune system. Almost half a century later, in the 1950's, much more was known about the immune system and the possible existence of tumor-specific antigens [2]. It was around this same time that Sir MacFarlane Burnet and Lewis Thomas proposed the immunosurveillance hypothesis, which suggested that cancer is suppressed by the adaptive immune system in immunocompetent individuals [3,4]. Even though much more was known of the immune system and cancer biology by that time, the immunosurveillance hypothesis was challenged and debated over the next half century. Now, this concept is widely accepted among immunologists and other scientists, owing to our deeper understanding of the tumor immunology and through the development of immunodeficient mouse models [5,6].

While immunosurveillance is a known process that prevents outgrowth of neoplastic tissue, occasional immunological escape can lead to cancer progression through a process known as cancer immunoediting, involving what has come to be known as the 3 E's (**Figure 1.1**) [5]. Throughout this process, cancerous cells alter their gene expression and/or accumulate mutations to facilitate a microenvironment that is favorable for their progression. For instance, downregulation of major histocompatibility complex I (MHC I)

expression decreases cytotoxic CD8 T lymphocyte (CTL) recognition. Tumor cells may also secrete chemical factors to facilitate an immunosuppressive environment and recruit an array of immune cells to help maintain this environment. Clinically detectable tumors are those that have escaped the native immunosuppression, leading to the need for clinical intervention, typically involving surgical resection, chemotherapy, or radiotherapy. Recent biomedical efforts have aimed at harnessing the inherent tumor-killing abilities of our immune system, by attempting to induce an immunotherapeutic response against the cancer [7-11]. In fact, two such therapies (Provenge and Yervoy) have recently reached FDA approval for clinical use [12,13]. The basic objective of a cancer vaccine is to allow the immune system to recognize distinct antigenic markers displayed on, or expressed by, cancer cells that are not typically present (or present at low levels) in healthy tissue, and to target such cells for destruction. These markers, known as tumor associated antigens (TAAs), vary widely among different cancer types and the identities of many have been elucidated [14].

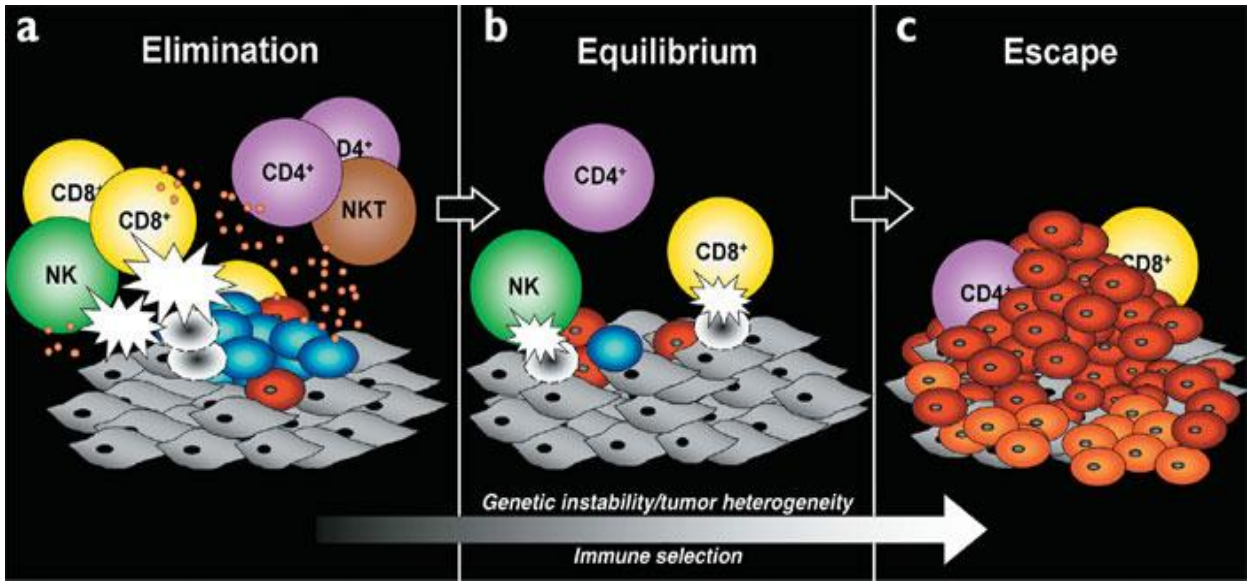

Figure 1.1. Cancer immunoediting encompasses three process. (a) Elimination corresponds to immunosurveillance. (b) Equilibrium represents the process by which the immune system iteratively selects and/or promotes the generation of tumor cell variants with increasing capacities to survive immune attack. (c) Escape is the process wherein the immunologically sculpted tumor expands in an uncontrolled manner in the immunocompetent host. In **a** and **b**, developing tumor cells (blue), tumor cell variants (red) and underlying stroma and nontransformed cells (gray) are shown; in **c**, additional tumor variants (orange) that have formed as a result of the equilibrium process are shown. Different lymphocyte populations are as marked. The small orange circles represent cytokines and the white flashes represent cytotoxic activity of lymphocytes against tumor cells. Figure taken from Dunn G.P. *et al* [5]. Copyright Nature Publishing Group. Reproduced with permission.

1.1.2 CD8 T cells and Dendritic Cells in Tumor Immunology

Many cancer vaccines have the general end goal of inducing a strong CTL mediated immune response [11]. CTL are adaptive immune cells responsible for the killing of host cells, critical for diseases like viral infections and cancer. Mature naïve CD8 T cells emerge from the thymus, and scour the secondary lymph organs and periphery in search of their cognate epitope (8-11mer peptide derived from a protein antigen). More specifically, CTL are activated through engagement of their T cell receptor (TCR) with an epitope-bound MHC I molecule. MHC I is expressed on all nucleated cells of the body and serves as a checkpoint

mechanism for immunological discrimination between self and non-self (or diseased self). In addition to TCR binding, co-stimulation by receptors on the surface of activated professional antigen presenting cells (APCs, *e.g*., dendritic cells and macrophages) is also critical for activation of naïve T cells; otherwise tolerance or anergy may be induced.

Normally, cytosolic (self and foreign) proteins and peptides are processed and displayed by MHC I receptors on both normal tissue and APCs. Conversely, extracellular material is actively endocytosed, degraded, and displayed primarily on MHC II receptors exclusively by professional antigen presenting cells, including dendritic cells (DCs), macrophages, and B cells. MHC II-displayed antigens recognized by cognate CD4 helper T cells primarily favors a humoral (*i.e.*, B cell/antibody) response, although APC/CD4 T cell interactions can also serve to enhance CTL-mediated responses, depending on the cytokine profile and other co-stimulatory ligands molecules present. For induction of a CD8 T cell mediated response against cancer, it is required that the extracellular TAA be endocytosed by the antigen presenting cell and reshuffled to the MHC I presentation pathway, a process known as cross-presentation.

DCs are the body's most potent antigen presenting cells and are also known to be particularly efficient at cross-presentation, and are therefore one of the major targets of cancer immunotherapeutic strategies [15]. DCs develop from hematopoietic stem cell-derived progenitors within the bone-marrow, and represent a heterogeneous APC population of multiple known and probably yet to be described subsets (**Figure 1.2**) [16]. A particular subset of DC may be migratory or resident within physiologically distinct locations (*e.g.,* lymph node), with each location housing a phenotypically unique DC [17]. Although all

DCs carry out many of the same basic functions for mediation of adaptive immunity, different subsets may have specialized functions for inducing a particular type of response (*e.g.,* CTL-mediated or antibody-mediated) biased toward diseases or infection commonly encountered in their particular microenvironment. However distinct, many of the DCs roles are likely complementary to each other, and the enlistment of multiple subsets simultaneously during infection or vaccination are likely to help shape and produce an effector adaptive immune response strong enough to eliminate or suppress the infection or disease.

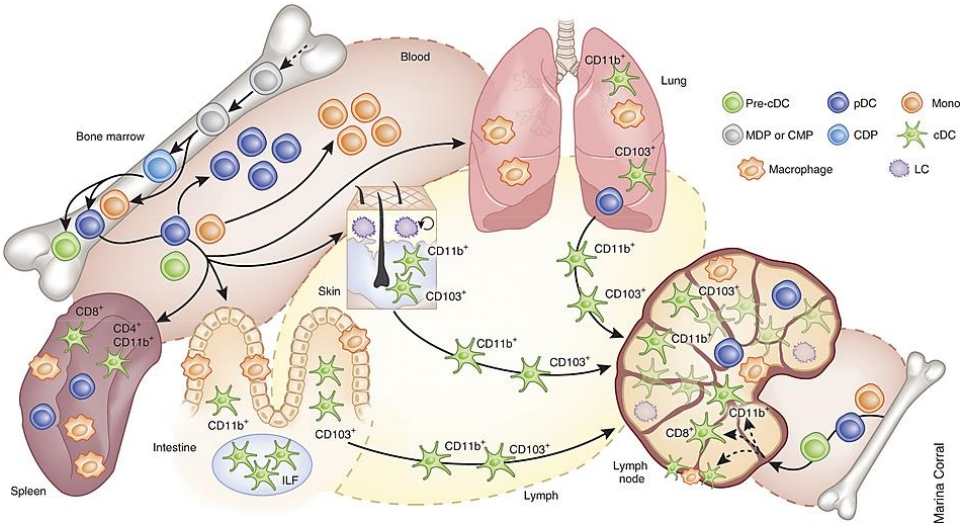

Figure 1.2. The various dendritic cell (DC) subsets derive from bone marrow progenitors. Common progenitors give rise to common DC progenitors and monocytes. And the former differentiate into plasmacytoid DCs (pDCs) or committed precursors to classical DCs (pre-cDCs). Pre-cDCs, pDCs and monocytes transit through the blood and seed peripheral organs, where pre-cDCs complete their differentiation. In the skin, dermal DCs consist of both $CD11b^+$ and $CD103^+$ classical DC subsets. Langerhans cells populate the epidermis and self-renew locally. A hallmark characteristic of classical DCs is their ability to migrate from tissues to draining lymph nodes after encountering antigen, to prime T cell responses. In contrast, macrophages mostly remain at the site of differentiation. Figure taken from Satpathy, A.T. *et al* [18]. Copyright Nature Publishing Group. Reproduced with permission.

Steady-state DCs are present in an immature state, where they are actively sampling their environment, endocytosing antigens, and checking for potential danger signals. Activation of DCs through various danger signals is necessary for mediating downstream adaptive immune responses [19,20]. Without activation, tolerance is likely to occur [20]. DCs are primarily activated through pattern recognition receptors (PRRs) that recognize a wide variety of conserved biological motifs knowns as pathogen-associated molecular patterns (PAMPs) or danger-associated molecular patterns (DAMPs) [21]. PRRs include Toll-like receptors (TLRs; plasma membrane or endolysosome), RIG-I-like receptors (cytoplasm), NOD-like receptors (cytoplasm), and C-type lectins (plasma membrane). They recognize a variety of pathogen-derived ligands, such as viral nucleic acids (*e.g.*, TLR3) or the gram-negative bacterial cell outer membrane component lipopolysaccharide (*i.e.*, TLR4). The type of danger signal(s) encountered will trigger different signaling pathways and help shape the magnitude and type of immune response mediated by the DC (or other immune cell). The TLR class of PRRs represent probably the most well-studied group of immune activators, and have been pursued as adjuvants for both pre-clinical and clinical studies for immunotherapies [22]. The known TLRs, their location, and ligands can be found in **Table 1**, compiled from sources reported in the literature [23-28].

TLR	Species	Cell Types	Natural Ligand
Plasma Membrane			
TLR1	Mouse/Human	Mo, MΦ, DC, B	Bacterial lipoproteins
TLR2	Mouse/Human	Mo, MΦ, DC, N, MC, NK	Bacterial peptidoglycans, HSP
TLR4	Mouse/Human	Mo, MΦ, DC, B, N, MC	LPS, HSP
TLR5	Mouse/Human	Mo, MΦ, DC, NK	Bacterial flagella
TLR6	Mouse/Human	Mo, MΦ, B, MC, NK	Bacterial lipoproteins
TLR10	Human	B, DC, N	Unknown
Endolysosome			
TLR3	Mouse/Human	DC, B, NK	dsRNA
TLR7	Mouse/Human	Mo, MΦ, DC, B	ssRNA
TLR8	Mouse/Human	Mo, MΦ, DC, MC	ssRNA
TLR9	Mouse/Human	Mo, MΦ, DC, B	CpG DNA
TLR11	Mouse	Mo, MΦ	profilin
TLR12	Mouse	Mo, MΦ, DC	profilin
Unknown			
TLR13	Mouse	Mo, MΦ, DC	bacterial ribosomal RNA

Table 1.1 A list of known TLRs along with their expression in known mice and/or human cells (non-exhaustive) with known natural ligands (many more synthetic ligands exist, see references [22,28,29]). Mo: monocyte, MΦ: macrophage, DC: dendritic cell, B: B cell, N: neutrophil, MC: mast cell, NK: natural killer cell

1.2 Immunotherapeutic Intervention of Cancer

For potential DC-mediated (or other pertinent APC) immunotherapy against cancer, vaccine strategies must (a) allow DC interaction with the antigenic material (*e.g.*, through passive or active targeting), (b) activate the DCs from an immature to a mature state where they can mediate downstream adaptive immune responses, and (c) allow the processing and presentation of the tumor antigens to CD8 T cells along with co-stimulatory factors.

Attempts to harness the capabilities of DCs and induce anti-cancer immune responses have included a variety of strategies. Perhaps the most straightforward strategy is to vaccinate with soluble whole protein antigen or peptide epitopes [30]. However, it is

necessary to incorporate an adjuvant to induce the activation of the immune system, otherwise tolerance may be induced. It is also difficult to ensure that proteins (or peptides) are accessing DCs *in vivo*. Whole tumor cell vaccination involves the homogenizing of autologous tumor tissue with subsequent re-administration [31]. This technique has the advantage of including multiple tumor antigens, including those yet to be characterized, that are derived from host tissue (*i.e.*, personalized vaccine therapy). *Ex vivo* antigen loading and reconstitution of autologous DCs that have been cultured and activated (e.g., Provenge) has shown promise as a strategy [12]. However, although an approved therapy for late stage prostate cancer, the process for Provenge therapy is labor and cost intensive relative to the reported benefit. Another *ex vivo* strategy being investigated is engineering autologous T cells with chimeric antigen receptors specific for a B cell leukemia overexpressed marker (CD19) antibody with the addition of built-in activation signals after TCR engagement, alleviating the necessity for APC co-stimulation and antigen training before effector functions can be carried out [32]. This strategy has demonstrated great potential for late stage leukemia and is currently undergoing further clinical investigation. However, as with any *ex vivo* strategy, the therapy will likely be costly and labor intensive, due to the inherent personalized nature of the treatment. Other approaches to cancer vaccination include monoclonal antibody-mediated targeting of markers [33], vaccination with recombinant microorganisms [34], and the use of engineered biomaterials [35-38].

1.3. Nanoparticles as Immunotherapeutic Platforms

Biomaterials have exhibited many advantages over other strategies for delivering therapeutics, including immune activating compounds, and for inducing immune responses [36,38]. Physical and chemical properties can be finely controlled with these materials. For instance, biomaterials possess the capacity for simultaneous encapsulation and/or conjugation of antigen and adjuvant. Encapsulation may provide protection to the adjuvant and antigens from being taken up by non-target cells, prevent enzymatic degradation, and facilitate their controlled release and co-delivery. Biomaterials that have been explored for application in cancer immunotherapy have included polymer scaffolds [39], microparticles [40], polymersomes [41], liposomes [42], and nanoparticles [37]. In fact, PLGA-based polymer scaffolds (reference [39]) and Qβ bacteriophage-derived virus-like particles (reference [43]) represent two biomaterial-based platforms that have reached clinical trials for cancer immunotherapy.

Nanoparticles have the potential to address important issues related to delivery of bioactive molecules, such as (i) reducing toxicity, (ii) protection from degradation/sequestration, (iii) increasing circulation times, (iv) targeting, and (v) increasing bioavailability [44-46]. Key particle variables, including size, surface charge, geometry, and the susceptibility to opsonization, all affect pharmacokinetic profiles [47]. Additionally, small size distributions of the nanomaterial allow for uniformity in antigen/adjuvant dosing. The size range of ~25-50 nm is optimal for receptor-mediated endocytosis (RME) and membrane wrapping kinetics of target cells, including antigen presenting cells [48]. What is also critical for the success of nanoparticles for delivery of

bioactive compounds is the capability to functionalize with multiple elements in a uniform and precise manner.

Certain types of nanoparticles represent a class of biomaterials explored as vaccine platforms due to the many advantages that they possess over other classes of biomaterials [37,49]. For instance, some nanoparticles possess the unique advantage of being optimal size for uptake by antigen presenting cells (~10-2,000 nm in diameter) while also being of optimal size for passive transport to the lymphatic system (~10-100 nm in diameter), where many target immune cells (*e.g.*, DCs and CD8 T cells) reside and interact [49,50]. In fact, it was shown that nanoparticles between 20-45 nm are taken up by 50% of lymph node-residing DC vs. only 5% for 100 nm particles [51]. **Figure 1.3** shows the size scale of different vaccine platforms/strategies and where they reside with respect to lymphatic transport and cellular uptake.

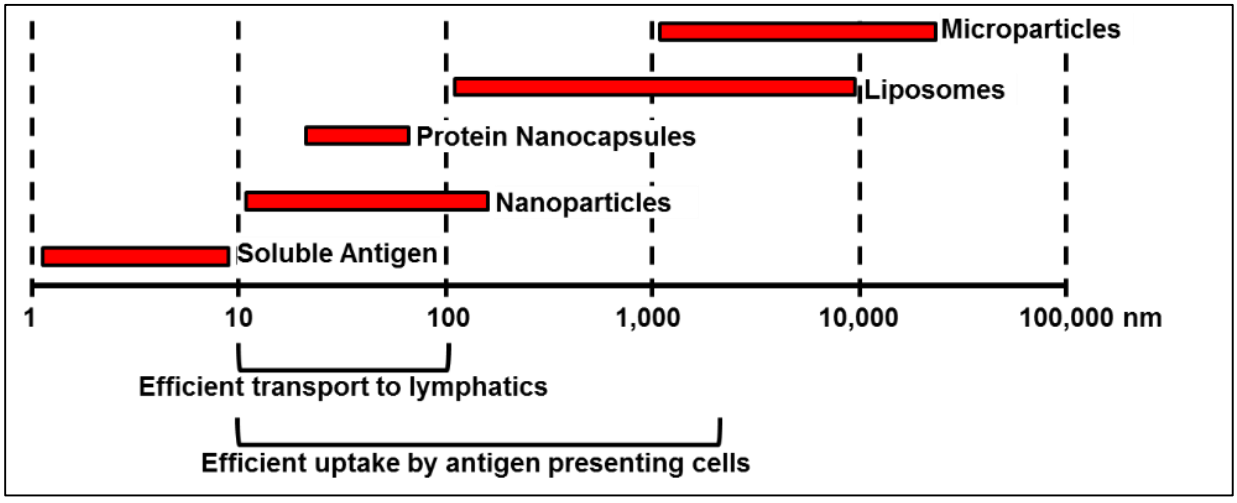

Figure 1.3. Comparison of the typical sizes of common vaccine delivery platforms are shown on a logarithmic scale. Also marked is the size range for efficient transport to the lymphatic system as well as optimal size for uptake by antigen presenting cells. Figure adapted from reference [49].

Nanoparticles possess the ability for encapsulation and/or multivalent display of both antigen and immunostimulatory compounds, allowing for simultaneous spatial and temporal co-delivery, potentially increasing the magnitude of the antigen-specific immune response [40,42,43,52-55]. Co-delivery ensures that the same APC responsible for antigen uptake is also the one being activated. Co-localization of antigen and adjuvant within the same endosomal compartment of the DC was shown to be critical for an effective anti-tumor responses [56]. Without simultaneous delivery, the vaccine has the risk of inducing tolerance rather than immunity. Nanoparticles explored for use in cancer immunotherapy have included polymer-based particles (e.g. PLGA) [57], inorganic nanoparticles (e.g. gold or silica) [52,58], and protein nanoparticles [54,59]. Caged protein nanoparticles possess many unique qualities that render them an attractive nano-scale platform for DC-based immunomodulation and other bionanotechnology applications [60-65].

1.4 Caged Protein Nanoparticles for Delivery of Bioactive Compounds and Antigens

1.4.1 Versatile Delivery Mechanisms for Drug/Adjuvant and Antigen

Conventional materials investigated for delivery of bioactive compounds include synthetic polymeric and liposomal nanoparticles [46]. These, however, may have limitations such as wide size distributions, difficulty in site-specific functionalization, low drug (or antigen) loading, and instability. Caged proteins represent a class of nanomaterial that may address many of these concerns [45,66-68]. Since the earliest example in drug delivery [69], advances have been made in understanding the architecture, assembly, physical properties, and biomedical applicability of these nanoparticulate systems. In general, protein

nanoparticles are caged structures with a well-defined geometry comprised of self-assembling monomers. Some common examples in the recent literature include virus-like particles (VLPs), ferritin cages, and heat shock proteins, which have emerged as robust platforms for medical and nanotechnology purposes [61,65]. The self-assembling nature of these particles results in nearly monodisperse size distributions, providing consistency between sample preparations and allowing for a more accurate measurement of antigen/drug loading and dosing for therapeutic or vaccination purposes. Many protein nanoparticles are produced recombinantly in microorganisms, such as *E. coli*, through well-established genetic engineering techniques. This allows the tools of biotechnology and protein engineering to be applied to the preparation of the nanoparticles. Amino acid mutations and/or deletions can be introduced in precise geometric locations within the nanoparticle, allowing for site-directed functionalization or altered electrostatic and/or hydrophobic properties [70-73]. Due to their multimeric nature, these alterations can be introduced at internal, external, or intersubunit interfaces, adding another level of control over engineered particle properties [74]. Furthermore, since proteins are naturally abundant within living cells, this class of nanoparticles should generally exhibit low toxicity.

Key aspects in nanoparticle drug delivery technologies are the containment and release of drugs (including adjuvant molecules like PAMPs and DAMPs) and or antigens within (or on) the particle, and these mechanisms are often related. Strategies available for a particulate system are dictated by its structure and dynamics, compounds delivered, and anticipated environmental/phyiological encounters. Many avenues exist for functionalizing a protein cage, and the primary approaches are described below (**Figure 1.4**).

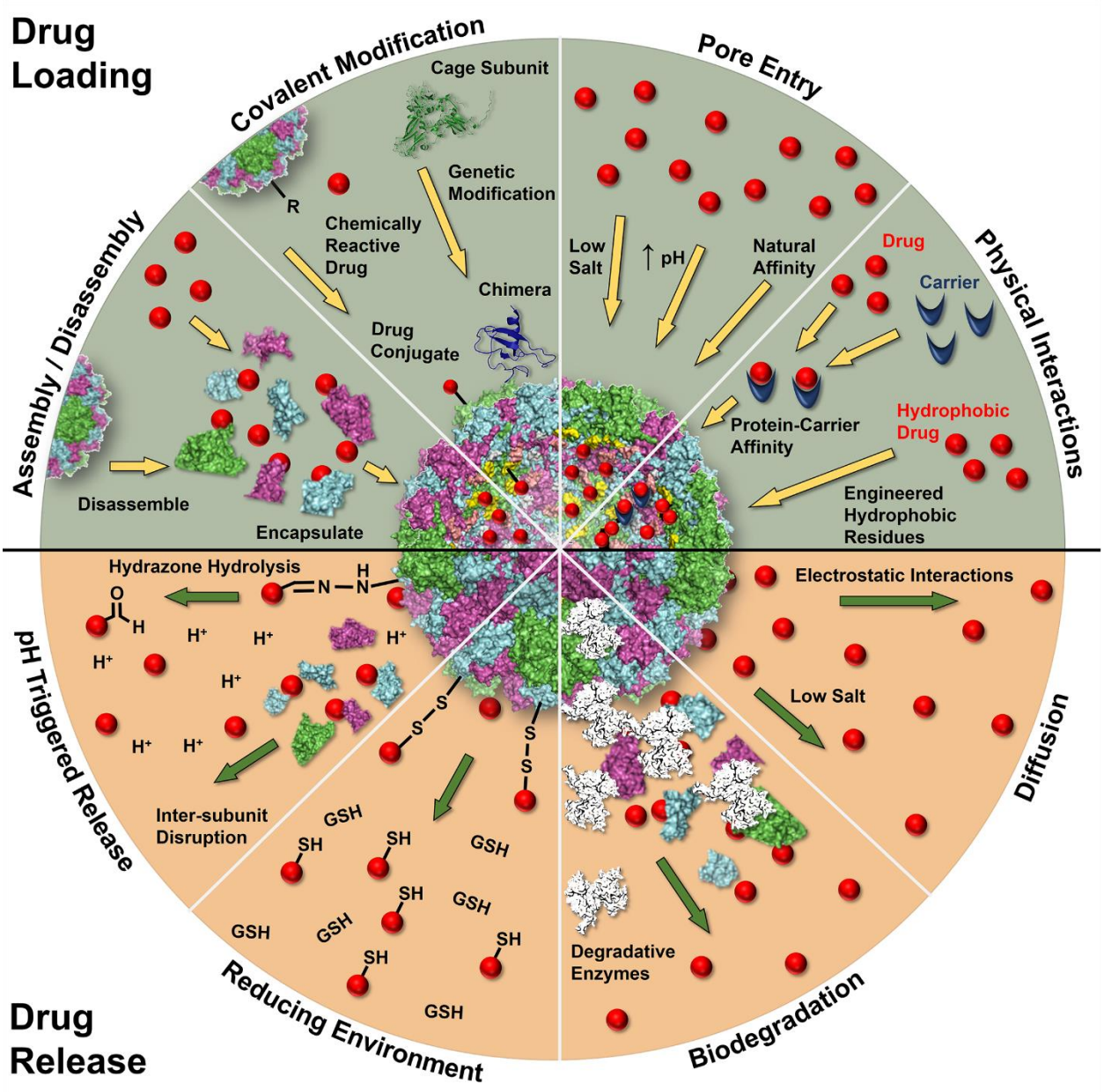

Figure 1.4. Summary of methods explored for drug loading (upper panel) and drug release (lower panel) in protein nanoparticle cages. R: any reactive amino acid side chain; GSH: glutathione. Representative protein cage scaffold is cowpea chlorotic mottle virus (PDB code 1CWP, assembly from VIPERdb; http://viperdb.scripps.edu/).

1.4.1.1 Recombinant Modification and Chimeric Fusions

One main advantage of using protein nanoparticles over other systems is the fine precision afforded by genetic engineering of functional sites at distinct locations on the nanoparticles, such as introduction of non-native amino acids [68]. For instance, a single cysteine point mutation introduces an exact number of new attachment sites, providing unique positions for drug conjugation and additional control in loading amounts [73]. The physicochemical character of the nanoparticle's hollow interior cavity can also be re-engineered to accommodate non-native hydrophobic [76] or charged molecules [77]. Knowledge of the protein crystal structure allows recombinant incorporation of peptides and/or entire proteins as N- or C-terminal chimeras or within loop regions [78-82].

1.4.1.2 Covalent Attachment

Covalent protein-drug conjugates are a common method of drug loading, and we refer to a prior review with thorough discussions of these strategies [68]. The tools of chemistry allow post-translational bioconjugation of small molecules to amino acid side chains (either native or recombinantly engineered), such as amines [83-86], carboxyls [83,87-89], cysteines [73,86,90,91], tyrosines [92], and non-native side chains through click chemistry [68,84].

Covalent attachment also allows for control over release kinetics. For example, molecules immobilized to adenovirus and ferritin through stable amide or thioether bonds are retained during physiologic conditions, but may be released during biodegradation [83,89,93]. Labile disulfide linkages permit release in reducing environments, and hydrazone bonds enable release in mildly acidic environments, both reported to occur

during endocytosis [73,83,90,91]. The selection of release mechanism depends on the chemical properties of the drug/antigen-protein conjugate (*e.g.*, chemical stability, release kinetics) and physiological needs (*e.g.*, the microenvironment encountered by nanoparticles).

1.4.1.3 Passive and Non-Covalent Loading

Protein particles often possess internal cavity surfaces with natural affinities for molecules such as nucleic acids or metals, and drugs with similar physical properties may be retained within the core. For example, single-stranded DNA can be encapsulated in hepatitis B VLPs (HBV) and Qβ nanoparticles through electrostatic interactions [94], and ferritin can chelate metal-based drugs like cisplatin [95]. Alternatively, the interior of protein nanoparticles may be redesigned to bind non-native molecules, such as in the genetic engineering of the internal E2 cavity to create a hydrophobic pocket for drug adsorption [76], introduction of siRNA binding motifs in HBV [96], or the directed evolution of lumazine synthase to increase the affinity for infectious HIV proteases through electrostatic interactions [77].

Drugs may also interact through non-specific physical interactions with a secondary carrier molecule, which has an affinity for the protein cage interior. For instance, after diffusing through natural pores, DOX and proflavin associate with the native RNA of cucumber mosaic virus and CPMV, respectively [97,98]. Forming a complex between drug and negatively-charged polymeric or metallic carriers may yield encapsulation of drug within the protein [99-102]. More stable encapsulation can be achieved through covalent

ligation of drug to the secondary carrier molecules (*e.g.*, MS2 bacteriophage RNA) [103-107], or of the protein capsule to the carrier molecule [108].

Utilizing non-specific interactions for encapsulation usually allows the slow non-triggered release of drug over time under physiologic conditions. Specific environmental conditions, however, can facilitate increased release rates. For example, the mildly acidic environment of the endosome increased drug solubility and accelerated release of hydrophobically-associated DOX [76], and glutathione reduction of cyclodextrins conjugated to protein nanoparticles enabled the release of the paclitaxel-cyclodextrin complexes [108].

1.4.1.4 Environmentally Triggered Changes

In loading mechanisms requiring diffusion of drug molecules, often, native pores of the caged structure enable access to the hollow interior. Some VLPs have gated pores, whereby low salt concentrations [109], basic pH [67], or osmotic shock [110] can cause the pores to swell open, allowing entry of the drug. Reversal of conditions then retains drug, preventing outward diffusion. In red clover necrotic mosaic VLPs, low magnesium and calcium levels, like that of the cytosol, promote opening of pores for intracellular drug release [109].

Native disassembly and reassembly of the protein cage under specific conditions also allows for drug encapsulation [95,96,103,104,111]. Protein nanoparticle assembly behavior can also be manipulated by reengineering the protein subunit interfaces [112]. Alternatively, VLPs may be isolated as subunits and assembled following purification, although this method can produce particles with size heterogeneity [88]. For drug release, this type of encapsulation may require biodegradation or introduction of repulsive

interactions at inter-subunit interfaces to induce environmentally-triggered disassembly [103,104,112,113].

1.4.2 Caged Protein Nanoparticles as Vaccine Platforms

One emerging area of research is to exploit the immune system's ability to recognize and interact with these protein platforms. Since subcutaneously-injected protein cages passively target lymphatics and are naturally recognized by many cells of the immune system, protein cages are particularly well-suited for delivering immune-modulating drugs for applications such as cancer immunotherapies or autoimmune disease treatment. For example, co-delivery of CpG DNA motifs and antigen in the E2 nanoparticle yields increased DC uptake and activation (discussed in Chapter 2), and increased antigen cross-presentation, compared to free forms of the drug [114]. CpG has also been non-specifically loaded to Qβ and HBV VLPs for *in vivo* delivery to DCs, and the inflammatory side-effects associated with the drug were alleviated [94]. Other immune-modulating drugs, such as IL-2 and IFN-γ, have also been explored for similar purposes [80,81].

While both viral and non-viral based protein nanoparticles have been researched for use in bionanotechnology, the latter may provide an extra advantage when it comes to immunologic properties. The innate immune system has evolved to become particularly adept at recognizing key pathogenic features, such as those of viruses. The use of non-viral nanoparticles that are structurally similar to viruses may benefit from mimicking a viral infection, without possessing any infectious or viral activity.

1.5 Pyruvate Dehydrogenase E2

Our research group has been exploring the therapeutic application of a non-viral protein nanoparticle derived from the E2 subunit of the pyruvate dehydrogenase multienzyme complex from *Bacillus stearothermophilus* [70-73,115]. The pyruvate dehydrogenase complex consists of a structural core (E2; dihydrolipoyl acetyltransferase), surrounded by two non-covalently bound protein subunits (E1 and E3, **Figure 1.5**), and is responsible for the conversion of pyruvate to acetyl-CoA, linking glycolysis to the citric acid (*i.e.*, Krebs) cycle, through catalytic oxidative decarboxylation [116].

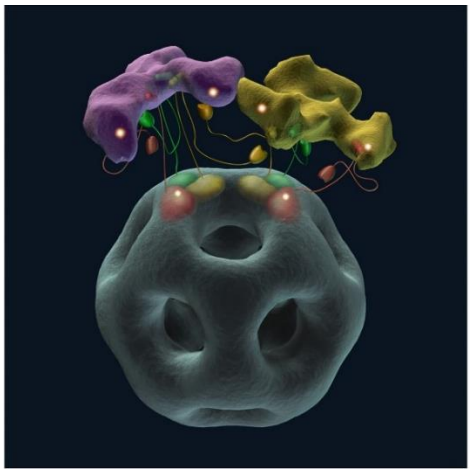

Figure 1.5. Model for active-site coupling in a hypothetical E1-E2-E3 complex. Three E1 tetramers (purple) and three E3 dimers (yellow) are shown in the outer protein shell above the inner icosahedron (gray) formed by 60 E2 catalytic domains. Figure taken from Milne *et al* [117]. Copyright American Society for Biochemistry and Molecular Biology. Reproduced with permission.

The native E2 subunit is a self-assembling multimeric protein comprised of 60 identical 428 amino acid monomers. The fully assembled E2 protein contains three distinctive regions: a catalytic structural core domain, a flexible peripheral subunit binding domain (binding region for the E1 and E3 subunits), and a lipoyl domain (**Figure 1.6**)

[116,118,119]. We have genetically distilled the E2 protein down to include only amino acids Pro175-Ala428 from the native sequence, preceded by a linker region with the sequence MLSVPG, leaving only the structural core domain [70]. The core recombinant E2 protein is a highly thermostable 24 nm dodecahedron caged structure, with 12 evenly spaced 5 nm openings to the internal core of the capsule [118,120,121].

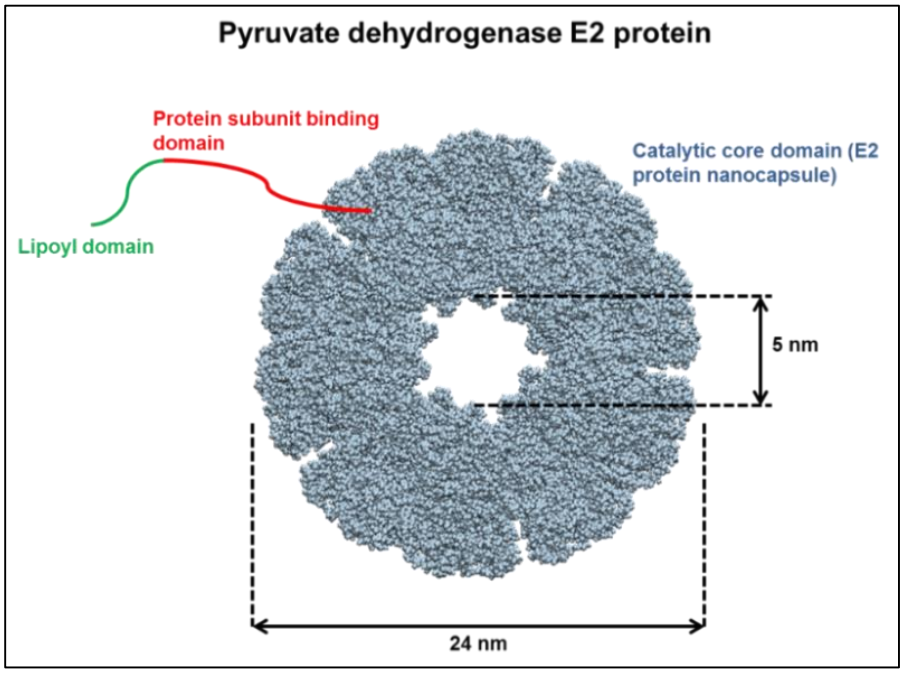

Figure 1.6. Shown is a graphic representation of the pyruvate dehydrogenase E2 subunit. For simplicity, only 1 protein subunit binding domain and lipoyl domain are shown (relative sizes not drawn to scale). The E2 core, which is the basis for our E2-WT nanocapsule, is shown as a fully assembled 60-mer complex looking at the 5-fold axis of symmetry.

Our research group has already demonstrated that with the single mutations of D381C (internal cavity) or E279C (exterior surface, discussed in Chapter 4), we are able to chemically conjugate a variety of guest molecules, including therapeutic molecules, in a site-directed manner to the reactive thiol side chain of cysteine (**Figure 1.7**) [70,73,122]. Our laboratory also demonstrated that by introducing solvent exposed hydrophobic residues in

the interior, small drugs can be encapsulated by hydrophobic interaction [115]. Encapsulated therapeutic anti-cancer molecules within E2 were able to be delivered *in vitro* to cancer cells with subsequent induced cytotoxicity [73,115]. Others have explored the E2 nanoparticle as a vaccine vehicle for inducing a helper CD4 T cell and antibody-mediated responses against HIV antigens, and also the ability to induce antigen specific CTL responses *in vivo* toward model antigens [123,124]. These immunological studies demonstrate the E2 particles' biosafety and also show that it may be a useful platform for inducing antigen-specific immune responses *in vivo*.

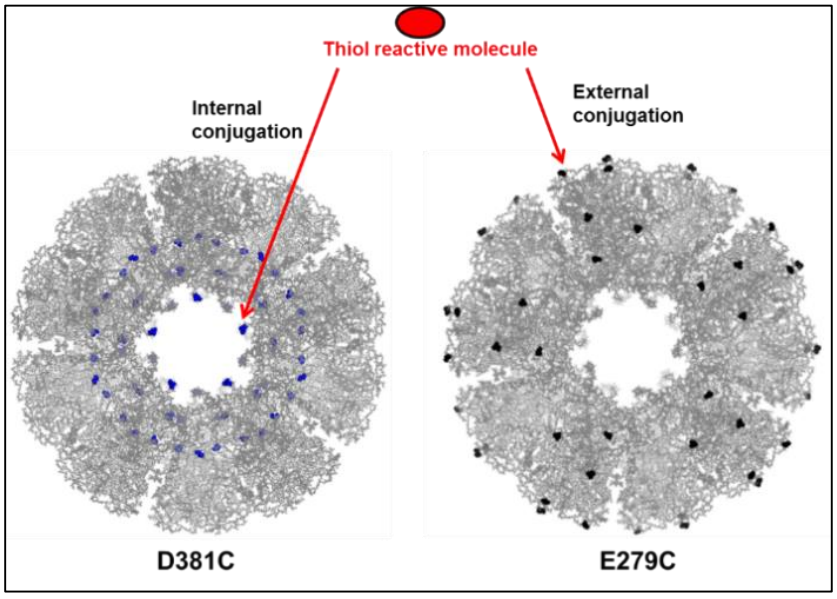

Figure 1.7. Depicted are two E2 mutants developed by our laboratory with non-native cysteine residues recombinantly introduced to either the internal surface (D381C; blue spheres) or the external surface (E279C; black spheres). A single mutation yields 60 cysteines in the fully assembled nanocapsule. A thiol reactive molecule is shown to depict the potential site-directed conjugation to the E2 particle.

1.8 Project Goals and Specific Aims of Individual Chapters

Viruses are known inducers of potent CTL responses, which is also critical for an immune response against cancer. Given this, our overall goal was to engineer the non-viral E2 nanoparticle to closely mimic viral properties and serve as a platform for the induction of cell-mediated responses against tumor antigens. More specifically, we aimed to target immune activating compounds/adjuvants simultaneously with antigenic epitopes for tumor antigen-specific CTL immunity, mediated by DCs *in vivo*. Further, we wanted to modulate the surface properties of the E2 nanoparticle to understand alterations in immunological interactions and attempt to enhance specificity and uptake by DCs. The particular aims and content of each chapter are listed below.

CHAPTER 2: We hypothesized that simultaneous delivery of CTL epitopes and CpG immune-activating DNA with the E2 nanoparticle would enhance DC cross-presentation of the associated epitopes. We then showed increased activation of DCs by delivery of CpG with the E2 nanoparticle and also demonstrate increased DC cross-presentation of model peptide epitopes (SIINFEKL) and T cell activation.

CHAPTER 3: We hypothesized that combination of CpG DNA and a melanoma-specific antigenic epitope from the gp100 TAA within the E2 nanoparticle that we could induce greater antigen-specific CD8 T cell activation compared to any other antigen formulation. We conjugated epitopes from the melanoma tumor antigen gp100, an overexpressed self-antigen, on the surface of E2 and covalently encapsulated CpG DNA within the E2 interior. We demonstrate, *in vitro*, increased CTL proliferation and IFN-γ secretion. *In vivo* we show

increased frequencies of melanoma-specific CD8 T cell induction which demonstrate the ability to lyse gp100-expresing melanoma cells.

CHAPTER 4: We studied the properties of the E2 nanoparticles following attachment of the hydrophilic polymer poly(ethylene) glycol, a known compound to increase *in vivo* circulation times of nanoparticles. An E2 mutant was developed to allow conjugation of exactly 60 PEG molecules, and we were able to saturate these attachment sites with PEG of various molecular weights. We show that the PEGylated nanoparticles exhibit decreased cellular uptake toward human macrophages and human breast cancer cells, with increasing PEG molecular weight corresponding to decreased cellular uptake. We also show that the PEGylated particles activate the human complement system, a humoral innate immune system component, in an *in vitro* assay, at moderate levels. The non-PEGylated E2 nanoparticle does not activate complement.

CHAPTER 5: We hypothesized that PEGylation of the E2 nanoparticle would decrease uptake toward many immune cell types and that surface display of CpG would increase cell uptake by DCs. Further, we hypothesized that the E2 nanoparticle would preferentially drain to the local lymph nodes of mice, and that surface display of CpG on the E2 nanoparticle, reported to target DC receptors, would increase lymph node retention and exhibit enhanced DC association. We show that PEGylation greatly decreased uptake by DCs, MΦ, B cells, T cells, and fibroblasts, and that CpG display greatly increases uptake by APCs. The E2 nanoparticle alone shows preferential accumulation in draining lymph nodes following subcutaneous administration. PEGylation allows further distribution of the nanoparticles, and surface display of CpG causes proximal accumulation and retention over

a greater period of time, compared to non-functionalized E2 or PEGylated E2. The CpG-functionalized E2 nanoparticle exhibits increased association with DCs in the lymph nodes.

CHAPTER 6: A brief summary and concluding remarks are provided on the dissertation followed by suggestions. We also provide future directions on developing and studying E2 platform as a biomaterial platform for CTL-mediated cancer immunotherapies and also for studying and altering DC-targeting effects *in vivo*, and strategies to combine targeting and surface functionalization with the cancer immunotherapy studies.

1.7 References

1. Ehrlich P: On the present state of chemotherapy. *Berichte Der Deutschen Chemischen Gesellschaft* 1909, 42:17-47.
2. Old LJ, Boyse EA: Immunology of Experimental Tumors. *Annu Rev Med* 1964, 15:167-186.
3. Burnet M: Cancer; a biological approach. I. The processes of control. *Br Med J* 1957, 1:779-786.
4. Lawrence HS: *Cellular and humoral aspects of the hypersensitive states; a symposium held at the New York Academy of Medicine*. P.B. Hoeber; 1959.
5. Dunn GP, Bruce AT, Ikeda H, Old LJ, Schreiber RD: Cancer immunoediting: from immunosurveillance to tumor escape. *Nat Immunol* 2002, 3:991-998.
6. Schreiber RD, Old LJ, Smyth MJ: Cancer immunoediting: integrating immunity's roles in cancer suppression and promotion. *Science* 2011, 331:1565-1570.
7. Berzofsky JA, Terabe M, Oh S, Belyakov IM, Ahlers JD, Janik JE, Morris JC: Progress on new vaccine strategies for the immunotherapy and prevention of cancer. *J Clin Invest* 2004, 113:1515-1525.
8. Blattman JN, Greenberg PD: Cancer immunotherapy: a treatment for the masses. *Science* 2004, 305:200-205.
9. Farkas AM, Finn OJ: Vaccines based on abnormal self-antigens as tumor-associated antigens: immune regulation. *Semin Immunol* 2010, 22:125-131.
10. Palucka K, Ueno H, Banchereau J: Recent developments in cancer vaccines. *J Immunol* 2011, 186:1325-1331.
11. Speiser DE, Romero P: Molecularly defined vaccines for cancer immunotherapy, and protective T cell immunity. *Semin Immunol* 2010, 22:144-154.
12. Cheever MA, Higano CS: PROVENGE (Sipuleucel-T) in prostate cancer: the first FDA-approved therapeutic cancer vaccine. *Clin Cancer Res* 17:3520-3526.
13. Topalian SL, Hodi FS, Brahmer JR, Gettinger SN, Smith DC, McDermott DF, Powderly JD, Carvajal RD, Sosman JA, Atkins MB, et al.: Safety, activity, and immune correlates of anti-PD-1 antibody in cancer. *N Engl J Med* 366:2443-2454.
14. Novellino L, Castelli C, Parmiani G: A listing of human tumor antigens recognized by T cells: March 2004 update. *Cancer Immunol Immunother* 2005, 54:187-207.
15. Heath WR, Carbone FR: Cross-presentation, dendritic cells, tolerance and immunity. *Annu Rev Immunol* 2001, 19:47-64.
16. Mildner A, Jung S: Development and function of dendritic cell subsets. *Immunity* 2014, 40:642-656.
17. Shortman K, Naik SH: Steady-state and inflammatory dendritic-cell development. *Nat Rev Immunol* 2007, 7:19-30.
18. Satpathy AT, Wu X, Albring JC, Murphy KM: Re(de)fining the dendritic cell lineage. *Nat Immunol* 2012, 13:1145-1154.
19. Banchereau J, Steinman RM: Dendritic cells and the control of immunity. *Nature* 1998, 392:245-252.
20. Steinman RM, Hawiger D, Liu K, Bonifaz L, Bonnyay D, Mahnke K, Iyoda T, Ravetch J, Dhodapkar M, Inaba K, et al.: Dendritic cell function in vivo during the steady state: a role in peripheral tolerance. *Ann N Y Acad Sci* 2003, 987:15-25.
21. Takeuchi O, Akira S: Pattern recognition receptors and inflammation. *Cell* 2010, 140:805-820.
22. Steinhagen F, Kinjo T, Bode C, Klinman DM: TLR-based immune adjuvants. *Vaccine* 2011, 29:3341-3355.
23. Andrade WA, Souza Mdo C, Ramos-Martinez E, Nagpal K, Dutra MS, Melo MB, Bartholomeu DC, Ghosh S, Golenbock DT, Gazzinelli RT: Combined action of nucleic acid-sensing Toll-like

receptors and TLR11/TLR12 heterodimers imparts resistance to Toxoplasma gondii in mice. *Cell Host Microbe* 2013, 13:42-53.
24. Beutler BA: TLRs and innate immunity. *Blood* 2009, 113:1399-1407.
25. Hedayat M, Netea MG, Rezaei N: Targeting of Toll-like receptors: a decade of progress in combating infectious diseases. *Lancet Infect Dis* 2011, 11:702-712.
26. Oldenburg M, Kruger A, Ferstl R, Kaufmann A, Nees G, Sigmund A, Bathke B, Lauterbach H, Suter M, Dreher S, et al.: TLR13 recognizes bacterial 23S rRNA devoid of erythromycin resistance-forming modification. *Science* 2012, 337:1111-1115.
27. Shin HJ, Youn HS: TBK1-targeted suppression of TRIF-dependent signaling pathway of Toll-like receptors by helenalin. *Life Sci* 2013, 93:847-854.
28. Uematsu S, Akira S: Toll-Like receptors (TLRs) and their ligands. *Handb Exp Pharmacol* 2008:1-20.
29. Kay E, Scotland RS, Whiteford JR: Toll-like receptors: Role in inflammation and therapeutic potential. *Biofactors* 2014, 40:284-294.
30. Hariharan K, Braslawsky G, Black A, Raychaudhuri S, Hanna N: The Induction of Cytotoxic T-Cells and Tumor-Regression by Soluble-Antigen Formulation. *Cancer Research* 1995, 55:3486-3489.
31. Hsueh EC, Essner R, Foshag LJ, Ollila DW, Gammon G, O'Day SJ, Boasberg PD, Stern SL, Ye X, Morton DL: Prolonged survival after complete resection of disseminated melanoma and active immunotherapy with a therapeutic cancer vaccine. *Journal of Clinical Oncology* 2002, 20:4549-4554.
32. Porter DL, Levine BL, Kalos M, Bagg A, June CH: Chimeric antigen receptor-modified T cells in chronic lymphoid leukemia. *N Engl J Med* 2011, 365:725-733.
33. Ueno H, Klechevsky E, Schmitt N, Ni L, Flamar AL, Zurawski S, Zurawski G, Palucka K, Banchereau J, Oh S: Targeting human dendritic cell subsets for improved vaccines. *Seminars in Immunology* 2011, 23:21-27.
34. Kim SH, Castro F, Gonzalez D, Maciag PC, Paterson Y, Gravekamp C: Mage-b vaccine delivered by recombinant Listeria monocytogenes is highly effective against breast cancer metastases. *Br J Cancer* 2008, 99:741-749.
35. Ali OA, Mooney DJ: Immunologically active biomaterials for cancer therapy. *Curr Top Microbiol Immunol* 344:279-297.
36. Kim J, Mooney DJ: In Vivo Modulation of Dendritic Cells by Engineered Materials: Towards New Cancer Vaccines. *Nano Today* 2011, 6:466-477.
37. Krishnamachari Y, Geary SM, Lemke CD, Salem AK: Nanoparticle delivery systems in cancer vaccines. *Pharm Res* 2011, 28:215-236.
38. Reddy ST, Swartz MA, Hubbell JA: Targeting dendritic cells with biomaterials: developing the next generation of vaccines. *Trends in Immunology* 2006, 27:573-579.
39. Ali OA, Emerich D, Dranoff G, Mooney DJ: In situ regulation of DC subsets and T cells mediates tumor regression in mice. *Sci Transl Med* 2009, 1:8ra19.
40. Wischke C, Zimmermann J, Wessinger B, Schendler A, Borchert HH, Peters JH, Nesselhut T, Lorenzen DR: Poly(I:C) coated PLGA microparticles induce dendritic cell maturation. *Int J Pharm* 2009, 365:61-68.
41. Scott EA, Stano A, Gillard M, Maio-Liu AC, Swartz MA, Hubbell JA: Dendritic cell activation and T cell priming with adjuvant- and antigen-loaded oxidation-sensitive polymersomes. *Biomaterials* 33:6211-6219.
42. Faham A, Altin JG: Antigen-Containing Liposomes Engrafted with Flagellin-Related Peptides Are Effective Vaccines That Can Induce Potent Antitumor Immunity and Immunotherapeutic Effect. *Journal of Immunology* 2010, 185:1744-1754.
43. Goldinger SM, Dummer R, Baumgaertner P, Mihic-Probst D, Schwarz K, Hammann-Haenni A, Willers J, Geldhof C, Prior JO, Kundig TM, et al.: Nano-particle vaccination combined with TLR-

7 and -9 ligands triggers memory and effector CD8(+) T-cell responses in melanoma patients. *Eur J Immunol*.
44. Farokhzad OC, Langer R: Impact of nanotechnology on drug delivery. *ACS Nano* 2009, 3:16-20.
45. Maham A, Tang Z, Wu H, Wang J, Lin Y: Protein-based nanomedicine platforms for drug delivery. *Small* 2009, 5:1706-1721.
46. Wagner V, Dullaart A, Bock AK, Zweck A: The emerging nanomedicine landscape. *Nat Biotechnol* 2006, 24:1211-1217.
47. Li SD, Huang L: Pharmacokinetics and biodistribution of nanoparticles. *Mol Pharmaceutics* 2008, 5:496-504.
48. Albanese A, Tang PS, Chan WC: The effect of nanoparticle size, shape, and surface chemistry on biological systems. *Annu Rev Biomed Eng* 2012, 14:1-16.
49. Bachmann MF, Jennings GT: Vaccine delivery: a matter of size, geometry, kinetics and molecular patterns. *Nat Rev Immunol* 2010, 10:787-796.
50. Manolova V, Flace A, Bauer M, Schwarz K, Saudan P, Bachmann MF: Nanoparticles target distinct dendritic cell populations according to their size. *Eur J Immunol* 2008, 38:1404-1413.
51. Reddy ST, van der Vlies AJ, Simeoni E, Angeli V, Randolph GJ, O'Neil CP, Lee LK, Swartz MA, Hubbell JA: Exploiting lymphatic transport and complement activation in nanoparticle vaccines. *Nat Biotechnol* 2007, 25:1159-1164.
52. Brinas RP, Sundgren A, Sahoo P, Morey S, Rittenhouse-Olson K, Wilding GE, Deng W, Barchi JJ: Design and Synthesis of Multifunctional Gold Nanoparticles Bearing Tumor-Associated Glycopeptide Antigens as Potential Cancer Vaccines. *Bioconjugate Chemistry* 2012, 23:1513-1523.
53. Zhang RX, Zhang S, Li M, Chen CY, Yao QZ: Incorporation of CD40 ligand into SHIV virus-like particles (VLP) enhances SHIV-VLP-induced dendritic cell activation and boosts immune responses against HIV. *Vaccine* 2010, 28:5114-5127.
54. Speiser DE, Schwarz K, Baumgaertner P, Manolova V, Devevre E, Sterry W, Walden P, Zippelius A, Conzett KB, Senti G, et al.: Memory and Effector CD8 T-cell Responses After Nanoparticle Vaccination of Melanoma Patients. *Journal of Immunotherapy* 2010, 33:848-858.
55. Kasturi SP, Skountzou I, Albrecht RA, Koutsonanos D, Hua T, Nakaya HI, Ravindran R, Stewart S, Alam M, Kwissa M, et al.: Programming the magnitude and persistence of antibody responses with innate immunity. *Nature* 470:543-547.
56. Nierkens S, den Brok MH, Sutmuller RPM, Grauer OM, Bennink E, Morgan ME, Figdor CG, Ruers TJM, Adema GJ: In vivo colocalization of antigen and CpG within dendritic cells is associated with the efficacy of cancer immunotherapy (vol 68, pg 5390, 2008). *Cancer Research* 2008, 68:6859-6859.
57. Zhang Z, Tongchusak S, Mizukami Y, Kang YJ, Ioji T, Touma M, Reinhold B, Keskin DB, Reinherz EL, Sasada T: Induction of anti-tumor cytotoxic T cell responses through PLGA-nanoparticle mediated antigen delivery. *Biomaterials* 2011, 32:3666-3678.
58. Cho NH, Cheong TC, Min JH, Wu JH, Lee SJ, Kim D, Yang JS, Kim S, Kim YK, Seong SY: A multifunctional core-shell nanoparticle for dendritic cell-based cancer immunotherapy. *Nat Nanotechnol* 6:675-682.
59. Kar UK, Jiang JN, Champion CI, Salehi S, Srivastava M, Sharma S, Rabizadeh S, Niazi K, Kickhoefer V, Rome LH, et al.: Vault Nanocapsules as Adjuvants Favor Cell-Mediated over Antibody-Mediated Immune Responses following Immunization of Mice. *PLoS One* 2012, 7.
60. Pokorski JK, Steinmetz NF: The art of engineering viral nanoparticles. *Mol Pharm* 2011, 8:29-43.
61. Manchester M, Destito G, Schneemann A: Biomedical Nanotechnology Using Virus-Based Nanoparticles. *Viruses and Nanotechnology* 2009, 327:95-122.
62. Lin YH, MaHam A, Tang ZW, Wu H, Wang J: Protein-Based Nanomedicine Platforms for Drug Delivery. *Small* 2009, 5:1706-1721.

63. Plummer EM, Manchester M: Viral nanoparticles and virus-like particles: platforms for contemporary vaccine design. *Wiley Interdisciplinary Reviews-Nanomedicine and Nanobiotechnology* 2011, 3:174-196.
64. Lee LA, Niu ZW, Wang Q: Viruses and Virus-Like Protein Assemblies-Chemically Programmable Nanoscale Building Blocks. *Nano Research* 2009, 2:349-364.
65. Douglas T, Young M: Viruses: Making friends with old foes. *Science* 2006, 312:873-875.
66. Yildiz I, Shukla S, Steinmetz NF: Applications of viral nanoparticles in medicine. *Curr Opin Biotechnol* 2011, 22:901-908.
67. Uchida M, Klem MT, Allen M, Suci P, Flenniken M, Gillitzer E, Varpness Z, Liepold LO, Young M, Douglas T: Biological containers: Protein cages as multifunctional nanoplatforms. *Adv Mater* 2007, 19:1025-1042.
68. Smith MT, Hawes AK, Bundy BC: Reengineering viruses and virus-like particles through chemical functionalization strategies. *Curr Opin Biotechnol* 2013, 24:620-626.
69. Wu M, Brown WL, Stockley PG: Cell-specific delivery of bacteriophage-encapsidated ricin A chain. *Bioconjug Chem* 1995, 6:587-595.
70. Dalmau M, Lim S, Chen HC, Ruiz C, Wang SW: Thermostability and Molecular Encapsulation Within an Engineered Caged Protein Scaffold. *Biotechnol Bioeng* 2008, 101:654-664.
71. Dalmau M, Lim S, Wang SW: pH-Triggered Disassembly in a Caged Protein Complex. *Biomacromolecules* 2009, 10:3199-3206.
72. Molino NM, Bilotkach K, Fraser DA, Ren D, Wang SW: Cell Uptake and Complement Responses Toward Polymer-Functionalized Protein Nanocapsules. *Biomacromolecules* 2012.
73. Ren DM, Kratz F, Wang SW: Protein Nanocapsules Containing Doxorubicin as a pH-Responsive Delivery System. *Small* 2011, 7:1051-1060.
74. Uchida M, Klem MT, Allen M, Suci P, Flenniken M, Gillitzer E, Varpness Z, Liepold LO, Young M, Douglas T: Biological containers: Protein cages as multifunctional nanoplatforms. *Advanced Materials* 2007, 19:1025-1042.
75. Molino NM, Wang SW: Caged protein nanoparticles for drug delivery. *Curr Opin Biotechnol* 2014, 28:75-82.
76. Ren DM, Dalmau M, Randall A, Shindel MM, Baldi P, Wang SW: Biomimetic Design of Protein Nanomaterials for Hydrophobic Molecular Transport. *Adv Funct Mater* 2012, 22:3170-3180.
77. Worsdorfer B, Woycechowsky KJ, Hilvert D: Directed evolution of a protein container. *Science* 2011, 331:589-592.
78. Franco D, Liu W, Gardiner DF, Hahn BH, Ho DD: CD40L-containing virus-like particle as a candidate HIV-1 vaccine targeting dendritic cells. *J Acquir Immune Defic Syndr* 2011, 56:393-400.
79. Jeon JO, Kim S, Choi E, Shin K, Cha K, So IS, Kim SJ, Jun E, Kim D, Ahn HJ, et al.: Designed Nanocage Displaying Ligand-Specific Peptide Bunches for High Affinity and Biological Activity. *ACS Nano* 2013.
80. Juarez V, Pasolli HA, Hellwig A, Garbi N, Arregui AC: Virus-Like Particles Harboring CCL19, IL-2 and HPV16 E7 Elicit Protective T Cell Responses in HLA-A2 Transgenic Mice. *Open Virol J* 2012, 6:270-276.
81. Kaczmarczyk SJ, Sitaraman K, Young HA, Hughes SH, Chatterjee DK: Protein delivery using engineered virus-like particles. *Proc Natl Acad Sci U S A* 2011, 108:16998-17003.
82. Zhang R, Zhang S, Li M, Chen C, Yao Q: Incorporation of CD40 ligand into SHIV virus-like particles (VLP) enhances SHIV-VLP-induced dendritic cell activation and boosts immune responses against HIV. *Vaccine* 2010, 28:5114-5127.
83. Aljabali AA, Shukla S, Lomonossoff GP, Steinmetz NF, Evans DJ: CPMV-DOX delivers. *Mol Pharm* 2013, 10:3-10.
84. Rhee JK, Baksh M, Nycholat C, Paulson JC, Kitagishi H, Finn MG: Glycan-targeted virus-like nanoparticles for photodynamic therapy. *Biomacromolecules* 2012, 13:2333-2338.

85. Shan L, Cui S, Du C, Wan S, Qian Z, Achilefu S, Gu Y: A paclitaxel-conjugated adenovirus vector for targeted drug delivery for tumor therapy. *Biomaterials* 2012, 33:146-162.
86. Suci P, Kang S, Gmur R, Douglas T, Young M: Targeted Delivery of a Photosensitizer to Aggregatibacter actinomycetemcomitans Biofilm. *Antimicrob Agents Chemother* 2010, 54:2489-2496.
87. Abbing A, Blaschke UK, Grein S, Kretschmar M, Stark CM, Thies MJ, Walter J, Weigand M, Woith DC, Hess J, et al.: Efficient intracellular delivery of a protein and a low molecular weight substance via recombinant polyomavirus-like particles. *J Biol Chem* 2004, 279:27410-27421.
88. Zhao Q, Chen W, Chen Y, Zhang L, Zhang J, Zhang Z: Self-assembled virus-like particles from rotavirus structural protein VP6 for targeted drug delivery. *Bioconjug Chem* 2011, 22:346-352.
89. Zochowska M, Paca A, Schoehn G, Andrieu JP, Chroboczek J, Dublet B, Szolajska E: Adenovirus dodecahedron, as a drug delivery vector. *PLoS One* 2009, 4:e5569.
90. Flenniken ML, Liepold LO, Crowley BE, Willits DA, Young MJ, Douglas T: Selective attachment and release of a chemotherapeutic agent from the interior of a protein cage architecture. *Chem Commun (Camb)* 2005:447-449.
91. Toita R, Murata M, Abe K, Narahara S, Piao JS, Kang JH, Ohuchida K, Hashizume M: Biological evaluation of protein nanocapsules containing doxorubicin. *Int J Nanomed* 2013, 8:1989-1999.
92. Kovacs EW, Hooker JM, Romanini DW, Holder PG, Berry KE, Francis MB: Dual-surface-modified bacteriophage MS2 as an ideal scaffold for a viral capsid-based drug delivery system. *Bioconjugate Chem* 2007, 18:1140-1147.
93. Kang YJ, Park DC, Shin HH, Park J, Kang S: Incorporation of Thrombin Cleavage Peptide into a Protein Cage for Constructing a Protease-Responsive Multifunctional Delivery Nanoplatform. *Biomacromolecules* 2012, 13:4057-4064.
94. Storni T, Ruedl C, Schwarz K, Schwendener RA, Renner WA, Bachmann MF: Nonmethylated CG motifs packaged into virus-like particles induce protective cytotoxic T cell responses in the absence of systemic side effects. *J Immunol* 2004, 172:1777-1785.
95. Yang Z, Wang XY, Diao HJ, Zhang JF, Li HY, Sun HZ, Guo ZJ: Encapsulation of platinum anticancer drugs by apoferritin. *Chem Commun* 2007:3453-3455.
96. Choi KM, Choi SH, Jeon H, Kim IS, Ahn HJ: Chimeric Capsid Protein as a Nanocarrier for siRNA Delivery: Stability and Cellular Uptake of Encapsulated siRNA. *ACS Nano* 2011, 5:8690-8699.
97. Yildiz I, Lee KL, Chen K, Shukla S, Steinmetz NF: Infusion of imaging and therapeutic molecules into the plant virus-based carrier cowpea mosaic virus: Cargo-loading and delivery. *J Controlled Release* 2013.
98. Zeng Q, Wen H, Wen Q, Chen X, Wang Y, Xuan W, Liang J, Wan S: Cucumber mosaic virus as drug delivery vehicle for doxorubicin. *Biomaterials* 2013, 34:4632-4642.
99. Liu XY, Wei W, Huang SJ, Lin SS, Zhang X, Zhang CM, Du YG, Ma GH, Li M, Mann S, et al.: Bio-inspired protein-gold nanoconstruct with core-void-shell structure: beyond a chemo drug carrier. *J Mater Chem B* 2013, 1:3136-3143.
100. Ma-Ham AH, Wu H, Wang J, Kang XH, Zhang YY, Lin YH: Apoferritin-based nanomedicine platform for drug delivery: equilibrium binding study of daunomycin with DNA. *J Mater Chem* 2011, 21:8700-8708.
101. Ren Y, Wong SM, Lim LY: Folic acid-conjugated protein cages of a plant virus: a novel delivery platform for doxorubicin. *Bioconjug Chem* 2007, 18:836-843.
102. Zhen ZP, Tang W, Chen HM, Lin X, Todd T, Wang G, Cowger T, Chen XY, Xie J: RGD-Modified Apoferritin Nanoparticles for Efficient Drug Delivery to Tumors. *ACS Nano* 2013, 7:4830-4837.

103. Ashley CE, Carnes EC, Phillips GK, Durfee PN, Buley MD, Lino CA, Padilla DP, Phillips B, Carter MB, Willman CL, et al.: Cell-specific delivery of diverse cargos by bacteriophage MS2 virus-like particles. *ACS Nano* 2011, 5:5729-5745.
104. Galaway FA, Stockley PG: MS2 viruslike particles: a robust, semisynthetic targeted drug delivery platform. *Mol Pharm* 2013, 10:59-68.
105. Pan Y, Jia TT, Zhang Y, Zhang K, Zhang R, Li JM, Wang LN: MS2 VLP-based delivery of microRNA-146a inhibits autoantibody production in lupus-prone mice. *Int J Nanomed* 2012, 7:5957-5967.
106. Pan Y, Zhang Y, Jia T, Zhang K, Li J, Wang L: Development of a microRNA delivery system based on bacteriophage MS2 virus-like particles. *FEBS J* 2012, 279:1198-1208.
107. Wu M, Sherwin T, Brown WL, Stockley PG: Delivery of antisense oligonucleotides to leukemia cells by RNA bacteriophage capsids. *Nanomedicine* 2005, 1:67-76.
108. Niikura K, Sugimura N, Musashi Y, Mikuni S, Matsuo Y, Kobayashi S, Nagakawa K, Takahara S, Takeuchi C, Sawa H, et al.: Virus-like particles with removable cyclodextrins enable glutathione-triggered drug release in cells. *Mol Biosyst* 2013, 9:501-507.
109. Lockney DM, Guenther RN, Loo L, Overton W, Antonelli R, Clark J, Hu M, Luft C, Lommel SA, Franzen S: The Red clover necrotic mosaic virus capsid as a multifunctional cell targeting plant viral nanoparticle. *Bioconjug Chem* 2011, 22:67-73.
110. Chou MI, Hsieh YF, Wang M, Chang JT, Chang D, Zouali M, Tsay GJ: In vitro and in vivo targeted delivery of IL-10 interfering RNA by JC virus-like particles. *J Biomed Sci* 2010, 17:51.
111. Ji XT, Huang L, Huang HQ: Construction of nanometer cisplatin core-ferritin (NCC-F) and proteomic analysis of gastric cancer cell apoptosis induced with cisplatin released from the NCC-F. *J Proteomics* 2012, 75:3145-3157.
112. Choi SH, Choi K, Kwon IC, Ahn HJ: The incorporation of GALA peptide into a protein cage for an acid-inducible molecular switch. *Biomaterials* 2010, 31:5191-5198.
113. Dalmau M, Lim SR, Wang SW: Design of a pH-Dependent Molecular Switch in a Caged Protein Platform. *Nano Lett.* 2009, 9:160-166.
114. Molino NM, Anderson AKL, Nelson EL, Wang SW: Biomimetic Protein Nanoparticles Facilitate Enhanced Dendritic Cell Activation and Cross-Presentation. *ACS Nano* 2013, In Press.
115. Ren DM, Dalmau M, Randall A, Shindel MM, Baldi P, Wang SW: Biomimetic Design of Protein Nanomaterials for Hydrophobic Molecular Transport. *Advanced Functional Materials* 2012, 22:3170-3180.
116. Perham RN: Domains, motifs, and linkers in 2-oxo acid dehydrogenase multienzyme complexes: a paradigm in the design of a multifunctional protein. *Biochemistry* 1991, 30:8501-8512.
117. Milne JL, Wu X, Borgnia MJ, Lengyel JS, Brooks BR, Shi D, Perham RN, Subramaniam S: Molecular structure of a 9-MDa icosahedral pyruvate dehydrogenase subcomplex containing the E2 and E3 enzymes using cryoelectron microscopy. *J Biol Chem* 2006, 281:4364-4370.
118. Milne JLS, Shi D, Rosenthal PB, Sunshine JS, Domingo GJ, Wu XW, Brooks BR, Perham RN, Henderson R, Subramaniam S: Molecular architecture and mechanism of an icosahedral pyruvate dehydrogenase complex: a multifunctional catalytic machine. *Embo Journal* 2002, 21:5587-5598.
119. Domingo GJ, Orru S, Perham RN: Multiple display of peptides and proteins on a macromolecular scaffold derived from a multienzyme complex. *Journal of Molecular Biology* 2001, 305:259-267.
120. Allen MD, Perham RN: The catalytic domain of dihydrolipoyl acetyltransferase from the pyruvate dehydrogenase multienzyme complex of Bacillus stearothermophilus - Expression, purification and reversible denaturation. *Febs Letters* 1997, 413:339-343.
121. Izard T, Aevarsson A, Allen MD, Westphal AH, Perham RN, de Kok A, Hol WG: Principles of quasi-equivalence and Euclidean geometry govern the assembly of cubic and dodecahedral cores of pyruvate dehydrogenase complexes. *Proc Natl Acad Sci U S A* 1999, 96:1240-1245.

122. Molino NM, Bilotkach K, Fraser DA, Ren DM, Wang SW: Complement Activation and Cell Uptake Responses Toward Polymer-Functionalized Protein Nanocapsules. *Biomacromolecules* 2012, 13:974-981.
123. Caivano A, Doria-Rose NA, Buelow B, Sartorius R, Trovato M, D'Apice L, Domingo GJ, Sutton WF, Haigwood NL, De Berardinis P: HIV-1 Gag p17 presented as virus-like particles on the E2 scaffold from Geobacillus stearothermophilus induces sustained humoral and cellular immune responses in the absence of IFN gamma production by CD4+T cells. *Virology* 2010, 407:296-305.
124. Jaworski JP, Krebs SJ, Trovato M, Kovarik DN, Brower Z, Sutton WF, Waagmeester G, Sartorius R, D'Apice L, Caivano A, et al.: Co-immunization with multimeric scaffolds and DNA rapidly induces potent autologous HIV-1 neutralizing antibodies and CD8+ T cells. *PLoS One* 7:e31464.

CHAPTER 2

BIOMIMETIC PROTEIN NANOPARTICLES FACILITATE ENHANCED DENDRITIC CELL ACTIVATION AND CROSS-PRESENTATION

Portions of this chapter have been slightly modified and published as: Molino NM, Anderson AK, Nelson EL, Wang SW: Biomimetic protein nanoparticles facilitate enhanced dendritic cell activation and cross-presentation. *ACS Nano* 2013, 7:9743-9752.

2.1 Background

Although recent years have seen advances in cancer therapies, common treatment strategies (*e.g.,* chemotherapy, radiation therapy, and surgical resection) still rely on techniques that lack specificity and risk side effects, including toxicity [1]. Recently, a more targeted approach to cancer therapy has included harnessing the body's immune system for tumor destruction. While cancer vaccination is a promising strategy, critical barriers to becoming a viable treatment include immune tolerance and the inability to provoke a robust enough immune response to overcome the weak immunogenicity of many cancer antigens [1,2].

In contrast, the natural immune system has evolved to become particularly adept at recognizing key geometries and pathogenic features, most notably those of viruses. Viruses, virus-like particles (VLPs), and other protein nanoparticles have proven to be well-suited as vaccine platforms [3], and examples of their development exist in the clinic (*e.g.,* Gardasil) and many others in clinical trials [3,4]. VLPs typically contain a hollow core and multiple interfaces (*i.e.,* internal, external, and inter-subunit) for engineering functional elements [3,5-7], allowing fine control over physical properties such as particle stability, surface chemistry, and biological interactions [6,8-11]. However, many viral-based vaccine platforms exhibit strong self-adjuvanting properties that may not always be desired, depending on the preferred immunotherapeutic outcome [3,12]. Additionally, VLPs and attenuated viruses may be difficult to produce and purify in large quantities using common protein expression systems, and therefore alternative platforms should be explored [12].

Our group has been developing the structural core of the non-viral E2 subunit of pyruvate dehydrogenase as a protein nanoparticle platform for therapeutic application [8-11,13,14]. E2 is a caged protein structure exhibiting unusually high thermostability and is comprised of 60 identical self-assembling monomers that produce a hollow dodecahedral capsule ~25 nm in diameter [13,15-17]. This size falls within the narrow size range of 20-45 nm, which is reported to be optimal for passive diffusion to regions of high immune activity (*i.e.* the lymph nodes) for uptake by the body's most potent antigen presenting cell, the dendritic cell (DC) [7,18,19]. Because E2 is a non-viral particle, it does not possess any infectious ability or native biological function for entrance into mammalian cells. We have engineered an E2 particle that contains recombinantly introduced internal cysteine residues for packaging of bioactive molecules and cellular delivery [11]. Other groups have explored E2 as a platform for inducing helper T cell and humoral responses to HIV *in vivo* [20,21]. These recent studies, along with our demonstrated ability to modulate immune interaction with E2 *in vitro* and to deliver therapeutic molecules to cells, has prompted us to explore the redesign of our protein nanoparticle as a viral-mimicking DC-based vaccine platform [9-11].

DCs have been identified as the key target for cell mediated immunotherapies because of their antigen processing capabilities and orchestration of downstream adaptive immune responses [22-24]. Important for cancer, DCs are particularly efficient at capturing and presenting endogenous antigen *via* major histocompatibility receptor type I (MHC I) (*i.e.,* cross-presentation), leading to a strong CD8 T cell effector response [22,23,25]. Viruses are strong inducers of CD8 T cell immunity, and therefore nanoparticles by virtue of their similar size, have been explored for the delivery of antigens to DCs [24,26,27]. In addition to the

packaging of antigen, nanoparticles may also encapsulate DC-activating molecules (*e.g.*, CpG DNA motifs) to mediate the magnitude and type of immune response [28].

Reports have shown that a requisite for a strong anti-tumor response includes simultaneous co-delivery of antigen and activator to the same DC subcellular compartment, as would happen with a natural viral infection [29,30]. Many current strategies employ systemic delivery of antigen together with adjuvant, thereby not likely meeting this criteria, as it places a high constraint on both free antigen and activator arriving in the same DC subcellular compartment simultaneously *in vivo*. Recent attempts to overcome this barrier have included use of nanoparticles for packaged delivery of vaccine components [3,31,32]. Furthermore, nanoparticles protect the molecular cargo while also shielding the host from toxic or immune-impairing side-effects, which have been linked to systemic delivery of Toll-like receptor (TLR) agonists in humans [33-35]. A nanoparticle vaccine to mimic the natural properties of viruses for a cell-mediated immune response should deliver antigen to DCs, facilitate increased levels of antigen cross-presentation, and provide necessary signals to induce immune activation.

Natural viruses display repeating patterns of antigen, and they also package genetic material. Therefore, we hypothesized that by mimicking the simultaneous packaging and transport of a repeated MHC I-restricted peptide epitope and a DNA-based DC activator (single-stranded DNA containing nonmethylated CG motifs; CpG) within the non-viral E2 particle, we can induce DC maturation and antigen cross-presentation to a greater extent than with free CpG or free peptide, respectively. No studies to date have demonstrated the modular "reprogramming" of an empty protein nanoscaffold shell of non-infectious origin

for eliciting immune response to the most potent antigen-presenting cell. We report, for the first time, the biomimetic design and characterization of a protein nanoparticle that is functionalized with CpG and peptide epitopes, for which release can be triggered by DC uptake (**Figure 2.1A**). The DC-activating properties of acid-releasable, encapsulated CpG are measured, and we also evaluate the CD8 T cell-activating properties of DCs that have been loaded with E2 nanoparticles harboring both CpG and antigen.

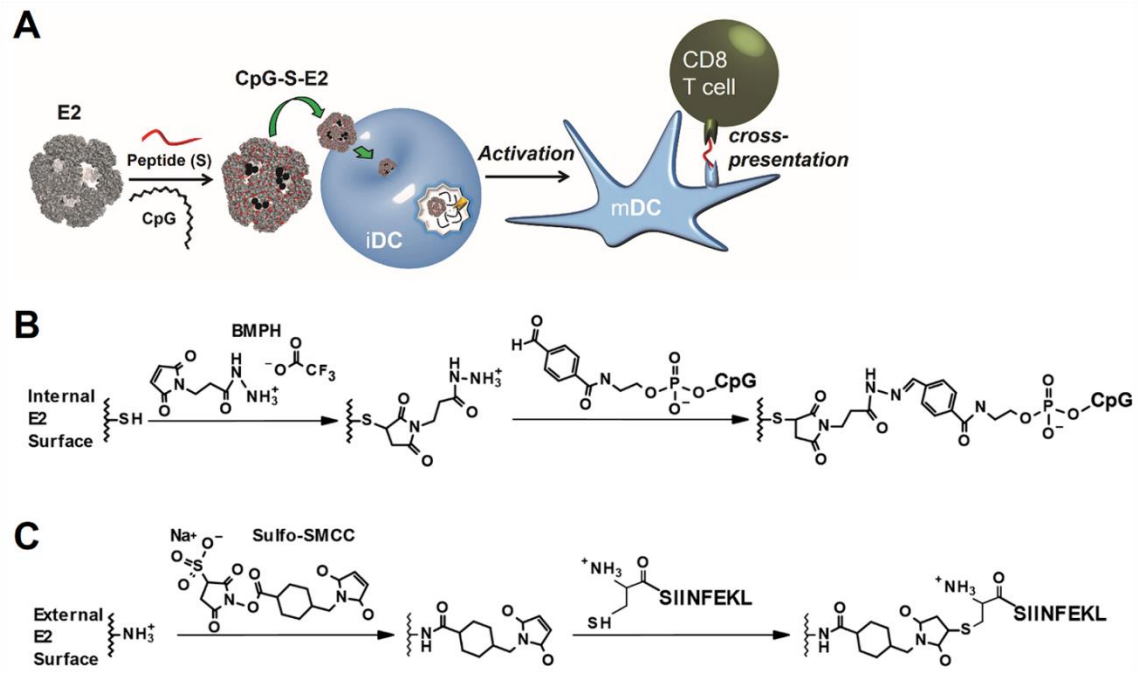

Figure 2.1. Schematics of this overall investigation and its chemical conjugation strategies. **A)** The E2 protein nanoparticle is first covalently combined with CpG activator internally and antigenic peptide (S) externally. The multifunctional particle (CpG-S-E2) is then incubated with immature dendritic cells (iDCs). After entering the acidic endosomal environment, the CpG molecules are released for interaction with Toll-like receptor 9, inducing activation to a mature phenotype (mDC). The co-delivery of CpG and peptide enhance cross-presentation of the associated MHC class I-restricted peptide epitopes to CD8 T cells). **B)** Conjugation of 5'-aldehyde-terminated CpG to E2's internal cysteines. **C)** Conjugation of SIINFEKL peptide to E2's external lysines.

2.2 Methods

2.2.1 Materials

All buffer reagents were purchased from Fisher Scientific, unless otherwise noted. The oligodeoxynucleotide Toll-like receptor 9 ligand CpG 1826 (5'-tccatgacgttcctgacgtt-3') (CpG) was synthesized with a phosphorothioated backbone and 5' benzaldehyde modification by TriLink Biotechnologies. The CpG 1826 oligonucleotide with a 5' Alexa Fluor 488 modification was synthesized by Integrated DNA Technologies. The MHC I immunodominant peptide SIINFEKL ($OVA_{257-264}$) was synthesized with an N-terminal cysteine by Genscript. All cell culture media was comprised of RPMI 1640 (Mediatech) supplemented with 10% heat-inactivated fetal bovine serum (Gibco), 1 mM sodium pyruvate (Hyclone), 2 mM L-glutamine (Lonza), 100 units/ml penicillin (Hyclone), 100 μg/ml streptomycin (Hyclone), 50 μM 2-mercaptoethanol (Fisher), 0.1 mM non-essential amino acids (Lonza) (complete RPMI media). NP-40 and chlorophenol red β–galactoside were from Sigma.

2.2.2 Cell Lines

B3Z, a CD8 T cell hybridoma containing a T cell receptor specific for the MHC I ovalbumin epitope SIINFEKL in the context of H-$2K^b$, was kindly provided by Prof. Nilabh Shastri (University of California, Berkeley). Cells were maintained in complete RPMI media at less than 7×10^5 cells/ml [36].

2.2.3 E2 Nanocapsule Preparation

The D381C E2 protein (E2) was prepared as previously described [13]. D381C is an E2 mutant with a non-native cysteine introduced to the internal cavity of the nanoparticle for site-directed functionalization. Briefly, proteins were expressed in *E. coli*, cells were lysed, and soluble cell lysates were applied to a HiPrep Q Sepharose anion exchange column (GE Healthcare) followed by a Superose 6 (GE Healthcare) size exclusion column for purification. The purified proteins were analyzed by dynamic light scattering (Zetasizer Nano ZS, Malvern) for size measurements. Electrospray ionization mass spectrometry and SDS-PAGE were performed for molecular weight and purity confirmation. Final protein preparations were stored in 50 mM potassium phosphate at pH 7.4 with 100 mM NaCl at 4°C for short-term and -80°C for long-term storage.

Lipopolysaccharide (LPS), a component of gram-negative bacterial cell walls, is recognized by Toll-like receptor 4 expressing immune cells (*e.g.* DCs), causing potentially unwanted immune activation. Residual LPS was removed following the method described by Aida and Pabst [37]. Briefly, Triton X-114 (Sigma) was added to the purified protein at 1% (v/v), chilled to 4°C, vortexed vigorously, and heated to 37°C. The mixture was then centrifuged at 18,000 × g and 37°C for 30 seconds, and the protein-containing aqueous portion was separated from the detergent. This total process repeated ≥ 8 times. Residual Triton was removed with detergent removal spin columns (Pierce). LPS levels were below 8 EU (0.8 ng) per milligram of E2 protein (LAL ToxinSensor gel clot assay, Genscript), significantly lower than levels that activate DCs in our assays.

2.2.4 CpG and Peptide Conjugation

For CpG conjugation (**Figure 2.1B**), the cysteines of the E2 internal cavity were first reduced with 10-fold excess of TCEP (Pierce) for 30 minutes followed by incubation with the N-(β-maleimidopropionic acid) hydrazide (BMPH) linker (Pierce) at a 10-fold excess for 2 hr at room temperature (RT). Unreacted linker was removed using Zeba Spin Desalting columns with a 40 kDa cutoff (Pierce). The aldehyde-modified CpG 1826 was added at 5-fold excess over protein monomer, incubated overnight at RT, and excess CpG removed by desalting spin columns. Conjugation was estimated by SDS-PAGE and measured by band intensity analysis with the NIH ImageJ software normalized to protein concentration measured with the BCA assay (Pierce). Conjugation measurements are given as an average number of CpG molecules per E2 particle (n=3). For CpG acid-hydrolysis assays, the conjugated-E2 nanocapsules were dialyzed against 50 mM potassium phosphate with 100 mM NaCl at either pH 7.4 (negative control) or pH 5 using drop dialysis membranes (Millipore) for 60-90 minutes. The nanoparticles were then removed from dialysis, incubated at 37°C for an additional 1 hr, and examined by SDS-PAGE.

For peptide conjugation (**Figure 2.1C**), the E2 protein was first incubated with sulfosuccinimidyl 4-(*N*-maleimidomethyl)cyclohexane-1-carboxylate (SMCC, Pierce) at a 20-fold excess to protein monomer for 30 minutes at room temperature followed by removal of unreacted linker by desalting spin columns. SMCC-functionalized E2 was combined with a 10-fold excess to protein monomer of the CSIINFEKL (TCEP reduced) peptide for 2 hr at RT. Excess peptide was removed by desalting spin columns. Conjugation of the peptide to the E2 protein was assessed by SDS-PAGE, and the number of peptides attached per particle was

measured by the difference in free thiol concentration (*i.e.* unreacted peptides) between a conjugation reaction with and without the SMCC cross-linker (non-specific loss of free thiols over the incubation time). Free thiol concentration was determined using Ellman's assay (Pierce), following manufacturer's instructions. Conjugation measurements are given as an average ± standard deviation of CSIINFEKL peptides per E2 particle (n=3).

For particles to which both peptide and CpGs were attached, the reaction schemes for the individual components were carried out as described above. The CpG oligonucleotide was conjugated first, followed by peptide conjugation with extent of conjugation of both components assessed by SDS-PAGE. Transmission electron micrographs of 2% uranyl acetate stained nanoparticles on Cu 150 mesh Formvar-carbon coated grids were obtained on a JEM1200EX (JEOL) with a BioScan600W digital camera (Gatan).

2.2.5 Bone Marrow-Derived Dendritic Cells (BMDCs)

Bone marrow-derived dendritic cells (BMDCs) were prepared following the method described by Lutz *et al* [38]. Briefly, the femurs and tibias were rinsed in 70% ethanol, epiphyses removed, and the marrow flushed. Cells were broken up to a single cell suspension and applied to a 70 μm cell strainer (Fisher). Red blood cells were depleted with ACK lysing buffer (Lonza), followed by washing with PBS. The marrow cells were plated at 2×10^5 cells/ml (10 ml total) on sterile bacteriological Petri dishes (Fisher) in complete RPMI media supplemented with 20 ng/ml murine recombinant GM-CSF (eBioscience) (DC media). Cells were maintained at 37°C and 5% CO_2, and 10 ml fresh DC media was added on day 3. On day 6, 50% of the media was replaced, and the non-adherent cells were pelleted and

added back to the plates. Loosely and non-adherent cells were collected and used as immature BMDCs on day 8.

2.2.6 BMDC Activation

Immature BMDCs (iDCs) harvested on day 8 were plated at 5×10^5 cells/well in 24-well plates and allowed to settle overnight. The E2 nanocapsule, unbound CpG, CpG-conjugated nanocapsules, or 100 ng/ml LPS (positive control) were added and incubated with cells for 24 hours at 37°C. After collecting DCs by gentle pipetting, surface expression of CD11c, MHC II, and CD86 was assessed by labeling with fluorescently-tagged monoclonal antibodies (eBioscience for FITC-anti-CD11c and FITC-anti-CD86 and Biolegend for PE-anti-MHC II). Cells were analyzed by flow cytometry, collecting 5×10^4 events per sample, using the Accuri C6 (BD Biosciences). The data is reported as fold-increase in percent positive cells ($n \geq 4$ independent experiments), relative to iDCs.

2.2.7. BMDC Uptake of E2 and CpG

CpG-E2 (at ~25 CpG molecules per E2 nanoparticle) were reacted with AlexaFluor 488 carboxylic acid succinimidyl ester (Invitrogen) for 1.5 hours at room temperature to yield ~25 dye molecules per E2 nanoparticle (AF-CpG-E2), giving a dye-to-CpG ratio of 1:1. Unbound CpG with a 5' AlexaFluor 488 (AF-CpG) was synthesized by Integrated DNA Technologies at a dye-to-CpG ratio of 1:1. Immature BMDCs harvested on day 8 of culture were incubated with unbound AF-CpG or AF-CpG-E2 particle at equivalent CpG concentrations for 2 hours at 37°C, harvested, and analyzed by flow cytometry (n=3).

2.2.8 Antigen Display and B3Z Assays

BMDCs harvested on day 8 were plated at 2.5×10^5 per well in 48 well plates and allowed to settle overnight. The E2 nanocapsule, SIINFEKL peptide (with or without unbound CpG), the SIINFEKL-conjugated E2 (S-E2, with or without unbound CpG), or the CpG and SIINFEKL double conjugated E2 (CpG-S-E2) nanocapsule were added for 18 hours. Cell surface display of the SIINFEKL epitope in the context of H-$2k^b$ was labeled with PE-tagged monoclonal antibody 25-D1.16 (Biolegend) and measured with flow cytometry (collecting 5×10^4 events per sample). The data is presented as MFI ($n \geq 4$ independent experiments) relative to DCs only (non-specific antibody labeling of BMDCs).

For the T cell activation assays, BMDCs harvested on day 8 were plated at 1×10^5 cells/well in a 96-well plate and allowed to settle overnight. The E2 nanocapsule, SIINFEKL peptide (with or without unbound CpG), S-E2 (with or without unbound CpG), or CpG-S-E2 were added to the BMDCs, washed away after 1 hr, and the B3Z CD8 T cells added at 1×10^5 cells/well for an additional 12 or 48 hr. The B3Z cells are activated by the SIINFEKL epitope in the context of H-$2k^b$, which can be measured by lacZ activity [36]. Cells were washed with PBS and incubated with 100 µl Z buffer (100 mM 2-mercaptoethanol, 9 mM $MgCl_2$, 0.125% NP-40, and 0.15 mM chlorophenol red β–galactoside) for 4 hours at 37°C. Following incubation, 50 µl of stop buffer (300 mM glycine and 15 mM EDTA in water) was added and absorbance at 570 nm was measured. The data is presented as an average absorbance relative to unbound SIINFEKL peptide ($n \geq 4$ independent experiments, unless otherwise noted).

2.2.9 Statistical Analysis

Statistical analyses were carried out using InStat version 3.10. Data is reported as mean ± standard deviation (SD) of at least four independent experiments (unless otherwise noted), with the value of a single independent experiment being the average of at least two replicates for that set. Statistical significance was determined by performing a one-way analysis of variance (ANOVA) followed by a Bonferroni post-test over pairs within the group. P-values less than 0.05 were considered significant.

2.3 Results and Discussion

2.3.1 E2 Can Be Simultaneously Functionalized with CpG Activator and Antigenic Peptide Epitopes

To induce a sufficiently strong CD8 T cell immune response, both antigen and activator molecules should co-localize within the same DC endosomal compartment [30]. Therefore, in the design of E2 as a vaccine platform, the combination of antigenic peptides and CpG within the same particle is critical. Our previously characterized E2 containing the functional amino acid mutation D381C (referred to as E2 in this study) was used as the starting scaffold [13]. The design of this E2 nanoparticle enabled encapsulation of an endosomal TLR ligand (*i.e.,* CpG for TLR 9) for release in the acidic environment that occurs during DC endocytosis and processing of antigen [39].

CpG molecules were successfully and stably encapsulated within core of the E2 nanoparticle. The synthetic CpG molecule was conjugated to the internal E2 cysteine

residues (CpG-E2), forming an acid-labile hydrazone bond (**Figure 2.1B**). The CpG-E2 lane in the SDS-PAGE gel of **Figure 2.2A** revealed two distinct bands, corresponding to an E2 monomer without a CpG conjugate (theoretical molecular weight is 28105 Da for an E2 monomer or 28288 Da for a monomer + cross-linker) and with an attached CpG (theoretical molecular weight of 34879 Da). Dynamic light scattering (DLS) measured a hydrodynamic diameter of 28.0 ± 0.9 nm for CpG-E2 (**Figure 2.2C**), which is within the optimal reported DC uptake size range [7,18,19].

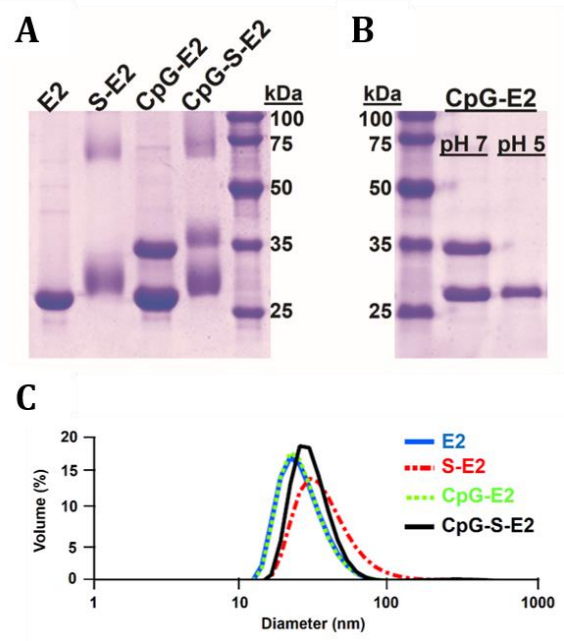

Figure 2.2. SDS-PAGE and DLS analysis of different E2 protein nanoparticles. **A)** Functionalization of the E2 nanoparticle (E2) with the SIINFEKL peptide (S-E2), CpG 1826 (CpG-E2), and simultaneous conjugation with CpG and SIINFEKL (CpG-S-E2). The unmodified E2 monomer has a theoretical molecular weight of 28105 Da. The 28-32 kDa band in lane S-E2 supports heterogeneous conjugation of the SIINFEKL peptide to the external E2 lysines, with each peptide adding a mass of 1285 Da to the E2 subunit. The CpG-E2 lane displays two bands, corresponding to an unmodified E2 monomer and a CpG-conjugated monomer (34879 Da). The CpG-S-E2 lane shows bands associated with attachment of both CpG and SIINFEKL peptide, supporting simultaneous conjugation. **B)** Incubation of CpG-E2 at pH 5 results in near-complete hydrolysis of the CpG activator from the E2 monomer. Incubation at pH 7 retains the CpG-E2 conjugate. **C)** Representative dynamic light scattering graph of the functionalized nanoparticles. A total of three independent experiments were carried out on each nanoparticle, with n=3 size measurements for each experiment.

Relatively high amounts of CpG were packaged and contained within the E2 core. The presence of 2 distinct bands in **Figure 2.2A** indicates incomplete conjugation to all 60 available internal cysteine residues, likely due to steric limitations within the ~ 12 nm cavity [17]. Encapsulation amounts were estimated to be 22 ± 3 CpG molecules per E2 particle, corresponding to ~ 36% of theoretical maximum. The ratio we report here is comparable to those obtained for CpG encapsulation within other VLP systems, which has relied on non-covalent interactions within the viral core, and is even higher than values reported for synthetic nanoparticle systems [34,40,41].

We observed pH-dependent release of the encapsulated CpG at acidic endosomal conditions. **Figure 2.2B** shows that the CpG molecules are fully released from the E2 monomers after 1 hr at pH 5 and 37°C. Our previous studies showed that the E2 particle alone remains intact below pH 5, and therefore the observed CpG release is likely due to hydrazone hydrolysis, rather than protein instability [8,11]. Incubation at 37°C for 1 hr at pH 7.4 did not result in loss of the CpG-conjugates, confirming the stability of the covalent linkage at normal physiologic conditions (**Figure 2.2B**). Therefore, we have engineered an E2 particle for pH-responsive encapsulation of CpG activator molecules that should only become available following exposure to an acidic environment (*e.g.,* the endosome). This feature may be important for *in vivo* application, imparting the potential to protect the host from global immune activation and inflammation, problems of CpG which have been alleviated by nanoparticle delivery [28,42]. While enzymatic degradation is not a major concern with the nuclease-resistant phosphorothioated CpG used in this study, others have shown that porous caged protein complexes can indeed protect the molecular cargo from enzymatic degradation [34,43].

To examine the DC cross-presentation of non-native E2-attached antigen, critical for a CD8 T cell response toward endogenous targets, we conjugated the MHC I-restricted SIINFEKL epitope from the model antigen ovalbumin (OVA) to E2's external lysines (**Figure 2.1C**). The lane in **Figure 2.2A** containing the SIINFEKL-conjugated E2 particle (S-E2) shows a broad band in the 28-32 kDa range, consistent with our expected heterogeneous peptide conjugation to the E2 monomer, since crystallographic structure of E2 (PDB code 1B5S) reveals multiple surface lysines as potential conjugation sites [16]. The high molecular weight bands of lighter intensities observed for the SIINFEKL-containing constructs (S-E2 and CpG-S-E2) are due to reaction with sulfo-SMCC; these bands are also present in E2 + sulfo-SMCC alone, and suggest a small population of cross-linked E2 subunits. Measurement of peptide conjugation yielded a ratio of 2.9 ± 0.3 peptides per protein monomer, comparable to reported SIINFEKL conjugation with other VLP systems [44]. DLS size measurements showed a size of 34.8 ± 4.2 nm (**Figure 2.2C**), within the reported optimal size range for vaccine delivery [7,18,19].

To achieve multiple functionalities, we first encapsulated CpG and subsequently conjugated the SIINFEKL epitope to purified CpG-E2. This multifunctional E2 particle (CpG-S-E2) displayed an average particle diameter of 29.9 ± 1.5 nm and SDS-PAGE revealed 2 broad signals, corresponding to E2 monomers (with and without conjugated CpG) with varying peptide conjugation amounts (**Figure 2.2A**). Further confirmation of intact particles was obtained with transmission electron microscopy (TEM) (**Figure 2.3**), which shows non-aggregated multifunctional particles with a diameter of ~ 30 nm, consistent with DLS data. This demonstrates our ability to combine both antigenic peptides and CpG to a single E2

protein nanocapsule *via* stable covalent linkages that retain the optimal particle size for DC-based vaccines. Upon mild acidification, CpG is released and able to interact with TLR 9.

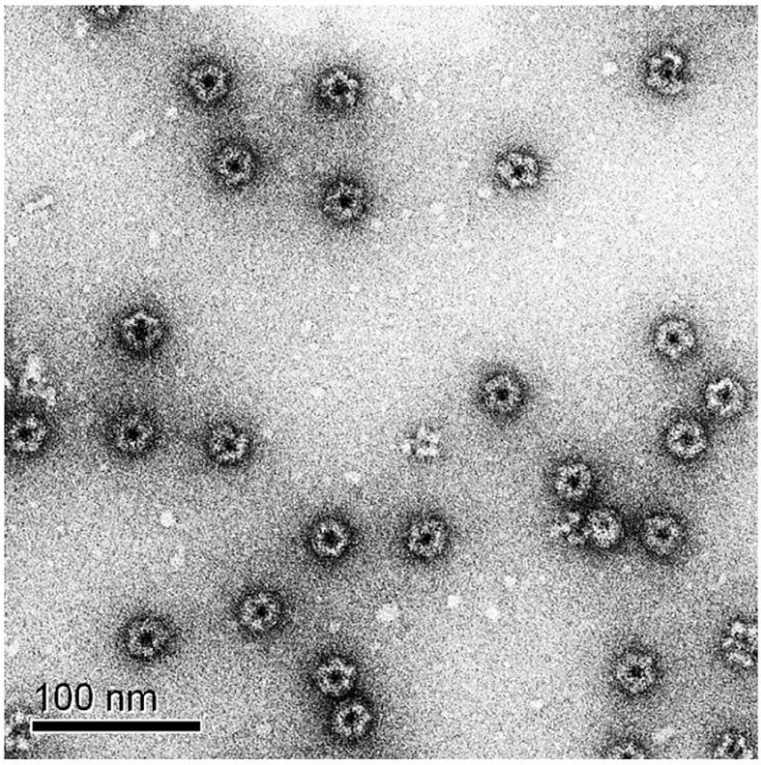

Figure 2.3. Transmission electron micrograph of 2% uranyl acetate stained CpG-S-E2 confirms monodisperse, intact, non-aggregated nanoparticles with a diameter of ~ 30 nm.

2.3.2 CpG Activation of BMDCs is Enhanced Following E2 Encapsulation

We expected that by combining the CpG activator within a protein nanoparticle of optimal DC uptake size, the concentrations necessary to activate DCs could be decreased, relative to unbound CpG. Delivery of the small CpG oligonucleotides in a 25-nm protein nanoparticle could allow for more efficient shuttling to endosomal compartments where TLR 9 is located. This could also potentially decrease the dose needed in a therapeutic application, while simultaneously shielding interaction of the CpG with systemic components that could degrade the CpG or cause nonspecific immune activation [34].

CpG induced greater bone marrow-derived dendritic cell (BMDC) activation following encapsulation within the E2 nanoparticle. BMDCs were incubated with varying amounts of the E2 particle alone, unbound CpG, and the CpG-E2 particle. Flow cytometry was used to measure the fold-change in percent positive cells, relative to immature DCs (iDCs), for the DC activation markers MHC II and CD86. CD11c served as our activation-invariant marker, and LPS served as our positive control for DC activation. The E2 particle alone, at the concentrations tested, did not have any significant effect on the expression levels of CD11c, MHC II or CD86, relative to iDCs (**Figure 2.4**). Incubation of unbound CpG with BMDCs showed no significant increased expression of activation markers at 0.02 and 0.1 μg/ml and induced only a modest increase in the relative MHC II and CD86 expression levels at 0.5 μg/ml (**Figure 2.4**). However, encapsulation of CpG activators within the internal cavity of E2 (CpG-E2) resulted in significant increases in the relative expression levels of MHC II at 0.1 and 0.5 μg/ml CpG and CD86 at 0.02, 0.1, and 0.5 μg/ml CpG, compared to unbound CpG at equivalent concentrations.

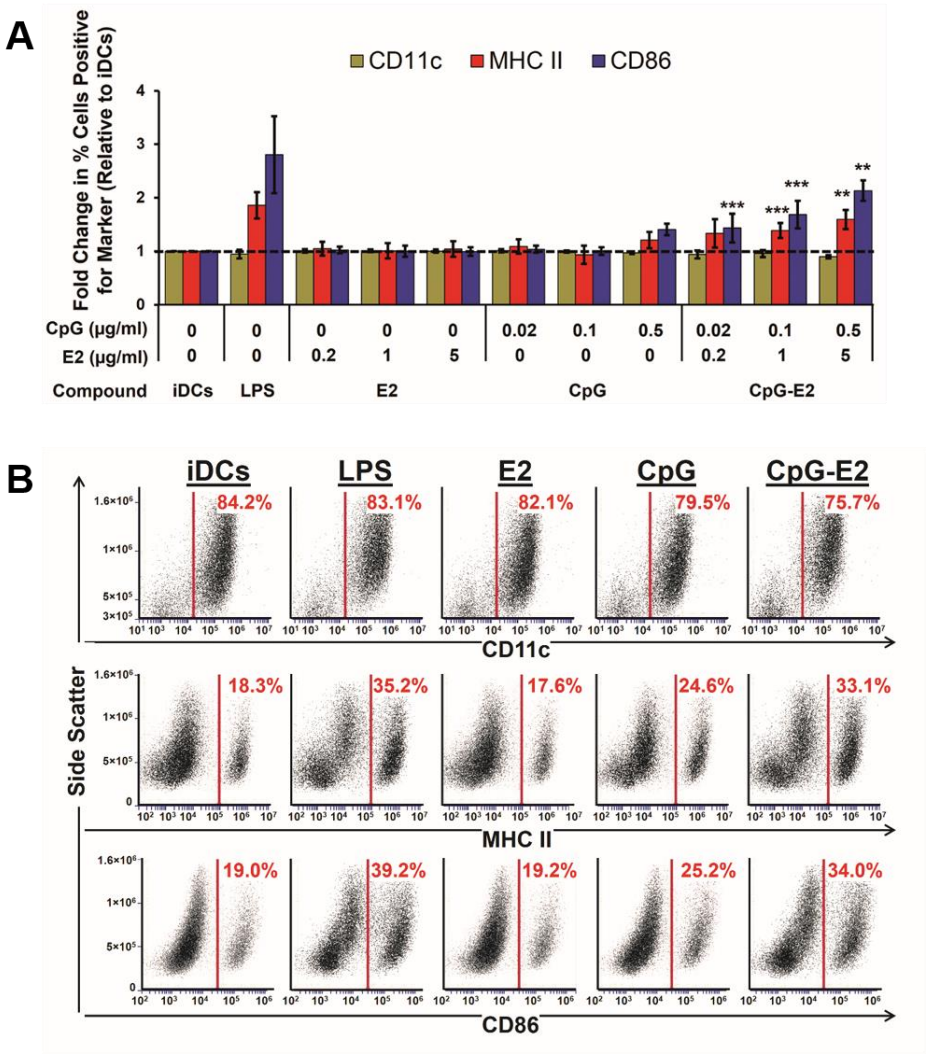

Figure 2.4. BMDC activation by CpG is enhanced following encapsulation in the E2 protein nanoparticle (CpG-E2). LPS at 100 ng/ml served as positive control and the activation-invariant marker was CD11c. **A)** MFI showed significantly greater DC activation with the CpG-E2 nanoparticle, at 0.1 and 0.5 µg/ml CpG for MHC II and CD86 markers and 0.02 µg/ml for CD86, compared to free CpG at equivalent concentrations. Data is presented as mean ± SD ($n \geq 4$ independent experiments). ** $p < 0.01$, *** $p < 0.001$, relative to unbound CpG at equivalent concentration for the given marker. **B)** A representative BMDC activation experiment analyzed by flow cytometry following 24 hours incubation with E2, CpG-E2, or free CpG (0.5 µg/ml equivalent CpG concentration). Rows display different surface markers, and columns correspond to the different compounds added to DCs (iDCs = immature DCs). Events to the right of the red bar are considered positive for the specific marker.

This demonstrates that CpG, at concentrations that do not measurably activate BMDCs *in vitro,* can do so if combined within the E2 particle, which itself does not cause activation. Significant increases in the activation markers over background can be observed at 25-fold lower concentration of CpG when encapsulated within E2 relative to unbound form, where 0.02 μg/ml E2-encapsulated CpG induces roughly the same amount of increased MHC II and CD86 expression as 0.5 μg/ml unbound CpG. Our observed relative increase in DC-activation is comparable to that reported for nanoparticle studies using alternative activators that also showed significant added therapeutic benefit *in vivo* [45,46].

One explanation for our observed DC activation increase from CpG in nanoparticle-bound form could be that unbound CpG is below the 20-nm lower reported limit for optimal DC uptake size. This would be consistent with the observations of Wu *et al.* showing that the aggregation of CpG is necessary for the *in vitro* activation of DCs [47]. Indeed, incubation with fluorescently labeled CpG-E2 (at 0.5 μg/ml CpG) showed greater than 25-fold increase in MFI, relative to unbound fluorescent CpG at an equivalent concentration (**Figure 2.5**). This data supports increased uptake of CpG by BMDC when it is encapsulation within the 25-nm E2 nanoparticle, compared to free CpG. As noted earlier, optimal sizes for vaccine delivery to lymph residing DCs *in vivo* have been reported to be between 20-45 nm, and the CpG-E2 particle falls within this narrow range [19]. Our observations showing specific activation of DCs with a 25-nm CpG-containing E2 protein nanoparticle may be important for vaccine design, since it is mature DCs that display antigen and orchestrate downstream adaptive immune responses.

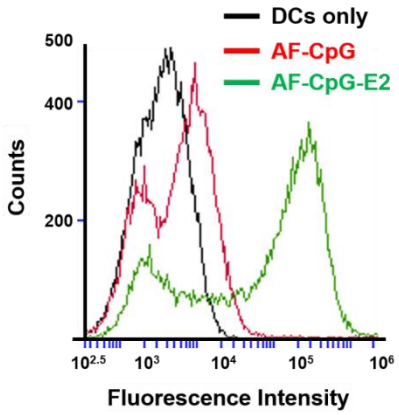

Figure 2.5. BMDCs show increased uptake of E2-encapsulated CpG, relative to unbound CpG. A representative BMDC uptake experiment analyzed by flow cytometry following 2 hours incubation with 0.5 μg/ml Alexa Fluor 488-conjugated CpG (AF-CpG) or Alexa Fluor 488-conjugated CpG-E2 (AF-CpG-E2, 0.5 μg/ml CpG). A shift in the MFI of > 25-fold was observed when incubated with AF-CpG-E2, relative to AF-CpG, indicative of increased uptake.

2.3.3 DCs Can Display E2-bound MHC Class I Epitopes

We assessed the ability of DCs to process the $OVA_{257-264}$ peptide conjugated to E2 and to display this epitope in the context of H-$2K^b$ (MHC I). BMDCs were incubated with the SIINFEKL peptide at varying concentrations in either unbound form or conjugated to E2, followed by antibody staining for MHC I presentation of the epitope. Averaged MFI values are reported as relative to DCs alone (**Figure 2.6A**), and representative dot plots are presented in **Figures 2.6C and 2.6D**. Unbound SIINFEKL showed a relative MFI increase over background (DC only) of 3.3 ± 1.7 at a concentration of 0.5 μg/ml ($p < 0.01$). No statistically significant increase in MFI at a concentration of 0.02 or 0.1 μg/ml was observed. At 0.1 and 0.5 μg/ml SIINFEKL delivered as S-E2 to BMDCs, we observed a 2.2 ± 0.6 and 4.6 ± 1.4-fold increase in antibody labeling for SIINFEKL display, respectively, relative to DC only ($p < 0.001$). No statistically significant display was measured for S-E2 at 0.02 μg/ml SIINFEKL concentration.

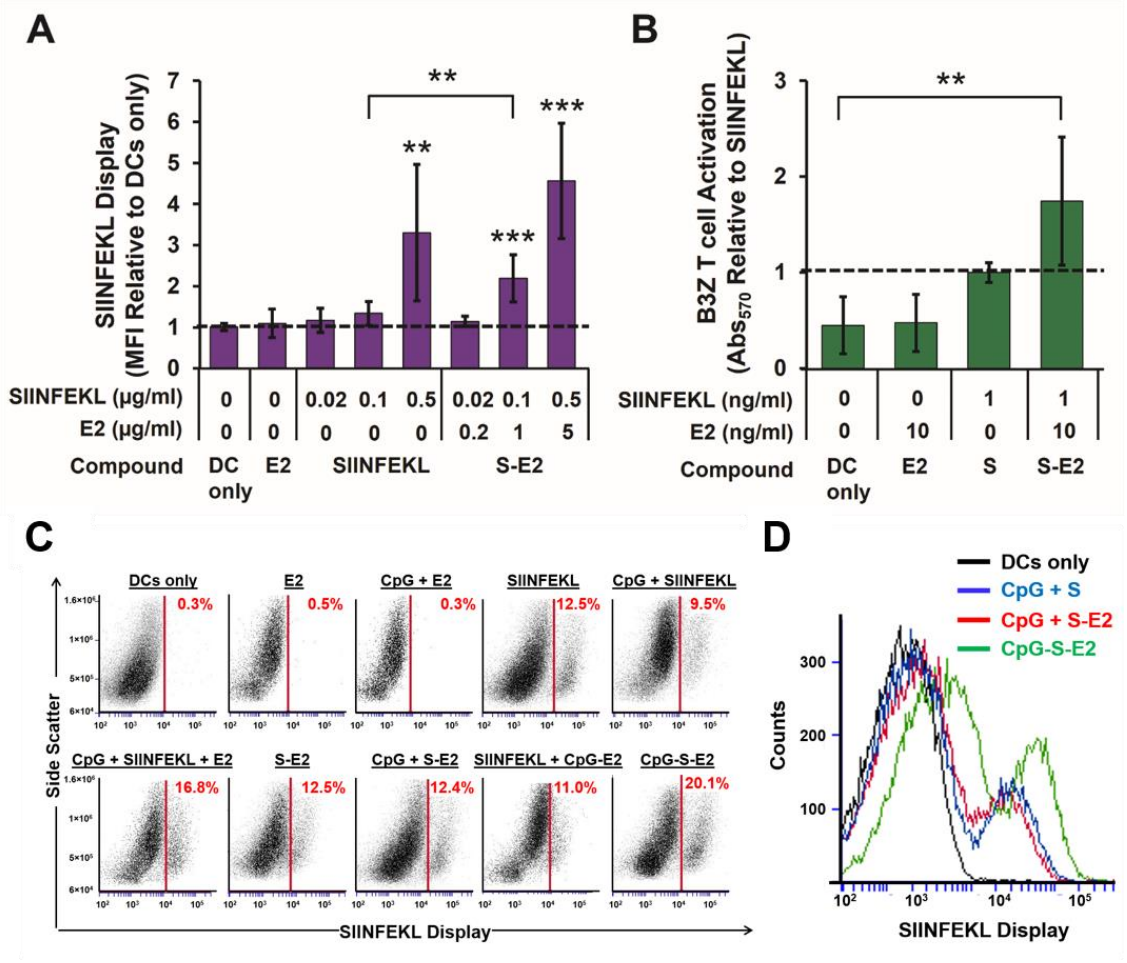

Figure 2.6. A and B) BMDCs process and display E2-bound SIINFEKL (S) epitopes and activate cognate CD8 T cells. **C and D)** Depicted are representative BMDC cross-presentation experiment analyzed by flow cytometry following incubation with antigen (0.5 µg/ml equivalent SIINFEKL concentration) and staining with monoclonal antibody 25-D1.16. **A)** MFI measurement of BMDCs showed greater SIINFEKL display when incubated with S-E2 compared to free SIINFEKL peptide at 0.1 µg/ml peptide concentration (** $p < 0.01$). **B)** The SIINFEKL-bound E2 group (S-E2) in the B3Z assay showed a 1.7 ± 0.7-fold increase in T cell activation, relative to unbound SIINFEKL. The S-E2 group showed significant B3Z activation above background (DC only), whereas unbound SIINFEKL was statistically within background levels. For both panels A & B, data is presented as mean ± SD ($n \geq 4$ independent experiments); ** $p < 0.01$ and *** $p < 0.001$, relative to DC only. **C)** Representative dot plot with the events to the right of the red bars are considered positive for SIINFEKL display in the context of H-2K^b. **D)** Overlay of representative histograms of DCs only, unbound CpG + unbound SIINFEKL (S), unbound CpG + S-E2, and CpG-S-E2.

Our data shows that peptide antigens covalently bound to E2 (S-E2) are able to be processed for display by BMDCs at levels comparable to those of free unbound peptide. In unbound form, peptides can potentially bind surface MHC I markers without needing to be internalized and processed in subcellular compartments. However, in the case of S-E2, the covalent peptide attachment requires intracellular processing. This suggests that the E2 particle is taken up by DC, and the SIINFEKL peptide is cleaved and processed for display on MHC I (*i.e.*, cross-presented). Interestingly, at a SIINFEKL concentration of 0.1 μg/ml there is a significant increase in relative display levels when delivered in E2-bound form (S-E2), relative to unbound form (SIINFEKL, $p < 0.01$) (**Figure 2.6A**). This result shows that conjugating antigen to the E2 protein nanoparticle through stable bonds does not preclude processing and display, and may increase or prolong antigen presentation.

This enhanced presentation effect has been reported before with antigens encapsulated in PLGA nanoparticles and with peptides bound to poly(propylene sulfide) nanoparticles [48,49]. In fact, Hirosue *et al*. showed that when SIINFEKL peptides were bound to nanoparticles through reducible disulfide bonds rather than more stable linkages, DCs exhibited greater cross-presentation to CD8 T cells [48]. In our study, the SIINFEKL peptides are immobilized through succinimidyl thioether bonds, and Baldwin *et al*. have shown that this type of bond can become labile in physiological reducing environments, such as that of the endosome [50]. The kinetics for reduction of disulfide bonds is much faster than that of succinimidyl thioethers, and design of these linkages may be one variable for controlled release of antigen upon cellular uptake.

For a strong cellular mediated immune response against cancer, DCs must display antigen and also engage antigen-specific CD8 T cells. The B3Z hybridoma CD8 T cell, expressing a T cell receptor specific for SIINFEKL in the context of H-2K^b, was incubated overnight with antigen-pulsed BMDC, and SIINFEKL recognition by the CD8 T cell was measured. The results shown in **Figure 2.6B** demonstrate that BMDC loaded with the S-E2 nanoparticle have the capability to functionally engage CD8 T cells, a critical event linking innate and adaptive immunity for a cell-mediated effector response. While no statistically significant difference is evident based on averages, the S-E2-pulsed BMDCs exhibited ~ 2-fold greater T cell activation in four out of five separate experiments compared to the free peptide. Therefore, a modest increase in T cell activation may be evident when DCs are incubated with S-E2 rather than unbound peptide, consistent with our observed result of increased antigen display (**Figure 2.6**). Taken together, our data shows that the BMDCs can internalize the S-E2 particle, process the covalently bound peptides for display *via* MHC I, and activate complementary CD8 T cells.

2.3.4 Simultaneous Delivery of Peptide and CpG within E2 Enhances Antigen Display

Since free CpG can enhance cross-presentation in BMDC [51], and subcellular co-localization of antigen and adjuvant correlates to a more efficacious anti-tumor immune response *in vivo* [30], we combined the OVA peptide with the CpG activator in a single multifunctional E2 particle (CpG-S-E2). Control studies showed that the conjugation of peptides did not interfere with the DC-activating capacity of the CpG-functionalized

nanoparticle (**Figure 2.7**), with no significant difference in relative expression levels of CD11c, MHC II, and CD86 between the CpG-E2 and CpG-S-E2 particles.

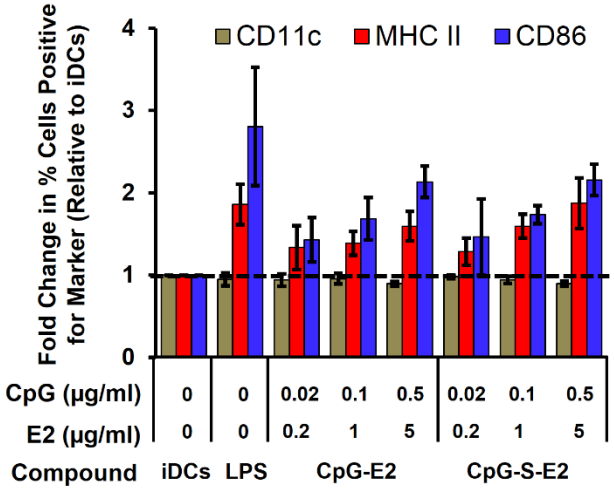

Figure 2.7. No significant difference was observed between the CpG-E2 particle and CpG-S-E2 particle with respect to BMDC activation at a given CpG concentration. Activation extent was determined by measuring MFI for the expression of MHC II and CD86 (n ≥ 4 independent experiments).

Antigen display experiments showed that the CpG-S-E2 particle induced significantly greater BMDC cross-presentation compared to unbound CpG + S-E2, with ~2.5-fold increase in relative MFI at 0.1 µg/ml and 0.5 µg/ml SIINFEKL. In fact, at SIINFEKL concentrations of 0.1 and 0.5 µg/ml, CpG-S-E2 facilitated significantly greater display than any other SIINFEKL formulation ($p < 0.001$) (**Figure 2.8**), with representative flow cytometry dot plots and histograms presented in the second row of **Figure 2.6C** and **Figure 2.6D**, respectively. Importantly, while no significant amount of MHC I presentation was detected in BMDCs above background (DC only) at 0.02 µg/ml SIINFEKL for both unbound SIINFEKL peptide and S-E2 (**Figure 2.6A**), there is a 1.6 ± 0.4 increase in MFI over background when delivered as CpG-S-E2 ($p < 0.05$; **Figure 2.8**). This shows that combining CpG and peptide within the

same E2 particle decreases the amount necessary to induce detectable levels of BMDC antigen display. These results also demonstrate that simultaneous delivery of activator and antigen by use of a protein nanoparticle can significantly enhance the antigen display and cross-presentation capabilities of DCs.

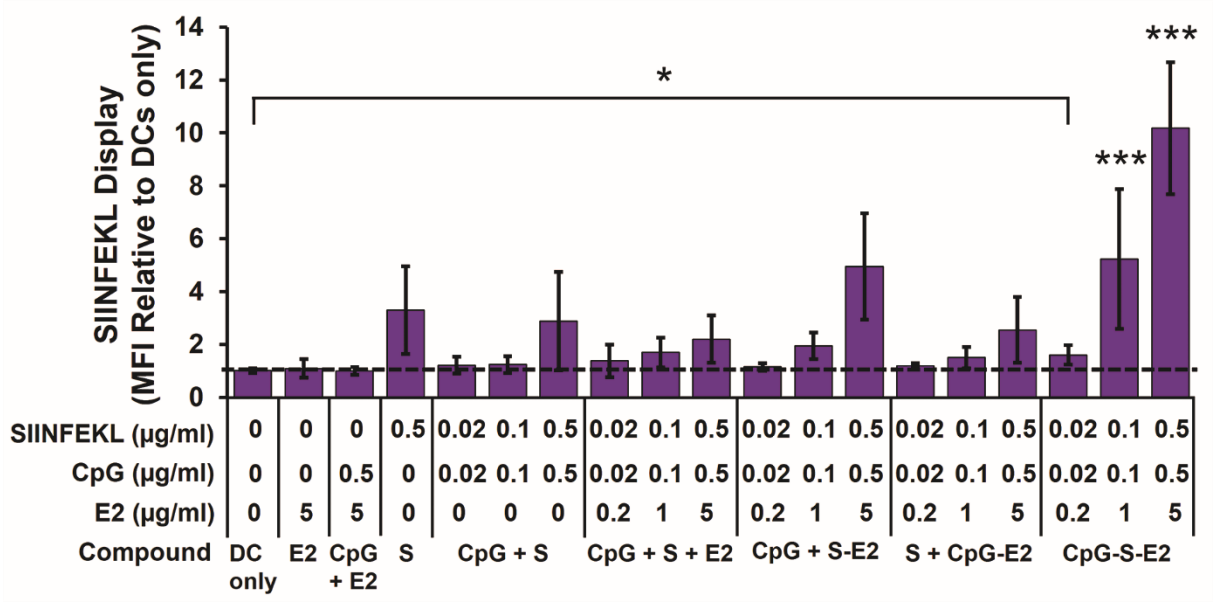

Figure 2.8. Simultaneous spatial and temporal delivery of CpG and SIINFEKL (S) with the E2 nanoparticle increases BMDC cross-presentation. MFI showed significantly more SIINFEKL display following simultaneous conjugation of SIINFEKL and CpG to E2 (CpG-S-E2), compared to all other SIINFEKL and CpG delivery formulations at SIINFEKL concentrations of 0.1 and 0.5 µg/ml (*** $p < 0.001$, for all comparisons at the same SIINFEKL concentration). At a SIINFEKL concentration of 0.02 µg/ml, CpG-S-E2 showed significant MFI above DC-only background (* $p < 0.05$), whereas MFI of all other SIINFEKL formulations at 0.02 µg/ml SIINFEKL were not statistically different from DC-only background. Data is presented as mean ± SD ($n \geq 4$ independent experiments).

The B3Z assay confirmed these cross-presentation observations, with ~2.5-fold increase in T cell activation at 1 ng/ml peptide concentration delivered as CpG-S-E2, compared to any of the other formulations containing unbound SIINFEKL ($p < 0.05$, **Figure**

2.9). This further confirms our ability to specifically increase antigen display and CD8 T cell activation by simultaneous spatial and temporal dosing of activator and antigen within the E2 nanoparticle. While no statistically significant difference was observed between the CpG-S-E2 or unbound CpG + S-E2 groups within the B3Z assay following 12 hours incubation (**Figure 2.9A**), T cell activation of the CpG-S-E2 group was higher every time the experiment was performed (n = 5 independent experiments), with an average 1.4-fold increase over CpG + S-E2. Following 48 hour incubation of BMDCs with B3Z T cells, there was indeed a statistically significant increase in T cell activation for the CpG-S-E2 group compared to CpG + S-E2 of ~ 1.5-fold ($p < 0.05$, **Figure 2.9B**). In fact, at 48 hours incubation, CpG-S-E2 was the only SIINFEKL formulation that exhibited statistically greater CD8 T cell activation over DC-only background ($p < 0.001$). Together, this data shows that simultaneous delivery of CpG and antigen on a nanoparticle (CpG-S-E2) facilitates prolonged antigen display.

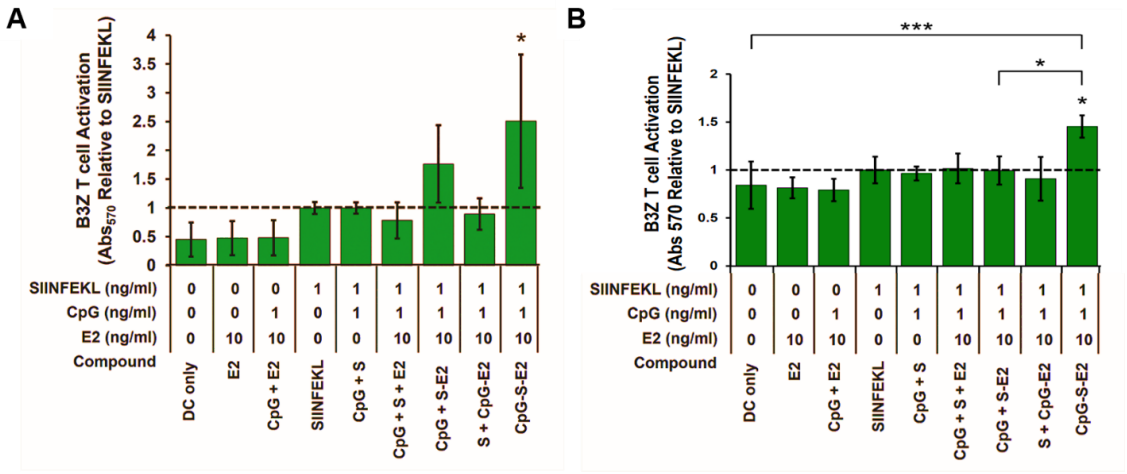

Figure 2.9. B3Z T cell activation of BMDCs pulsed with different groups. **A)** Simultaneous CpG and SIINFEKL conjugation to E2 (CpG-S-E2) showed significantly greater CD8 T cell activation than any other formulation with unbound SIINFEKL (S) peptide after 12 hours incubation. Data is presented as mean ± SD (n ≥ 4 independent experiments for all groups, except n = 3 for groups [S + CpG-E2] and [CpG + S +E2]). Significance was determined by a one-way ANOVA followed by a Bonferroni post-test comparing the set of data for DC-only control and all formulations containing SIINFEKL peptide. * $p < 0.05$, relative to all formulations containing unbound SIINFEKL. **B)** BMDC incubated with CpG-S-E2 facilitate greater CD8 T cell activation than any other peptide delivery strategy after 48 hour incubation. Significantly greater B3Z activation was achieved for BMDCs incubated with CpG-S-E2, relative to all unbound SIINFEKL formulations (* $p < 0.05$). Comparisons with CpG + S-E2 (* $p < 0.05$) and with DC-only background (*** $p < 0.001$) also yielded statistically significant differences. Data is presented as mean ± SD (n ≥ 3 independent experiments), and significance was determined by a one-way ANOVA followed by a Bonferroni post-test.

Peptide epitopes delivered in the E2 nanoparticle enable increased DC-mediated activation of CD8 T cells, and simultaneous delivery of peptide and CpG activator to DCs with E2 further increases and prolongs B3Z activation, compared to unbound peptide and S-E2. While T cell activation differences reported here appear modest, a cancer immunotherapeutic study using free CpG reported relative B3Z activation increases which were similar to our observations using the CpG-S-E2 particle [52]. The 2-fold difference reported for the B3Z assay in this previous report translated to animal death or survival,

showing that even small relative increases with *in vitro* CD8 T cell activation can signify noticeable therapeutic immune response differences.

Prior studies with PLGA nanoparticle systems have also shown relative B3Z activation increases comparable to our observations [49], and potent anti-tumor effects following peptide encapsulation [46]. These past studies, however, used synthetic nanoparticles that did not covalently associate with the antigen, and thus were subject to loss of the antigen by diffusion over time [46]. Therefore, while having similar effects on cross-presentation *in vitro*, the non-viral E2 nanoparticle has the additional advantage of stable covalent peptide display on the external surface, similar to viruses, ensuring delivery to the BMDCs in a packaged size reported optimal for *in vivo* DC-based vaccination [7,19]. Our results here show that we can specifically activate BMDCs with the CpG-S-E2 particle, and that associated antigen can be processed for display *via* MHC I to CD8 T cells at greater levels than with unbound peptides or nanoparticle-conjugated peptides with free CpG.

2.4 Conclusions

In this work, we have designed a multifunctional protein nanoparticle platform based on the E2 core scaffold of pyruvate dehydrogenase for immune modulation. This is the first investigation to demonstrate that a non-infectious protein scaffold of non-viral origin can be re-engineered to mimic viral properties, giving enhancement of DC response and antigen presentation compared to free DC activator and antigen alone. The nanoparticle structure was designed to allow for simultaneous arrival of both immune-activator and antigen to the DC, which mimics the natural activity of viruses. Upon internalization by DC, release of both DC activator and antigen is specifically triggered by the acidic and reducing environment of the endosome. This controlled release is important because systematic circulation of DC activators may result in inflammation and toxic side effects while weakening the antigen-specific response. CpG DNA motifs were covalently bound internally within the E2 capsule through acid-labile hydrazone linkages that hydrolyze at acidic endosomal conditions. Delivery of CpG to BMDCs *in vitro* was able to induce cell activation at concentrations lower than required in unbound form, effectively decreasing the dose needed for DC maturation. Peptide epitopes that were bound to the external surface of the E2 nanoparticle were able to be processed by BMDCs *in vitro* for MHC I display, likely through cross-presentation, and the DCs were able to further functionally engage antigen specific CD8 T cells.

The combination of both CpG and peptide epitopes on a single multifunctional E2 particle increased MHC I display and CD8 T cell activation, relative to unbound forms of the individual components. This shows the ability to enhance cross-presentation of nanoparticle-associated antigens by co-delivering an endosomally restricted TLR 9 ligand.

With the use of a model antigen, we demonstrate the potential of engineering a non-viral protein nanoparticle system to induce a CD8 T cell mediated immune response, which is necessary for anti-cancer responses and mimics the activity of viruses, without being infectious. Decreasing the amount of adjuvant molecules needed for DC-activation while increasing antigen cross-presentation may help reduce unwanted side effects or altered immune responses (*e.g.*, tolerance) evident with the systemic administration of these individual components. This provides the groundwork for optimizing the design of an E2 nanoparticle for targeting therapeutically relevant antigenic peptides to the immune system for anti-cancer responses. More broadly, it demonstrates that using biomimetic strategies which emulate viruses, such as in size, symmetry, and simultaneous intracellular delivery of antigen and activator to DCs, can be an effective strategy for eliciting immune response.

2.5 Acknowledgements

We thank the laboratories of Prof. Paolo Casali and Prof. Wendy Liu at UCI for providing excess animal tissue and the laboratory of Prof. Aaron Esser-Kahn for use of their flow cytometer. We thank Prof. Nilabh Shastri at UC Berkeley for providing the B3Z CD8 T cell hybridoma cell line. DLS and mass spectrometry were carried out at the UCI Laser Spectroscopy Facility and the UCI Mass Spectrometry Facility, respectively. We are also grateful to Dr. Sergey Ryazantsev for assistance with obtaining TEM images in the EMi Laboratory at UCLA. This work was supported by NIH (R21 EB010161) and the University of California Cancer Research Coordinating Committee.

2.6 References

1. Aly HA: Cancer therapy and vaccination. *J Immunol Methods* 2012, 382:1-23.
2. Klebanoff CA, Acquavella N, Yu ZY, Restifo NP: Therapeutic cancer vaccines: are we there yet? *Immunological Reviews* 2011, 239:27-44.
3. Plummer EM, Manchester M: Viral nanoparticles and virus-like particles: platforms for contemporary vaccine design. *Wiley Interdisciplinary Reviews-Nanomedicine and Nanobiotechnology* 2011, 3:174-196.
4. Kushnir N, Streatfield SJ, Yusibov V: Virus-like particles as a highly efficient vaccine platform: Diversity of targets and production systems and advances in clinical development. *Vaccine* 2012, 31:58-83.
5. Pokorski JK, Steinmetz NF: The art of engineering viral nanoparticles. *Mol Pharm* 2011, 8:29-43.
6. Uchida M, Klem MT, Allen M, Suci P, Flenniken M, Gillitzer E, Varpness Z, Liepold LO, Young M, Douglas T: Biological containers: Protein cages as multifunctional nanoplatforms. *Advanced Materials* 2007, 19:1025-1042.
7. Bachmann MF, Jennings GT: Vaccine delivery: a matter of size, geometry, kinetics and molecular patterns. *Nature Reviews Immunology* 2010, 10:787-796.
8. Dalmau M, Lim S, Wang SW: Design of a pH-dependent molecular switch in a caged protein platform. *Nano Lett* 2009, 9:160-166.
9. Molino NM, Bilotkach K, Fraser DA, Ren D, Wang SW: Cell Uptake and Complement Responses Toward Polymer-Functionalized Protein Nanocapsules. *Biomacromolecules* 2012, 13:974–981.
10. Ren DM, Dalmau M, Randall A, Shindel MM, Baldi P, Wang SW: Biomimetic Design of Protein Nanomaterials for Hydrophobic Molecular Transport. *Advanced Functional Materials* 2012, 22:3170-3180.
11. Ren DM, Kratz F, Wang SW: Protein Nanocapsules Containing Doxorubicin as a pH-Responsive Delivery System. *Small* 2011, 7:1051-1060.
12. Grgacic EV, Anderson DA: Virus-like particles: passport to immune recognition. *Methods* 2006, 40:60-65.
13. Dalmau M, Lim S, Chen HC, Ruiz C, Wang SW: Thermostability and Molecular Encapsulation Within an Engineered Caged Protein Scaffold. *Biotechnol Bioeng* 2008, 101:654-664.
14. Dalmau M, Lim S, Wang SW: pH-Triggered Disassembly in a Caged Protein Complex. *Biomacromolecules* 2009, 10:3199-3206.
15. Domingo GJ, Chauhan HJ, Lessard IAD, Fuller C, Perham RN: Self-assembly and catalytic activity of the pyruvate dehydrogenase multienzyme complex from Bacillus stearothermophilus. *European Journal of Biochemistry* 1999, 266:1136-1146.
16. Izard T, Aevarsson A, Allen MD, Westphal AH, Perham RN, de Kok A, Hol WG: Principles of quasi-equivalence and Euclidean geometry govern the assembly of cubic and dodecahedral cores of pyruvate dehydrogenase complexes. *Proc Natl Acad Sci U S A* 1999, 96:1240-1245.
17. Milne JLS, Shi D, Rosenthal PB, Sunshine JS, Domingo GJ, Wu XW, Brooks BR, Perham RN, Henderson R, Subramaniam S: Molecular architecture and mechanism of an icosahedral pyruvate dehydrogenase complex: a multifunctional catalytic machine. *Embo Journal* 2002, 21:5587-5598.
18. Reddy ST, Rehor A, Schmoekel HG, Hubbell JA, Swartz MA: In vivo targeting of dendritic cells in lymph nodes with poly(propylene sulfide) nanoparticles. *Journal of Controlled Release* 2006, 112:26-34.
19. Reddy ST, van der Vlies AJ, Simeoni E, O'neil CP, Swartz MA, Hubbell JA: Exploiting lymphatic transport and complement activation in nanoparticle vaccines. *Tissue Engineering Part A* 2008, 14:734-735.

20. Caivano A, Doria-Rose NA, Buelow B, Sartorius R, Trovato M, D'Apice L, Domingo GJ, Sutton WF, Haigwood NL, De Berardinis P: HIV-1 Gag p17 presented as virus-like particles on the E2 scaffold from Geobacillus stearothermophilus induces sustained humoral and cellular immune responses in the absence of IFN gamma production by CD4+T cells. *Virology* 2010, 407:296-305.
21. Jaworski JP, Krebs SJ, Trovato M, Kovarik DN, Brower Z, Sutton WF, Waagmeester G, Sartorius R, D'Apice L, Caivano A, et al.: Co-Immunization with Multimeric Scaffolds and DNA Rapidly Induces Potent Autologous HIV-1 Neutralizing Antibodies and CD8(+) T Cells. *Plos One* 2012, 7:e31464.
22. Apetoh L, Locher C, Ghiringhelli F, Kroemer G, Zitvogel L: Harnessing dendritic cells in cancer. *Semin Immunol* 2011, 23:42-49.
23. Tacken PJ, de Vries IJ, Torensma R, Figdor CG: Dendritic-cell immunotherapy: from ex vivo loading to in vivo targeting. *Nat Rev Immunol* 2007, 7:790-802.
24. Ueno H, Klechevsky E, Schmitt N, Ni L, Flamar AL, Zurawski S, Zurawski G, Palucka K, Banchereau J, Oh S: Targeting human dendritic cell subsets for improved vaccines. *Seminars in Immunology* 2011, 23:21-27.
25. Joffre OP, Segura E, Savina A, Amigorena S: Cross-presentation by dendritic cells. *Nat Rev Immunol* 2012, 12:557-569.
26. Reddy ST, Swartz MA, Hubbell JA: Targeting dendritic cells with biomaterials: developing the next generation of vaccines. *Trends in Immunology* 2006, 27:573-579.
27. Joshi MD, Unger WJ, Storm G, van Kooyk Y, Mastrobattista E: Targeting tumor antigens to dendritic cells using particulate carriers. *Journal of Controlled Release* 2012, 161:25-37.
28. Bourquin C, Anz D, Zwiorek K, Lanz AL, Fuchs S, Weigel S, Wurzenberger C, von der Borch P, Golic M, Moder S, et al.: Targeting CpG oligonucleotides to the lymph node by nanoparticles elicits efficient antitumoral immunity. *J Immunol* 2008, 181:2990-2998.
29. Burgdorf S, Scholz C, Kautz A, Tampe R, Kurts C: Spatial and mechanistic separation of cross-presentation and endogenous antigen presentation. *Nature Immunology* 2008, 9:558-566.
30. Nierkens S, den Brok MH, Sutmuller RPM, Grauer OM, Bennink E, Morgan ME, Figdor CG, Ruers TJM, Adema GJ: In vivo colocalization of antigen and cytidyl guanosyl within dendritic cells is associated with the efficacy of cancer immunotherapy. *Cancer Research* 2008, 68:5390-5396.
31. Krishnamachari Y, Geary SM, Lemke CD, Salem AK: Nanoparticle Delivery Systems in Cancer Vaccines. *Pharmaceutical Research* 2011, 28:215-236.
32. Peek LJ, Middaugh CR, Berkland C: Nanotechnology in vaccine delivery. *Advanced Drug Delivery Reviews* 2008, 60:915-928.
33. Wilson NS, Behrens GMN, Lundie RJ, Smith CM, Waithman J, Young L, Forehan SP, Mount A, Steptoe RJ, Shortman KD, et al.: Systemic activation of dendritic cells by Toll-like receptor ligands or malaria infection impairs cross-presentation and antiviral immunity. *Nature Immunology* 2006, 7:165-172.
34. Storni T, Ruedl C, Schwarz K, Schwendener RA, Renner WA, Bachmann MF: Nonmethylated CG motifs packaged into virus-like particles induce protective cytotoxic T cell responses in the absence of systemic side effects. *Journal of Immunology* 2004, 172:1777-1785.
35. Steinhagen F, Kinjo T, Bode C, Klinman DM: TLR-based immune adjuvants. *Vaccine* 2011, 29:3341-3355.
36. Sanderson S, Shastri N: LacZ inducible, antigen/MHC-specific T cell hybrids. *Int Immunol* 1994, 6:369-376.
37. Aida Y, Pabst MJ: Removal of endotoxin from protein solutions by phase separation using Triton X-114. *J Immunol Methods* 1990, 132:191-195.
38. Lutz MB, Kukutsch N, Ogilvie AL, Rossner S, Koch F, Romani N, Schuler G: An advanced culture method for generating large quantities of highly pure dendritic cells from mouse bone marrow. *J Immunol Methods* 1999, 223:77-92.

39. Rodriguez A, Regnault A, Kleijmeer M, Ricciardi-Castagnoli P, Amigorena S: Selective transport of internalized antigens to the cytosol for MHC class I presentation in dendritic cells. *Nat Cell Biol* 1999, 1:362-368.
40. Zwiorek K, Bourquin C, Battiany J, Winter G, Endres S, Hartmann G, Coester C: Delivery by cationic gelatin nanoparticles strongly increases the immunostimulatory effects of CpG oligonucleotides. *Pharmaceutical Research* 2008, 25:551-562.
41. Roman BS, Irache JM, Gomez S, Tsapis N, Gamazo C, Espuelas MS: Co-encapsulation of an antigen and CpG oligonucleotides into PLGA microparticles by TROMS technology. *European Journal of Pharmaceutics and Biopharmaceutics* 2008, 70:98-108.
42. Tacken PJ, Zeelenberg IS, Cruz LJ, van Hout-Kuijer MA, van de Glind G, Fokkink RG, Lambeck AJA, Figdor CG: Targeted delivery of TLR ligands to human and mouse dendritic cells strongly enhances adjuvanticity. *Blood* 2011, 118:6836-6844.
43. Sioud M, Leirdal M: Design of nuclease resistant protein kinase calpha DNA enzymes with potential therapeutic application. *J Mol Biol* 2000, 296:937-947.
44. Peacey M, Wilson S, Baird MA, Ward VK: Versatile RHDV virus-like particles: Incorporation of antigens by genetic modification and chemical conjugation. *Biotechnology and Bioengineering* 2007, 98:968-977.
45. Molinari P, Crespo MI, Gravisaco MJ, Taboga O, Moron G: Baculovirus capsid display potentiates OVA cytotoxic and innate immune responses. *Plos One* 2011, 6:e24108.
46. Zhang Z, Tongchusak S, Mizukami Y, Kang YJ, Ioji T, Touma M, Reinhold B, Keskin DB, Reinherz EL, Sasada T: Induction of anti-tumor cytotoxic T cell responses through PLGA-nanoparticle mediated antigen delivery. *Biomaterials* 2011, 32:3666-3678.
47. Wu CCN, Lee JD, Raz E, Corr M, Carson DA: Necessity of oligonucleotide aggregation for toll-like receptor 9 activation. *Journal of Biological Chemistry* 2004, 279:33071-33078.
48. Hirosue S, Kourtis IC, van der Vlies AJ, Hubbell JA, Swartz MA: Antigen delivery to dendritic cells by poly(propylene sulfide) nanoparticles with disulfide conjugated peptides: Cross-presentation and T cell activation. *Vaccine* 2010, 28:7897-7906.
49. Shen H, Ackerman AL, Cody V, Giodini A, Hinson ER, Cresswell P, Edelson RL, Saltzman WM, Hanlon DJ: Enhanced and prolonged cross-presentation following endosomal escape of exogenous antigens encapsulated in biodegradable nanoparticles. *Immunology* 2006, 117:78-88.
50. Baldwin AD, Kiick KL: Tunable degradation of maleimide-thiol adducts in reducing environments. *Bioconjug Chem* 2011, 22:1946-1953.
51. Datta SK, Redecke V, Prilliman KR, Takabayashi K, Corr M, Tallant T, DiDonato J, Dziarski R, Akira S, Schoenberger SP, et al.: A subset of Toll-like receptor ligands induces cross-presentation by bone marrow-derived dendritic cells. *J Immunol* 2003, 170:4102-4110.
52. den Brok MH, Sutmuller RP, Nierkens S, Bennink EJ, Toonen LW, Figdor CG, Ruers TJ, Adema GJ: Synergy between in situ cryoablation and TLR9 stimulation results in a highly effective in vivo dendritic cell vaccine. *Cancer Res* 2006, 66:7285-7292.

CHAPTER 3

VIRAL-MIMICKING PROTEIN NANOCAPSULES ENHANCE CYTOTOXIC T CELL RESPONSES TOWARD A TUMOR ANTIGEN

3.1 Background

Recent years have brought an improved understanding of the interplay between cancer and the immune system, leading to increased interest in immunotherapy for treatment of the disease [1,2]. Traditional cancer management strategies (*e.g.*, surgical resection, radiation therapy, or chemotherapy) have been the mainstay and continual research is constantly improving upon these strategies. However, recent investigations have revealed that the immune system possesses many unique advantages for disease eradication [3-5]. The adaptive immune response toward cancer is inherently targeted, given that lymphocytes recognize a very specific epitope or antigen [2]. Antigen-specific immune cells are trained within secondary lymphoid organs (*i.e.,* lymph node or spleen) to attack tumor-associated antigens (TAAs), with subsequent migration to the periphery for surveillance. When the target antigen is encountered, the cell or organism bearing that TAA is destroyed or neutralized, leaving healthy tissue largely unharmed.

For immunological suppression of cancer, a robust $CD8^+$ cytotoxic T lymphocyte (CTL) response is required, due to CTLs' natural ability to lyse cells expressing TAA epitopes presented in the context of major histocompatibility receptor type I (MHC I), which all nucleated cells express [6,7]. Various clinically promising strategies for therapeutic vaccination against TAAs have included administration of whole protein antigen [8], mature peptide epitopes [9], cell lysate [10,11], adoptive transfer of tumor reactive CTL [12], and engineering T cells with chimeric antigen receptors [13,14]. Chimeric antigen-containing T cells have shown particularly promising results and complete regression of late stage leukemia in multiple patients [13,14].

Peptide vaccines possess the advantage of requiring less biochemical processing for antigen display to CTL, compared to other strategies [9,15,16]. Peptides also allow for easy incorporation of multiple epitopes without significantly increasing formulation complexity or requiring production and purification of multiple recombinant protein antigens. Peptides represent a synthetically simple and relatively inexpensive TAA-targeted vaccine alternative to many of the other promising strategies mentioned above [9,15,16]. For instance, while chimeric antigen receptor engineering of autologous T cells may confer great success to cancer vaccination, the labor intensive process and need for highly skilled scientists may render this intervention financially unattainable for widespread clinical application.

Peptide epitope vaccines are not without their own drawbacks, however. Purified peptide typically display hydrodynamic radii well below the reported optimal size range for efficient vaccine delivery [17]. While at the physical size range of peptides, they likely diffuse away from the injection site and into the lymphatics, they are also likely to enter local capillary vasculature. At this small size they are also below the reported ~20-2000 nm size range for efficient uptake by APCs within the lymph and may be subject to rapid degradation by *in vivo* peptidase enzymes [17,18]. Therefore alterations in the current delivery paradigm should be explored to reveal their full potential [19-21].

It has been established that antigen preparation resulting in particulate formulations are advantageous, particularly with respect to antigen presenting cell (APC) recognition and uptake [17,22-24]. Particulate formation is hypothesized to occur for the common human vaccine adjuvant, alum, forming antigen depots at the site of injection [24]. Other common strategies to form particulate antigens include oil immersions and immune stimulating

complexes [24]. It was determined that particles in the range of 20-2000 nm are most effectively drained to lymphatics and taken up by APCs, including dendritic cells (DCs), a key mediator of CTL immunity [17,25,26]. Nanoparticles have been explored for the delivery of tumor antigens to the immune system for vaccination, including polymers (*e.g.,* PLGA), liposomes, saccharide-based particulate materials, and metallic nanoparticles [27].

Beyond size, geometry can play a key role in DC interactions, most notably the geometry of viruses [17,28,29]. Viruses are a natural pathogen the immune system has evolved to recognize quite efficiently, and mimicking this capability may be advantageous for inducing robust CTL responses against low-immunogenic targets like tumor antigens. Viruses are generally comprised of one or a few protein monomers that assemble into symmetrical hollow structures with repeating antigens and geometric features. The core of the viral capsid contains the genetic material for perpetuation of virus production in the infected cell. The immune system has evolved sensing mechanisms (*e.g.*, Toll-like receptors; TLRs) to recognize common pathogenic features of viruses, adding another advantage to pursuing mimicry of these elegant infectious agents [30,31]. While mirroring these various features of viruses for vaccine formulation is desired, the natural infectivity of the virus must be avoided. Platforms explored to accomplish this have include virus-like particles (VLPs) (*i.e.* the native viral capsules without the genetic payload) or other cage-like protein structures (*e.g.,* E2, see Chapter 1). In fact, Qβ-based VLP platforms are current undergoing clinical trial for the delivery of melanoma-derived CTL epitopes [32,33]. Potential drawbacks of using VLPs as opposed to other caged structures, may be issues related to difficulty in preparation and high immunogenicity to the capsid itself, which could detract from the TAA-specific response whose induction is being attempted [34].

Our research group has previously demonstrated that by combining peptide epitopes from the model antigen ovalbumin along with endolysosomal-releasable TLR9-activating nonmethylated CpG DNA within the E2 nanoparticle for simultaneous delivery to DCs, we observed enhanced activation and cross-presentation capabilities (See Chapter 2) [35]. Enhanced cross-presentation by DCs is an immunological attribute that would potentially allow increased CTL activation toward the antigen payload. Additionally, the co-delivery of danger signal may allow the immune system to overcome the low immunogenicity or tolerance to tumor antigens.

A tumor antigen that has been explored clinically is gp100, which is overexpressed in over 90% of melanoma cases [36]. The overexpressed gp100 TAA is a self-antigen and a differentiation marker for melanocytes. Therefore, with this particular class of TAA, a sufficiently strong response is required to overcome central tolerance. Although mounting an immune response against a self-antigen has the potential for autoimmune responses, vaccination against self-antigen TAA's in mice and in humans has indicated tumor eradication without debilitating autoimmunity [13,14,37,38]. Therefore, we hypothesized that by vaccination with a gp100 CTL-restricted epitope and CpG simultaneously packaged within the E2 nanoparticle, we will observe increased antigen-specific CTL immunity, relative to other antigen formulations.

3.2 Methods

3.2.1 Materials

All buffer reagents were purchased from Fisher Scientific, unless otherwise noted. The oligodeoxynucleotide Toll-like receptor 9 ligand CpG 1826 (5'-tccatgacgttcctgacgtt-3') (CpG) was synthesized with a phosphorothioated backbone and 5' benzaldehyde modification by TriLink Biotechnologies. The KVPRNQDWL peptide ($gp100_{25\text{-}33}$) was from Genscript, and the custom $gp100_{25\text{-}33}$ was synthesized with an N-terminal cysteine by Thinkpeptides (Proimmune). All cell culture media was comprised of RPMI 1640 (Mediatech) supplemented with 10% heat-inactivated fetal bovine serum (Hyclone), 1 mM sodium pyruvate (Hyclone), 2 mM L-glutamine (Lonza), 100 units/ml penicillin (Hyclone), 100 μg/ml streptomycin (Hyclone), 50 μM 2-mercaptoethanol (Sigma), and 0.1 mM non-essential amino acids (Lonza) (complete RPMI media). Carboyxyfluorescein diacetate, succinimidyl ester (CFSE) and flow cytometry antibodies were purchased from eBioscience.

3.2.2 Mice and Cell Lines

Female C57Bl/6 mice and pmel-1 mice (C57Bl/6 background, transgenic T-cell receptor specific for the murine $gp100_{25\text{-}33}$ epitope in the context of H2-D^b with cross-reactivity for the human homologue used in these studies [38]) were purchased from Jackson Laboratories, and used at 6-12 weeks of age. The B16-F10 murine melanoma cell line was purchased from ATCC and cultured in DMEM media supplemented with 10% FBS according to vendor instructions.

3.2.3 E2 Purification

The D381C E2 protein (E2) was prepared as previously described [39]. D381C is an E2 mutant with a non-native cysteine introduced to the internal cavity of the nanoparticle for site-directed functionalization. Briefly, proteins were expressed in *E. coli*, cells were lysed, and soluble cell lysates were applied to a HiPrep Q Sepharose anion exchange column (GE Healthcare) followed by a Superose 6 (GE Healthcare) size exclusion column for purification. The purified proteins were analyzed by dynamic light scattering (Zetasizer Nano ZS, Malvern) for size measurements. Electrospray ionization mass spectrometry and SDS-PAGE were performed for molecular weight and purity confirmation. Final protein preparations were stored in 50 mM potassium phosphate at pH 7.4 with 100 mM NaCl at 4°C for short-term and -80°C for long-term storage.

Lipopolysaccharide (LPS), a component of gram-negative bacterial cell walls, is recognized by Toll-like receptor 4 expressing immune cells (*e.g.* DCs), causing potentially unwanted immune activation. Residual LPS was removed following the method described by Aida and Pabst [40]. Briefly, Triton X-114 (Sigma) was added to the purified protein at 1% (v/v), chilled to 4°C, vortexed vigorously, and heated to 37°C. The mixture was then centrifuged at 18,000 × g and 37°C for 30 seconds, and the protein-containing aqueous portion was separated from the detergent. This total process repeated ≥ 8 times. Residual Triton was removed with detergent removal spin columns (Pierce). LPS levels were below 8 EU (0.8 ng) per milligram of E2 protein (LAL ToxinSensor gel clot assay, Genscript).

3.2.4 CpG and gp100 Peptide Conjguation

CpG and cysteine-terminated peptides were conjugated as described in Chapter 2.2.4 [35], with the exception that the peptide sequence used for these studies was CKVPRNQDWL, a CTL-restricted epitope from human gp100.

For measurement of peptide conjugation ratios, $gp100_{25\text{-}33}$-conjugated E2 (gp-E2) was analyzed by high performance liquid chromatography (HPLC, Shimadzu) with a Zorbex C18 column over a 35 minute linear gradient from 5% aqueous acetonitrile to 100% acetonitrile. A standard curve was produced with TCEP-reduced CKVPRNQDWL peptide over a range of $0.06\text{-}2\times10^{-3}$ M. Peptide and E2 were combined at a 10:1 molar ratio, with respect to the E2 monomer concentration (*i.e.* 36 μM E2 monomer with 360 μM peptide). Negative controls consisted of adding water in place of the SMCC linker to the E2 nanoparticle, and reactions were otherwise carried out as described previously [35]. Without removing free peptide, gp-E2 was compared to the negative control reaction (E2 + H_2O + CKVPRNQDWL) to measure differences in free peptide.

3.2.5 Bone Marrow-Derived Dendritic Cells

Bone marrow-derived dendritic cells (BMDCs) were prepared following the method described by Lutz *et al* [41]. Briefly, the femurs and tibias were rinsed in 70% ethanol, epiphyses removed, and the marrow flushed. Cells were broken up to a single cell suspension and applied to a 70 μm cell strainer (Fisher). Red blood cells were depleted with ACK lysing buffer (Lonza), followed by washing with PBS. The marrow cells were plated at 2×10^5 cells/ml (10 ml total) on sterile bacteriological Petri dishes (Fisher) in complete RPMI media supplemented with 20 ng/ml murine recombinant GM-CSF (eBioscience) (DC media).

Cells were maintained at 37°C and 5% CO_2, and 10 ml fresh DC media was added on day 3. On day 6, 50% of the media was replaced, and the non-adherent cells were pelleted and added back to the plates. Loosely and non-adherent cells were collected and used as immature BMDCs on day 8.

3.2.6 pmel-1 CD8 T Cell Isolation and CFSE Labeling

The spleens and lymph nodes from 8-12 week old female pmel-1 mice were isolated following euthanization under 100% $C0_2$ and were crushed through a 70 μm cell strainer in to ice cold PBS and centrifuged at 300×g for 5 minutes. The pellet was treated with 5 mL ACK lysing buffer (Lonza) for 2 minutes to remove red blood cells, brought to 25 mL with ice cold PBS, centrifuged, washed 1 more time with 10 mL PBS, and prepared at 1×10^8 cells/mL. The CD8 T cells were purified with the EasySep CD8 T cell negative isolation kit from STEMCELL according to the manufacturer's instructions. The CD8 T cells were prepared at 2×10^7 cells/mL in PBS and diluted with an equal volume of PBS containing 5 μM of the intracellular dye CFSE (1×10^7 cells/mL and 2.5 μM CFSE final) and incubated at room temperature for 10 minutes. The reaction was quenched by 10-fold dilution with 37°C RPMI containing 10% FBS, centrifuged, and washed one more time with PBS. The CFSE-labeled CD8 T cells were used for further immunological assays.

3.2.7 pmel-1 CD8 T Cell Proliferation and IFN-γ Secretion Assays

BMDCs (5×10^3 cells/well in 96 well plate) were cultured in complete RPMI media at 37°C containing 1000, 100, or 10 nM $gp100_{25\text{-}33}$ in various formulation including, free peptide, free peptide + free CpG, free peptide + free CpG + free E2, free peptide + CpG-conjugated E2 (CpG-E2; internal conjugation to thiol), $gp100_{25\text{-}33}$-conjugated E2 (gp-E2;

external conjugation to amines) + free CpG, or CpG and $gp100_{25\text{-}33}$ simultaneously conjugated to E2 (CpG-gp-E2). Control groups included E2 alone and CpG-E2 alone. Equivalent amounts of E2, peptide, and CpG were used in all formulation for direct comparison. Both CpG and peptide are roughly 10% (w/w), relative to E2, in their conjugated form [33]. After 4 hours, the BMDCs were centrifuged at 300×g, the plates were washed 2× with 37°C PBS, and cells were re-suspended in fresh 37°C complete RPMI. Freshly prepared CFSE-labeled pmel-1 CD8 T cells were added to the antigen-pulsed BMDCs at 5×10^4 cells/well and cultured at 37°C for 72 hr. Negative control wells consisted of co-culture without any antigen stimulation and positive control included αCD3/αCD28 Dynabeads (Gibco) added at a 1:1 ratio with T cells.

The supernatant from the cultures was collected and assayed for IFN-γ by the Mouse IFN-γ ELISA Ready-Set-Go kit (eBioscience), following the manufacturer's instructions. Data is reported as IFN-γ concentration relative to BMDCs pulsed with free $gp100_{25\text{-}33}$ peptide alone. Cells were harvested, stained with APC-tagged anti-CD8, and analyzed by an Accuri C6 flow cytometer for CFSE dilution of $CD8^+$ cells. Data is reported as proliferation index (PI), relative to the free $gp100_{25\text{-}33}$ peptide formulation [42]. PI was calculated as

$$\mathrm{PI} = \frac{\sum_0^i N_i}{\sum_0^i \frac{N_i}{2^i}}$$

where *i* is the number of divisions and *N* is the number of cells within that division.

3.2.8 Animal Immunizations

Animal studies were carried out in accordance with approved protocols according to IACUC at University of California Irvine. Six to 12 week old C57Bl/6 wild-type females were injected subcutaneously bilaterally at the base of the tail with various formulations of the $gp100_{25\text{-}33}$ peptide in PBS. Formulations included free peptide + free CpG, free peptide + CpG-E2, gp-E2 + free CpG, and CpG-gp-E2, and were administered as 50 μg of nanoparticle or equivalent amount of free peptide or CpG (~10% w/w). After 7 days, animals were euthanized under 100% CO_2 and were analyzed *ex vivo* for an antigen-specific immune response. Formulations tested in this study are listed in **Table 3.1**.

Formulation	**Label**
Free peptide	gp100
Free peptide + Free CpG	gp100 + CpG
Free peptide + Free CpG + Free E2	gp100 + CpG + E2
Free peptide + CpG-conjugated E2	gp100 + CpG-E2
Peptide-conjuagted E2 + Free CpG	gp-E2 + CpG
Peptide and CpG-conjugated E2	CpG-gp-E2

Table 3.1. List of various $gp100_{25\text{-}33}$ formulations used in this study, and the label they are referred to as. Free peptide refers to the sequence KVPRNQDWL, whereas peptides linked to the E2 nanoparticle contain an N-terminal CYS for conjugation. Similarly, free CpG does not contain any modifications to the 5' or 3' terminus, whereas CpG linked to the interior of the E2 cavity contain a 5' aldehyde group for conjugation.

3.2.9 IFN-γ ELISpot

Spleen and draining lymph nodes (inguinal, axillary, brachial, and iliac) were collected and analyzed separately. Single cell suspensions were prepared by crushing through a 70 μm cell strainer into ice cold PBS. Splenocytes were treated with ACK lysing buffer for 2 minutes and quenched with a 5-fold volume of PBS after pelleting at 300×g for 5

minutes. Cells were prepared in complete RPMI and added at ranging concentrations to ELISpot plates (PVDF membrane 96-well plates, Millipore), pre-coated overnight with anti-mouse IFN-γ antibody from the Mouse IFN-γ ELISpot Ready-Set-Go kit (eBioscience). Cells were incubated for 24 hours at 37°C in the presence of either 10μg/mL $gp100_{25\text{-}33}$ or irrelevant peptide (SIINFEKL). Negative control consisted of normal culture media and positive control wells contained 1.5% PHA-M (Gibco). Spots were developed according to the kit manufacturer's protocol and were detected and analyzed by the Cellular Technology Ltd. ELISpot reader and Immunospot Analysis Pack software, respectively.

3.2.10 Flow Cytometry Staining

Isolated splenocyte and lymph node cells were analyzed by flow cytometry to determine the percentages of various cell types present following immunization. Cell markers analyzed included CD11c, F4/80, B220, CD3, CD4, CD8, PD-1, and FoxP3. Fluorescently-tagged antibodies for the above surface markers were mixed with cells in PBS + 1% BSA (FACS buffer) on ice for 30 minutes, followed by 2 washes with FACS buffer.

3.2.11 CTL Lysis Assays

To examine the specific lysis of cells bearing the gp100 TAA, splenocytes from immunized animals were cultured in complete RPMI at 8×10^6/well in 24-well plates in the presence of 10 μg/mL $gp100_{25\text{-}33}$ for 24 hours, washed 2× with PBS to remove unbound peptide, and cultured in fresh complete RPMI for an additional 96 hours. B16-F10 melanoma cells (H-$2D^{b+}$ and $gp100^{+}$) or negative control EL4 cells (H-$2D^{b+}$ and $gp100^{-}$) were plated at 5×10^3 cell/well in a round-bottom 96 well tissue culture-treated plate along with the *ex vivo* stimulated splenocytes at an effector to target ratio of 50:1. Cytotoxicity was

measured by lactose dehydrogenase release with the CytoTox 96 non-radioactive cytotoxicity assay (Promega) following the manufacturer's instructions. Data is reported as % lysis as calculated according to the following equation:

$$\%\ Lysis = \frac{(coculture\ LDH\ release) - (spontaneous\ LDH\ release)}{(maximum\ LDH\ release) - (spontaneous\ LDH\ release)} \text{x } 100$$

3.2.12 Statistical Analysis

Statistical analyses were carried out using Microsoft Excel and GraphPad Prism. Data is reported as mean ± standard error of the mean (S.E.M.) of at least three independent experiments (unless otherwise noted), with the value of a single independent experiment being the average of at least two replicates for that set. Statistical significance was determined by performing a one-way analysis of variance (ANOVA) followed by a Tukey's range test over all statistical means. P-values less than 0.05 were considered significant.

3.3 Results and Discussion

3.3.1 Conjugation of CpG and gp100$_{25-33}$ to E2

CpG and gp100 peptides were successfully and simultaneously conjugated to the E2 nanoparticle (CpG-gp-E2). The CpG was successfully conjugated to the recombinantly introduced cysteine within the interior cavity of the E2 protein (CpG-E2) as described previously at a ratio of 22 ± 3 CpG per nanoparticle (~10% w/w) [35]. The cysteine-containing human gp100$_{25-33}$ MHC I-restricted epitope (CKVPRNQDWL) was successfully conjugated to the exterior amines of the E2 nanoparticle through SMCC chemistry (cysteine to amine cross-linking). While the peptide epitope chosen for this study was derived from the human gp100 protein, is has strong cross-reactivity with the mouse MHC I molecule H-2D^b (mouse homologous epitope is EGSRNQDWL) [38], allowing testing of a human vaccine on an animal model. HPLC analysis revealed a conjugation ratios of 3.9 ± 0.6 peptides/monomer (234 ± 36 peptides/nanoparticle), similar to what we observed for other peptides [35].

SDS-PAGE analysis showed a signal with molecular weight range of 30-35 kDa, consistent with each peptide + linker adding 1,592 Da to the E2 monomer (28105 Da). Similarly two distinct bands in the molecular weight range of 30-35 kDA and 35-40 kDa demonstrate simultaneous conjugation of both CpG and the gp100 peptide to the E2 monomers (**Figure 3.1A**). The similarities between the SDS-PAGE signals, but discrepancy in measured conjugation ratios between the current peptide under investigation and our previously reported peptide could be due to differences in the assays used to quantify attachment [35]. In the present study, we employed HPLC analysis (free peptide) as

described in the Methods section, whereas the Ellman's assay (free thiols) was used for our previous studies [35]. Dynamic light scattering size measurements of the gp-E2 and CpG-gp-E2 nanoparticles revealed a diameter of 31.6 ± 1.3 nm and 30.2 ± 0.7 nm, respectively, displaying particle sizes within the reported optimal size range for vaccines and lack of aggregation (**Figure 3.1B**) [17]. These nanoparticle diameters are also comparable to that observed for the conjugation of the model epitope SIINFEKL to E2 in our previous studies, an indication of size consistency between different epitope conjugations, important for downstream application [35]. This demonstrates the versatility of the E2 nanoparticle as a platform for attachment of different epitopes, where the same functionalization protocol may be applied to different peptides, easily exchanging epitopes to alter the vaccine target.

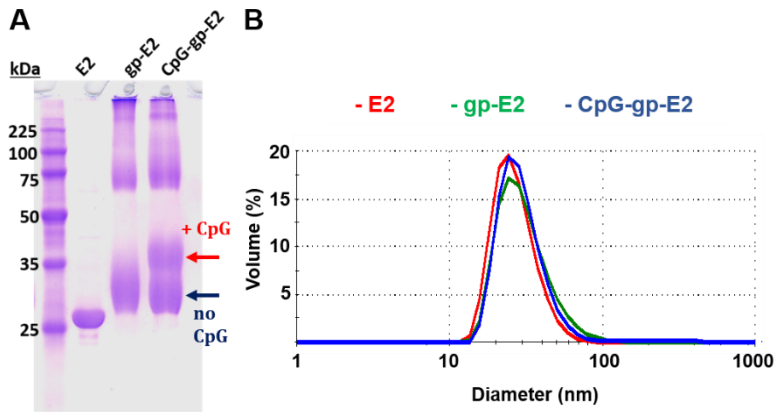

Figure 3.1. Physicochemical characterization of the gp-E2 and CpG-gp-E2 nanoparticles. **A)** Functionalization of the E2 nanoparticle (E2) with the KVPRNQDWL peptide (gp-E2) showing band signal in the 30-35 kDa range. The unmodified E2 monomer has a theoretical molecular weight of 28,105 Da, and the 30-35 kDa band in lane gp-E2 supports heterogeneous conjugation of the gp100$_{25\text{-}33}$ peptide to the external E2 lysines, with each peptide + linker adding a mass of 1,592 kDa to the E2 subunit. Simultaneous conjugation of gp100$_{25\text{-}33}$ peptide and CpG DNA is shown in the right-most land (CpG-gp-E2). Each CpG molecule + linker ads a theoretical molecular weight of 6,774 kDa to the E2 monomer, causing two distinct broad signals in the 30-35 kDa (red arrow) and 35-40 kDa (blue arrow) range. **B)** Representative DLS curves reveal nanoparticle sizes within the optimal reported vaccine size range without aggregation.

The gp100 antigen is a TAA clinically pursued as a target for cancer vaccination [43]. As noted, the chosen 9-mer peptide KVPRNQDWL allows the study of a human epitope in a murine model [38,44]. Additionally, this class of TAA is a differentiation marker and self-antigen and is therefore inherently more difficult to mount an immune response against due to central tolerance. Therefore, the ability to elicit an antigen-specific immune response with this model may provide insight to delivery platforms in general and reveal important formulation parameters critical for superior immunotherapies. In fact, it has already been demonstrated that for this particular TAA, a multi-faceted approach is usually necessary to overcome tolerance and mount an effective anti-tumor response [38]. We hypothesized that the simultaneous combination of CpG and a gp100-derived peptide epitope within in a viral mimicking nanoparticle formulation may provide a superior and more simplified approach.

3.3.2 E2 Co-Delivery of gp100$_{25\text{-}33}$ and CpG Enhance CD8 T Cell Activation

The CpG-gp-E2 nanoparticle increased CTL-specific IFN-γ secretion, compared to other formulations. Bone marrow-derived dendritic cells (BMDCs) pulsed with formulations containing 10, 100, and 1000 nM gp100$_{25\text{-}33}$ were co-cultured with purified naïve pmel-1 CD8 T cells for 72 hours. Over all concentrations tested, the CpG-gp-E2 nanoparticle formulation exhibited increased IFN-γ, compared to other formulations (**Figure 3.2**). There was a statistically significant increase in relative IFN-γ secretion over other groups, with the exception of gp100 + CpG-E2. While no significant differences between groups are observed at the 10 nM level, the CpG-gp-E2 formulation exhibited the highest levels of relative IFN-γ in 2 out 3 experiments.

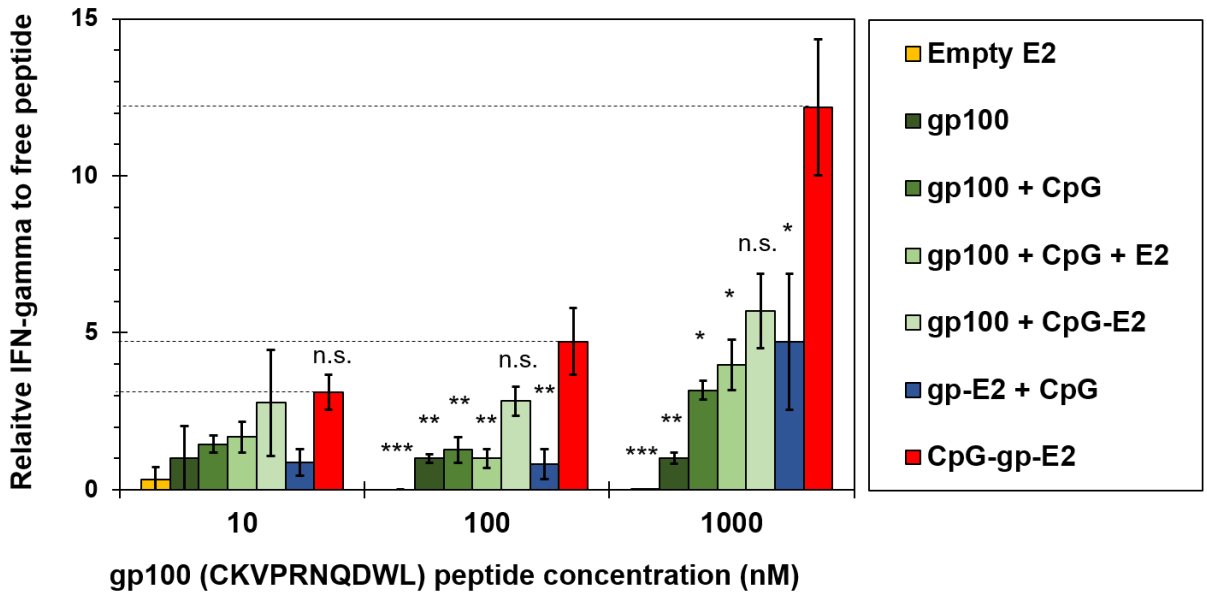

Figure 3.2. Pmel-1 CD8 T cells show enhanced IFN-γ secretion in the presence of BMDCs pulsed with CpG-gp-E2 nanoparticle compared to other formulations over 10, 100, and 1000 nM gp100 peptide. IFN-γ levels measured with ELISA were normalized to the free gp100 peptide formulation as baseline, and are presented as mean ± S.E.M. (n=3) and were analyzed using a one-way ANOVA followed by Tukey's test for post-hoc analysis comparing all means within each concentration (* $p < 0.05$; ** $p < 0.01$; *** $p < 0.001$).

Additionally, we observed a dose response of cytokine secretion, where increasing antigen concentrations correspond to increased IFN-γ levels. Interestingly, while increasing CpG-gp-E2 dose positively correlated with cytokine secretion (19 ± 11, 273 ± 74, and 10599 ± 3821 pg/mL for 10, 100, and 1000 nM $gp100_{25\text{-}33}$, respectively), the greatest relative increase of CpG-gp-E2 over the $gp100_{25\text{-}33}$ + CpG-E2 formulation was observed at the 100 nM concentration (**Figure 3.2**). This observation may be explained by the dynamics of the assay. Elevated unbound peptide concentrations in a closed environment may allow efficient epitope binding to empty surface MHC on the BMDCs, thereby creating a high avidity antigen display scenario without the necessity for internalization and processing, while simultaneously efficiently activating BMDCs with the CpG-E2 nanoparticle [35].

Our results indicate that the combination of peptide and CpG within a viral-mimicking E2 platform enhances the ability to induce antigen-specific IFN-γ secretion, a cytokine well known to support the effector functions of CTL. Naturally, virus-infected cells are known inducers of Type II interferon (*i.e.* IFN-γ) [45], and this is also critical for anti-cancer immunity and suppression [46]. In fact, IFN-γ was shown to play a key role in gp100-positive melanoma sensitization to the lytic activity of CTL [47]. Our ability to increase antigen-specific IFN-γ secretion may contribute to the superior functionality of the E2 nanoparticle as a viral-mimicking melanoma peptide vaccine platform.

The CpG-gp-E2 nanoparticle also facilitated increased C8 T cell proliferation, another indicator of T cell activation. We observed a significant increase in pmel-1 CD8 T cell proliferation over 72 hours for the CpG-gp-E2 formulation, compared to all other formulations at the 100 nM concentration level (**Figure 3.3**). The CTL population in all formulations expanded up to ~7 divisions; however the CpG-gp-E2 nanoparticle formulation induced a higher population of C8 T cell to divide multiple times, indicating a stronger proliferative response (**Figure 3.3A**). Consistent with the IFN-γ ELISA data, the largest relative difference between the CpG-gp-E2 formulation was observed at 100 nM $gp100_{25\text{-}33}$. In fact, 100 nM was the only concentration that showed statistically significant differences in relative proliferation index (PI) between groups. This supports the notion of antigen-specific CTL dysfunction and/or deletion at high antigen doses [48-50]. Our observation can be considered a positive result, as this would imply that a lower antigen dose would provide the highest benefit with regard to an antigen-specific immune response. Furthermore, the CpG-gp-E2 dose required for optimal activation appears to be lower than that of the free unbound components, a desirable attribute for potential clinical development.

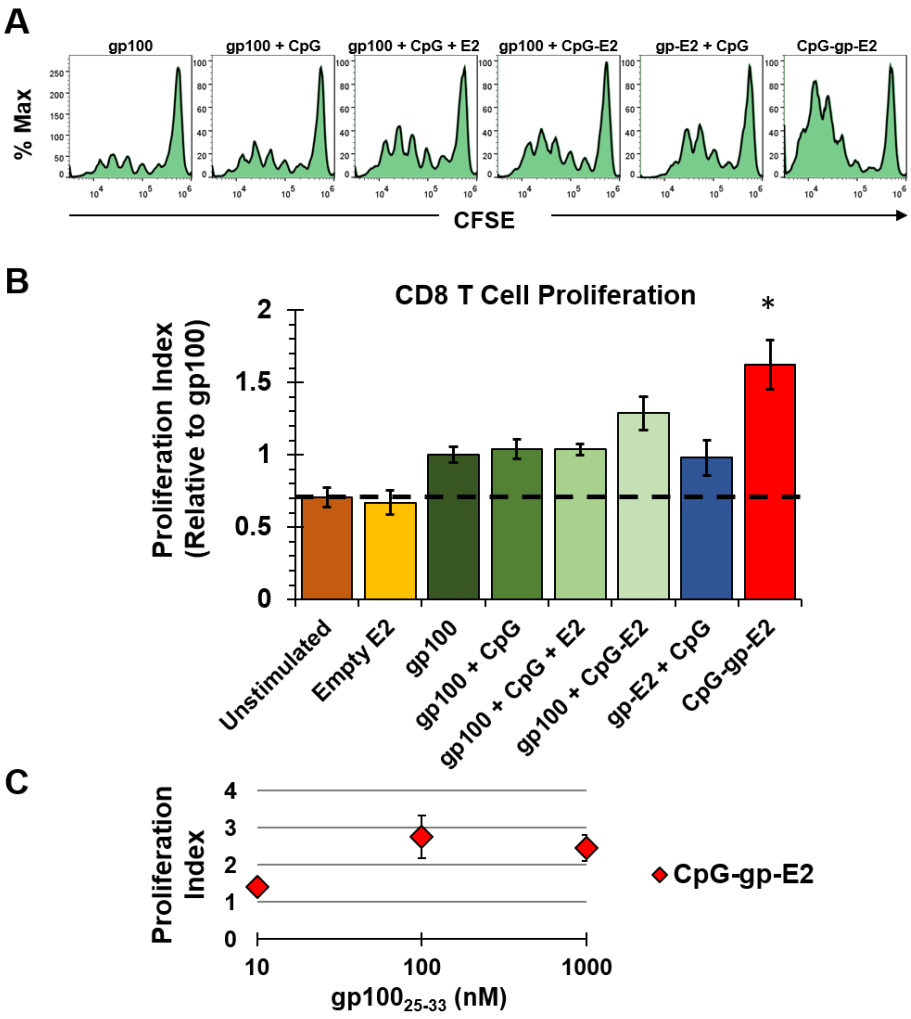

Figure 3.3. Pmel-1 CD8 T cells exhibit increase proliferative capacity over 72 hours when cultured in the presence of BMDCs pulsed with the CpG-gp-E2 nanoparticle, compared to other formulations of gp100$_{25-33}$, at the same peptide concentration. **(A)** Representative flow cytometry histograms of CFSE-labeled CD8 T cells show increased proliferation in the CpG-gp-E2 group, where each successive peak to the left of the rightmost peak (undivided cells) depicts a single cell division. **(B)** The CpG-gp-E2 platform induced the greatest CTL proliferative capacity over 72 hours, as measured by proliferation index (PI). CpG-gp-E2 was the only formulation to display statistically significant levels above unstimulated background. Data is presented as mean PI ± S.E.M., relative to the free gp100 peptide formulation. Data was analyzed with a one-way ANOVA followed by Tukey's test for post-hoc analysis, where * is $p < 0.05$, compared to unstimulated (no peptide) cells. **(C)** pmel-1 CD8 T cell in the presence of BMDC-pulsed CpG-gp-E2 nanoparticle display the greatest PI at the 100 nM concentration (data is mean ± S.E.M.).

Our IFN-γ and proliferation results are remarkably similar to those observed using a PLGA nanoparticle system simultaneously delivering the $gp100_{25\text{-}33}$ peptide with a TLR4 agonist [51]. While direct comparisons are difficult due to differences in particular assays used, this previous study reported similar relative IFN-γ levels to ours and also observed a decrease in CTL proliferative capacity at higher antigen doses in their nanoparticle formulation of peptide [51]. Additionally, the PLGA nanoparticle mentioned above was co-delivered with a passively encapsulated TLR4 (expressed on the outer cell membrane) agonist, relying on non-specific release in the extracellular environment, rather than endolysosome-triggered release. The differences between the CpG-gp-E2 nanoparticle and the PLGA system just discussed (*i.e.* endosomal vs. surface TLR ligand and passive release of activator vs. endosomal-triggered release) may have major implications *in vivo*.

3.3.3 E2 Delivery of CpG Increases Antigen Presenting Cell Numbers in Secondary Lymphoid Organs

Following immunization of wild-type mice with the different gp100 formulations, the nanoparticle containing the covalently packaged CpG (CpG-E2 and CpG-gp-E2 formulations) induced enlargement of the spleens and draining lymph nodes (dLN) (**Figure 3.4A**). This is an indication that either lymphocytes are actively proliferating in these organs, other cells are infiltrating these organs, or a combination of the two. Nanoparticle-mediated delivery of CpG was shown to effectively enter draining lymph nodes, where increases in dLN size and spleen size were observed over 1 week [52]. Enumeration of different cells within the draining lymph nodes and spleens of immunized mice revealed an increase in the number

antigen presenting cells (APCs), including DCs, macrophages (MΦ), and B cells, and also increased numbers of T cells (**Figure 3.4B**).

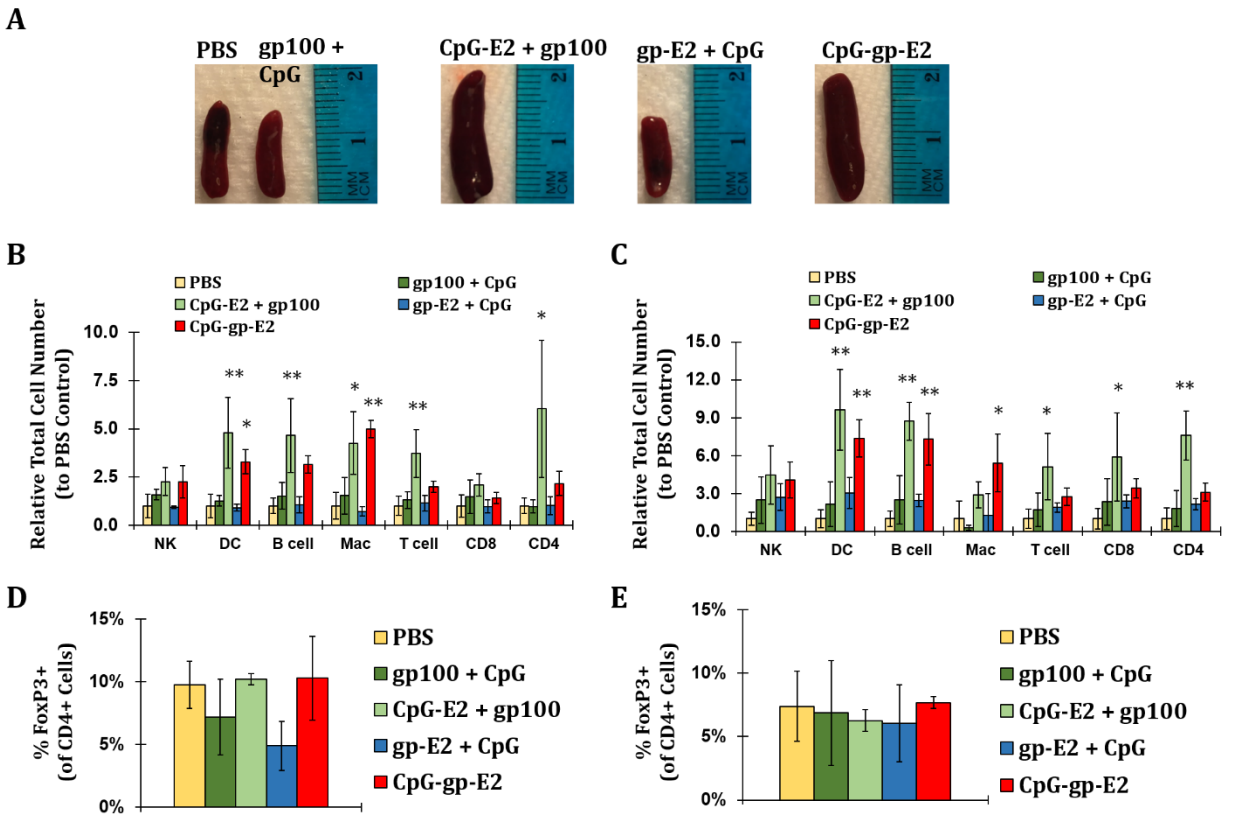

Figure 3.4. CpG-gp-E2 and CpG-E2 + gp100 exhibit increased secondary lymphoid organ size and increased numbers of antigen presenting cells and lymphocytes. **A)** Spleens from mice immunized with the different antigen formulations show increases sizes for the CpG-gp-E2 and CpG-E2 + gp100 formulation. Total cell numbers of different cells measured in the **B)** spleen and **C)** draining lymph nodes by flow cytometry of immunized animals and the frequency of FoxP3 expressing CD4 T cells **D)** spleen and **E)** lymph node. Data is presented as average ± S.D. total cell numbers relative to PBS control of at least 3 independent experiments. Statistical significance was determined by ANOVA followed by a post hoc Tukey's test. * $p < 0.05$; ** $p < 0.01$ compared to the PBS background control.

APCs showed the largest increase in relative numbers in both the dLN and spleen, compared to mice injected with PBS. It is known that CpG can induce proliferation of B cells in mice [53,54], and it is likely that E2 is allowing more efficient delivery of the CpG to these cells, compared to free CpG [52]. The increase in CD11c+ cells (primarily DCs) and F4/80+ cells (primarily MΦ) indicates an increase in recruitment or infiltration of these cells types to these organs. While F4/80 is considered a surface marker for MΦ, it is also known to be expressed on Langerhans cells, which are a subset of DCs present within the subcutaneous space [55]. Therefore, it is possible that the local Langerhans cells within the site of E2 administration are picking up the nanoparticles quite efficiently due to their size and virus-like nature [17], whereby activation signals from the endolysosomally-released CpG is initiating migration to the draining lymph nodes [56]. In any case, while lymphocytes such as B cells and T cells undergo rapid expansion in secondary lymphoid organs during the immune response, APCs such as DCs and MΦ are not currently known to expand at such rapid rates in these organs. It is possible that developing APCs are expanding for infiltration into these organs, since certain cytokine factors are known to cause large increases in systemic DC numbers [57,58]. Increased numbers of these potent APCs within the secondary lymphoid organs is a desirable effect, since these cells are responsible for the orchestration of the adaptive immune response [59,60].

Interestingly, only the free peptide administered with CpG-E2 demonstrated significant increases in CD4 T cells in the dLNs and all T cells within the spleen. This could be explained by a phenomenon known as homeostatic T cell proliferation, whereby particular cytokines (namely IL-7) support CD4 T cell expansion under non-antigen-stimulating conditions [61,62]. Epithelial, accessory cells, and some DCs of the lymphatics

express TLR9 and are also known to secrete IL-7, and therefore interaction of the CpG-E2 nanoparticle with these cell types may mediate the observed non-specific proliferative response [63-65]. Alternatively, the increased APC activation in the microenvironment due to delivery of CpG may allow activation of autoreactive CD4 T cells with normally low affinity for the self-antigens [61]. While the CpG-gp-E2 nanoparticle also delivers CpG in the same format as CpG-E2, there are an abundance of immunodominant CTL epitopes bound to CpG-gp-E2. The high affinity CTL epitopes on a virus-mimicking nanoparticle may mediate, *via* APCs, a cytokine environment less conducive to homeostatic CD4 T cell proliferation and more favorable for the activation of $CD8^+$ T cells [66]. CpG delivery to lymph nodes is known to induce high levels of type I interferons, important CTL development [67]. The apparent lack of elevated $CD8^+$ T cell number in the secondary lymphoid organs of mice immunized with CpG-gp-E2 is likely to due to the fact that antigen-specific CTL will exit these organs during the first week of viral infection, which we are closely mimicking [68]. Similarly, the elevated levels of $CD8^+$ T cells in the formulation containing CpG-E2 may be evident because these $CD8^+$ T cells are the result of non-antigen-specific proliferation, and are therefore not triggered to exit the secondary lymphoid organs [69].

The lower number of total T cells for CpG-gp-E2 nanoparticle compared to the free gp100 peptide + CpG-E2 nanoparticle formulation is not likely due to increases in regulatory T cells (Treg) (**Figure 3.4D** and **3.4E**). As noted, while both the CpG-gp-E2 and CpG-E2 nanoparticles show increased T cell numbers (including $CD8^+$), only CpG-E2 exhibits significant increases relative to mice immunized with PBS alone. One possible explanation, other than T cells exiting the lymph nodes, could be the induction of FoxP3+ CD4 T cells that have the potential to cause local immunological suppression [70,71]. However, we show that

after a single immunization, all of the antigen formulations shows similar frequency of FoxP3+ CD4 T cells, indicating that Treg induction is not occurring in this time frame or immunization regimen.

The T cells from the mice immunized with CpG-gp-E2 are likely not experiencing exhaustion (**Figure 3.5**). A marker of T cell exhaustion is the programmed death receptor 1 (PD-1) [72], which is upregulated in many aspects of the immunological control of lymphocytes [73,74]. However, relative PD-1 expression to PBS immunized mice did not exhibit any significant differences within the lymph nodes or spleen, comparing total cells, T cells, CD4 T cells, CD8+ T cells, or FoxP3+ CD4 T cells. While a low level, albeit not statistically significant, increase is observed for CD8+ T cells, particularly in the lymph nodes, it is expected that some level of PD-1 increase would occur transiently following immunization to control over immune response [75]. T cell deletion is a normal physiologic event that follows the rapid proliferation during viral infections [76], and therefore this observation is consistent with our mimicking of a virus infection with the CpG-gp-E2 nanoparticle.

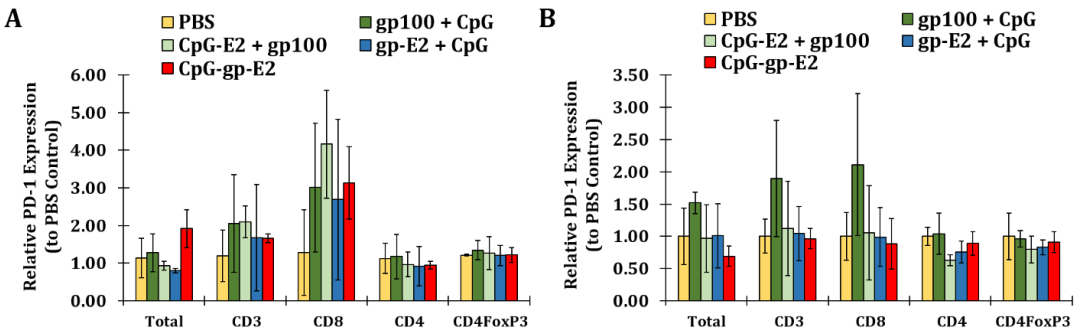

Figure 3.5. The nanoparticle formulations do not induce increased expression of PD-1. PD-1 expression was measured by flow cytometry in the **A)** lymph nodes and **B)** spleens of immunized animals. Data is presented as average ± S.D. total cell numbers relative to PBS control from at least 3 independent experiments. Statistical significance was determined by ANOVA followed by post hoc Tukey's test.

3.3.4 CpG-gp-E2 Immunization Shows Increased Tumor Antigen-Specific CTL

The CpG-gp-E2 formulation induces an increased frequency of gp100-specific CTL (**Figure 3.6**). IFN-γ ELISpot analysis of lymph node cells (**Figure 3.6A**) and splenocytes (**Figure 3.6B**) from mice receiving a single immunization of 5 μg of the $gp100_{25\text{-}33}$ peptide in the different formulations demonstrated a large increase in the number of gp100-specific spots for the CpG-gp-E2 viral-mimicking antigen formulation compared to all other formulations. While statistically significant differences are not measured in the lymph node under the spot frequency analysis reported in **Figure 3.6A**, when the data was compared relative to the negative control peptide (SIINFEKL; a further measure of specificity, rather than total spots), the CpG-gp-E2 formulation shows significant increases ($p < 0.05$), compared to the $gp100_{25\text{-}33}$ + free CpG and gp-E2 + free CpG formulations. We observed spot frequencies among total cells that were comparable to previously reported nanoparticle formulations delivering the $gp100_{25\text{-}33}$ epitope [77]. This previous study administered two booster immunization, whereas we observe the expansion of gp100-specific $CD8^+$ T cells following a single immunization. While multiple administrations may be necessary to achieve optimal anti-TAA effects, the requirement for less total vaccine formulation is a very desirable attribute, from a practical and physiological standpoint. Interestingly, the CpG-E2 nanoparticle formulated with free $gp100_{25\text{-}33}$ peptide induced the next highest frequency of TAA-specific CTL, with no statistically significant differences to the CpG-gp-E2 formulation within the lymph nodes. This implies that within the initial draining lymph nodes of the immunization site (*i.e.*, the local response), packaging CpG within the E2 nanoparticle already greatly enhances the CTL response toward peptide antigens, potentially through non-specific interactions with the peptide and/or enhanced or targeted adjuvanting effects

of CpG, which is a molecular adjuvant that is currently under clinical investigation in humans for cancer therapy [78]

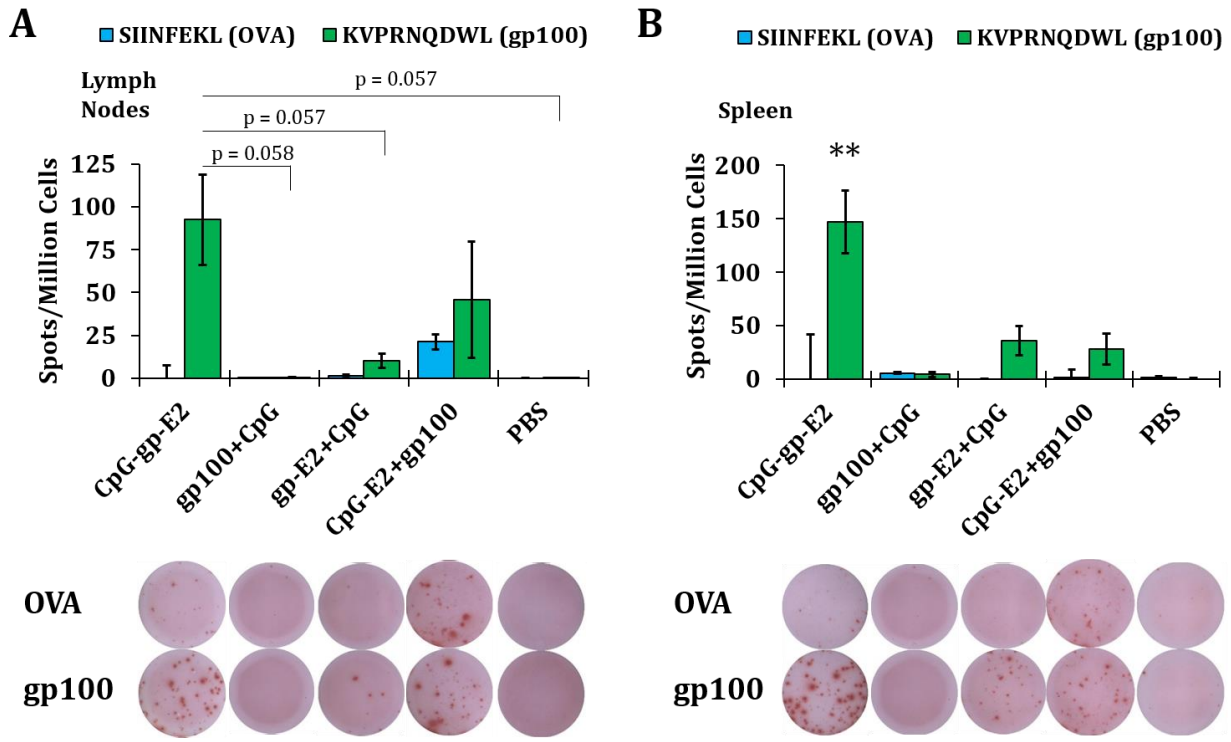

Figure 3.6. Immunization with CpG-gp-E2 results in increased gp100-specific CTL. Cells were cultured *ex vivo* from the **A)** lymph nodes and **B)** spleens of mice immunized with different formulations in the presence of KVPRNQDWL peptide (gp100) or irrelevant SIINFEKL peptide (OVA) and analyzed for IFN-γ secreting cells by ELISpot. The lower panels show representative wells from the immunization groups for negative control irrelevant peptide (OVA) and tumor antigen peptide (gp100). Data is presented as average ± S.E.M. spots per millions cells from at least 3 independent experiments. Statistical significance was determined by ANOVA followed by a post hoc Tukey's test. ** $p < 0.01$ compared to all other antigen formulations.

We also demonstrate spot frequencies similar to previous investigations using nanoparticle formulations for melanoma-specific TAAs (other than gp100), and which also demonstrated strong anti-tumor capacities of the induced CTL [51,79,80]. These studies also reported multiple administrations, whereas we have achieved our results from a single immunization. VLP delivery of CTL epitopes along with CpG demonstrated strong CTL responses against many MHC I-restricted epitopes [81], and these same particles are undergoing clinical trial for vaccination against melanomas in humans [32,33], demonstrating the power of viral mimicry in cancer immunotherapies. Remarkably, we have achieved this effect without the use of attenuated viruses and without the need for multiple administrations.

3.3.5 CpG-gp-E2 Immunized Mice Show Enhanced Melanoma Cell-Specific Lysis

CpG-containing E2 nanoparticles formulated with the $gp100_{25\text{-}33}$ epitope induce increased TAA-specific cytolytic ability (**Figure 3.7**). Splenocytes re-stimulated with the $gp100_{25\text{-}33}$ peptide for 72 hours were co-cultured with the gp100-positive B16-F10 metastatic melanoma cell line. Interestingly, even though the CpG-gp-E2 nanoparticle induced a significantly greater frequency of gp100-specific CTL (**Figure 3.6B**), compared to the CpG-E2 + $gp100_{25\text{-}33}$ formulation, splenocytes from the animals immunized with these two formulations demonstrated similar lytic capacities toward the B16-F10 melanoma line. In any case, this is consistent with our ELISpot (**Figure 3.6**) and *in vitro* pmel-1 assays (**Figure 3.2** and **Figure 3.3**) that demonstrate CpG-packaged within E2 exhibit increases antigen-specific CTL responses, compared to the other formulations. Importantly, with a

single immunization, we are able to achieve a specific lysis of the B16 melanoma cell line at levels comparable to that of immunization + booster using heat shock protein nanoparticles [77]. This observations further supports the notion that simultaneous spatial and temporal delivery of antigen and activator are important [82]. Optimization of immunization schedule and E2 amounts may yield even greater gp100-specific CTL frequencies with elevated lytic capacity, in a manner comparable to that seen with heat shock protein-based nanoparticles, where specific lysis increased with a third immunization, relative to 2 immunizations [77].

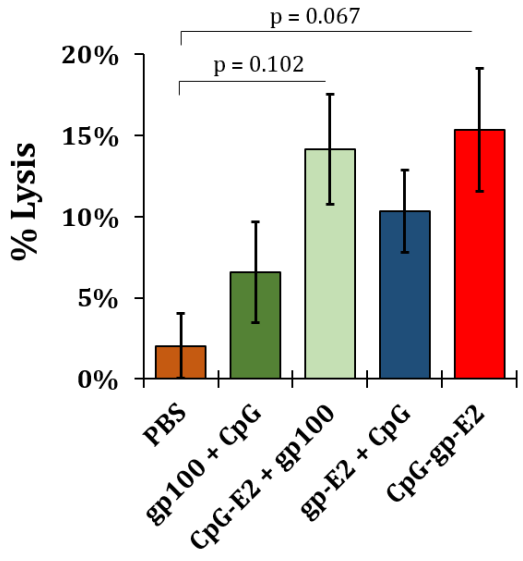

Figure 3.7. Splenocytes from mice immunized with CpG-gp-E2 and CpG-E2 + gp100 antigen formulations exhibit enhanced melanoma cell lytic ability *ex vivo*. Lysis was measured against the B16-F10 melanoma cell line by release of lactate dehydrogenase. Data is presented as average ± S.E.M. % lysis of 3 independent experiments. Statistical significance was determined by ANOVA followed by a post hoc Tukey's test.

Lysis of the gp100-expressing B16 cell line is an important observation, since this melanoma in particular is known to exhibit low immunogenicity and is difficult to mount effective immune responses against [44,83,84]. Additionally, gp100 is a self-antigen, and therefore the central tolerance to this antigen renders it even more difficult to induce a functional response, as the $gp100_{25\text{-}33}$-specific CTL that exist naturally in the animal would

presumably have a lower binding affinity for the epitope, compared to those antigens that are exogenous. With antigens such as this, the formulation of the antigen or the immunotherapeutic approach is particularly critical to the success of the anti-tumor response [84]. Even though immunogenicity may be lower for the gp100 overexpressed self-TAA, it is a known and demonstrated to be tumor regression antigen in humans, and therefore a therapeutically attractive TAA for targeting in a clinical setting [85].

3.4 Conclusions

We have successfully and simultaneously packaged CpG within the interior of the E2 nanoparticle and displayed multiple copies of the $gp100_{25\text{-}33}$ MHC I-restricted epitope on the surface of E2. These nanoparticles demonstrated superior *in vitro* $CD8^+$ T cell antigen-specific activation as measured by IFN-γ cytokine release and proliferation. The delivery of CpG within the E2 nanoparticle induces an increase in the number of DCs, MΦ, B cells, and T cells within the lymph nodes and spleen of immunized animals, without inducing increased $FoxP3^+$ CD4 T cell frequency or PD-1 expression. Further, we showed that the frequency of gp100-specifc $CD8^+$ T cells *in vivo* is increased for the CpG-gp-E2 nanoparticle formulation, supporting the hypothesis that simultaneous delivery of antigen and activator in a virus-mimicking format enhances cell-mediated anti-tumor antigen immunotherapies. The CTL from the immunized animals also show superior lytic capacity, compared to free peptide and free CpG administered together in unconjugated form. This demonstrates that the virus-mimicking E2 nanoparticle is an attractive immunotherapeutic platform for vaccination against tumor associated antigens.

3.5 References

1. Dunn GP, Bruce AT, Ikeda H, Old LJ, Schreiber RD: Cancer immunoediting: from immunosurveillance to tumor escape. *Nat Immunol* 2002, 3:991-998.
2. Schreiber RD, Old LJ, Smyth MJ: Cancer immunoediting: integrating immunity's roles in cancer suppression and promotion. *Science* 2011, 331:1565-1570.
3. Berzofsky JA, Terabe M, Oh S, Belyakov IM, Ahlers JD, Janik JE, Morris JC: Progress on new vaccine strategies for the immunotherapy and prevention of cancer. *J Clin Invest* 2004, 113:1515-1525.
4. Blattman JN, Greenberg PD: Cancer immunotherapy: a treatment for the masses. *Science* 2004, 305:200-205.
5. Ozols RF, Herbst RS, Colson YL, Gralow J, Bonner J, Curran WJ, Jr., Eisenberg BL, Ganz PA, Kramer BS, Kris MG, et al.: Clinical cancer advances 2006: major research advances in cancer treatment, prevention, and screening--a report from the American Society of Clinical Oncology. *J Clin Oncol* 2007, 25:146-162.
6. Klebanoff CA, Gattinoni L, Restifo NP: CD8+ T-cell memory in tumor immunology and immunotherapy. *Immunol Rev* 2006, 211:214-224.
7. Klebanoff CA, Gattinoni L, Torabi-Parizi P, Kerstann K, Cardones AR, Finkelstein SE, Palmer DC, Antony PA, Hwang ST, Rosenberg SA, et al.: Central memory self/tumor-reactive CD8+ T cells confer superior antitumor immunity compared with effector memory T cells. *Proc Natl Acad Sci U S A* 2005, 102:9571-9576.
8. Hariharan K, Braslawsky G, Black A, Raychaudhuri S, Hanna N: The Induction of Cytotoxic T-Cells and Tumor-Regression by Soluble-Antigen Formulation. *Cancer Research* 1995, 55:3486-3489.
9. Slingluff CL, Jr.: The present and future of peptide vaccines for cancer: single or multiple, long or short, alone or in combination? *Cancer J* 2011, 17:343-350.
10. Fadul CE, Fisher JL, Hampton TH, Lallana EC, Li Z, Gui J, Szczepiorkowski ZM, Tosteson TD, Rhodes CH, Wishart HA, et al.: Immune response in patients with newly diagnosed glioblastoma multiforme treated with intranodal autologous tumor lysate-dendritic cell vaccination after radiation chemotherapy. *J Immunother* 2011, 34:382-389.
11. Sondak VK, Sosman JA: Results of clinical trials with an allogenic melanoma tumor cell lysate vaccine: Melacine. *Semin Cancer Biol* 2003, 13:409-415.
12. Rosenberg SA, Restifo NP, Yang JC, Morgan RA, Dudley ME: Adoptive cell transfer: a clinical path to effective cancer immunotherapy. *Nat Rev Cancer* 2008, 8:299-308.
13. Kalos M, Levine BL, Porter DL, Katz S, Grupp SA, Bagg A, June CH: T Cells with Chimeric Antigen Receptors Have Potent Antitumor Effects and Can Establish Memory in Patients with Advanced Leukemia. *Science Translational Medicine* 2011, 3.
14. Porter DL, Levine BL, Kalos M, Bagg A, June CH: Chimeric antigen receptor-modified T cells in chronic lymphoid leukemia. *N Engl J Med* 2011, 365:725-733.
15. Arens R, van Hall T, van der Burg SH, Ossendorp F, Melief CJ: Prospects of combinatorial synthetic peptide vaccine-based immunotherapy against cancer. *Semin Immunol* 2013, 25:182-190.
16. Yamada A, Sasada T, Noguchi M, Itoh K: Next-generation peptide vaccines for advanced cancer. *Cancer Sci* 2013, 104:15-21.
17. Bachmann MF, Jennings GT: Vaccine delivery: a matter of size, geometry, kinetics and molecular patterns. *Nat Rev Immunol* 2010, 10:787-796.
18. Neundorf I, Rennert R, Franke J, Kozle I, Bergmann R: Detailed analysis concerning the biodistribution and metabolism of human calcitonin-derived cell-penetrating peptides. *Bioconjug Chem* 2008, 19:1596-1603.

19. Chong SF, Sexton A, De Rose R, Kent SJ, Zelikin AN, Caruso F: A paradigm for peptide vaccine delivery using viral epitopes encapsulated in degradable polymer hydrogel capsules. *Biomaterials* 2009, 30:5178-5186.
20. Wang F, Bade E, Kuniyoshi C, Spears L, Jeffery G, Marty V, Groshen S, Weber J: Phase I trial of a MART-1 peptide vaccine with incomplete Freund's adjuvant for resected high-risk melanoma. *Clin Cancer Res* 1999, 5:2756-2765.
21. Buyuktimkin B, Wang Q, Kiptoo P, Stewart JM, Berkland C, Siahaan TJ: Vaccine-like controlled-release delivery of an immunomodulating peptide to treat experimental autoimmune encephalomyelitis. *Mol Pharm* 2012, 9:979-985.
22. Foged C, Hansen J, Agger EM: License to kill: Formulation requirements for optimal priming of CD8(+) CTL responses with particulate vaccine delivery systems. *European Journal of Pharmaceutical Sciences* 2012, 45:482-491.
23. Aguilar JC, Rodriguez EG: Vaccine adjuvants revisited. *Vaccine* 2007, 25:3752-3762.
24. Fox CB, Kramer RM, Barnes VL, Dowling QM, Vedvick TS: Working together: interactions between vaccine antigens and adjuvants. *Ther Adv Vaccines* 2013, 1:7-20.
25. Reddy ST, van der Vlies AJ, Simeoni E, Angeli V, Randolph GJ, O'Neil CP, Lee LK, Swartz MA, Hubbell JA: Exploiting lymphatic transport and complement activation in nanoparticle vaccines. *Nat Biotechnol* 2007, 25:1159-1164.
26. Manolova V, Flace A, Bauer M, Schwarz K, Saudan P, Bachmann MF: Nanoparticles target distinct dendritic cell populations according to their size. *Eur J Immunol* 2008, 38:1404-1413.
27. Krishnamachari Y, Geary SM, Lemke CD, Salem AK: Nanoparticle delivery systems in cancer vaccines. *Pharm Res* 2011, 28:215-236.
28. Plummer EM, Manchester M: Viral nanoparticles and virus-like particles: platforms for contemporary vaccine design. *Wiley Interdisciplinary Reviews-Nanomedicine and Nanobiotechnology* 2011, 3:174-196.
29. Douglas T, Young M: Viruses: Making friends with old foes. *Science* 2006, 312:873-875.
30. Uematsu S, Akira S: Toll-Like receptors (TLRs) and their ligands. *Handb Exp Pharmacol* 2008:1-20.
31. Kay E, Scotland RS, Whiteford JR: Toll-like receptors: Role in inflammation and therapeutic potential. *Biofactors* 2014, 40:284-294.
32. Speiser DE, Schwarz K, Baumgaertner P, Manolova V, Devevre E, Sterry W, Walden P, Zippelius A, Conzett KB, Senti G, et al.: Memory and effector CD8 T-cell responses after nanoparticle vaccination of melanoma patients. *J Immunother* 2010, 33:848-858.
33. Goldinger SM, Dummer R, Baumgaertner P, Mihic-Probst D, Schwarz K, Hammann-Haenni A, Willers J, Geldhof C, Prior JO, Kundig TM, et al.: Nano-particle vaccination combined with TLR-7 and -9 ligands triggers memory and effector CD8(+) T-cell responses in melanoma patients. *Eur J Immunol* 2012, 42:3049-3061.
34. Grgacic EV, Anderson DA: Virus-like particles: passport to immune recognition. *Methods* 2006, 40:60-65.
35. Molino NM, Anderson AK, Nelson EL, Wang SW: Biomimetic protein nanoparticles facilitate enhanced dendritic cell activation and cross-presentation. *ACS Nano* 2013, 7:9743-9752.
36. Barrow C, Browning J, MacGregor D, Davis ID, Sturrock S, Jungbluth AA, Cebon J: Tumor antigen expression in melanoma varies according to antigen and stage. *Clin Cancer Res* 2006, 12:764-771.
37. Finkelstein SE, Heimann DM, Klebanoff CA, Antony PA, Gattinoni L, Hinrichs CS, Hwang LN, Palmer DC, Spiess PJ, Surman DR, et al.: Bedside to bench and back again: how animal models are guiding the development of new immunotherapies for cancer. *Journal of Leukocyte Biology* 2004, 76:333-337.

38. Overwijk WW, Theoret MR, Finkelstein SE, Surman DR, de Jong LA, Vyth-Dreese FA, Dellemijn TA, Antony PA, Spiess PJ, Palmer DC, et al.: Tumor regression and autoimmunity after reversal of a functionally tolerant state of self-reactive CD8+ T cells. *J Exp Med* 2003, 198:569-580.
39. Dalmau M, Lim S, Chen HC, Ruiz C, Wang SW: Thermostability and molecular encapsulation within an engineered caged protein scaffold. *Biotechnol Bioeng* 2008, 101:654-664.
40. Aida Y, Pabst MJ: Removal of endotoxin from protein solutions by phase separation using Triton X-114. *J Immunol Methods* 1990, 132:191-195.
41. Lutz MB, Kukutsch N, Ogilvie AL, Rossner S, Koch F, Romani N, Schuler G: An advanced culture method for generating large quantities of highly pure dendritic cells from mouse bone marrow. *J Immunol Methods* 1999, 223:77-92.
42. Roederer M: Interpretation of cellular proliferation data: avoid the panglossian. *Cytometry A* 2011, 79:95-101.
43. Di Pucchio T, Pilla L, Capone I, Ferrantini M, Montefiore E, Urbani F, Patuzzo R, Pennacchioli E, Santinami M, Cova A, et al.: Immunization of stage IV melanoma patients with Melan-A/MART-1 and gp100 peptides plus IFN-alpha results in the activation of specific CD8(+) T cells and monocyte/dendritic cell precursors. *Cancer Res* 2006, 66:4943-4951.
44. Overwijk WW, Tsung A, Irvine KR, Parkhurst MR, Goletz TJ, Tsung K, Carroll MW, Liu CL, Moss B, Rosenberg SA, et al.: gp100/pmel 17 is a murine tumor rejection antigen: Induction of "self"-reactive, tumoricidal T cells using high-affinity, altered peptide ligand. *Journal of Experimental Medicine* 1998, 188:277-286.
45. Goodbourn S, Didcock L, Randall RE: Interferons: cell signalling, immune modulation, antiviral response and virus countermeasures. *J Gen Virol* 2000, 81:2341-2364.
46. Dunn GP, Koebel CM, Schreiber RD: Interferons, immunity and cancer immunoediting. *Nat Rev Immunol* 2006, 6:836-848.
47. Bohm W, Thoma S, Leithauser F, Moller P, Schirmbeck R, Reimann J: T cell-mediated, IFN-gamma-facilitated rejection of murine B16 melanomas. *J Immunol* 1998, 161:897-908.
48. AlexanderMiller MA, Leggatt GR, Sarin A, Berzofsky JA: Role of antigen, CD8, and cytotoxic T lymphocyte (CTL) avidity in high dose antigen induction of apoptosis of effector CTL. *Journal of Experimental Medicine* 1996, 184:485-492.
49. Busch DH, Pamer EG: MHC class I peptide stability: Implications for immunodominance, in vitro proliferation, and diversity of responding CTL. *Journal of Immunology* 1998, 160:4441-4448.
50. Critchfield JM, Racke MK, Zunigapflucker JC, Cannella B, Raine CS, Goverman J, Lenardo MJ: T-Cell Deletion in High Antigen Dose Therapy of Autoimmune Encephalomyelitis. *Science* 1994, 263:1139-1143.
51. Zhang Z, Tongchusak S, Mizukami Y, Kang YJ, Ioji T, Touma M, Reinhold B, Keskin DB, Reinherz EL, Sasada T: Induction of anti-tumor cytotoxic T cell responses through PLGA-nanoparticle mediated antigen delivery. *Biomaterials* 2011, 32:3666-3678.
52. Bourquin C, Anz D, Zwiorek K, Lanz AL, Fuchs S, Weigel S, Wurzenberger C, von der Borch P, Golic M, Moder S, et al.: Targeting CpG oligonucleotides to the lymph node by nanoparticles elicits efficient antitumoral immunity. *J Immunol* 2008, 181:2990-2998.
53. Jiang W, Lederman MM, Harding CV, Rodriguez B, Mohner RJ, Sieg SF: TLR9 stimulation drives naive B cells to proliferate and to attain enhanced antigen presenting function. *Eur J Immunol* 2007, 37:2205-2213.
54. Kim YH, Lee SH, Yoo YC, Lee J, Park JH, Park SR: Kinetic Analysis of CpG-Induced Mouse B Cell Growth and Ig Production. *Immune Netw* 2012, 12:89-95.
55. Hume DA, Robinson AP, MacPherson GG, Gordon S: The mononuclear phagocyte system of the mouse defined by immunohistochemical localization of antigen F4/80. Relationship between macrophages, Langerhans cells, reticular cells, and dendritic cells in lymphoid and hematopoietic organs. *J Exp Med* 1983, 158:1522-1536.

56. Najar HM, Dutz JP: Topical TLR9 agonists induce more efficient cross-presentation of injected protein antigen than parenteral TLR9 agonists do. *Eur J Immunol* 2007, 37:2242-2256.
57. Edukulla R, Woller N, Mundt B, Knocke S, Gurlevik E, Saborowski M, Malek N, Manns MP, Wirth T, Kuhnel F, et al.: Antitumoral immune response by recruitment and expansion of dendritic cells in tumors infected with telomerase-dependent oncolytic viruses. *Cancer Res* 2009, 69:1448-1458.
58. Maraskovsky E, Brasel K, Teepe M, Roux ER, Lyman SD, Shortman K, McKenna HJ: Dramatic increase in the numbers of functionally mature dendritic cells in Flt3 ligand-treated mice: multiple dendritic cell subpopulations identified. *J Exp Med* 1996, 184:1953-1962.
59. Steinman RM: Dendritic cells and the control of immunity: enhancing the efficiency of antigen presentation. *Mt Sinai J Med* 2001, 68:160-166.
60. Hume DA: Macrophages as APC and the dendritic cell myth. *J Immunol* 2008, 181:5829-5835.
61. Min B, Yamane H, Hu-Li J, Paul WE: Spontaneous and homeostatic proliferation of CD4 T cells are regulated by different mechanisms. *J Immunol* 2005, 174:6039-6044.
62. Tan JT, Dudl E, LeRoy E, Murray R, Sprent J, Weinberg KI, Surh CD: IL-7 is critical for homeostatic proliferation and survival of naive T cells. *Proc Natl Acad Sci U S A* 2001, 98:8732-8737.
63. El Kebir D, Jozsef L, Pan W, Wang L, Filep JG: Bacterial DNA activates endothelial cells and promotes neutrophil adherence through TLR9 signaling. *J Immunol* 2009, 182:4386-4394.
64. Hara T, Shitara S, Imai K, Miyachi H, Kitano S, Yao H, Tani-ichi S, Ikuta K: Identification of IL-7-producing cells in primary and secondary lymphoid organs using IL-7-GFP knock-in mice. *J Immunol* 2012, 189:1577-1584.
65. Kroncke R, Loppnow H, Flad HD, Gerdes J: Human follicular dendritic cells and vascular cells produce interleukin-7: a potential role for interleukin-7 in the germinal center reaction. *Eur J Immunol* 1996, 26:2541-2544.
66. Kolumam GA, Thomas S, Thompson LJ, Sprent J, Murali-Krishna K: Type I interferons act directly on CD8 T cells to allow clonal expansion and memory formation in response to viral infection. *J Exp Med* 2005, 202:637-650.
67. Sun S, Zhang X, Tough DF, Sprent J: Type I interferon-mediated stimulation of T cells by CpG DNA. *J Exp Med* 1998, 188:2335-2342.
68. Lawrence CW, Braciale TJ: Activation, differentiation, and migration of naive virus-specific CD8+ T cells during pulmonary influenza virus infection. *J Immunol* 2004, 173:1209-1218.
69. Tough DF, Borrow P, Sprent J: Induction of bystander T cell proliferation by viruses and type I interferon in vivo. *Science* 1996, 272:1947-1950.
70. Liston A, Gray DH: Homeostatic control of regulatory T cell diversity. *Nat Rev Immunol* 2014, 14:154-165.
71. Josefowicz SZ, Lu LF, Rudensky AY: Regulatory T cells: mechanisms of differentiation and function. *Annu Rev Immunol* 2012, 30:531-564.
72. Wherry EJ, Ha SJ, Kaech SM, Haining WN, Sarkar S, Kalia V, Subramaniam S, Blattman JN, Barber DL, Ahmed R: Molecular signature of CD8+ T cell exhaustion during chronic viral infection. *Immunity* 2007, 27:670-684.
73. Thibult ML, Mamessier E, Gertner-Dardenne J, Pastor S, Just-Landi S, Xerri L, Chetaille B, Olive D: PD-1 is a novel regulator of human B-cell activation. *Int Immunol* 2013, 25:129-137.
74. Jin HT, Ahmed R, Okazaki T: Role of PD-1 in regulating T-cell immunity. *Curr Top Microbiol Immunol* 2011, 350:17-37.
75. Fife BT, Bluestone JA: Control of peripheral T-cell tolerance and autoimmunity via the CTLA-4 and PD-1 pathways. *Immunol Rev* 2008, 224:166-182.
76. Schlub TE, Sun JC, Walton SM, Robbins SH, Pinto AK, Munks MW, Hill AB, Brossay L, Oxenius A, Davenport MP: Comparing the kinetics of NK cells, CD4, and CD8 T cells in murine cytomegalovirus infection. *J Immunol* 2011, 187:1385-1392.

77. Wang XY, Chen X, Manjili MH, Repasky E, Henderson R, Subjeck JR: Targeted immunotherapy using reconstituted chaperone complexes of heat shock protein 110 and melanoma-associated antigen gp100. *Cancer Res* 2003, 63:2553-2560.
78. Dorn A, Kippenberger S: Clinical application of CpG-, non-CpG-, and antisense oligodeoxynucleotides as immunomodulators. *Curr Opin Mol Ther* 2008, 10:10-20.
79. Hamdy S, Molavi O, Ma Z, Haddadi A, Alshamsan A, Gobti Z, Elhasi S, Samuel J, Lavasanifar A: Co-delivery of cancer-associated antigen and Toll-like receptor 4 ligand in PLGA nanoparticles induces potent CD8+ T cell-mediated anti-tumor immunity. *Vaccine* 2008, 26:5046-5057.
80. Xu Z, Ramishetti S, Tseng YC, Guo S, Wang Y, Huang L: Multifunctional nanoparticles co-delivering Trp2 peptide and CpG adjuvant induce potent cytotoxic T-lymphocyte response against melanoma and its lung metastasis. *J Control Release* 2013, 172:259-265.
81. Storni T, Ruedl C, Schwarz K, Schwendener RA, Renner WA, Bachmann MF: Nonmethylated CG motifs packaged into virus-like particles induce protective cytotoxic T cell responses in the absence of systemic side effects. *J Immunol* 2004, 172:1777-1785.
82. Nierkens S, den Brok MH, Sutmuller RPM, Grauer OM, Bennink E, Morgan ME, Figdor CG, Ruers TJM, Adema GJ: In vivo colocalization of antigen and cytidyl guanosyl within dendritic cells is associated with the efficacy of cancer immunotherapy. *Cancer Research* 2008, 68:5390-5396.
83. Zoller M: IFN-treatment of B16-F1 versus B16-F10: relative impact on non-adaptive and T-cell-mediated immune defense in metastatic spread. *Clin Exp Metastasis* 1988, 6:411-429.
84. Finkelstein SE, Heimann DM, Klebanoff CA, Antony PA, Gattinoni L, Hinrichs CS, Hwang LN, Palmer DC, Spiess PJ, Surman DR, et al.: Bedside to bench and back again: how animal models are guiding the development of new immunotherapies for cancer. *J Leukoc Biol* 2004, 76:333-337.
85. Kirkin AF, Dzhandzhugazyan K, Zeuthen J: The immunogenic properties of melanoma-associated antigens recognized by cytotoxic T lymphocytes. *Exp Clin Immunogenet* 1998, 15:19-32.

CHAPTER 4

Complement Activation and Cell Uptake Responses toward Polymer-Functionalized Protein Nanocapsules

Portions of this chapter have been slightly modified and published as: Molino NM, Bilotkach K, Fraser DA, Ren D, Wang SW: Cell Uptake and Complement Responses Toward Polymer-Functionalized Protein Nanocapsules. *Biomacromolecules* 2012, 13:974–981.

4.1 Background

The use of conventional nanoparticulates such as liposomes, polymers, or gold nanoparticles for bionanotechnology applications, including imaging, therapeutics, biosensing, catalysis, and diagnostics, has been increasingly reported [1,2]. Although these particles have been extensively investigated, many issues still exist which raise concern for therapeutic and biomedical applications, including toxicity, physical stability, and heterogeneity [3,4].

More recently, recombinant protein-based nanoparticles are being explored as alternatives for such applications [3,5-8]. One major advantage of protein nanoparticles over conventional polymeric or inorganic particles is the ability to manipulate precisely their architecture, size, surface functionality, and assembly using recombinant tools and protein engineering. Furthermore, due to their highly organized structure, these systems provide monodisperse capsules that can be engineered at their internal, external, or intersubunit interfaces at specific locations, allowing for high control over surface properties [9]. Protein-based particles have included virus-like particles (e.g. Cowpea mosaic virus, adenovirus) [10-12], and particles of non-viral origin (e.g. ferritin cages, heat shock protein) [3].

However, applicability of these protein complex systems for certain purposes may be affected by the biological responses towards them. For example, particles of viral origin may be particularly prone to immunological recognition and clearance. Attachment of polyethylene glycol (PEG) to nanoparticles has been proposed as enabling evasion by phagocytic immune cells and reducing blood plasma protein (e.g. complement proteins) adsorption [13-16]. While studies of cellular immune responses to PEGylated virus-like

particles are well-documented [12,17], information on humoral innate immune responses to such particles is less prevalent.

In this work, we created a modified protein nanoparticle scaffold with general applicability for site-directed surface attachment of different classes of molecules, and we examined cellular uptake and complement responses. The model protein is the dihydrolipoyl acyltransferase enzyme (E2 subunit) of the pyruvate dehydrogenase multienzyme complex. Prior work has shown that this assembly of enzymes can be distilled down to its structural core scaffold (E2-WT) to yield a 24-nm protein nanocapsule composed of 60 identical self-assembling subunits that maintains its structural integrity over a wide range of temperatures and pH values [18-21]. In its folded state, the internal hollow cavity of the E2 particle is accessible by small molecules through its openings at the 5-fold axes of symmetry. Redesigning the internal surface enables encapsulation of fluorescent dyes and small molecule drugs, with applicability toward drug delivery [18,22]. Inter-subunit interactions can also be re-engineered to introduce environmentally-triggered behavior not observed in the native scaffold [23,24]. The E2 scaffold is of non-viral origin, and therefore does not possess any infectious ability in its native wild-type state, which may render it less immunogenic than virus-like particles. Even so, attaching short peptides to the N-terminus via recombinant methods enables surface display of antigens for vaccine development [5,25,26]. In this latter case of surface functionalization, the recombinant approach requires extensive DNA manipulation for each different antigen and is not applicable for larger proteins or non-protein based moieties (e.g., synthetic polymers or carbohydrates).

Our investigation examined uptake of this protein scaffold before and after PEGylation by primary human macrophages and by a human breast cancer cell line. We also

investigated the capacity of E2-WT and surface-modified E2 nanocapsules to activate human serum complement proteins *in vitro*, by assaying for C4 consumption (an early marker in the classical/lectin pathway) and generation of the cleavage fragment, C5a. C5a is an anaphylatoxin released following complement activation via the alternative, classical, or lectin pathways, and is therefore a good indicator of complement terminal pathway activation and inflammation. Complement activation can set the course for subsequent adaptive immunological responses, and such responses to PEGylated icosahedral protein nanoparticles of non-viral origin have not yet to our knowledge been reported. Performing these immune assays with the wild-type and PEGylated E2 particle will allow us to determine *in vitro* whether any changes in uptake and complement activation are provoked. This characterization will help determine general applicability of the E2 particle for future bionanotechnological applications.

4.2 Methods

4.2.1 Materials

All buffer reagents were supplied by EMD Chemicals (Gibbstown, NJ), unless otherwise stated. Dithiothreitol (DTT), isopropyl β-D-thiogalactopyranoside (IPTG), dimethylsulfoxide (DMSO), and potassium phosphate were supplied by Fisher Scientific (Pittsburgh, PA). Phenylmethylsulfonyl fluoride (PMSF) and tris(2-carboxyethyl)-phosphine hydrochloride (TCEP) were supplied by Pierce (Rockford, IL), and sodium azide was from Merck KGaA (Gibbstown, NJ). Restriction endonucleases (BamHI, NdeI), T4 DNA ligase, RNase, DNase, and DpnI were from New England Biolabs (Ipswitch, MA) and *PfuUltra*

High-Fidelity DNA polymerase was from Stratagene (Gibbstown, NJ). Dye molecules Alexa Fluor 532 C_5-maleimide (AF532) and Alexa Fluor 488 succinimidyl ester (AF488) were purchased from Invitrogen (Carlsbad, CA). Polyethylene glycol (PEG) reagents used were methyl-PEG_{24}-maleimide (PEG1200-maleimide, Pierce), methyl-PEG-maleimide with PEG range of 1800-2200 Da (PEG2000-maleimide, Nanocs, New York, NY), and methyl-PEG-maleimide with PEG range of 4500-5500 Da (PEG5000-maleimide, Nanocs). Host *E. coli* strains were DH5α (Zymo Research, Orange, CA) and BL21(DE3) (Stratagene, La Jolla, CA). Normal human serum (NHS) was isolated from whole blood and complement activity was confirmed in standard hemolytic assays (data not shown). The MicroVue C5a EIA kit was purchased from Quidel (San Diego, CA).

4.2.2 Design and Construction of Surface Cysteine Mutants

To enable chemical attachment of non-native molecules to the surface of the protein nanocapsules, we selected several potential external sites to perform site-directed mutagenesis to cysteine. The thiol side chain of cysteine is advantageous because it enables chemical conjugation at specific sites constructed via protein engineering. Although the E2-WT subunit has one native cysteine, crystallographic structure and our prior investigations [18] demonstrated that this native site is buried within the protein and not accessible for chemical conjugation. Selection criteria included external surface accessibility while retaining interactions likely to preserve the protein's 60-mer structure and stability [20]. Other criteria included locations in loop regions to minimize disruption to secondary structure (alpha-helices, beta strands), and avoidance of the N-terminus and inter-subunit interface interactions [20,23,24,27]. To retain molecular accessibility into the interior

hollow cavity, we also favored positions that did not occlude the native 5-nm entrances to this cavity. Selection was performed using the quaternary protein structure 1b5s (Protein Data Bank) viewed through PyMOL [28]. Based on these criteria, a set of five sites were selected for mutagenesis to cysteine: threonine 219 (T219C), aspartic acid 278 (D278C), glutamic acid 279 (E279C), threonine 334 (T334C), and methionine 338 (M338C).

The starting DNA template encodes the wild-type E2 scaffold (E2-WT) in a pGEM vector and includes amino acids 174-427, as described previously [18]. To perform site-directed mutagenesis, we cloned the E2-WT gene into pGEM-3Z (Promega) and followed a modified version of the Stratagene QuickChange protocol. The starting DNA template encodes the wild-type E2 scaffold (E2-WT) in a pGEM vector and includes amino acids 174-427, as described previously [1]. We used oligonucleotides with the sequence listed in **Table 4.1** as the primers for mutagenesis. Sequences listed in Table S-1 are forward oligonucleotides; the reverse sequences used are complementary to the forward primers listed here. Gene sequences of the mutants were confirmed by DNA sequencing and cloned into the expression vector pET-11a. Plasmids were transformed into *E. coli* strain BL21(DE3) for protein expression. The resulting clones were screened and sequenced, and the mutated E2 genes were ligated into the expression vector pET-11a at the *Nde*I and *Bam*HI sites.

Mutant	Oligonucleotide sequences
T219C	5'– GCC ATG GTT CAC TCT AAA CAC **TGC** GCG CCA CAC GTT ACC CTG ATG – 3'
E279C	5'– CTG AAC ACC TCT ATT GAC GAC **TGC** ACC GAA GAA ATC ATC CAG – 3'
D278C	5'– GTT CTG AAC ACC TCT ATT GAC **TGC** GAG ACC GAA GAA ATC ATC CAG – 3'
T334C	5'– GCT CGT GAC GGT AAA CTG **TGC** CCT GGT GAA ATG AAA GGC – 3'
M338C	5'– C GGT AAA CTG ACT CCT GGT GAA **TGC** AAA GGC GCG TCT TGC – 3'

Table 4.1. Sequences of forward oligonucleotides used for mutagenesis. Codons in bold denote mutated sites.

4.2.3 Protein Expression and Purification

Protein expression was performed following previously-reported protocol [18]. In summary, cells were grown in Luria-Bertani (LB) media containing 100 μg/ml ampicillin and induced at OD_{600} 0.7-0.9 with 1 mM IPTG at 37 °C for 3.5 hours. For scale-up, purification, and analysis, we selected one of the mutants (E279C) based on criteria described in Results and Discussion. Purification was performed as previously described[18] and included using a Q-Sepharose anion exchange column and a Superose 6 size exclusion column (GE Healthcare), with the exception that 1 mM DTT was added to all of the lysis, purification, and storage buffers to prevent cross-linking of protein nanocapsules in solution. Proteins were stored at 4 °C for short-term or -80 °C for long-term storage in 50 mM potassium phosphate (pH 7.4) and 100 mM NaCl (herein referred to as "phosphate buffer") containing 0.02 % sodium azide, 1 mM DTT, and 5 mM EDTA. Protein concentrations were quantified using a Micro-BCA kit (Pierce).

4.2.4 Confirmation of Structural Assembly and Thermostability

Stability and structural analyses of the protein nanocapsules were carried out as previously described [18]. Briefly, secondary protein folding was characterized with far-UV circular dichroism (CD) on a Jasco 810 spectropolarimeter (Jasco, Easton, MD). The thermostability of the five mutants was screened by heating the soluble fractions of freshly lysed cells to elevated temperatures ranging between 37 – 95 °C, followed by centrifugation to remove insoluble proteins. Thermostabilities of the purified E279C mutant were quantified by measuring molar ellipticity at 222 nm from 40 °C to 95 °C. The onset of unfolding (T_o) and midpoint of unfolding (T_m) temperatures were determined using a nonlinear least squares fitting program in MATLAB according to the method by Greenfield [29]. Protein molecular weights were confirmed via electrospray ionization mass spectrometry (ESI-MS, Micromass LCT Premier Mass Spectrometer, Waters) using E2-WT and fluorotriazines as standards for calibration. Particle size was determined using dynamic light scattering (DLS) with a Zetasizer Nano ZS instrument (Malvern, Westborough, MA). Because the E2 assembly comprises 60 identical subunits which are associated by non-covalent interactions, ESI-MS data yields the molecular weight of a single subunit while the milder conditions of DLS measure the size of the particle in solution. Molecular weight (ESI-MS), T_m, T_o, and particle size are presented as an average ± standard deviation of three separately prepared samples. Transmission electron microscopy (TEM, Philips CM20) was performed on protein samples stained with 2% uranyl acetate on carbon-coated Formvar grids.

4.2.5 Functionalization with Polyethylene Glycol (PEG) and Dye Molecules

Stock PEG1200-maleimide, PEG2000-maleimide and PEG5000-maleimide solutions were prepared in DMSO under argon gas, stored dessicated at -20 °C, and brought to room temperature immediately before use. Purified E279C protein was incubated with 8.5 molar excess of TCEP for 40 minutes at room temperature, and PEG-maleimide was added to E279C (1 mg/ml) at a 20-fold molar excess with respect to the E2 subunit and reacted for 2 hours at room temperature with agitation. DTT, TCEP, and excess PEG-maleimide were removed with Zeba desalting columns (40 kDa MWCO, Pierce) using phosphate buffer as the exchange solution. Protocols for attaching dye molecules are described in Supporting Information. AlexaFluor 532 C5-maleimide (AF532M) was conjugated to Cys, and AlexaFluor 488 succinimidyl ester (AF488) reacted with primary amines (lysines) on the protein nanocapsule. The resulting PEG- and dye-conjugated particles were analyzed as described above.

4.2.6 Functionalization with Dye Molecules

Reactivity of the engineered Cys thiols with small molecules was quantified by conjugating AlexaFluor 532 C5-maleimide (AF532M) to the surface-accessible side chains. Conjugation and analysis was performed according to protocol presented in Dalmau et al.[1]. Purified E279C (1.4 mg/ml) and E2-WT (1.3 mg/ml) were reduced with 8.5 molar excess of TCEP and reacted with AF532M at a 3:1 (dye:protein subunit) molar ratio. Unreacted dye was removed using drop dialysis ("V" series membrane, Millipore).

To label primary amines, proteins in phosphate buffer were reacted with AlexaFluor 488 succinimidyl ester (AF488) at a 3:1 and 4:1 (dye:protein subunit) for E2-WT and PEG-

conjugated E279C, respectively. These ratios were chosen to yield an equimolar conjugation ratio of dye-to-subunit, enabling direct comparison in subsequent uptake assays. Samples were agitated in the dark at room temperature for 1.5 hours. Excess dye was removed using desalting columns (Zeba, 40 kDa MWCO), with phosphate buffer as the exchange solution. Dye conjugation was quantified by measuring absorbance at 495 nm and calibrated with a standard curve. Protein concentration was determined using micro-BCA, allowing for dye:protein subunit ratio quantification (average ± standard deviation for at least 3 batches).

4.2.7 Cellular Uptake by Macrophages and Breast Cancer Cells

All blood samples were collected in accordance with the guidelines and approval of the University of California Irvine Institutional Review Board. Human monocyte derived macrophages (HMDM) were derived from human peripheral blood monocytes as previously described[30] and MDA-MB-231 breast cancer cells (ATCC, Manassas, VA) were cultured as described previously [22]. HMDM (harvested using Versene-EDTA) were resuspended at 1×10^6 cells/ml in phagocytosis buffer (RPMI 1640, 25 mM HEPES, 5 mM $MgCl_2$). MDA-MB-231 cells were plated at 2×10^5 cells/well in Dulbecco's Modified Eagle's Medium supplemented with 10 % fetal bovine serum and 1 % L-glutamine. AF488-labeled protein (E2-WT control and PEGylated E279C) were added to the cell suspensions at a range of concentrations (1, 10, or 30 μg/ml) and incubated for 1 hour (for HMDM, n=4) or 4 hours (for MDA-MB-231, n=3) at 37 °C and 5% CO_2. Uptake of AF488-labeled protein was analyzed by flow cytometry using the FACSCalibur (Becton Dickinson, San Jose, CA). Data is presented as an average ± standard deviation of mean fluorescence intensity (MFI) value relative to

control (E2-WT) MFI values. Statistical significance was determined using a two-tailed Student's t-test assuming unequal variances.

4.2.8 Complement Activation Assays

Activation of the classical/lectin complement pathway by E2-WT and PEGylated E279C was measured using a C4-depletion assay as previously described in detail [31,32]. Briefly, proteins were diluted to a final concentration of 1 mg/ml in phosphate buffer and incubated with an equal volume of normal human serum (NHS) for 30 minutes at 30 °C to allow for complement activation, prior to incubation of serial dilutions with antibody-sensitized sheep erythrocytes (EA) in the presence of C4-depleted normal guinea pig serum. Phosphate buffer and aggregated human IgG antibody served as the negative and positive controls, respectively. IgG antibody (10 mg/ml) was incubated at 63°C for 15 minutes, diluted to 2 mg/ml, and centrifuged at 13,000 RPM for 5 minutes to remove large aggregates. Samples and controls were then quantified by measuring the amount of EA lysis over the range of dilutions, with lower cell lysis corresponding to greater C4 consumption in the initial NHS/E2 mixture. Dilutions were optimized to ensure that sub-maximal lysis was observed in the most dilute samples. Details of data analysis are described in Supporting Information. Data is reported as % C4 remaining relative to phosphate buffer averaged over 10 independent experiments and statistical significance was determined using a two-tailed Student's t-test assuming unequal variances.

Since the C4-assay measures early activation, it was important to evaluate whether activation progressed to terminal complement pathway activation. Therefore, production of C5a was measured to determine the activation extent of the entire complement pathway and whether the alternative pathway may be involved. Human serum was incubated with both

PEGylated and non-functionalized E2 protein using the same procedures as described for the C4 depletion assays with the exception that EDTA was added to final concentration of 20 mM following incubation to arrest further complement activation, and C5a production (and its more stable cleavage product, C5a-des-Arg) was measured using the MicroVue C5a EIA kit following the manufacturer's instructions. Data is reported as absolute C5a concentration averaged over 3 separate experiments, and statistical significance was determined using a two-tailed Student's t-test assuming unequal variances.

Levels of background endotoxin in the samples and solutions were determined using a Pyrogent Plus Gel Clot LAL Assay (Lonza, Walkersville, MD). Endotoxin concentrations in protein nanoparticle samples were nearly 80 times lower than the minimum values which activate complement *in vitro* [33]. This indicates that any complement activity observed is not due the presence of endotoxins.

4.2.9 Analysis of Complement Assay Data

Analysis was performed as previously described [2]. Raw data from absorbance (Abs) measurements taken at 405 nm was converted to red blood cell % lysis using the equation

$$\%\ Lysis = \frac{Abs_{Sample} - Abs_{DVGB\ buffer\ control}}{Abs_{water\ control} - Abs_{DVGB\ buffer\ control}}$$

Next, the lysis data was normalized to a z-value using the equation

$$Z - value = -\ln(1 - \%\ lysis)$$

and z-values between 0.2 and 2 (the linear range on a graph of % lysis versus normal human serum dilution) were plotted against serum dilution on a log-log plot. The slope of the z-

value data was used to determine the serum dilution at which z-value is equal to 1 (i.e. the point at which 50% cell lysis occurs), and from this dilution the percent C4 remaining protein consumption relative to the phosphate buffer was determined using the equation

$$\%\ C4\ remaining = 100 \times \frac{Dilution_{sample\ when\ z-value\ is\ 1}}{Dilution_{phosphate\ buffer\ when\ z-value\ is\ 1}}$$

4.3 Results and Discussion

4.3.1 All Surface Cysteine Mutants Were Expressed, Soluble, and Thermostable

All five mutants with external cysteines (Cys) yielded soluble proteins and were overexpressed at the relatively high levels observed for the wild-type E2 scaffold (E2-WT) (**Figure 4.1A**). Our thermostability screen showed that all mutants remain soluble up to approximately 80 °C, which is remarkably stable and similar to the thermostability of E2-WT (**Figure 4.1B**). Our previous investigations found that protein scaffold solubility and correct 60-mer assembly is closely coupled [18]; therefore, these thermostability results suggest correct quaternary complex assembly of all five Cys mutants.

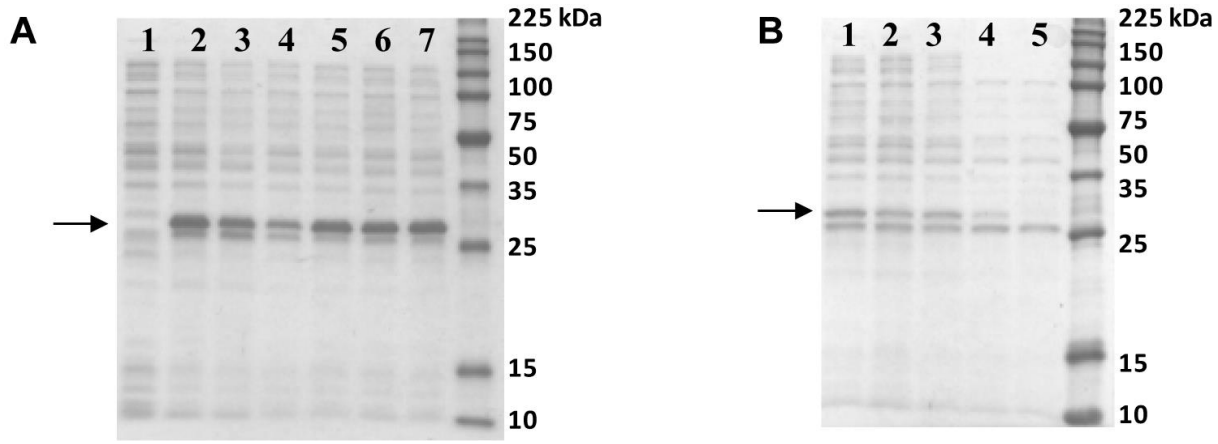

Figure 4.1. SDS-PAGE of mutants with introduced external cysteine residues. **A**: The soluble fraction of BL21(DE3) cell lysates show that all Cys mutants are expressed and soluble. Lanes: (1) pET-11a (no gene), (2) E2-WT, (3) T219C, (4) E279C, (5) D278C, (6) T334C, and (7) M338C. **B**: Temperature screens show that all Cys mutants remain soluble and assembled until approximately 80 °C. Shown is one representative data set, for the E279C soluble fraction after heating for 20 min at (1) 37, (2) 60, (3) 70, (4) 80, and (5) 95 °C. The arrows highlight the bands with the E2 subunit.

Because protein nanocapsule structure, expression, and thermostability appeared comparable between all mutants, we chose one mutant to investigate further based on examining the PDB crystallographic structure of the E2 scaffold. Position 279C (**Figure 4.2**) is surface accessible, does not obstruct the entrance leading to the internal hollow cavity, and gives relatively uniform spacing over the external surface to minimize steric hindrance for chemical coupling. Therefore, E279C was chosen for subsequent studies.

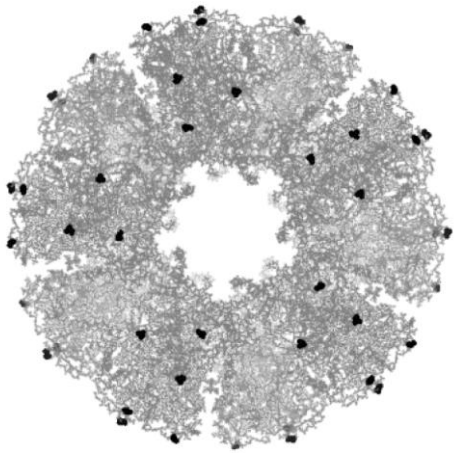

Figure 4.2. Fully assembled E2 scaffold with position 279 highlighted in black. This protein assembly consists of 60 identical subunits, each with one cysteine-279. Structure is displayed at the five-fold axis of symmetry and generated by PyMOL (DeLano 2002).

4.3.2 E279C Exhibits Characteristics Similar to E2-WT

Following purification of E279C, ESI-MS results revealed a single, distinct peak with a molecular weight of 28091 ± 1 Da corresponding to a single subunit of the nanocapsule, (theoretical is 28091 Da), confirming high purity and incorporation of Cys into E279C (**Figure 4.3D**). Protein folding, quaternary structure and assembly, and thermostability of the E279C mutant were similar to those of the E2-WT scaffold. DLS analysis of intact 60-mer particles showed a single peak with an average hydrodynamic diameter of 28.0 ± 0.8 nm, compared to the previously-reported value of 26.6 ± 0.6 nm for E2-WT (**Figure 4.3A**) [18]. DLS also revealed that the DTT reducing agent added to the phosphate buffer prevented cross-linking between Cys and subsequent aggregation of the protein; removal of DTT yielded large aggregates > 100 nm.

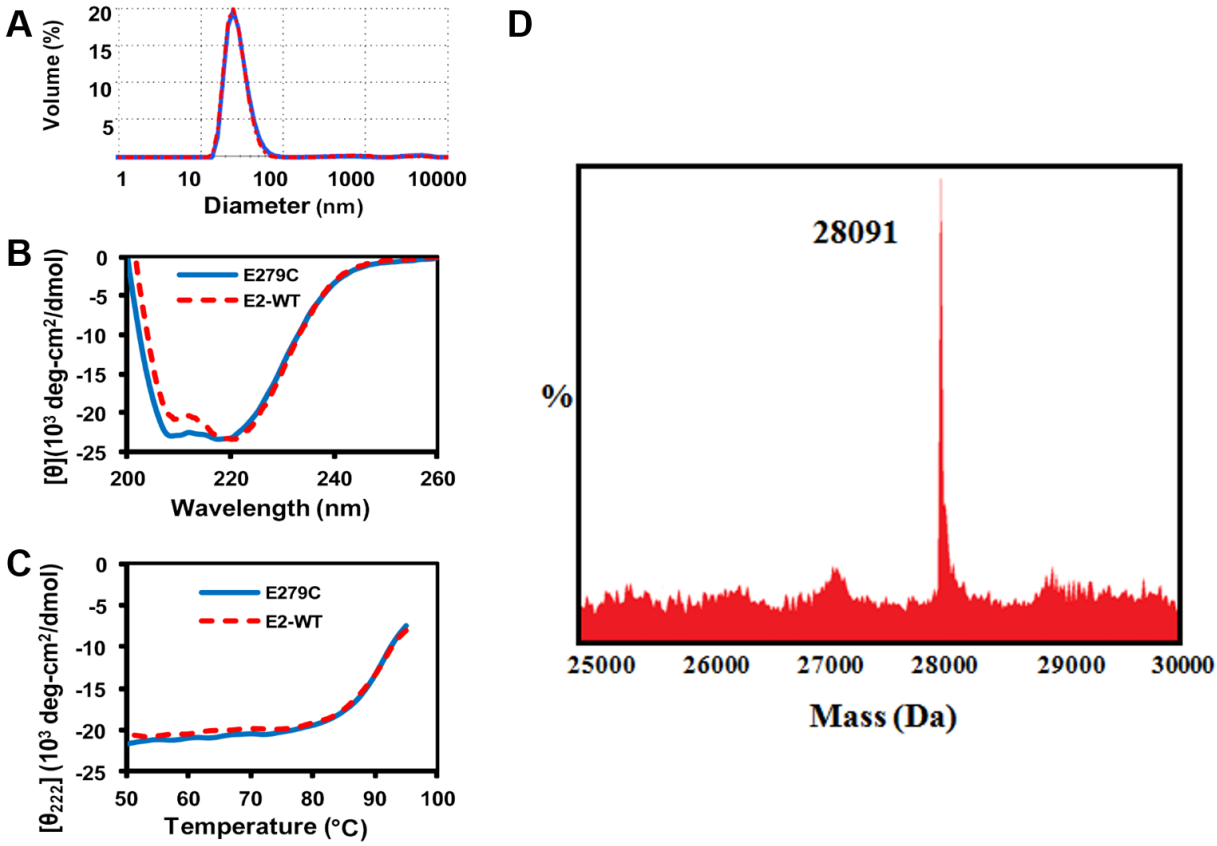

Figure 4.3. Representative characterization data of purified E279C. **A**) DLS measurement of E2-WT (26.6 ± 0.6 nm, n=3, red dashed line) and E279C (28.0 ± 0.8 nm, n=3, blue solid line). **B**) Molar ellipticity versus wavelength shows characteristic minima at 208 and 222 nm for E2-WT and E279C, indicative of high alpha-helical structure. **C**) Thermostability profile (50-95 °C) measuring ellipticity at 222 nm. The calculated average T_o and T_m for E279C are 80.0 ± 1.5 °C and 89.5 ± 1.9 °C, respectively (n=3). **D)** Electrospray ionization mass spectrometry analysis of E279C mutantexhibits a single peak at 28091 Da (theoretical = 28091 Da).

The CD wavelength scans revealed molar ellipticity minima at 208 and 222 nm, indicative of the E2 scaffold's characteristic high alpha-helical content (**Figure 4.3B**). Additionally, a thermostability scan at 222 nm showed that the E279C protein is highly stable, with an onset of unfolding temperature (T_o) of 80.0 ± 1.5 °C and a midpoint of unfolding temperature (T_m) of 89.5 ± 1.9 °C, both of which are close to E2-WT values (**Figure**

4.3C). Protein solubility (**Figure 4.1**) and correct 60-mer assembly have been found to be closely coupled in the E2 complex [18]. This demonstrates that introduction of a non-native cysteine residue into the external surface of the E2-WT subunit does not alter its overall conformation, assembly, or thermostability, rendering it a good candidate for further applications and studies.

4.3.3 Nanocapsule Surface can be Functionalized with Both Small Molecule Dyes and Polymeric Macromolecules

The E2 scaffold is a self-assembled complex of 60 subunits; therefore, a single cysteine mutation theoretically yields 60 accessible thiol sites on the external surface of the protein nanocapsule. To evaluate the chemical accessibility of these thiols, we reacted AlexaFluor 532 C5-maleimide (AF532) with protein and obtained conjugation ratios of 15.2 ± 1.7 and 58.3 ± 12.5 (dye molecules per protein nanocapsule) for E2-WT and E279C, respectively. These values are comparable to those obtained for Cys engineered into the internal hollow cavity of E2 [18]. Although the E2-WT control indicates a low level of nonspecific interactions or conjugation to AF532 [34], the significantly higher conjugation ratio of AF532 to E279C mutant shows that the engineered surface cysteines are indeed accessible for conjugation to near-saturation.

Conjugation of PEG with the E279C particle was confirmed through ESI-MS (**Figure 4.4**). Since PEG1200-maleimide from our source is monodisperse, we expected a distinct peak for PEG1200-E279C at 29330 Da for a single PEG conjugated subunit. The presence of this single peak at 29330 ± 1 Da (**Figure 4.4**) and the absence of the non-functionalized

E279C peak at 28091 Da show that Cys-279 had reacted with PEG to near-completion. The specificity of the PEG reagents for E279C thiols was further confirmed by performing the PEGylation procedures with E2-WT; ESI-MS yielded a peak for non-functionalized E2-WT only, demonstrating no detectable reaction with the E2-WT control.

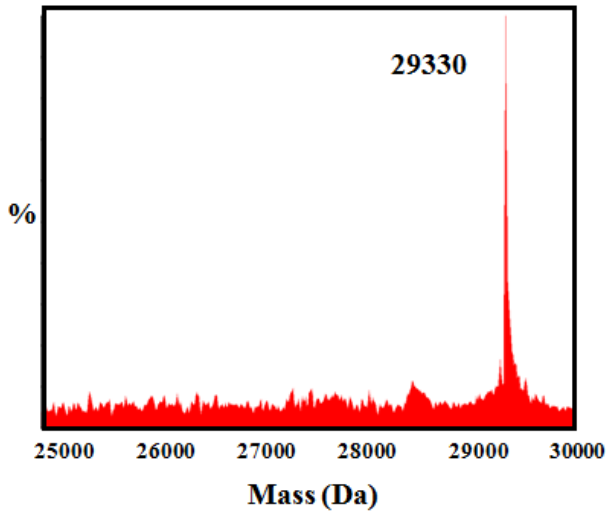

Figure 4.4. Electrospray ionization mass spectrometry analysis of PEG1200-E279C exhibits a single peak at 29330 Da (theoretical = 29330 Da). The lack of a secondary peak at 28091 Da reveals no detectable unreacted E279C and indicates incorporation of a single PEG1200 chain on a single E279C subunit. ESI-MS analysis for PEG2000-E279C and PEG5000-E279C could not obtain a single observable peak; the commercial source reports a range of molecular weights within 10% of 2000 Da and 5000 Da for PEG2000-maleimide and PEG5000-maleimide, respectively.

Characterization of PEGylated particles confirmed that intact structure and thermostability had been retained after functionalization (**Figure 4.5**). DLS measured the hydrodynamic particle diameters to be 37.3 ± 3.6, 41.6 ± 6.4, and 41.4 ± 4.6 nm for PEG1200-E279C, PEG2000-E279C, and PEG5000-E279C, respectively (**Figure 4.5**). The average particle diameters are within the expected range, and secondary aggregation peaks are absent. CD data showed that PEGylation does not affect the structural integrity or the high

thermostability of the nanocapsules, with the onset of unfolding (T_o) at 79.7 ± 1.8 °C, and the midpoint of unfolding transition temperature (T_m) at 89.2 ± 1.3 °C for PEG1200-E279C (**Figure 4.5**). TEM micrographs of PEG1200-E279C further confirm the presence of intact particles following the conjugation reaction (**Figure 4.5 C**). A summary of the physicochemical characterization for the E279C and PEG1200-E279C particles can be found in **Table 4.2**.

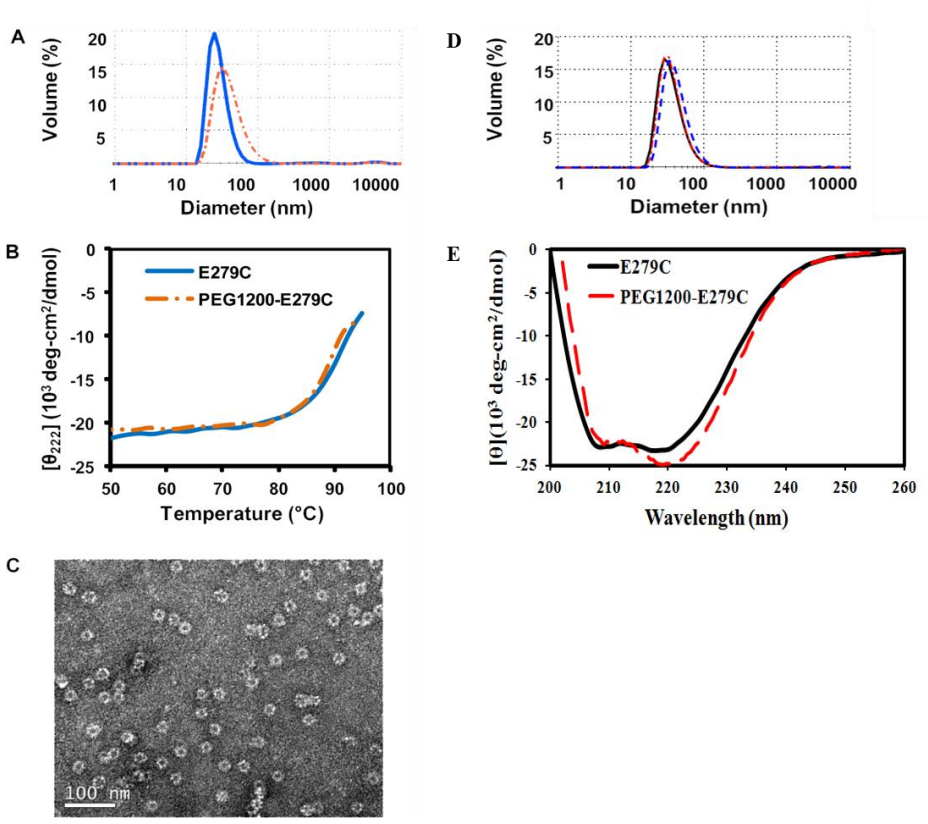

Figure 4.5. Representative characterization data of PEGylated E279C particles. **A**) DLS measurement of particle sizes of E279C (28.0 ± 0.8 nm, n=3, solid blue line) and PEG1200-E279C (37.3 ± 3.6 nm, n=3, orange dashed line). **B**) Thermostability profile of PEG1200-E279C at 222 nm. The calculated average T_o and T_m for PEG1200-E279C are 79.7 ± 1.8 °C and 89.2 ± 1.3 °C, respectively (n=3). **C**) Transmission electron micrograph of PEG1200-E279C particles. **D)** DLS size measurement of E279C and PEGylated E279C mutants. DLS showing representative size measurements of PEG1200-E279C (37.3 ± 3.6 nm, black line), PEG2000-E279C (41.6 ± 6.4 nm, red dashes) and PEG5000-E279C (41.4 ± 4.6 nm, blue dashes). **E)** Molar ellipticity versus wavelength shows characteristic minima at 208 and 222 nm for E279C and PEG1200-E279C. PEGylation of the E279C mutant does not disrupt the characteristic high alpha helical structure.

	E279C	PEG1200-E279C
Single Subunit Mass (Da)	28091 ± 1	29330 ± 1
Average Particle Diameter (nm)	28.0 ± 0.8	37.3 ± 3.6
DLS Average Histogram Peak Height (nm)	26.1 ± 1.9	29.7 ± 2.6
Molar Ellipticity Minima (nm)	208, 222	208, 222
Midpoint of Unfolding Temperature (°C)	89.5 ± 1.9	89.2 ± 1.3

Table 4.2. Summary of characterization of the PEGylated (PEG1200-E279C) and non-PEGylated (E279C) protein nanocapsules.

Our strategy leaves solvent-exposed lysines on the PEGylated nanoparticles available for secondary functionalization. These reactive sites can be used to couple a range of molecules to the particle, including fluorescent dyes or therapeutic compounds. We demonstrated the availability of these sites by labeling with AF488. DLS analysis confirmed intact PEG1200-E279C protein particles conjugated with AF488, with an average particle size of 37.8 ± 2.2 nm. Using our labeling conditions, quantification of labeling revealed dye:protein subunit ratios of 1.0 ± 0.2, 1.1 ± 0.2, 1.4 ± 0.1, and 1.3 ± 0.5 for E2-WT, PEG1200-E279C, PEG2000-E279C, and PEG5000-E279C, respectively. These nanocapsules, functionalized with two different chemical entities, were used to investigate *in vitro* cellular uptake. The ability to introduce multiple functionality to the protein particles is important toward applicability. Our prior work demonstrates that by functionalizing the E2 particles with doxorubicin, we can obtain drug loading, pH-dependent release, and cytotoxicity toward breast cancer cells [22].

4.3.4 PEGylation Inhibits Cellular Uptake of Nanoparticles

Uptake by HMDM (from multiple donors) and the MDA-MB-231 human breast cancer cell line were significantly lower for PEGylated E279C nanoparticles relative to non-PEGylated (E2-WT control) in all protein concentrations tested (**Figure 4.6**). For HMDM cells, uptake levels, relative to E2-WT, decreased to 74.8 ± 13.8, 54.6 ± 15.7, and 36.3 ± 8.3 % MFI for PEG1200-E279C, PEG2000-E279C, and PEG5000-E279C, respectively, at a protein concentration of 1 μg/ml. A similar trend was seen at 10 μg/ml (76.3 ± 12.4, 59.4 ± 21.0, and 32.6 ± 8.3 % MFI, respectively) (**Figure 4.6**). Observing uptake properties in the absence of serum allows us to determine the intrinsic recognizability of our particle without other contributing factors (e.g. opsonins or antibodies). For MDA-MB-231 cells, relative uptake levels decreased to 70.8 ± 13.9, 62.4 ± 10.5, and 37.4 ± 7.2 % MFI, respectively, for 30 μg/ml protein, with a similar trend also seen at 10 μg/ml (75.3 ± 9.1, 67.3 ± 9.3, 46.8 ± 5.8 % MFI, respectively) (**Figure 4.6**).

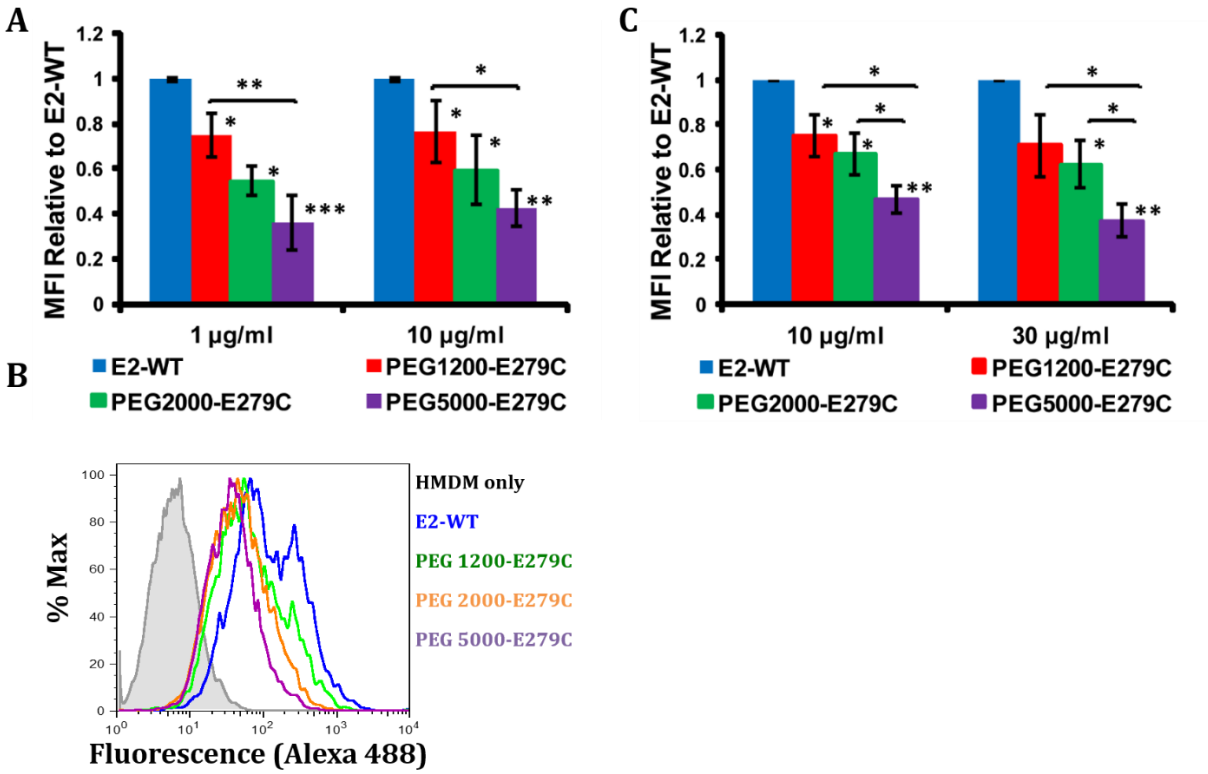

Figure 4.6. PEGylation decreases cellular uptake of the E2 protein nanocapsule. **A)** Uptake of E2-WT and PEGylated E279C by human monocyte derived macrophages. Mean fluorescence intensity (MFI) values were normalized to E2-WT MFI. Significant differences in uptake between E2-WT and PEGylated proteins are indicated (*p < 0.05, **p < 0.01, ***p < 0.001; n=4). **B)** Representative histogram of fluorescence intensity of human macrophages incubated with 10 mg/ml Alexa488-labeled PEGylated and unfunctionalized E2 proteins. Measured by flow cytometry. **C)** Uptake of E2-WT and PEGylated E279C by MDA-MB-231 cells. Mean fluorescence intensity (MFI) values were normalized to E2-WT MFI. Significant differences in uptake between E2-WT and PEGylated proteins are indicated (*p < 0.05, **p < 0.01; n=3).

PEGylation of biomaterials and nanoparticles has been utilized as a strategy to evade immune recognition, improve solubility, and increase *in vivo* half-life [15,16,35-38]. For nanoparticles similar in size to ours, reduced *in vitro* cellular uptake has been observed following PEG functionalization [16,39,40]. Our data is consistent with this and also shows the trend of reduced uptake with increasing PEG chain length, with PEG5000-E279C particles showing significantly less uptake compared to PEG1200-E279C over the particle concentrations examined. This dependence on PEG content was also observed in previous studies with gold nanoshells [41] and virus-like particles [16], and showed that the phenomenon of reduced cellular uptake of biomaterials was greatly diminished as the PEG molecular weight was further increased from 5 kDa to 20 kDa, indicating some structural feature of high molecular weight PEGs that increase cellular recognition [41].

Our observation of reduced cellular uptake with increasing PEG content may have implications for modulating the cellular recognition of our particle *in vivo*. This effect is possibly due to inhibition of specific receptor-mediated interactions, which has been proposed for other protein particle systems [16,40]. Explanations in the studies mentioned have suggested shifting of polymer architecture from mushroom-like to brush-like or increased effective shielded area [16,41]. Vonarbourg et al. showed that the ability of PEG to mask particles was increased as particle diameter decreased from 100 to 20 nm, which is similar to the size of our protein nanocapsule [42], Decreased cellular uptake is a property that could decrease immunogenicity and potentially allow longer *in vivo* circulation times of our particle. Conversely, decreased cellular recognition may also reduce efficacy for applications such as drug delivery, where it may be beneficial to evade the phagocytic

immune cells while remaining recognizable by target cells. Previous studies have overcome this barrier by affinity ligand functionalization of the PEG free ends [36,40,43].

4.3.5 PEGylation of Protein Nanocapsule Activates Complement

We characterized the capacity of our protein nanocapsules to activate complement, an innate immune mechanism that initiates inflammation and recognizes and clears foreign pathogenic material. Following protein nanoparticle incubation with serum (as a source of complement proteins), a higher percentage of C4 remaining in the sample corresponds to a lower degree of classical/lectin complement pathway activation, with no activation when 100 % of C4 remains. Unmodified E2-WT promotes only a small degree of classical/lectin complement activation, with 97.6 ± 10.8 % C4 remaining after incubation with human serum, relative to phosphate buffer alone (**Figure 4.7**). In comparison, PEG1200-E279C consistently exhibited an enhanced activation of complement relative to non-PEGylated E2-WT within individual assays, with 79.7 ± 6.0 % C4 remaining. Heat-aggregated IgG (positive control) gave near-complete consumption of C4 over all the dilutions tested, showing full activation. Observed inter-assay variability may be due to donor variability in sheep erythrocytes and guinea pig serum. Our data indicate that PEGylation of the E279C nanocapsules moderately increases classical/lectin complement activation.

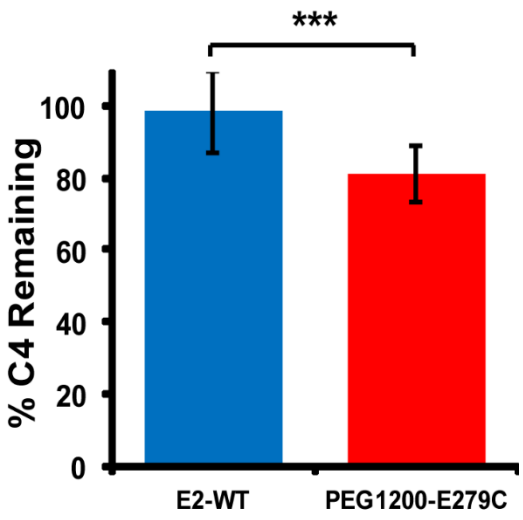

Figure 4.7. *In vitro* classical/lectin complement activation by E2-WT and PEG1200-E279C, as measured by C4 depletion in human serum. Higher percent C4 remaining corresponds to lower activation and is relative to phosphate buffer (negative control). Heat-aggregated human IgG (positive control) showed near-complete C4 consumption. Significant differences in activation are indicated (***$p < 0.001$).

Since C4 is a protein involved early in the classical/lectin pathway, it is not a definitive marker of full pathway activation, nor does it provide information about possible involvement of the alternative pathway. We therefore additionally measured C5a production in human serum following incubation with the E2 protein nanoparticles, with a higher amount of C5a produced *in vitro* corresponding to a greater degree of complement activation. C5a serum concentrations resulting from incubation with E2-WT and PEG1200-E279C averaged 40.1 ± 6.0 ng/ml and 87.6 ± 10.1 ng/ml, respectively (**Figure 4.8**). Both E2-WT and PEG1200-E279C produced greater amounts of C5a in human serum relative to the phosphate buffer background (11.2 ± 3.3 ng/ml) and significantly less than the heat-aggregated IgG positive control (239.0 ± 89.2 ng/ml).

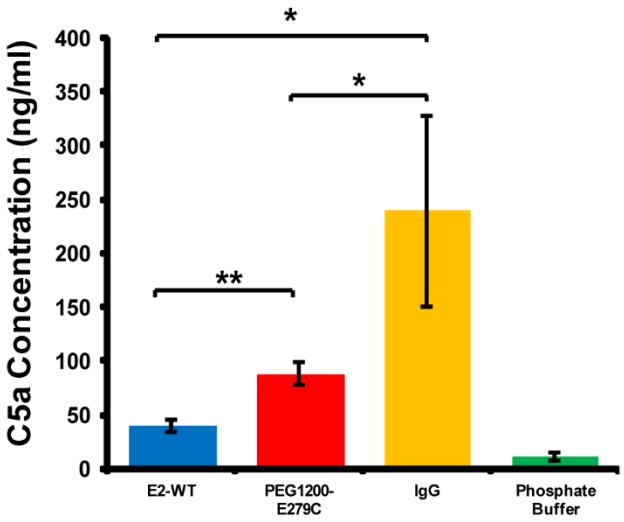

Figure 4.8. Measurement of C5a concentration in human serum following incubation with E2-WT, PEGylated E279C, phosphate buffer, and aggregated human IgG. A higher amount of C5a indicates greater complement activation. Significant differences in concentration are indicated (*$p < 0.05$, **$p < 0.01$). E2-WT, PEG1200-E279C, and IgG all showed significantly greater C5a concentrations relative to phosphate buffer ($p < 0.001$).

In both the C4 depletion and C5a production assay results, the PEGylated E279C mutant consistently induced more complement activity compared to E2-WT. Our data indicates that the unmodified protein nanoparticle is a weak activator of complement relative to a known strong classical pathway activator (aggregated IgG). Measurements of background endotoxin levels in our serum/protein solutions was determined to be approximately 80 times lower than the minimum amount reported to activate complement, indicating that any observed complement activation is due to the properties of the sample itself and not contaminating levels of endotoxin [33]. Furthermore, free PEG1200-maleimide at levels comparable to that of residual PEG1200-maleimide after PEG1200-E279C purification exhibited no complement activation, further indicating that the activation observed is due to the attachment of PEG on the protein nanoparticle. PEGylation of these particles moderately activate the classical/lectin pathway, and given that relative amounts of C5a produced are similar to relative consumption amounts observed in the C4

assays, this suggests that the alternative pathway does not substantially contribute to or amplify complement activation by these particles.

The adsorption of proteins on nanomaterial surfaces can have many adverse *in vivo* effects such as opsonization of the nanomaterial or triggering inflammation, and it has been suggested that PEGylation can minimize such effects [13,14,37,42,44]. While nanoparticle conjugation with PEG and reduction of PEGylated nanoparticle size has been observed to reduce complement activation *in vitro*, it does not eliminate it completely [37,45-47]. In contrast, the rapid clearance of PEGylated nanoparticles *in vivo* and PEG-mediated complement activation *in vitro* and *in vivo* have also been reported previously [37,44,47-50], although the mechanism of activation is still unclear. One explanation for the apparent contradictory observations in these prior investigations may be that PEG is masking the complement activation properties of the particle itself, but is introducing a lower, yet non-negligible, amount of polymer-mediated complement activation. This would in part explain why we have observed complement activation after PEGylation of a particle that intrinsically is not a strong activator, an observation also made with liposomal systems [50]. However, since only modest activation due to PEG relative to the positive control was observed, and also because reported concentrations of protein particles used for *in vivo* applications are typically much lower than those which activate complement in our *in vitro* assay [25,35,38,40], we expect that the complement activation is likely to be less significant when *in vivo* conditions are examined.

4.4 Conclusions

We have engineered a protein nanocapsule (E279C), based on the E2 scaffold, which can be functionalized on the surface with various molecules. This scaffold properly assembles and remains highly thermostable, even following conjugation with synthetic polymers. We found that introducing PEG on the surface of this scaffold decreased cellular uptake by both human monocyte derived macrophages and a human breast cancer cell line. PEGylation of the protein nanocapsule also moderately increased complement activation capacity relative to the unfunctionalized E2-WT scaffold, which itself yields a low level of activation. PEG activates weakly the classical/lectin pathways with little, if any, alternative pathway amplification. Our work demonstrates a generally applicable strategy of generating surface modifications to this protein nanocapsule platform, and that these modifications can alter cellular uptake and complement activation properties.

4.5 References

1. De M, Ghosh PS, Rotello VM: Applications of Nanoparticles in Biology. *Advanced Materials* 2008, 20:4225-4241.
2. Nie S, Xing Y, Kim GJ, Simons JW: Nanotechnology applications in cancer. *Annu Rev Biomed Eng* 2007, 9:257-288.
3. Lin YH, MaHam A, Tang ZW, Wu H, Wang J: Protein-Based Nanomedicine Platforms for Drug Delivery. *Small* 2009, 5:1706-1721.
4. Forrest ML, Aillon KL, Xie YM, El-Gendy N, Berkland CJ: Effects of nanomaterial physicochemical properties on in vivo toxicity. *Advanced Drug Delivery Reviews* 2009, 61:457-466.
5. Domingo GJ, Orru S, Perham RN: Multiple display of peptides and proteins on a macromolecular scaffold derived from a multienzyme complex. *Journal of Molecular Biology* 2001, 305:259-267.
6. Koudelka KJ, Manchester M: Chemically modified viruses: principles and applications. *Curr Opin Chem Biol* 2010, 14:810-817.
7. Steinmetz NF: Viral nanoparticles as platforms for next-generation therapeutics and imaging devices. *Nanomedicine-Nanotechnology Biology and Medicine* 2010, 6:634-641.
8. Strable E, Finn MG: Chemical modification of viruses and virus-like particles. *Curr Top Microbiol Immunol* 2009, 327:1-21.
9. Uchida M, Klem MT, Allen M, Suci P, Flenniken M, Gillitzer E, Varpness Z, Liepold LO, Young M, Douglas T: Biological containers: Protein cages as multifunctional nanoplatforms. *Advanced Materials* 2007, 19:1025-1042.
10. Douglas T, Young M: Viruses: Making friends with old foes. *Science* 2006, 312:873-875.
11. Lee LA, Niu ZW, Wang Q: Viruses and Virus-Like Protein Assemblies-Chemically Programmable Nanoscale Building Blocks. *Nano Research* 2009, 2:349-364.
12. Manchester M, Destito G, Schneemann A: Biomedical Nanotechnology Using Virus-Based Nanoparticles. *Viruses and Nanotechnology* 2009, 327:95-122.
13. Shan XQ, Yuan Y, Liu CS, Tao XY, Sheng Y, Xu F: Influence of PEG chain on the complement activation suppression and longevity in vivo prolongation of the PCL biomedical nanoparticles. *Biomedical Microdevices* 2009, 11:1187-1194.
14. Sant S, Poulin S, Hildgen P: Effect of polymer architecture on surface properties, plasma protein adsorption, and cellular interactions of pegylated nanoparticles. *J Biomed Mater Res A* 2008, 87:885-895.
15. Dobrovolskaia MA, McNeil SE: Immunological properties of engineered nanomaterials. *Nat Nanotechnol* 2007, 2:469-478.
16. Steinmetz NF, Manchester M: PEGylated viral nanoparticles for biomedicine: the impact of PEG chain length on VNP cell interactions in vitro and ex vivo. *Biomacromolecules* 2009, 10:784-792.
17. Ludwig C, Wagner R: Virus-like particles - universal molecular toolboxes. *Current Opinion in Biotechnology* 2007, 18:537-545.
18. Dalmau M, Lim S, Chen HC, Ruiz C, Wang SW: Thermostability and molecular encapsulation within an engineered caged protein scaffold. *Biotechnol Bioeng* 2008, 101:654-664.
19. Domingo GJ, Chauhan HJ, Lessard IAD, Fuller C, Perham RN: Self-assembly and catalytic activity of the pyruvate dehydrogenase multienzyme complex from Bacillus stearothermophilus. *European Journal of Biochemistry* 1999, 266:1136-1146.
20. Izard T, Aevarsson A, Allen MD, Westphal AH, Perham RN, de Kok A, Hol WG: Principles of quasi-equivalence and Euclidean geometry govern the assembly of cubic and dodecahedral cores of pyruvate dehydrogenase complexes. *Proc Natl Acad Sci U S A* 1999, 96:1240-1245.

21. Milne JLS, Shi D, Rosenthal PB, Sunshine JS, Domingo GJ, Wu XW, Brooks BR, Perham RN, Henderson R, Subramaniam S: Molecular architecture and mechanism of an icosahedral pyruvate dehydrogenase complex: a multifunctional catalytic machine. *Embo Journal* 2002, 21:5587-5598.
22. Ren DM, Kratz F, Wang SW: Protein Nanocapsules Containing Doxorubicin as a pH-Responsive Delivery System. *Small* 2011, 7:1051-1060.
23. Dalmau M, Lim S, Wang SW: Design of a pH-dependent molecular switch in a caged protein platform. *Nano Lett* 2009, 9:160-166.
24. Dalmau M, Lim S, Wang SW: pH-triggered disassembly in a caged protein complex. *Biomacromolecules* 2009, 10:3199-3206.
25. Caivano A, Doria-Rose NA, Buelow B, Sartorius R, Trovato M, D'Apice L, Domingo GJ, Sutton WF, Haigwood NL, De Berardinis P: HIV-1 Gag p17 presented as virus-like particles on the E2 scaffold from Geobacillus stearothermophilus induces sustained humoral and cellular immune responses in the absence of IFN gamma production by CD4+T cells. *Virology* 2010, 407:296-305.
26. Domingo GJ, Caivano A, Sartorius R, Barba P, Backstrom M, Piatier-Tonneau D, Guardiola J, De Berardinis P, Perham RN: Induction of specific T-helper and cytolytic responses to epitopes displayed on a virus-like protein scaffold derived from the pyruvate dehydrogenase multienzyme complex. *Vaccine* 2003, 21:1502-1509.
27. Zhou ZH, Liao WC, Cheng RH, Lawson JE, McCarthy DB, Reed LJ, Stoops JK: Direct evidence for the size and conformational variability of the pyruvate dehydrogenase complex revealed by three-dimensional electron microscopy - The "breathing" core and its functional relationship to protein dynamics. *Journal of Biological Chemistry* 2001, 276:21704-21713.
28. DeLano W: The PyMOL molecular graphics system. DeLano Scientific; 2002.
29. Greenfield N: Using circular dichrois collected as a function of temperature to determine the thermodynamics of protein unfolding and binding interactions. *Nat Protocols* 2006, 1:2527-2535.
30. Fraser DA, Tenner AJ: Innate immune proteins C1q and mannan-binding lectin enhance clearance of atherogenic lipoproteins by human monocytes and macrophages. *J Immunol* 2010, 185:3932-3939.
31. Cribbs DH, Velazquez P, Soreghan B, Glabe CG, Tenner AJ: Complement activation by cross-linked truncated and chimeric full-length beta-amyloid. *NeuroReport* 1997, 8:3457-3462.
32. Webster SD, Tenner AJ, Poulos TL, Cribbs DH: The mouse C1q A-chain sequence alters beta-amyloid-induced complement activation. *Neurobiol Aging* 1999, 20:297-304.
33. Kaca W, Roth R: Activation of Complement by Human Hemoglobin and by Mixtures of Hemoglobin and Bacterial-Endotoxin. *Biochimica Et Biophysica Acta-General Subjects* 1995, 1245:49-56.
34. Smyth DG, Nagamatsu A, Fruton JS: Some reactions of N-Ethylmaleimide. *Journal of the American Chemical Society* 1960, 82:4600-4604.
35. De Geest B, Snoeys J, Van Linthout S, Lievens J, Collen D: Elimination of innate immune responses and liver inflammation by PEGylation of adenoviral vectors and methylprednisolone. *Hum Gene Ther* 2005, 16:1439-1451.
36. Eto Y, Gao JQ, Sekiguchi F, Kurachi S, Katayama K, Maeda M, Kawasaki K, Mizuguchi H, Hayakawa T, Tsutsumi Y, et al.: PEGylated adenovirus vectors containing RGD peptides on the tip of PEG show high transduction efficiency and antibody evasion ability. *Journal of Gene Medicine* 2005, 7:604-612.
37. Mosqueira VCF, Legrand P, Gulik A, Bourdon O, Gref R, Labarre D, Barratt G: Relationship between complement activation, cellular uptake and surface physicochemical aspects of novel PEG-modified nanocapsules. *Biomaterials* 2001, 22:2967-2979.

38. Raja KS, Wang Q, Gonzalez MJ, Manchester M, Johnson JE, Finn MG: Hybrid virus-polymer materials. 1. Synthesis and properties of PEG-decorated cowpea mosaic virus. *Biomacromolecules* 2003, 4:472-476.
39. Kelf TA, Sreenivasan VK, Sun J, Kim EJ, Goldys EM, Zvyagin AV: Non-specific cellular uptake of surface-functionalized quantum dots. *Nanotechnology* 2010, 21:285105.
40. Ogawara KI, Rots MG, Kok RJ, Moorlag HE, van Loenen AM, Meijer DKF, Haisma HJ, Molema G: A novel strategy to modify adenovirus tropism and enhance transgene delivery to activated vascular endothelial cells in vitro and in vivo. *Human Gene Therapy* 2004, 15:433-443.
41. Kah JC, Wong KY, Neoh KG, Song JH, Fu JW, Mhaisalkar S, Olivo M, Sheppard CJ: Critical parameters in the pegylation of gold nanoshells for biomedical applications: an in vitro macrophage study. *J Drug Target* 2009, 17:181-193.
42. Vonarbourg A, Passirani C, Saulnier P, Simard P, Leroux JC, Benoit JP: Evaluation of pegylated lipid nanocapsules versus complement system activation and macrophage uptake. *J Biomed Mater Res A* 2006, 78:620-628.
43. Jung Y, Park HJ, Kim PH, Lee J, Hyung W, Yang J, Ko H, Sohn JH, Kim JH, Huh YM, et al.: Retargeting of adenoviral gene delivery via Herceptin-PEG-adenovirus conjugates to breast cancer cells. *Journal of Controlled Release* 2007, 123:164-171.
44. Moghimi SM, Szebeni J: Stealth liposomes and long circulating nanoparticles: critical issues in pharmacokinetics, opsonization and protein-binding properties. *Prog Lipid Res* 2003, 42:463-478.
45. Danielsson A, Elgue G, Nilsson BM, Nilsson B, Lambris JD, Totterman TH, Kochanek S, Kreppel F, Essand M: An ex vivo loop system models the toxicity and efficacy of PEGylated and unmodified adenovirus serotype 5 in whole human blood. *Gene Ther* 2010, 17:752-762.
46. Gbadamosi JK, Hunter AC, Moghimi SM: PEGylation of microspheres generates a heterogeneous population of particles with differential surface characteristics and biological performance. *FEBS Lett* 2002, 532:338-344.
47. Hamad I, Al-Hanbali O, Hunter AC, Rutt KJ, Andresen TL, Moghimi SM: Distinct polymer architecture mediates switching of complement activation pathways at the nanosphere-serum interface: implications for stealth nanoparticle engineering. *ACS Nano* 2010, 4:6629-6638.
48. Arima Y, Toda M, Iwata H: Complement activation on surfaces modified with ethylene glycol units. *Biomaterials* 2008, 29:551-560.
49. Moghimi SM, Andersen AJ, Hashemi SH, Lettiero B, Ahmadvand D, Hunter AC, Andresen TL, Hamad I, Szebeni J: Complement activation cascade triggered by PEG-PL engineered nanomedicines and carbon nanotubes: the challenges ahead. *J Control Release* 2010, 146:175-181.
50. Szebeni J, Baranyi L, Savay S, Milosevits J, Bunger R, Laverman P, Metselaar JM, Storm G, Chanan-Khan A, Liebes L, et al.: Role of complement activation in hypersensitivity reactions to doxil and HYNICPEG liposomes: Experimental and clinical studies. *Journal of Liposome Research* 2002, 12:165-172.

CHAPTER 5

Lymphatic Drainage and Enhanced Dendritic Cell Interactions with PEGylated and CpG-Functionalized Protein Nanoparticles

5.1 Background

Biomaterials possess many advantages as platforms for immunotherapy, including the ability to simultaneously encapsulate and protect vaccine payloads (*e.g.,* antigens and immune activators), protect the host from non-specific inflammation, and allow efficient interaction between an antigen and antigen presenting cells (APCs) [1-4]. The capability to package and allow for controlled release of immune-modulating compounds renders biomaterial a unique and potentially advantageous platform for vaccine delivery. The administration of vaccine components (antigen and/or immune-stimulants) as separate components in soluble or suspended form has inherent drawbacks related to inefficient interaction with antigen presenting cells and non-specific triggering of systemic inflammation, detracting from the desired antigen-specific response [5-8].

Biomaterials are being engineered for a variety of vaccine therapies [7]. Platforms such as polymer scaffolds may be implanted, allowing for recruitment of APCs and local inflammatory cells to the site of the scaffold, thereby mimicking a local infection [9,10]. In fact, this type of technology has entered into clinical trials for the treatment of skin cancer [11]. Rather than attracting APCs to the biomaterial, nanoparticles and microparticles are platforms suitable for administration that can efficiently drain to the lymphatics and interact with dendritic cells (DCs) and other immune cells in their natural environment [2,4,6,7,12]. Nanoparticles, in particular, represent a powerful tool for approaches in targeting DCs, the immune system's most powerful mediator between innate and adaptive immunity, for cellular mediated responses [3,4,13,14]. CD8 cytotoxic T cell (CTL) responses are critical for viral infections, cancer, and other intracellular infections [15].

DCs are an APC of the adaptive arm of immunity that are particularly efficient at sampling their environment and processing antigen, trafficking throughout the lymphatics, and translating danger signals to orchestrate the most appropriate adaptive immune response, to more effectively carry out targeted effector functions with long-lasting immunological memory [16,17]. Therefore, DCs represent a major target of nanoparticle and other biomaterial vaccine formulations, when attempting to synthetically shape the immune response [3,13,14,18]. Nanoparticles are of optimal size for dendritic cell uptake, and many (< 100 nm) are able to drain freely from the subcutaneous and intradermal space to the local lymphatics, where many DCs reside [4,7]. Therefore, many nanoparticle platforms have been explored for use as vaccines where interaction with DCs is a desired application, such as with cancer vaccines [12].

Biomaterials, including nanoparticles, must also be designed such that interaction with non-target cell types and adsorption of opsonins should be decreased in an attempt to hone in on the physiological location and cell types desired. The most common approach to decrease these undesired interactions is to functionalize with hydrophilic polymers, most notably poly(ethylene) glycol [19-23]. This approach can be used in conjunction with display of other moieties to further alter cellular specificty [24].

Although nanoparticles, including virus-like particles [13], possess a natural ability to passively target the lymphatic system and access APCs, their affinity for DCs may be enhanced by surface functionalization with different functionalities (*e.g.,* by altering surface charge or display or targeting molecules) [1,14,25-27]. Researchers have attempted to engineer various formulations of antigens, including biomaterials, for the specific targeting

of DCs (or even particular DC subsets) [3,14]. The most common examples in the literature for attempts at targeting DCs have been the utilization of antibodies [3,24,28,29]. Although promising, antibodies, in general, exhibit inherent challenges for their use in cell-specific targeting. From a practical standpoint, monoclonal antibodies can be costly and difficult to produce and purify, especially at larger scales. Antibodies are also physically bulky biomacromolecules that may increase the sizes of associated nanoparticle beyond the optimal size range for DC-based immunotherapies. The large size may also limit the total number of antibodies that can be conjugated to the nanoparticle surface, thereby limiting the achievable avidity. Also, it is often difficult to conjugate to sites on an antibody that guarantees its orientation will allow the variable region to recognize its target or that the linker itself will not bind within the variable region, although conjugation strategies are being developed to overcome this barrier [30].

As an alternative approach, aptamers (*e.g.,* peptide) or recombinant proteins have been explored to specifically target DCs, which represent synthetically simpler molecules than their antibody counterparts [31-33]. Additionally, while not explored specifically as a targeting ligand, one group recently uncovered the importance of DEC-205 expression for the *in vivo* uptake of the Toll-like receptor 9 (TLR 9) ligand CpG [34]. DEC-205 is a frequently targeted DC receptor in synthetic vaccine design [14,26,29], and therefore CpG offers a potentially novel ligand with dual purpose for DC targeting and activation.

While many nanoparticle platforms are being explored for DC-mediated immunotherapies for T cell response, protein nanoparticle possess distinctive properties that render them a particularly attractive biomaterial for vaccination [4,35,36]. Protein

nanoparticle display many of the same structural and chemical features of natural viruses, which the immune system have evolved to become particularly adept at recognizing and mounting an immune response [35,37,38]. Important for cell-mediated responses, DCs are known to be particularly efficient at cross-presenting viral antigens to induce potent CD8 T cell responses [39], and as such many nanoparticle platforms' intent is to mimic viral properties to induce immunity towards the synthetically associated antigen [7].

The E2 nanoparticle our group has been developing has the distinct advantage of displaying many virus-like properties without being of viral origin. Additionally, we have already demonstrated the capability of inducing an antigen-specific immune response *in vivo* (**Chapter 3**) and the ability to reduce cellular interactions following PEGylation (**Chapter 4**) [40]. While the biodistribution of other protein nanoparticles has been explored following a range of administration routes, including subcutaneous [41-43], we sought to understand the distribution of the E2 nanoparticle in particular following subcutanous administration. We also observed changes in cell uptake, biodistribution, and cellular distribution following surface functionalization with PEG and the nucleic acid aptamer CpG. In this study, we hypothesized that PEGylation could provide a mechanism to reduce cellular interaction with a variety of immune and non-immune cell types, and that PEG could serve as a linker to attach CpG DNA to specifically target DCs.

5.2 Methods

5.2.1 Materials

All buffer reagents were purchased from Fisher Scientific, unless otherwise noted. The oligodeoxynucleotide Toll-like receptor 9 ligand CpG 1826 (5'-tccatgacgttcctgacgtt-3') (CpG) was synthesized with a phosphorothioated backbone and 5' thiol linker by TriLink Biotechnologies. The methyl-PEG-NHS (mPEG; molecular weight 2000 Da) and maleimide-PEG-NHS (mal-PEG; molecular weight 2000 Da) were purchased from Nanocs. Alexa Fluor 488 C5-maleimide was from Life Technologies. All cell culture media, unless otherwise noted, was comprised of RPMI 1640 (Mediatech) supplemented with 10% heat-inactivated fetal bovine serum (Gibco), 1 mM sodium pyruvate (Hyclone), 2 mM L-glutamine (Lonza), 100 units/ml penicillin (Hyclone), 100 μg/ml streptomycin (Hyclone), 50 μM 2-mercaptoethanol (Fisher), 0.1 mM non-essential amino acids (Lonza) (complete RPMI media).

5.2.2 Animals and Cell Lines

For generation of bone marrow-derived dendritic cells and for *in vivo* biodistribution assays, wild-type C57Bl/6 female mice aged 6-12 weeks were used (Jackson Laboratories). All experiments were performed under approved protocol by the IACUC at the University of California, Irvine. Animals were housed and maintained by the ULAR.

The NIH 3T3 mouse fibroblast cell line was purchased from ATCC. B3Z, a CD8 T cell hybridoma, was kindly provided by Prof. Nilabh Shastri (University of California, Berkeley). CH12, a B cell lymphoma line was kindly provided by Prof. Paolo Casali (University of Texas

Health Science Center at San Antonio). Murine bone marrow-derived macrophages were kindly provided by Prof. Wendy Liu [86]. NIH 3T3 cells were purchased from ATCC and maintained in DMEM + 10% FBS.

5.2.3 E2 Nanocapsule Preparation

The D381C E2 protein (E2) was prepared as previously described [44]. D381C is an E2 mutant with a non-native cysteine introduced to the internal cavity of the nanoparticle for site-directed functionalization. Briefly, proteins were expressed in *E. coli*, cells were lysed, and soluble cell lysates were applied to a HiPrep Q Sepharose anion exchange column (GE Healthcare) followed by a Superose 6 (GE Healthcare) size exclusion column for purification. The purified proteins were analyzed by dynamic light scattering (Zetasizer Nano ZS, Malvern) for size measurements. Electrospray ionization mass spectrometry and SDS-PAGE were performed for molecular weight and purity confirmation. Final protein preparations were stored in 50 mM potassium phosphate at pH 7.4 with 100 mM NaCl (phosphate buffer) at 4°C for short-term and -80°C for long-term storage.

Lipopolysaccharide (LPS), a component of gram-negative bacterial cell walls, is recognized by Toll-like receptor 4 expressing immune cells (*e.g.* DCs), causing potentially unwanted immune activation. Residual LPS was removed following the method described by Aida and Pabst [45]. Briefly, Triton X-114 (Sigma) was added to the purified protein at 1% (v/v), chilled to 4°C, vortexed vigorously, and heated to 37°C. The mixture was then centrifuged at 18,000 × g and 37°C for 30 seconds, and the protein-containing aqueous portion was separated from the detergent. This total process repeated ≥ 8 times. Residual

Triton was removed with detergent removal spin columns (Pierce). LPS levels were below 8 EU (0.8 ng) per milligram of E2 protein (LAL ToxinSensor gel clot assay, Genscript).

5.2.4 Bone Marrow-Derived Dendritic Cells (BMDCs)

Bone marrow-derived dendritic cells (BMDCs) were prepared following the method described by Lutz *et al* [46]. Briefly, the femurs and tibias were rinsed in 70% ethanol, epiphyses removed, and the marrow flushed. Cells were broken up to a single cell suspension and applied to a 70 μm cell strainer (Fisher). Red blood cells were depleted with ACK lysing buffer (Lonza), followed by washing with PBS. The marrow cells were plated at 2×10^5 cells/ml (10 ml total) on sterile bacteriological Petri dishes (Fisher) in complete RPMI media supplemented with 20 ng/ml murine recombinant GM-CSF (eBioscience). Cells were maintained at 37°C and 5% CO_2, and 10 ml fresh DC media was added on day 3. On day 6, 50% of the media was replaced, and the non-adherent cells were pelleted and added back to the plates. Loosely and non-adherent cells were collected and used as immature BMDCs on day 8.

5.2.5 Internal Conjugation with Alexa Fluor 488 and External Conjugated of poly(ethylene) glycol and CpG

The Alexa Fluor 488 C5-maleimide was conjugated to the internal cysteine of E2 (E2) by combining with E2 at a 3-fold molar excess to E2's thiols for 2 hr at room temperature. The unreacted excess dye was removed by the Zeba Spin Desalting Columns with a 40 kDa molecular weight cutoff (desalting column; Pierce) to phosphate buffer for *in vitro* assays. This same reaction was buffer exchanged to phosphate buffered saline (PBS, Fisher Scientific) at the final step for *in vivo* assays.

The mPEG-NHS linker was conjugated to the external primary amines on E2 (mPEG-E2) by incubating with E2 at a 25-fold molar ratio to the E2 monomer for 2 hr at room temperature. The unreacted mPEG-NHS was removed by the Zeba Spin desalting column to phosphate buffer for *in vitro* assays or to PBS for *in vivo* assays. The same exact procedure was carried out to conjugate the mal-PEG-NHS to the external amines of the E2 nanoparticle. To the mal-PEG-functionalized E2 nanoparticle (mal-PEG-E2), a 10-fold molar excess (to E2 monomer) of TCEP-reduced CpG-SH was added and incubated for 2 hr at room temperature followed by an overnight incubation at 4°C. The external CpG-conjugated E2 (CpG-PEG-E2) was incubated the L-cysteine (Fisher) at a 20-fold excess to E2 monomer to quench unreacted maleimide groups. In order to remove unreacted CpG-SH and L-cysteine, the CpG-PEG-E2 was desalted to phosphate buffer for *in vitro* assays and to PBS for *in vivo* assays. All nanoparticles were characterized by BCA for determining protein concentration, SDS-PAGE for determining successful conjugation, and DLS for measuring particle size. All proteins were 0.22 μM filtered and stored at -80°C.

5.2.6 In Vitro Uptake Assays

Cells (BMDCs, BMDMs, CH12 B cells, B3Z T cells, and NIH 3T3 cells) were harvested and plated in a 96-well plate at 200,000 cells/well in duplicate wells in 200 μL of complete RPMI media. The E2, mPEG-E2, or CpG-PEG-E2 proteins were added to the cells at a final concentration of 5 μg/mL and 1 μg/mL for 1 hr at 37°C. Cells were subsequently harvested (gentle pipetting for BMDCs, BMDMs, CH12, and B3Z and 0.5% Trypsin for releasing NIH 3T3 cells) and prepared in PBS + 1% BSA (Fisher) and 0.02% Sodium Azide (FACS buffer). Cells were analyzed for fluorescence by flow cytometry on the BD AccuriC6 flow cytometer. MFI

was recorded and reported as relative to cells only (background fluorescence) as a measure of nanoparticle uptake. Data is presented as an average ± standard deviation of at least 3 independent experiments.

For inhibition of cellular uptake, well-established pathway-specific inhibitors and conditions were used [54]. Cells were incubated for 1 hr at 37°C with 1 μM Cytochalasin D (macropinocytosis and phagocytosis), 30 min with 5 mM amiloride HCl (macropinocytosis), 20 min with 10 μg/mL chlorpromazine (clathrin-mediated endocytosis), or 20 min with 25 μg/mL nystatin (lipid raft-mediated endocytosis). The E2 protein was then added for an additional 1 hr at 37°C and cells were harvested for analysis. For discrimination of surface bound versus internalized fluorescent particles, cells were incubated with 0.5% trypsin for 30 min at 37°C to remove surface-bound proteins. For BMDCs, staining for the surface marker CD11c was used as a control to confirm cleavage of surface receptors by trypsin.

5.2.7 Biodistribution and In Vivo Cell Interaction

Proteins (50 μg in PBS) were administered subcutaneously in the left hock region of 6-12 week old female C57BL/6 wild-type mice. Following a period of 6 hr or 48 hr animals were euthanized under 100% CO_2 and organs were excised and processed for fluorescence measurement using flow cytometry.

The spleen, thymus, ipsilateral and contralateral lymph nodes (LN; popliteal, inguinal, axillary/brachial, cervicals, iliac, renal, and mesenteric) were isolated separately for individual analysis and minced through a 70 μM cell strainer to prepare a single cell suspension. The heart, kidney, and liver were cut into ~1 mm squares and added to a 1.5 mL centrifuge tube containing 1 mL of Liberase TM (0.25 U/mL for heart and liver and 0.5 U/mL

for kidney) in PBS, incubated at 37°C for 30 min (heart and liver) or 45 min (kidney). The lung and skin from the injection site (and contralateral hock, for comparison) were cut into ~1 mm squares and incubated with 0.5 mg/mL Collagenase D (Roche) in PBS for 30 min at 37°C. All tissues were subsequently minced through a 70 μM cell strainer to remove connective tissue and clumps of dead cells. Blood was collected and centrifuged at 300 × g for 5 min to separate cells from plasma. Cells from the draining lymph nodes (dLN) were prepared in FACS buffer and subsequently stained for CD11c (DCs), CD3 (T cells), B220 (B cells), and F4/80 (macrophages), and analyzed by flow cytometry. Blood plasma was centrifuged at 18,000 × g for 5 min to remove debris and analyzed for fluorescence in a 96-well plate reader at an excitation/emission wavelength of 490/525 nm.

5.2.8 Statistical Analysis

Statistical analyses were carried out using Microsoft Excel and GraphPad Prism. Data is reported as mean ± standard error of the mean (S.E.M.) or standard deviation (S.D.) of at least three independent experiments (unless otherwise noted), with the value of a single independent experiment being the average of at least two replicates for that set. Statistical significance was determined by performing a one-way analysis of variance (ANOVA) followed by a Tukey's range test over all statistical means. P-values less than 0.05 were considered significant.

5.3 Results and Discussion

5.3.1 Methyl-PEG and CpG Were Successfully Displayed on E2

Complete conjugation of thiol-reactive Alexa Fluor to the engineered internal cysteines of the E2 nanoparticle was previously confirmed [44]. The mPEG and CpG-SH were successfully conjugated to the E2 (**Figure 5.1**). SDS-PAGE analysis demonstrated a broad band for the mPEG-E2 nanoparticle in the molecular weight range of 30-50 kDa, indicative of a range of heterogeneous attachment of a polymer with molecular weight of 2000 ± 200 Da. Similar to what we observed with peptide attachment to surface amines (**Chapters 2 and 3**), there is a range of conjugation ratios to the E2 monomer. The CpG-PEG-E2 nanoparticle displayed 2 distinct bands, corresponding to an E2 monomer functionalized with the maleimide-PEG linker only, and an E2 monomer conjugated to the CpG-SH aptamer via the mal-PEG (**Figure 5.1**). The band pattern at molecular weights > 75 kDa within the SDS-PAGE gel is consistent with what we have observed for NSH-maleimide linkers previously (**Chapter 2**), and can also be seen in the reaction with L-cysteine only (no CpG-SH) [47]. This result also clearly demonstrates that each E2 monomer is not functionalized with a CpG molecules. Depending on the conformation of the PEG (*i.e.* brush or mushroom), the maleimide functionality may not be extended and easily accessible for reaction with the CpG-SH [48]. Using NIH ImageJ analysis of the SDS-PAGE gel of the CpG-PEG-E2 nanoparticle, we measured a conjugation ratio of 15.8 ± 5.2 CpG/E2 nanoparticle. While, HPLC analysis was attempted to measure conjugation ratios, as with the gp100 peptides described previously (**Chapter 3**), the CpG-PEG-E2 nanoparticle co-eluted partially with the free CpG-SH (see **Appendix A.2**). The optimal surface density of PEG is known to vary for conjugation

of aptamers [49], and the amount of aptamer required to observe maximal targeting effects varies as well [50,51]. Therefore the number CpG/particle measured in this study may provide sufficient surface density for observable targeting effects.

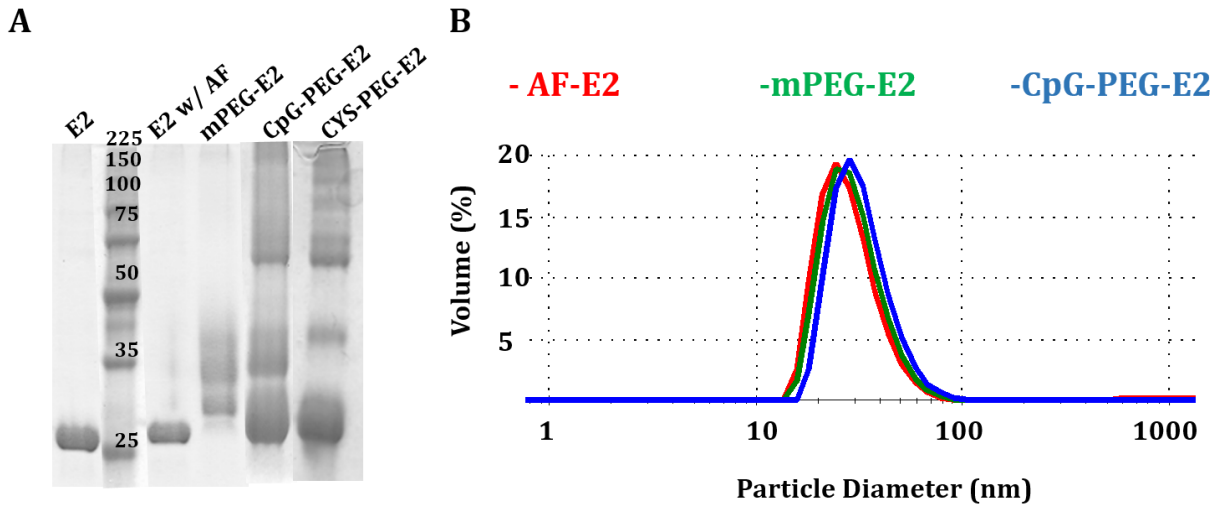

Figure 5.1. Characterization of the mPEG-E2 and CpG-PEG-E2 nanoparticles. **A)** SDS-PAGE analysis shows that the mPEG-E2 nanoparticle exhibits a broad band in the ~30-50 kDa range, indicative of heterogeneous attachment of a polymer with varying molecular weight. The CpG-PEG-E2 nanoparticle shows 2 distinct bands in the 28-34 kDa range (linker only) and in the 34-45 kDa range, linker + CpG (each PEG + CpG-SH adds ~8000 Da). **B)** DLS analysis revealed that the functionalized nanoparticles used in this study are within the optimal size reported for lymphatic transport for dendritic cell uptake (~20-45 nm) [4,18,52], with a lack of particle aggregation.

Dynamic light scattering (DLS) analysis revealed particle sizes of 29.1 ± 1.3, 30.4 ± 0.8, and 32.0 ± 0.8 for the E2, mPEG-E2, and CpG-PEG-E2 nanoparticles, respectively (**Figure 5.1**), comparable to our measured 26.8 ± 0.6 nm diameter for the base E2 nanoparticle. Functionalization with the various elements (fluorescent dye, hydrophilic polymers, and DNA) does not increase the particle size beyond what has been reported to be the optimal

range for nanoparticle access to the lymph nodes (LN) for interaction with DCs [4,18,52]. This is in agreement with our previous observed results for attachment of PEG to the surface of the E2 particle (**Chapter 4**) [40]. Additionally, DLS analysis demonstrated a lack of protein aggregation, indicating that the particle integrity had not been compromised due to the functionalization. The addition of a DNA aptamer to the PEG linker did not increase the particle size appreciably, whereas antibodies have been shown to increase the size of nanoparticle by > 100 nanometers [53].

5.3.2 E2 is Internalized by DCs through Various Mechanisms

We sought to understand whether the E2 nanoparticle is efficiently internalized by DCs, and also what mechanisms of internalization the DCs may employ. In our previous studies measuring DC uptake of E2 packaged with CpG in **Chapter 2** we did not directly determine whether the E2 nanoparticles are internalized, or simply surface bound (although the increase in DC activation would strongly indicate internalization of the E2 nanoparticles). While cellular targeting with nanoparticles can display both enhanced surface binding and/or uptake, the nanoparticle must be internalized for antigen processing.

DCs internalize the E2 nanoparticle through various mechanisms (**Figure 5.2**). BMDCs were cultured in the presence of the fluorescent nanoparticle, and were subsequently harvested and treated with trypsin to remove any surface bound particles. The addition of pharmacological uptake inhibitors to inhibit actin polymerization (cytochalasin D); clathrin-mediated endocytosis (chlorpromazine), lipid raft-mediated endocytosis

(nystatin), and macropinocytosis via inhibition of sodium-proton exchange (amiloride) [54], revealed multiple uptake mechanisms of E2 by BMDCs (**Figure 5.2**).

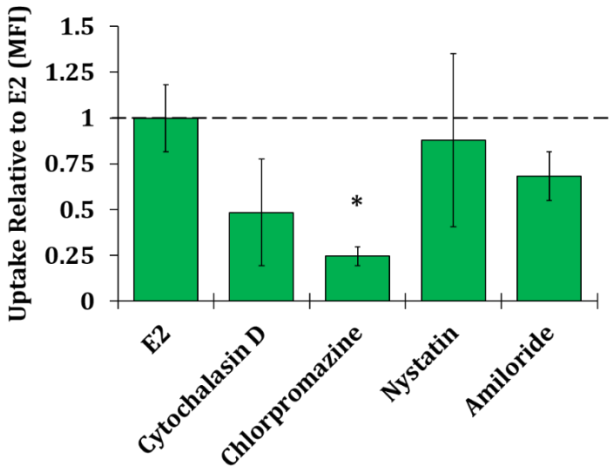

Figure 5.2. Incubation of BMDCs with various uptake inhibitors shows decreased uptake in the presence of cytochalasin D, chlorpromazine, and amiloride, indicating macropinocytic and clathrin-mediated uptake mechanisms. Conditions were chosen that have been well-established for these uptake inihibitors [54].

Our data demonstrates that blocking clathrin-mediated and macropinocytic mechanisms both decrease cellular uptake, indicating likely involvement of both mechanisms. This is consistent with observations that nanoparticles, in general, and viruses and virus-like particles exhibit cellular uptake via a wide variety of mechanisms [55-57]. Our data implicates E2 trafficking to the DC interior via macropinocytosis, likely by nature of its small optimal size relative to the larger macropinosomes [58], and also specific receptor interactions on the DC surface, triggering clathrin-coated pit formation to internalize the particle. The larger apparent effect of cytochalasin D on uptake, relative to amiloride (both reported macropinocytosis inhibitors), may be due F-actin's demonstrated variable role in clathrin-mediated uptake [59].

5.3.3 Surface Functionalization Alters Cellular Uptake

E2 associates with BMDCs significantly more than other cell types over varying concentrations (**Figure 5.3**). Besides BMDCs, other cell types tested against included bone marrow-derived macrophages (BMDMs), B cells (CH12), T cells (B3Z), and fibroblasts (NIH 3T3). Our data suggests that over a short time period, the BMDCs may take up the E2 protein more efficiently than other professional antigen presenting cells (*i.e.* BMDMs and B cells), where there is a statistically significant increase in fluorescence compared to all cell types at both 5 μg/mL and 1 μg/mL.

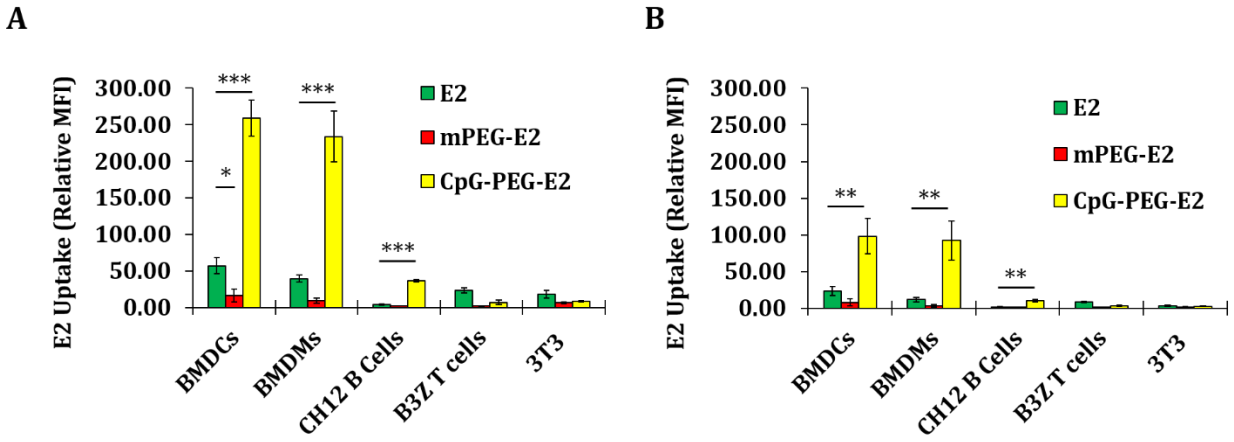

Figure 5.3. BMDCs show increased uptake of E2 *in vitro*, compared to other cell types ($p < 0.05$). Further, mPEG-E2 shows decreased cellular uptake for all cell types, and CpG-PEG-E2 shows enhanced uptake in antigen presenting cells (BMDCs, BMDMs, and CH12 B cells), compared to both E2. Cellular association was measured by recording the MFI of cells incubated with **A)** 5 μg/mL or **B)** 1 μg/mL of the E2 nanoparticle for 1 hr at 37°C. Data is reported as average ± S.D. relative to cellular background fluorescence of 3 independent experiments, and statistical significance was determined with a one-way ANOVA using a post-hoc Tukey's test; * $p < 0.05$, ** $p < 0.01$, *** $p < 0.001$.

Surface display of PEG with a molecular weight of 2000 Da decreased cellular uptake of E2 over the range of cell types tested (**Figure 5.3**). This is consistent with our previous study measuring cell uptake of the E2 nanoparticle with human macrophages (MΦ) and with human breast cancer cells (**Chapter 4**) [40], and is also consistent with the reported use of PEG to reduce cellular interactions against biomaterials, including protein nanocapsules [20,23]. This demonstrates the potential to modulate cellular interaction with the E2 nanoparticle though the use of PEG linkers. To test whether the bifunctional PEG linker used to attach the CpG aptamers exhibits the same shielding effect as mPEG, we capped the maleimide with L-cysteine (**Figure 5.1**). These cysteine-functionalized E2 nanoparticles still exhibit decreased cellular uptake, as shown with BMDCs (**Figure 5.4**), supporting our application of this polymer as a linker for ligands. Interestingly, mPEG exhibits the highest specificity for association with BMDCs *in vitro*, with significantly more BMDC fluorescence compared to B cells and T cells at all concentrations tested ($p < 0.05$). This is consistent with previous reports of PEG increasing DC specificity for nanoparticles *in vivo* [60].

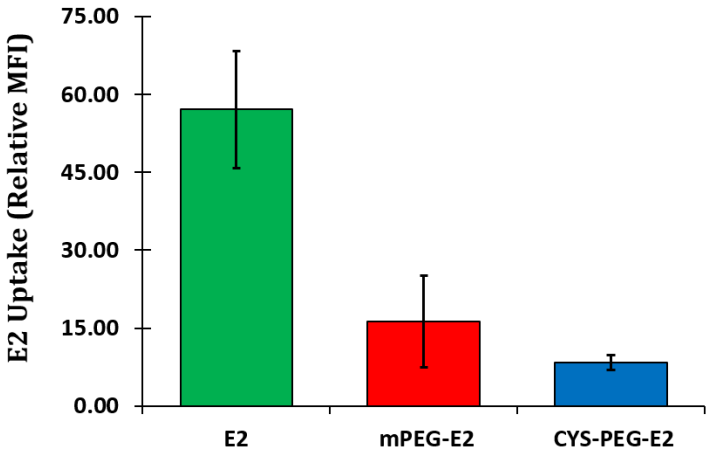

Figure 5.4. The bifunctional malemide-PEG-NHS, conjugated to E2 through NHS and capped with L-cysteine (CYS-PEG-E2) showed similar BMDC uptake reduction compared to the mPEG-E2 nanoparticle. Data for E2 and mPEG-E2 are from 3 independent experiments, and CYS-PEG-E2 is from a single experiment with duplicate wells. Data is mean MFI relative to cellular background ± S.D.

Display of the CpG DNA oligonucleotide on the surface of E2 significantly enhanced nanoparticle uptake with all APCs tested (**Figure 5.3**). Remarkably, there was ~5-fold increase in fluorescence associated with BMDCs, relative to the bare E2 nanoparticle, indicating a large increase in cell association. DNA is known to be a "sticky" molecule to cells [61], and therefore this raises the question whether display of CpG is simply causing an increase in non-specific binding to cell surface proteins of BMDCs (and other APCs), rather than increasing specific uptake. Treatment of the BMDCs, BMDMs, and B cells with trypsin showed that the majority of CpG-PEG-E2 nanoparticles were internalized by BMDCs and BMDMs, but not by B cells (**Figure 5.5**). This is in agreement with previous studies demonstrating *in vivo* that 30 nm nanoparticles were internalized by DCs and monocytes, but were mainly surface-associated with B cells [62]. We are the first, to our knowledge, to demonstrate an increase in DC targeting following display of a DNA aptamer that is a known TLR ligand. This is especially interesting, since the TLR for CpG is expressed within the endosome, rather than the outer membrane. CpG was previously reported to be a potential ligand for the receptor DEC-205 [34], a receptor involved in endocytosis and antigen processing [63]. DEC-205 is highly expressed on many DC subsets, and to a lesser degree on other cells of the immune system.

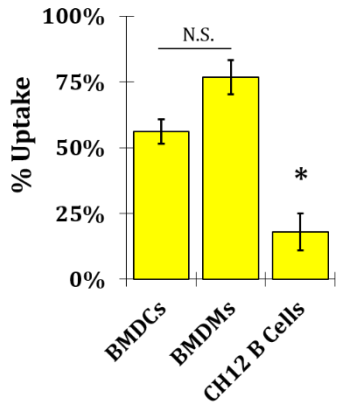

Figure 5.5. CH12 B cells show less CpG-PEG-E2 internalization compared to dendritic cells (BMDCs) and macrophages (BMDMs). Cells were incubated with 5 μg/mL of the CpG-PEG-E2 nanoparticle and subsequently treated with 0.5% trypsin to remove surface bound proteins. The percentage of fluorescence remaining following treatment with trypsin is shown. Data is reported as average S.E.M. of 3 independent experiments, and statistical significance was determined with a one way ANOVA followed by a post hoc Tukey's test (* $p < 0.05$). Significance for CH12 B cells was compared to both BMDCs and BMDMs.

As an alternative to antibody-targeting of nanoparticles to DEC-205 *in vivo* for enhanced vaccine properties [2,14,29,64], we explore the possibility of displaying a smaller, synthetically simpler DNA aptamer to achieve the same targeting capacity. As a broader impact to medicine, ligand-specific targeting of cells is a topic gaining traction in the clinical treatment of disease [65]. Aside from being a reported ligand for DEC-205, sensing of TLR danger signals are known to increase the macropinocytic activity of DCs within the microenvironment, likely an evolutionary advantage in clearing out potential pathogens in a timely manner [66]. Since B cells and MΦ are also known to express TLRs, including TLR9, it is possible that they would exhibit danger-signal induced macropinocytosis as well. Therefore, the display of CpG on the E2 nanoparticle may enhance DC uptake through multiple mechanism. However, while the observation of enhanced DC uptake *in vitro* is an exciting result, the apparent biodistribution and cellular association of the nanoparticle in a physiological setting will bear a larger impact on the potential application of this platform for targeted vaccinations.

Peptide aptamers represent another class of potential compounds for targeting nanoparticles or antigens to cells, including DCs [31,33,51]. We have explored the prospect

of attaching one such peptide (FYPSYHSTPQRP), reported to target human and mouse DCs, to the surface of the nanoparticle in a fashion similar to that for the CpG aptamers (see **Appendix A.1** for methods and **Appendix A.2** for particle characterization) [33]. Preliminary results for E2 nanoparticles displaying the peptide did not demonstrate any differences in dendritic cell association of the E2 nanoparticle (see **Appendix A.2**).

5.3.4 Surface Functionalization Alters E2 Biodistribution

Following subcutaneous (SC) administration, the E2 nanoparticle drains to most of LN ipsilateral to the injection site within the first 6 hr (**Figure 5.6A**). Virus-like nanoparticles were previously shown to remain at the site of SC injection, with continuous drainage to the popliteal LN, for up to 8 days [13]. Interestingly, in contrast to these previous reports, the draining lymph nodes (dLN) of mice injected with the E2 nanoparticle shows a drastic decrease at 48 hr compared to 6 hr, indicating lymphatic clearance (**Figure 5.6B**). Although decreased, fluorescent signal is still evident in the injection site and dLNs (**Figure 5.6B)**. This would indicate an initial burst of E2 from the site of injection toward the lymphatics early following subcutaneous administration, which is driven primarily by hydrostatic pressure. Once the fluid volume at the injection site has decreased, persistent presence of the E2 nanoparticle at the site of SC administration is to be expected, as it is known that the rate of protein diffusion away from this space is inversely proportional to molecular weight [67]. The E2 particle is not observed in any of the contralateral LN or in the mesenteric LN at either time point (**Figure 5.6C and 5.6C**). There is, however, fluorescence observed in the spleen ($p = 0.08$) and liver ($p = 0.2$) at 6 hr, albeit not at statistically significant levels (**Figure**

5.6C). This implies that a portion of the nanoparticle is exiting the subcutaneous space and away from the lymphatics into the blood stream, where it can access the spleen (the spleen does not contain afferent lymph vessels) and other blood draining organs. VLP systems reaching blood draining organs following subcutaneous administration have been observed previously [41]. However, the measured MFI seem to indicate that the majority of E2 is draining to the LN.

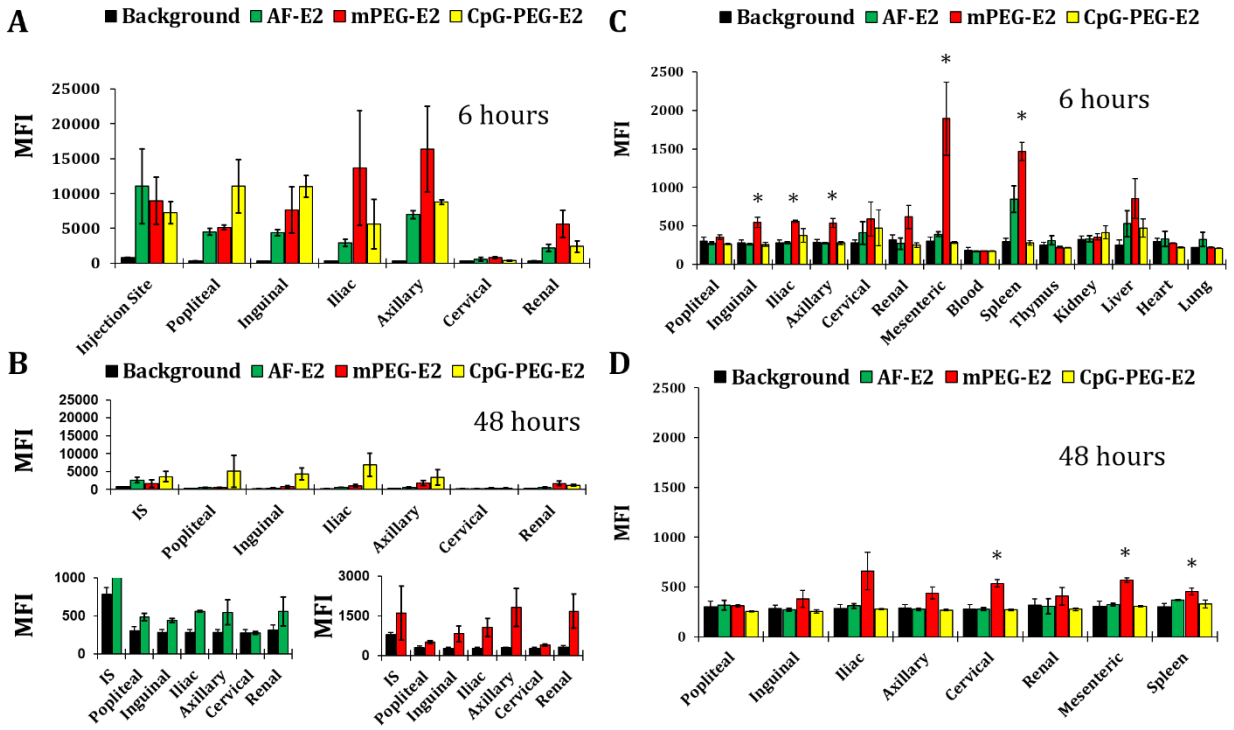

Figure 5.6. Measured fluorescence in secondary lymphoid organs and other blood draining organs following subcutaneous administration the various E2 nanoparticles. MFI was measured by flow cytometry of cells from the LN ipsilateral to the left hock injection site at **A)** 6 hr and **B)** 48 hr. The lower left panel in **B)** is zoomed in on the y-axis compared to the top panel, and shows only background and E2 (IS: injection site). Similarly the bottom right panel shows only mPEG-E2 and background (IS: injection site). **C and D)** The contralateral LN and blood draining organs were prepared and analyzed for cellular fluorescence at **C)** 6 hr and **D)** 48 hr. Data is presented as average ± S.E.M. MFI of 3 independent experiments. For statistical significance comparing each organ to background, a one way ANOVA was performed followed by a post hoc Tukey's test; * $p < 0.05$, ** $p < 0.01$.

The mPEG-E2 nanoparticle exhibited an altered distribution within the dLNs, compared to the non-surface-functionalized E2. Whereas the E2 nanoparticle showed a relatively even dissemination amongst the dLN, the mPEG-E2 nanoparticle showed a trend of increased fluorescence signal in the most distal dLN (*i.e.* axillary/brachial), compared to the most proximal (*i.e.* popliteal) at both time points, although statistical differences were not measured. Remarkably, the mPEG-E2 particle is observed in the contralateral and mesenteric LN, as well, a further indication of increased lymphatic drainage of PEGylated protein nanoparticles. Within blood draining organs, mPEG-E2 is found in the spleen and liver at elevated levels compared to E2, where statistically significant fluorescence was observed in the spleen above background ($p < 0.05$). Our observation is in agreement with previous literature reporting that PEGylation of particulate biomaterials enhances their ability to drain faster from the immunization site toward the dLN [68]. It is likely that a reduction in protein adsorption and cellular interactions within the injection site and initial lymphatics allows further distribution throughout the lymphatics and deposition in more distal sites. Interestingly, the mPEG-E2 nanoparticle was the only particle in this study that was also at measurable and significant levels in the blood plasma (**Figure 5.7**), where protein nanoparticles are shown to have rapid clearance [41-43]. Adenovirus VLPs used at gene therapy platforms had previously shown enhanced pharmacokinetic profiles following PEGylation, and our results are in agreement with these previous reports [69,70].

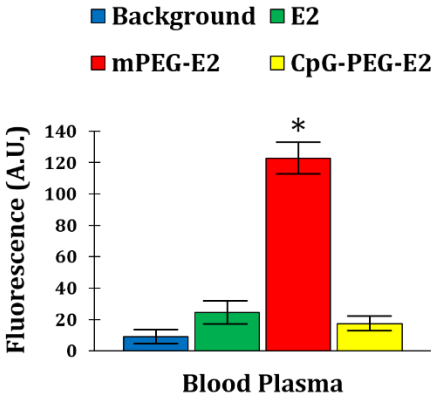

Figure 5.7. Blood plasma fluorescence was determined 6 hr following 50 μg subcutaneously administered E2 nanoparticles. Data is reported at average S.E.M. blood plasma fluorescence of 3 independent experiments. Statistical significance was determined with a one way ANOVA followed by a post hoc Tukey's test (* $p < 0.05$, compared to all other groups).

CpG-PEG-E2 shows a LN distribution similar to that of E2 at 6 hr, but exhibits a trend of increased presence in the dLN (**Figure 5.6**). The lack of CpG-PEG-E2 presence in the contralateral LN, mesenteric LN, and any blood draining organ other than the liver are a further indication of particle retention within the more proximal regions to the administration site. While fluorescence was not evident in the spleen, the dLN were shown to play a more important acute role in priming $CD8^+$ T cell responses toward viruses, which trigger cell-mediated immune responses that are also important for other diseases like cancer [72]. The CpG-PEG-E2 nanoparticle also displays increased dLN retention over time, where our results clearly show elevated fluorescence compared to E2 and mPEG-E2 at 48 hr (**Figure 5.6B**). CpG is a polysaccharide, and polysaccharide-based nanoparticles were also shown to be retained within the LN up to at least 48 hr [71]. Therefore, it may be the basic chemical properties of the CpG that are enabling retention, or it may be that the TLR-induced danger signaling associated with this aptamer creates a heightened level of APC activity within dLN, actively taking up large amounts of CpG-PEG-E2 before it can diffuse away. In

any case, LN retention of antigens is known to be an important variable for immunotherapy, particularly with biomaterials [2].

All of the E2 particles tested here showed a lack of significant fluorescence at 48 hr in the blood or blood draining organs of the mice, consistent with studies showing that nanoparticles with 30 nm diameters peak in non-lymphoid organs at 6-12 hr following SC injection [62]. While PEGylation is known to exhibit enhanced blood pharmacokinetic profiles for protein particles and also LN accumulation [60,70], PEGylated nanoparticles are also known to experience the accelerated blood clearance phenomenon [73]. While the fluorescence signal is decreased, the mPEG-E2 nanoparticle is still present at significant levels in the contralateral LN and spleen, whereas E2 is not.

5.3.5 E2 Nanoparticles Exhibit High Specificity for DCs In Vivo

At 6 hr, ~20% of the fluorescent cells are DCs (**Figure 5.8**). Although DC make up a minority of cells within the LN (< 5%), our results are consistent with the notion that APCs interact most efficiently with vaccine delivery vehicles in the size range of 20-2000 nm [4]. Biodistribution studies with 200 nm polystyrene beads showed a similar cellular trend, compared to the E2 [60]. We observe much higher DC interaction with the non-functionalized nanoparticle, compared to this previous study, where they show less than 5% of the nanoparticle containing cells are DCs [60]. PEGylation was demonstrated to increase DC specificity toward nanoparticles in this previous study as well [60]. Interestingly, we do not observe any measurable difference between cellular association with DCs, regardless of the surface functionality examined.

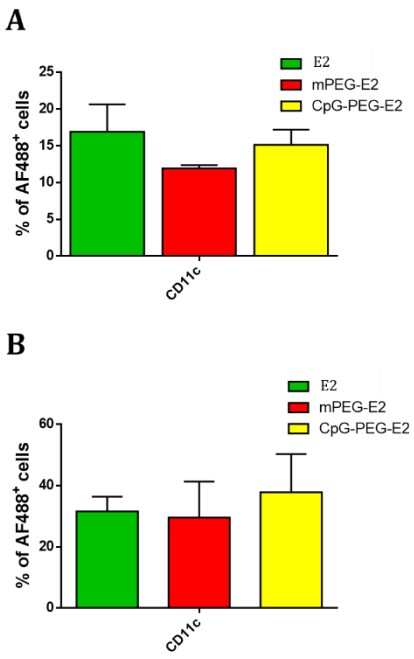

Figure 5.8. The percentage of Alexa Fluor 488 positive (AF488+) cells that were DCs was determined at **A)** 6 hr or **B)** 48 hr following subcutaneous administration. Data is reported as average ± S.E.M. of percentage of cells positive for AF488 of 3 independent experiments. Statistical significance was tested using a one way ANOVA followed by a post hoc Tukey's test. There is no statistical differences between the different nanoparticles tested.

5.3.6 mPEG-E2 and CpG-PEG-E2 Show Increased Association with APCs

Within a given population of cells, all of the nanoparticles tested interact with roughly the same percentage of a given subset of cells at 6 hr, regardless of surface functionality (**Figure 5.9A**). At 6 hr, ~50% of the DC population is associated with the E2 nanoparticle, a relatively high percentage compared to other nanoparticle studies looking at the same metric, including VLPs [13,62]. Additionally, a relatively low overall percentage of the B220+ population is associated with the nanoparticles, which also decreases over time (**Figure 5.9**), while the $CD11c^+$ and $F4/80^+$ populations show a less dramatic decrease, compared to T cell and B cell. Studies with VLPs have also shown ~2% B cell association at 48 hr, similar to our observations at 48 hr [13]. This implies that as the microenvironment of the LN is given time

to equilibrate following an initial burst of nanoparticle release from the injection site, interaction with cell types other than DCs and MΦ greatly decreases. For vaccine purposes, persistence within the APC population is critical for immunotherapeutic success, where CTL function is desired [2].

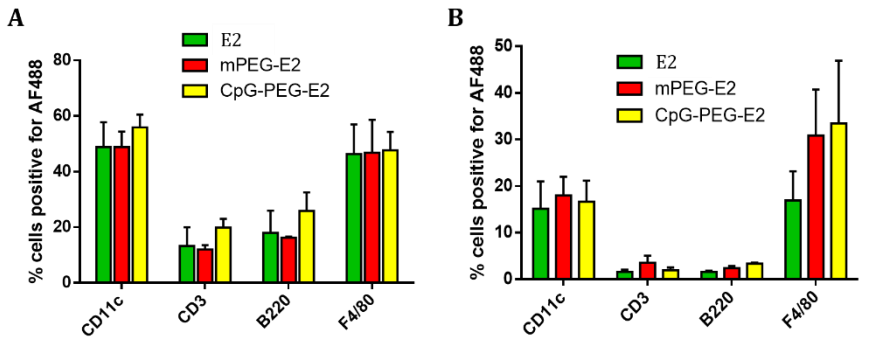

Figure 5.9. The percentage of a cellular population within the LN that are Alexa Fluor 488 positive (AF488+) was determined by flow cytometry after **A)** 6 hr or **B)** 48 hr following subcutaneous administration. Cells tested for AF488 were dendritic cells (CD11c), T cells (CD3), B cells (B220), and macrophages (F4/80). Data is reported as average ± S.E.M. of percentage of cells positive for AF488 of 3 independent experiments.

Interestingly, while PEGylation or display of CpG does not have any significant measurable effect on the amount of the DC population that interacts with E2, it appears that interaction with F4/80$^+$ cells is enhanced after 48 hours following PEGylation and display of CpG, compared to the base E2, although not at statistically significant levels. As noted, the F4/80$^+$ population could potentially represent the MΦ naturally present within the LN, or Langerhans DCs, which are present in the subcutaneous space where the nanoparticles are injected. Uptake and potential activation by the CpG of these cell types would trigger migration to the LN for T cell interaction.

We next asked the question whether the fluorescent B220^{+} cells are in fact B cells, or possibly B220+ plasmacytoid DCs (**Figure 5.10**) [81]. Interestingly, we found that at 48 hr, ~40% of the B220+ cells are also CD11c+, for all of the E2 nanoparticles. Therefore, at 48 hr, where ~50% of the fluorescent cells are B220+, < 25% are B cells. Plasmacytoid DCs were previously shown to interact with a Qβ–based VLP immunotherapy platform that is undergoing clinical trial for melanoma [13,82]. The observation of plasmacytoid DC interaction is considered a positive event for cancer immunotherapy, since this class of DCs express high levels of TLR9 and are potent producers of type I interferons, which strongly support cell-mediated anti-viral immunity and important also for cancer [83]. It is also possible, however, that the CD11c+B220+ cells are activated B cells, since some subsets of B cells are known to occasionally express CD11c [84,85].

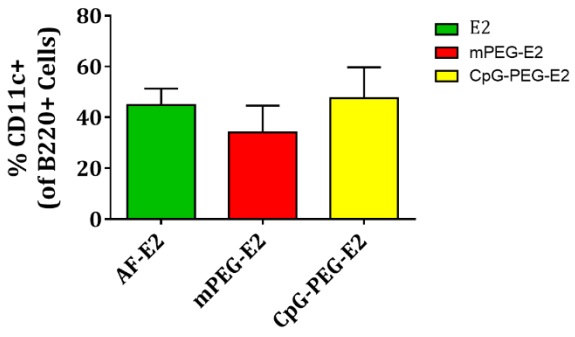

Figure 5.10. The percentage of Alexa Fluor 488 positive cells that were also B220+ were analyzed for CD11c expression (*i.e.* plasmacytoid DCs). Data is presented as average S.E.M. of the percentage of B220+ cells that are also CD11c+ of 3 independent experiments.

5.3.7 CpG-PEG-E2 Shows Increased DC Uptake

While LN fluorescence remains elevated for the CpG-PEG-E2 nanoparticle compared to mPEG-E2 and E2 (**Figure 5.6**), there is a lack in any statistical differences in cellular association between the nanoparticles (**Figure 5.9**). This begs the question as to whether the cells that are interacting with CpG-PEG-E2 are associating with more particles per cell, as we observed *in vitro* (**Figure 5.3**). At both 6 hr and 48 hr, the CpG-PEG-E2 nanoparticle showed a significant increase in DC fluorescence (**Figure 5.11**), indicating much higher uptake of CpG-PEG-E2 compared to the mPEG-E2 or E2 nanoparticles, in good agreement with our *in vitro* data (**Figure 5.3**). We also observe the trend of increased fluorescence of F4/80+ cells, for both mPEG-E2 (at 48 hr) and CpG-PEG-E2 (at 6 hr and 48 hr). PEGylation of nanoparticles was previously reported to increase specific uptake by DCs, and it could be that we observing that trend as well for MΦ or Langerhans cells [60].

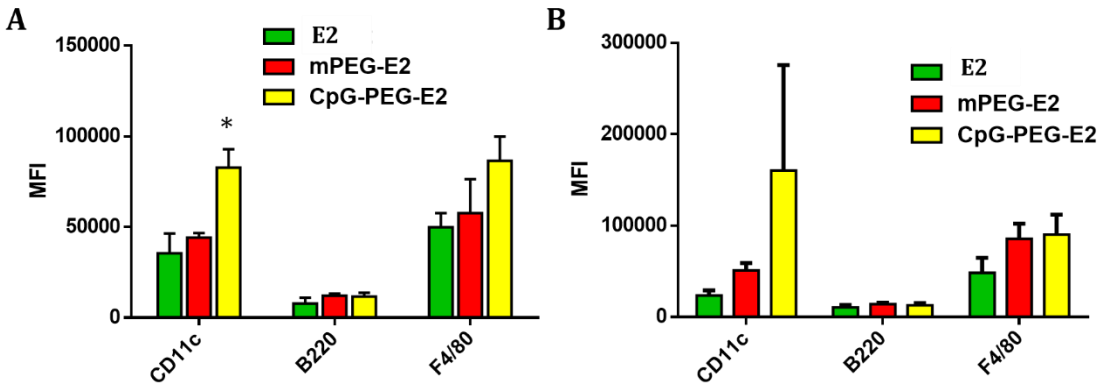

Figure 5.11. The MFI (E2 uptake extent on a single cell level) of Alexa Fluor 488 positive cells was determined by flow cytometry after **A)** 6 hr or **B)** 48 hr following subcutaneous administration. Cells tested for AF488 were dendritic cells (CD11c), B cells (B220), and macrophages (F4/80). Data is reported as average ± S.E.M. MFI of 3 independent experiments. Statistical significance was determined using a one way ANOVA followed by a post hoc Tukey's test (* $p < 0.05$).

As mentioned earlier, CpG was a reported ligand for DEC-205, and therefore we sought to understand whether DEC-205$^+$ DCs are responsible for the large increase in CpG-PEG-E2 association [34]. We observed an increase in fluorescence of DEC-205$^+$ DC for mice injected with the CpG-PEG-E2 nanoparticle at 6 hr, compared to E2 (**Figure 5.12A**). While there is an increase in fluorescence of DEC-205$^+$ DC at 6 hr for CpG-PEG-E2, the measured difference was not significant. However, the CpG-PEG-E2 nanoparticle showed increased fluorescence of DEC-205$^+$ DC in all 3 injections, compared to the E2 nanoparticle (**Figure 5.13A**, lower panel). Interestingly, the mPEG-E2 nanoparticle showed similar fluorescence compared to the CpG-PEG-E2 nanoparticle, indicating a possible increase in specificity for DEC-205$^+$ DCs simply by surface display of PEG [60]. At 48 hr all of the particles showed a similar fluorescence in the CD11c$^+$DEC-205$^+$ cell population. Therefore, remarkably, the large increase in fluorescence observed for DCs with the CpG-PEG-E2 nanoparticle is not due primarily to association with DEC-205$^+$ DCs, but rather other DC subsets. This is in stark contrast to the reports of CpG being a DEC-205 ligand. As mentioned earlier, TLR danger signals are known to enhance the macropinocytic activity of DCs [66]. Therefore, it is likely that the initial danger signaling triggered by the CpG on the surface of CpG-PEG-E2 is causing a burst of macropinocytic activity within the DC population. Macropinocytosis has the potential to uptake more E2 nanoparticles per macropinosome, compared to receptor-mediated endocytosis (*i.e.*, DEC-205-mediated). It could be that we are observing danger signal-induced uptake activity amongst all DC subsets outcompeting receptor-specific events.

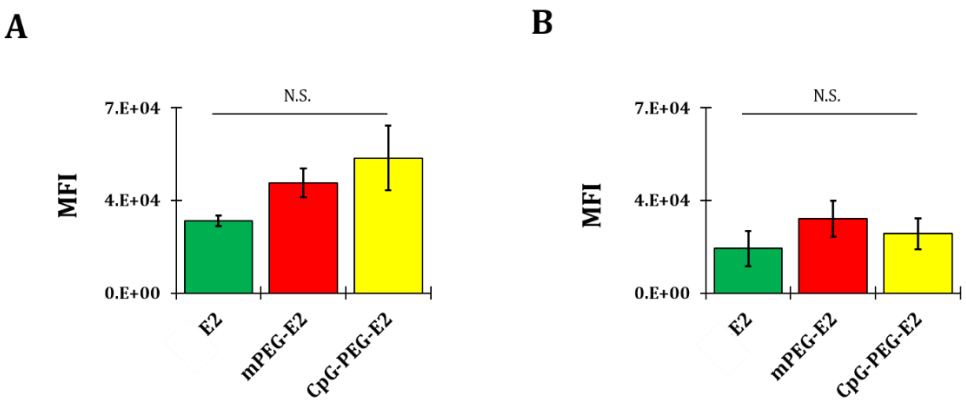

Figure 5.12. The MFI (E2 uptake extent on a single cell level) of Alexa Fluor 488 positive CD11c+/DEC-205+ cells was determined by flow cytometry after **A)** 6 hr or **B)** 48 hr following subcutaneous administration. Data is reported as average ± S.E.M. MFI of 3 independent experiments. The lower panel of **A)** shows the distribution of individual data points of the upper panel. Statistical significance was determined using a one way ANOVA followed by a post hoc Tukey's test.

5.4 Conclusions

We have demonstrated *in vitro* that the PEGylation of E2 reduces cellular uptake by both phagocytic and non-phagocytic cell lines. Surface display of CpG, a reported ligand for DEC-205, on a PEG linker significantly increased APC-specific uptake of the E2 nanoparticle. *In vivo*, the CpG-PEG-E2 nanoparticle showed a significant increase in cellular association with DCs within the dLN, compared to the other nanoparticles tested. The CpG-PEG-E2 nanoparticle also demonstrated increased LN retention over 48 hr, and less presence in blood draining organs, compared to the E2 and mPEG-E2 nanoparticles. All of the nanoparticles showed a similar distribution amongst the different cell types present within the LN.

5.5 References

1. Albanese A, Tang PS, Chan WC: The effect of nanoparticle size, shape, and surface chemistry on biological systems. *Annu Rev Biomed Eng* 2012, 14:1-16.
2. Andorko JI, Hess KL, Jewell CM: Harnessing biomaterials to engineer the LN microenvironment for immunity or tolerance. *AAPS J* 2015, 17:323-338.
3. Reddy ST, Swartz MA, Hubbell JA: Targeting dendritic cells with biomaterials: developing the next generation of vaccines. *Trends in Immunology* 2006, 27:573-579.
4. Bachmann MF, Jennings GT: Vaccine delivery: a matter of size, geometry, kinetics and molecular patterns. *Nat Rev Immunol* 2010, 10:787-796.
5. Mills KH: Designer adjuvants for enhancing the efficacy of infectious disease and cancer vaccines based on suppression of regulatory T cell induction. *Immunol Lett* 2009, 122:108-111.
6. Swartz MA, Hirosue S, Hubbell JA: Engineering approaches to immunotherapy. *Sci Transl Med* 2012, 4:148rv149.
7. Irvine DJ, Swartz MA, Szeto GL: Engineering synthetic vaccines using cues from natural immunity. *Nat Mater* 2013, 12:978-990.
8. Bolhassani A, Safaiyan S, Rafati S: Improvement of different vaccine delivery systems for cancer therapy. *Mol Cancer* 2011, 10:3.
9. Arany PR, Mooney DJ: At the edge of translation - materials to program cells for directed differentiation. *Oral Dis* 2011, 17:241-251.
10. Ali OA, Huebsch N, Cao L, Dranoff G, Mooney DJ: Infection-mimicking materials to program dendritic cells in situ. *Nat Mater* 2009, 8:151-158.
11. Nagda P: Implantable melanoma vaccine enters human clinical trials. *Immunotherapy* 2013, 5:1277.
12. Krishnamachari Y, Geary SM, Lemke CD, Salem AK: Nanoparticle delivery systems in cancer vaccines. *Pharm Res* 2011, 28:215-236.
13. Manolova V, Flace A, Bauer M, Schwarz K, Saudan P, Bachmann MF: Nanoparticles target distinct dendritic cell populations according to their size. *Eur J Immunol* 2008, 38:1404-1413.
14. Ueno H, Klechevsky E, Schmitt N, Ni L, Flamar AL, Zurawski S, Zurawski G, Palucka K, Banchereau J, Oh S: Targeting human dendritic cell subsets for improved vaccines. *Seminars in Immunology* 2011, 23:21-27.
15. Zhang N, Bevan MJ: CD8(+) T cells: foot soldiers of the immune system. *Immunity* 2011, 35:161-168.
16. Banchereau J, Steinman RM: Dendritic cells and the control of immunity. *Nature* 1998, 392:245-252.
17. Mildner A, Jung S: Development and function of dendritic cell subsets. *Immunity* 2014, 40:642-656.
18. Reddy ST, van der Vlies AJ, Simeoni E, Angeli V, Randolph GJ, O'Neil CP, Lee LK, Swartz MA, Hubbell JA: Exploiting lymphatic transport and complement activation in nanoparticle vaccines. *Nat Biotechnol* 2007, 25:1159-1164.
19. De Geest B, Snoeys J, Van Linthout S, Lievens J, Collen D: Elimination of innate immune responses and liver inflammation by PEGylation of adenoviral vectors and methylprednisolone. *Hum Gene Ther* 2005, 16:1439-1451.
20. Steinmetz NF, Manchester M: PEGylated viral nanoparticles for biomedicine: the impact of PEG chain length on VNP cell interactions in vitro and ex vivo. *Biomacromolecules* 2009, 10:784-792.
21. Franz S, Rammelt S, Scharnweber D, Simon JC: Immune responses to implants - a review of the implications for the design of immunomodulatory biomaterials. *Biomaterials* 2011, 32:6692-6709.

22. Jain A, Jain SK: PEGylation: an approach for drug delivery. A review. *Crit Rev Ther Drug Carrier Syst* 2008, 25:403-447.
23. Wattendorf U, Merkle HP: PEGylation as a tool for the biomedical engineering of surface modified microparticles. *J Pharm Sci* 2008, 97:4655-4669.
24. Cruz LJ, Tacken PJ, Fokkink R, Figdor CG: The influence of PEG chain length and targeting moiety on antibody-mediated delivery of nanoparticle vaccines to human dendritic cells. *Biomaterials* 2011, 32:6791-6803.
25. Boscardin SB, Hafalla JC, Masilamani RF, Kamphorst AO, Zebroski HA, Rai U, Morrot A, Zavala F, Steinman RM, Nussenzweig RS, et al.: Antigen targeting to dendritic cells elicits long-lived T cell help for antibody responses. *J Exp Med* 2006, 203:599-606.
26. Bonifaz LC, Bonnyay DP, Charalambous A, Darguste DI, Fujii S, Soares H, Brimnes MK, Moltedo B, Moran TM, Steinman RM: In vivo targeting of antigens to maturing dendritic cells via the DEC-205 receptor improves T cell vaccination. *J Exp Med* 2004, 199:815-824.
27. He C, Hu Y, Yin L, Tang C, Yin C: Effects of particle size and surface charge on cellular uptake and biodistribution of polymeric nanoparticles. *Biomaterials* 2010, 31:3657-3666.
28. Fay F, Scott CJ: Antibody-targeted nanoparticles for cancer therapy. *Immunotherapy* 2011, 3:381-394.
29. Cruz LJ, Rosalia RA, Kleinovink JW, Rueda F, Lowik CW, Ossendorp F: Targeting nanoparticles to CD40, DEC-205 or CD11c molecules on dendritic cells for efficient CD8(+) T cell response: a comparative study. *J Control Release* 2014, 192:209-218.
30. Kumar S, Aaron J, Sokolov K: Directional conjugation of antibodies to nanoparticles for synthesis of multiplexed optical contrast agents with both delivery and targeting moieties. *Nat Protoc* 2008, 3:314-320.
31. Jung SN, Kang SK, Yeo GH, Li HY, Jiang T, Nah JW, Bok JD, Cho CS, Choi YJ: Targeted delivery of vaccine to dendritic cells by chitosan nanoparticles conjugated with a targeting Peptide ligand selected by phage display technique. *Macromol Biosci* 2015, 15:395-404.
32. Yu W, Ming ZX, Fang W, Shuai W, Cheng WZ, Yan DZ, Qi YJ, Yun YJ: Design, expression, and characterization of a novel dendritic cell-targeted proteins. *Biochem Biophys Res Commun* 2015.
33. Curiel TJ, Morris C, Brumlik M, Landry SJ, Finstad K, Nelson A, Joshi V, Hawkins C, Alarez X, Lackner A, et al.: Peptides identified through phage display direct immunogenic antigen to dendritic cells. *J Immunol* 2004, 172:7425-7431.
34. Lahoud MH, Ahmet F, Zhang JG, Meuter S, Policheni AN, Kitsoulis S, Lee CN, O'Keeffe M, Sullivan LC, Brooks AG, et al.: DEC-205 is a cell surface receptor for CpG oligonucleotides. *Proc Natl Acad Sci U S A* 2012, 109:16270-16275.
35. Kaczmarczyk SJ, Sitaraman K, Young HA, Hughes SH, Chatterjee DK: Protein delivery using engineered virus-like particles. *Proc Natl Acad Sci U S A* 2011, 108:16998-17003.
36. Uchida M, Klem MT, Allen M, Suci P, Flenniken M, Gillitzer E, Varpness Z, Liepold LO, Young M, Douglas T: Biological containers: Protein cages as multifunctional nanoplatforms. *Advanced Materials* 2007, 19:1025-1042.
37. Plummer EM, Manchester M: Viral nanoparticles and virus-like particles: platforms for contemporary vaccine design. *Wiley Interdisciplinary Reviews-Nanomedicine and Nanobiotechnology* 2011, 3:174-196.
38. Yildiz I, Shukla S, Steinmetz NF: Applications of viral nanoparticles in medicine. *Curr Opin Biotechnol* 2011, 22:901-908.
39. Heath WR, Belz GT, Behrens GM, Smith CM, Forehan SP, Parish IA, Davey GM, Wilson NS, Carbone FR, Villadangos JA: Cross-presentation, dendritic cell subsets, and the generation of immunity to cellular antigens. *Immunol Rev* 2004, 199:9-26.

40. Molino NM, Bilotkach K, Fraser DA, Ren D, Wang SW: Cell Uptake and Complement Responses Toward Polymer-Functionalized Protein Nanocapsules. *Biomacromolecules* 2012, 13:974–981.
41. Cubas R, Zhang S, Kwon S, Sevick-Muraca EM, Li M, Chen C, Yao Q: Virus-like particle (VLP) lymphatic trafficking and immune response generation after immunization by different routes. *J Immunother* 2009, 32:118-128.
42. Kaiser CR, Flenniken ML, Gillitzer E, Harmsen AL, Harmsen AG, Jutila MA, Douglas T, Young MJ: Biodistribution studies of protein cage nanoparticles demonstrate broad tissue distribution and rapid clearance in vivo. *Int J Nanomedicine* 2007, 2:715-733.
43. Singh P, Prasuhn D, Yeh RM, Destito G, Rae CS, Osborn K, Finn MG, Manchester M: Bio-distribution, toxicity and pathology of cowpea mosaic virus nanoparticles in vivo. *J Control Release* 2007, 120:41-50.
44. Dalmau M, Lim S, Chen HC, Ruiz C, Wang SW: Thermostability and molecular encapsulation within an engineered caged protein scaffold. *Biotechnol Bioeng* 2008, 101:654-664.
45. Aida Y, Pabst MJ: Removal of endotoxin from protein solutions by phase separation using Triton X-114. *J Immunol Methods* 1990, 132:191-195.
46. Lutz MB, Kukutsch N, Ogilvie AL, Rossner S, Koch F, Romani N, Schuler G: An advanced culture method for generating large quantities of highly pure dendritic cells from mouse bone marrow. *J Immunol Methods* 1999, 223:77-92.
47. Molino NM, Anderson AK, Nelson EL, Wang SW: Biomimetic protein nanoparticles facilitate enhanced dendritic cell activation and cross-presentation. *ACS Nano* 2013, 7:9743-9752.
48. Jokerst JV, Lobovkina T, Zare RN, Gambhir SS: Nanoparticle PEGylation for imaging and therapy. *Nanomedicine (Lond)* 2011, 6:715-728.
49. Hak S, Helgesen E, Hektoen HH, Huuse EM, Jarzyna PA, Mulder WJ, Haraldseth O, Davies Cde L: The effect of nanoparticle polyethylene glycol surface density on ligand-directed tumor targeting studied in vivo by dual modality imaging. *ACS Nano* 2012, 6:5648-5658.
50. Ashley CE, Carnes EC, Phillips GK, Durfee PN, Buley MD, Lino CA, Padilla DP, Phillips B, Carter MB, Willman CL, et al.: Cell-specific delivery of diverse cargos by bacteriophage MS2 virus-like particles. *ACS Nano* 2011, 5:5729-5745.
51. Stefanick JF, Ashley JD, Kiziltepe T, Bilgicer B: A systematic analysis of peptide linker length and liposomal polyethylene glycol coating on cellular uptake of peptide-targeted liposomes. *ACS Nano* 2013, 7:2935-2947.
52. Reddy ST, Rehor A, Schmoekel HG, Hubbell JA, Swartz MA: In vivo targeting of dendritic cells in LN with poly(propylene sulfide) nanoparticles. *J Control Release* 2006, 112:26-34.
53. Aktas Y, Yemisci M, Andrieux K, Gursoy RN, Alonso MJ, Fernandez-Megia E, Novoa-Carballal R, Quinoa E, Riguera R, Sargon MF, et al.: Development and brain delivery of chitosan-PEG nanoparticles functionalized with the monoclonal antibody OX26. *Bioconjug Chem* 2005, 16:1503-1511.
54. Ivanov AI: Pharmacological inhibition of endocytic pathways: is it specific enough to be useful? *Methods Mol Biol* 2008, 440:15-33.
55. Win SJ, Ward VK, Dunbar PR, Young SL, Baird MA: Cross-presentation of epitopes on virus-like particles via the MHC I receptor recycling pathway. *Immunol Cell Biol* 2011, 89:681-688.
56. Kuhn DA, Vanhecke D, Michen B, Blank F, Gehr P, Petri-Fink A, Rothen-Rutishauser B: Different endocytotic uptake mechanisms for nanoparticles in epithelial cells and macrophages. *Beilstein J Nanotechnol* 2014, 5:1625-1636.
57. Mercer J, Helenius A: Virus entry by macropinocytosis. *Nat Cell Biol* 2009, 11:510-520.
58. Norbury CC: Drinking a lot is good for dendritic cells. *Immunology* 2006, 117:443-451.
59. Fujimoto LM, Roth R, Heuser JE, Schmid SL: Actin assembly plays a variable, but not obligatory role in receptor-mediated endocytosis in mammalian cells. *Traffic* 2000, 1:161-171.

60. Zhan X, Tran KK, Shen H: Effect of the poly(ethylene glycol) (PEG) density on the access and uptake of particles by antigen-presenting cells (APCs) after subcutaneous administration. *Mol Pharm* 2012, 9:3442-3451.
61. Renner WA, Jordan M, Eppenberger HM, Leist C: Cell-cell adhesion and aggregation: Influence on the growth behavior of CHO cells. *Biotechnol Bioeng* 1993, 41:188-193.
62. Kourtis IC, Hirosue S, de Titta A, Kontos S, Stegmann T, Hubbell JA, Swartz MA: Peripherally administered nanoparticles target monocytic myeloid cells, secondary lymphoid organs and tumors in mice. *PLoS One* 2013, 8:e61646.
63. Jiang W, Swiggard WJ, Heufler C, Peng M, Mirza A, Steinman RM, Nussenzweig MC: The receptor DEC-205 expressed by dendritic cells and thymic epithelial cells is involved in antigen processing. *Nature* 1995, 375:151-155.
64. Dhodapkar MV, Sznol M, Zhao B, Wang D, Carvajal RD, Keohan ML, Chuang E, Sanborn RE, Lutzky J, Powderly J, et al.: Induction of antigen-specific immunity with a vaccine targeting NY-ESO-1 to the dendritic cell receptor DEC-205. *Sci Transl Med* 2014, 6:232ra251.
65. van der Meel R, Vehmeijer LJ, Kok RJ, Storm G, van Gaal EV: Ligand-targeted particulate nanomedicines undergoing clinical evaluation: current status. *Adv Drug Deliv Rev* 2013, 65:1284-1298.
66. West MA, Wallin RP, Matthews SP, Svensson HG, Zaru R, Ljunggren HG, Prescott AR, Watts C: Enhanced dendritic cell antigen capture via toll-like receptor-induced actin remodeling. *Science* 2004, 305:1153-1157.
67. Wu F, Bhansali SG, Law WC, Bergey EJ, Prasad PN, Morris ME: Fluorescence imaging of the LN uptake of proteins in mice after subcutaneous injection: molecular weight dependence. *Pharm Res* 2012, 29:1843-1853.
68. Xie Y, Bagby TR, Cohen MS, Forrest ML: Drug delivery to the lymphatic system: importance in future cancer diagnosis and therapies. *Expert Opin Drug Deliv* 2009, 6:785-792.
69. Yao X, Yoshioka Y, Morishige T, Eto Y, Watanabe H, Okada Y, Mizuguchi H, Mukai Y, Okada N, Nakagawa S: Systemic administration of a PEGylated adenovirus vector with a cancer-specific promoter is effective in a mouse model of metastasis. *Gene Ther* 2009, 16:1395-1404.
70. O'Riordan CR, Song A: PEGylated adenovirus for targeted gene therapy. *Methods Mol Biol* 2008, 434:133-160.
71. Vicente S, Goins BA, Sanchez A, Alonso MJ, Phillips WT: Biodistribution and LN retention of polysaccharide-based immunostimulating nanocapsules. *Vaccine* 2014, 32:1685-1692.
72. Olson MR, McDermott DS, Varga SM: The initial draining LN primes the bulk of the CD8 T cell response and influences memory T cell trafficking after a systemic viral infection. *PLoS Pathog* 2012, 8:e1003054.
73. Abu Lila AS, Kiwada H, Ishida T: The accelerated blood clearance (ABC) phenomenon: clinical challenge and approaches to manage. *J Control Release* 2013, 172:38-47.
74. Kim YH, Lee SH, Yoo YC, Lee J, Park JH, Park SR: Kinetic Analysis of CpG-Induced Mouse B Cell Growth and Ig Production. *Immune Netw* 2012, 12:89-95.
75. Jiang W, Lederman MM, Harding CV, Rodriguez B, Mohner RJ, Sieg SF: TLR9 stimulation drives naive B cells to proliferate and to attain enhanced antigen presenting function. *Eur J Immunol* 2007, 37:2205-2213.
76. Swartz MA, Hubbell JA, Reddy ST: Lymphatic drainage function and its immunological implications: from dendritic cell homing to vaccine design. *Semin Immunol* 2008, 20:147-156.
77. Pal I, Ramsey JD: The role of the lymphatic system in vaccine trafficking and immune response. *Adv Drug Deliv Rev* 2011, 63:909-922.
78. Benvenuti F, Lagaudriere-Gesbert C, Grandjean I, Jancic C, Hivroz C, Trautmann A, Lantz O, Amigorena S: Dendritic cell maturation controls adhesion, synapse formation, and the duration of the interactions with naive T lymphocytes. *J Immunol* 2004, 172:292-301.

79. Hume DA, Robinson AP, MacPherson GG, Gordon S: The mononuclear phagocyte system of the mouse defined by immunohistochemical localization of antigen F4/80. Relationship between macrophages, Langerhans cells, reticular cells, and dendritic cells in lymphoid and hematopoietic organs. *J Exp Med* 1983, 158:1522-1536.
80. Hume DA: Macrophages as APC and the dendritic cell myth. *J Immunol* 2008, 181:5829-5835.
81. Reizis B, Bunin A, Ghosh HS, Lewis KL, Sisirak V: Plasmacytoid dendritic cells: recent progress and open questions. *Annu Rev Immunol* 2011, 29:163-183.
82. Speiser DE, Schwarz K, Baumgaertner P, Manolova V, Devevre E, Sterry W, Walden P, Zippelius A, Conzett KB, Senti G, et al.: Memory and effector CD8 T-cell responses after nanoparticle vaccination of melanoma patients. *J Immunother* 2010, 33:848-858.
83. Dunn GP, Bruce AT, Sheehan KC, Shankaran V, Uppaluri R, Bui JD, Diamond MS, Koebel CM, Arthur C, White JM, et al.: A critical function for type I interferons in cancer immunoediting. *Nat Immunol* 2005, 6:722-729.
84. Racine R, Chatterjee M, Winslow GM: CD11c expression identifies a population of extrafollicular antigen-specific splenic plasmablasts responsible for CD4 T-independent antibody responses during intracellular bacterial infection. *J Immunol* 2008, 181:1375-1385.
85. Baumjohann D, Preite S, Reboldi A, Ronchi F, Ansel KM, Lanzavecchia A, Sallusto F: Persistent antigen and germinal center B cells sustain T follicular helper cell responses and phenotype. *Immunity* 2013, 38:596-605.
86. Kim YK, Que R, Wang SW, Liu WF: Modification of biomaterials with a self-protein inhibits the macrophage response. *Adv Healthc Mater* 2014, 3:989-994.

CHAPTER 6

Concluding Remarks and Future Directions

6.1 E2 Enhances DC Activation and CTL Responses Toward Cancer Antigens

6.1.1. Concluding Remarks

The immune system is a powerful, targeted, and diverse biological network for the fight against cancer [1-3]. Dendritic cells (DCs) are a professional antigen presenting cell of the adaptive arm of immunity, and represent a critical link and orchestrator of adaptive immunity [4]. DCs are particularly efficient in priming CD8 T cells (CTL) toward exogenous antigen through cross-presentation, and CTL are the key effector cell in the fight against cancer cells.

We have demonstrated in this work that by simultaneous delivery of CTL epitopes and TLR9-activating CpG DNA within the viral-mimicking E2 nanoparticle, we can mediate an increase of immature DC activation and increase their capacity to cross-present attached antigen. Further, the DCs demonstrate an increased capacity to activate antigen-specific naïve CD8 T cells. We observed increased CTL proliferation and IFN-γ secretion for DCs pulsed with the E2 nanoparticle harboring both CpG and a melanoma antigen (gp100), compared to any other combination of antigen, activator, and nanoparticle. This supports our hypothesis that viral mimicry has distinct advantages in formulating tumor antigens.

The spleens and lymph nodes from mice receiving a single subcutaneous immunization with the multifunctional nanoparticles exhibited an increased frequency of gp100-specific CTL, compared to all other tumor antigen formulations tested. The CTL generated from the immunization also show an increased ability to specifically lyse gp100-expressing B16-F10 melanoma cell. Altogether, our data shows the applicability of the E2 nanoparticle as a viral-mimicking platform for cancer immunotherapy.

6.1.2. Future Directions

Now that we have shown the superior capacity of the E2 nanoparticle to generate increased CTL responses toward overexpressed tumor antigens *in vivo*, there are many exciting possibilities to explore as our platform is developed. While a single tumor antigen immunization with E2 was able to mount a significant CTL response, it remains to be seen whether the conditions we have tested here represent (a) the optimal antigen load per immunization, (b) the optimal number of immunizations, or (c) the optimal route of immunization [5]. Beyond these studies, we should test 3 different antigen payloads, such as 2.5 μg, 5 μg (used in this study), and 10 μg of the gp100 peptide. Also, we should test the effect of altering the number of immunizations and the immunization schedule (*i.e.,* one, two, or three immunizations, spaced at either 1 or 2 week intervals).

Once we have uncovered an immunization schedule which produces an optimal CTL response, the ultimate test of any vaccine is whether or not it can (a) protect from disease challenge, (b) mount an anti-tumor response of established disease, and (c) induce immunological memory, where protection from future disease challenge is observed. It will also be interesting to observe whether the immune response can be effective against metastases, where conventional cancer therapies face their largest challenges. The ability to discover and destroy metastases and non-detectable systemic cancer cells is where the immune system possesses the greatest potential.

Ideally, a cancer vaccine approach would also demonstrate applicability to a wide variety of disease types. While the ability to mount an anti-tumor response against melanoma (gp100) would be a prodigious achievement, the possibility of switching out the

tumor antigen-derived peptides on the surface of E2 with those of other cancer types would reveal the breadth of possibilities for the E2 nanoparticle platform. While the gp100 antigen is an overexpressed differentiation antigen (*i.e.*, a self-antigen) [6], it would be interesting to observe the response toward other classes of tumor antigens, such as cancer/testis class of antigen (*e.g.,* NY-ESO-1, currently under investigation in our research group) [7]. Developing a delivery platform whereby antigens could easily be swapped is a desirable attribute from a therapeutic and logistical development standpoint. It would also be important to understand the physical stability and shelf-life of the E2 vaccine platform. Vaccines should ideally display long term stability, perhaps as a solid, where they can be stored and delivered to areas that may not possess resources for sub-zero long term storage conditions [8].

Alternative TLR-activators should also be explored, to (a) understand how engaging alternative TLRs affect the activation extent and antigen presentation and (b) reveal the potential of combining multiple activators to a single E2 platform for synergistic effects. While TLR9 (receptor for CpG) is expressed abundantly in the immune system of a mouse, its expression is much more limited in a human [9]. Therefore, while ongoing trials may reveal CpG to be a clinically potent adjuvant for cancer immunotherapies, it will be important to have other tools in our arsenal, for easy exchange to encapsulate and deliver different activators. Each unique adjuvant molecule may favor one avenue of the adaptive response, and a particular disease or cancer type may benefit more from a particular ligand. Other potential intracellular receptors targets include TLR3, TLR7, and TLR8, all of which recognize nucleic acid-derived danger signals, similar to TLR9 (See Chapter 1) [10,11]. The ligands for TLR7 and TLR8 are small RNA and DNA sequences, which can potentially be packaged within E2 in mechanisms similar to that achieved for CpG (See Chapter 2). The

major known activator of TLR3 is the much larger double-stranded RNA (*i.e.*, poly(I:C)), and while this may display constraints with respect to internal packaging, TLR3 shows abundant expression in human DC subsets that also have increased cross-presentation capacities (*i.e.* CLEC9A^{+} DC subsets) [12]. We have pursued chemistries to explore immobilization of poly(I:C) on to the E2 nanoparticle surface (See Appendix A.2).

Finally, other mechanisms of peptide attachment should be explored also, such as recombinant display. While we have shown successful immobilization of peptide to the free amines of the E2 nanoparticle, the ability to explore other mechanisms of attachment will demonstrate the robustness of our system. This will (a) allow for the possibility to display multiple tumor-antigen CTL epitopes or (b) reveal potential for attachment of helper epitopes (MHC II-restricted, for CD4 T cell help), in addition to CTL epitopes. The enlistment of CD4 T helper cell activity, potentially through use of a promiscuous T helper epitope, may prove a critical aspect of cancer vaccination strategies, and we should have in place mechanisms for incorporation [13]. Certain TLR-ligands, such as that for TLR5, are peptide based, and this provides a mechanism of immune activator incorporation as well [14]. We have developed an arsenal of E2 nanoparticle variants for straight-forward recombinant incorporation of peptide on the surface (See Appendix A.1 and A.2). We have actually explored the possibility of recombinantly displaying flagellin-derived peptide (*i.e.* TLR5 ligand), model antigen epitopes (*i.e.* SIINFEKL from chicken ovalbumin), tumor antigen epitopes (*i.e.* SLLMWITQV from NY-ESO-1) [15], and peptides reported to target DCs (*i.e.* FYPSYHSTPQRP) [16].

6.2 Tuning Cellular Interactions and Lymphatic Drainage of E2

6.2.1. Concluding Remarks

The goal of any biomaterial *in vivo* is to mediate and enhance a therapeutic or biological function at a superior capacity compared to the natural physiological response or other intervening methods. Biomaterials, particularly on the nanoscale, have shown brilliant potential in their ability to sculpt the lymphatic microenvironment and help direct the immune response [17,18]. Virus-like particles and other protein nanocapsules closely mimic the geometry and pattern of natural viruses, rendering them an intriguing platform for cancer immunotherapy, since both virus infection and cancer require strong CTL-mediated immune responses for eradication or suppression.

Our E2 nanoparticle *in vitro* demonstrated the ability for efficient uptake by antigen presenting cells, including DCs, over a short period of time. We are able to tune the amount of uptake by surface display of poly(ethylene glycol) (PEG) hydrophilic polymers of various lengths. Additionally, while complement activation (which could neutralize a biomaterial) via PEGylation of biomaterials is a concern, we show that levels of complement activation provoked by our nanoparticle are much lower than that of known activators. Additionally, decreasing general cellular uptake by surface display of PEG provides the opportunity to explore display of targeting ligands to enhance target cell-specific uptake. To that end, we showed that conjugation of CpG DNA motifs, reported to be a DEC-205 ligand, to PEG linkers on the E2 surface greatly enhanced DC uptake *in vitro*.

Nanoparticles which display sizes similar to that of the E2 nanoparticle are reported to drain freely to lymphatics, for interaction with DCs [19]. Indeed, we showed that following subcutaneous injection, non-functionalized E2 drains primarily to the lymph nodes (LN) ipsilateral to the injection site. Following PEGylation, the nanoparticle tends to accumulate in more distal LN, and is also present as measurable amounts within the LN contralateral to the injection site. Surface immobilization of the CpG DNA with a PEG linker displayed nanoparticle accumulation in the LN most proximal to the injection site and these nanoparticles also demonstrated a tendency of enhanced LN retention over longer periods of time, compared to the other E2 nanoparticles tested. Each of the nanoparticles tested were shown to interact with a high percentage of DCs and F4/80+ cells (macrophages or Langerhans DCs), regardless of surface functionality. However, CpG display on the E2 results in an increase in DC fluorescence, indicating that CpG DNA motifs enhance the uptake of DCs, even if cellular distribution remains unaltered. Therefore, CpG may represent a potential ligand to functionalize biomaterials for enhanced DC uptake of antigen.

6.2.2. Future Directions

While CpG DNA aptamers showed promise as uptake modulators toward DCs, macrophages, and B cells *in vitro*, it would be interesting to explore other potential aptamers for similar purposes, such as peptides reported to enhance DC targeting [16]. In fact, we have explored this prospect with one such peptide (FYPSYHSTPQRP), although observation of potential targeting effects will require more work (See Appendix A.2). There is also the prospect of using phage display to identify possible leads on DC-targeting aptamers, as

others have attempted [16]. The choice of linker for aptamer disaplay may have an effect on (a) the density of aptamers we can conjugate and (b) the resulting effect on cell targeting and uptake kinetics [20-22]. While PEG with a molecular weight of 2000 Da was chosen for the current study, it would be interesting to measure differences in cell uptake with varying molecular weights of PEG, homogeneous PEG, or without PEG at all, using a zero-spacing linker like SMCC.

CpG is a TLR danger signal, which is known to enhance DC macropinocytic activity during early stages of activation [23]. Therefore, it would be interesting to observe whether the increase in uptake we observe is due to surface display and receptor engagement by the CpG, or whether the enhanced uptake effect is due to the activation induced by CpG. This could be tested by measuring DC uptake of the E2 nanoparticle with CpG packaged internally.

In vivo, while we measured LN and injection site fluorescence up to 48 hours, it would be interesting to measure at which point fluorescence is no longer detectable, to get a sense as to when the nanoparticles have been either degraded or cleared. It would also be interesting to note the activation level of DCs within the draining lymph nodes. PEGylation of nanoparticle has been shown previously to induce a low level of LN complement activation, which actually augmented the immune response [24]. With our CpG-conjugated nanoparticle, we would expect that any DC which takes in the nanoparticle would also be activated, rendering CpG a potential multifaceted targeting moiety, enhancing DC uptake and enhancing DC activation.

Beyond targeting and uptake, an important variable is to test whether or not these surface modifications enhance or detract from antigen specific immune responses. We have

shown in preliminary work that surface modification of E2 with PEG that is displaying an MHC I epitope does not preclude cross-presentation of those epitopes, which is a very important observation for vaccine success (See Appendix A.2). Further, the PEGylated and CpG-conjugated nanoparticles show contrasting lymph node draining patterns, where PEG allows further dispersion to distal LN, other organs, and the blood, while CpG conjugation to the E2 surface results in accumulation in proximal LN. Therefore, it would be interesting to understand whether less nanoparticle in more lymph nodes (mPEG-E2) or more nanoparticle in less lymph nodes (CpG-PEG-E2) is more important for a strong systemic anti-tumor CTL response, which will help dictate future design of the E2 nanoparticle as an optimal cancer vaccine platform.

6.3 References

1. Blattman JN, Greenberg PD: Cancer immunotherapy: a treatment for the masses. *Science* 2004, 305:200-205.
2. Dunn GP, Bruce AT, Ikeda H, Old LJ, Schreiber RD: Cancer immunoediting: from immunosurveillance to tumor escape. *Nat Immunol* 2002, 3:991-998.
3. Schreiber RD, Old LJ, Smyth MJ: Cancer immunoediting: integrating immunity's roles in cancer suppression and promotion. *Science* 2011, 331:1565-1570.
4. Banchereau J, Steinman RM: Dendritic cells and the control of immunity. *Nature* 1998, 392:245-252.
5. Cubas R, Zhang S, Kwon S, Sevick-Muraca EM, Li M, Chen C, Yao Q: Virus-like particle (VLP) lymphatic trafficking and immune response generation after immunization by different routes. *J Immunother* 2009, 32:118-128.
6. Overwijk WW, Tsung A, Irvine KR, Parkhurst MR, Goletz TJ, Tsung K, Carroll MW, Liu CL, Moss B, Rosenberg SA, et al.: gp100/pmel 17 is a murine tumor rejection antigen: Induction of "self"-reactive, tumoricidal T cells using high-affinity, altered peptide ligand. *Journal of Experimental Medicine* 1998, 188:277-286.
7. Scanlan MJ, Gure AO, Jungbluth AA, Old LJ, Chen YT: Cancer/testis antigens: an expanding family of targets for cancer immunotherapy. *Immunol Rev* 2002, 188:22-32.
8. Kumru OS, Joshi SB, Smith DE, Middaugh CR, Prusik T, Volkin DB: Vaccine instability in the cold chain: mechanisms, analysis and formulation strategies. *Biologicals* 2014, 42:237-259.
9. Krieg AM: Toll-like receptor 9 (TLR9) agonists in the treatment of cancer. *Oncogene* 2008, 27:161-167.
10. Kay E, Scotland RS, Whiteford JR: Toll-like receptors: Role in inflammation and therapeutic potential. *Biofactors* 2014, 40:284-294.
11. Uematsu S, Akira S: Toll-Like receptors (TLRs) and their ligands. *Handb Exp Pharmacol* 2008:1-20.
12. Caminschi I, Proietto AI, Ahmet F, Kitsoulis S, Shin Teh J, Lo JC, Rizzitelli A, Wu L, Vremec D, van Dommelen SL, et al.: The dendritic cell subtype-restricted C-type lectin Clec9A is a target for vaccine enhancement. *Blood* 2008, 112:3264-3273.
13. Fikes JD, Sette A: Design of multi-epitope, analogue-based cancer vaccines. *Expert Opin Biol Ther* 2003, 3:985-993.
14. Sfondrini L, Rossini A, Besusso D, Merlo A, Tagliabue E, Menard S, Balsari A: Antitumor activity of the TLR-5 ligand flagellin in mouse models of cancer. *J Immunol* 2006, 176:6624-6630.
15. Purbhoo MA, Sutton DH, Brewer JE, Mullings RE, Hill ME, Mahon TM, Karbach J, Jager E, Cameron BJ, Lissin N, et al.: Quantifying and imaging NY-ESO-1/LAGE-1-derived epitopes on tumor cells using high affinity T cell receptors. *J Immunol* 2006, 176:7308-7316.
16. Curiel TJ, Morris C, Brumlik M, Landry SJ, Finstad K, Nelson A, Joshi V, Hawkins C, Alarez X, Lackner A, et al.: Peptides identified through phage display direct immunogenic antigen to dendritic cells. *J Immunol* 2004, 172:7425-7431.
17. Andorko JI, Hess KL, Jewell CM: Harnessing biomaterials to engineer the lymph node microenvironment for immunity or tolerance. *AAPS J* 2015, 17:323-338.
18. Reddy ST, Swartz MA, Hubbell JA: Targeting dendritic cells with biomaterials: developing the next generation of vaccines. *Trends in Immunology* 2006, 27:573-579.
19. Bachmann MF, Jennings GT: Vaccine delivery: a matter of size, geometry, kinetics and molecular patterns. *Nat Rev Immunol* 2010, 10:787-796.
20. Zhan X, Tran KK, Shen H: Effect of the poly(ethylene glycol) (PEG) density on the access and uptake of particles by antigen-presenting cells (APCs) after subcutaneous administration. *Mol Pharm* 2012, 9:3442-3451.

21. Steinmetz NF, Manchester M: PEGylated viral nanoparticles for biomedicine: the impact of PEG chain length on VNP cell interactions in vitro and ex vivo. *Biomacromolecules* 2009, 10:784-792.
22. Stefanick JF, Ashley JD, Kiziltepe T, Bilgicer B: A systematic analysis of peptide linker length and liposomal polyethylene glycol coating on cellular uptake of peptide-targeted liposomes. *ACS Nano* 2013, 7:2935-2947.
23. West MA, Wallin RP, Matthews SP, Svensson HG, Zaru R, Ljunggren HG, Prescott AR, Watts C: Enhanced dendritic cell antigen capture via toll-like receptor-induced actin remodeling. *Science* 2004, 305:1153-1157.
24. Reddy ST, van der Vlies AJ, Simeoni E, Angeli V, Randolph GJ, O'Neil CP, Lee LK, Swartz MA, Hubbell JA: Exploiting lymphatic transport and complement activation in nanoparticle vaccines. *Nat Biotechnol* 2007, 25:1159-1164.

APPENDIX A.1

Appendix A.1 Detailed Protocols and Additional Methods

A.1.1 Bone Marrow-Derived Dendritic Cell Preparation

Extraction of marrow:

1. Beginning with euthanized mouse
    a. Spray animal with generous amount of 70% ethanol
    b. Make sure surgical tools are all sterile
        i. Curved forceps, straight forceps, curved scissors, straight scissors
2. Cut away the tissue from the hind legs of the animal
    a. I like to sever the Achilles tendon first and cut up towards the body
        i. For a good video on this, go to: http://www.jove.com/video/769/culture-of-myeloid-dendritic-cells-from-bone-marrow-precursors
    b. Make sure you remove enough skin and tissue to expose the hip joint
        i. It's common for bleeding to occur here, if you sever the femoral artery
3. Remove the hind legs from the animal by cutting at the hip joint
    a. Be very careful not to break the femur
        i. I like to flex the hip joint, so it is obvious where the joint is
4. Continue to remove tissue until the bones are exposed
    a. Remove the feet
    b. Separate the femur and tibia at the knee joint
        i. You can use all four leg bones, just the femur, or just the tibias, depending on how many cells you need
            1. All four bones → ~ 30-40 million cells
            2. 2X Femurs → 20-30 million cells
            3. 2X Tibias → 5-10 million cells
5. Rinse bones in 70% ethanol for about a minute (I use the lid of a petri dish)
6. Rinse the bones in a small amount of ice cold PBS (I use the lid of a petri dish)
7. Set the bones in ice cold PBS on ice (I use a petri dish)
8. Using straight scissors, cut both epiphyses from the bone and place back in ice cold PBS until next step
9. Prepare ~ 7 ml of ice cold PBS in a petri dish and fill a 3 ml syringe with ice cold PBS
    a. 27 gauge needle on end of syringe
10. Insert the needle into one end of the bone and flush out the marrow with PBS into the 7 mls of PBS in the petri dish

   a. The bone will go from brownish to bright white as the marrow is flushed to the dish
   b. Flush with more PBS as necessary to get all of the marrow out
11. Optional: Flush the open end of the epiphyses with PBS to get that marrow out
   a. Usually I don't need to get the maximal possible amount of marrow, though
12. Using a 10 ml serological pipette, pipette the marrow/PBS solution up and down for several minutes, until the marrow is broken up into a more homogeneous solution (single cell suspension)
13. Insert a 70 μm mesh tissue strainer to a 50 ml conical tube and apply the 10 mls of marrow to the mesh
   a. If there are red clumps on the mesh, you can break that up with the tip of the pipettes.
14. Rinse the petri dish with 10 ml of fresh ice cold PBS, and apply that to the strainer
15. Centrifuge the marrow cells at 300 x g for 5 minutes
16. Decant the supernatant, break up the pellet, and add 3 mls of ACK lysing buffer for 2 minutes at room temperature
   a. After 2 minutes, quench with 10-20 mls of ice cold PBS
17. Centrifuge at 300 x g for 5 minutes
18. Decant, break up pellet, and add 10-20 mls of PBS
   a. You should notice that the pellet is now white, instead of red
   b. Take 100 μl for cell counting
19. Centrifuge at 300 x g for 5 minutes
   a. This is a good time to count your cells

<u>Generation and Culturing of BMDCs:</u>

20. Resuspend the cells at 2 million cells/ml in pre-warmed BMDC media
21. From here, I follow the method of Lutz et al for culturing BMDCs
   a. Lutz, M. B.; Kukutsch, N.; Ogilvie, A. L.; Rossner, S.; Koch, F.; Romani, N.; Schuler, G. An Advanced Culture Method for Generating Large Quantities of Highly Pure Dendritic Cells from Mouse Bone Marrow. *J. Immunol. Methods* 1999, 223, 77-92.
22. Add 1 ml of cell suspension to a sterile bacteriological non-treated petri dish (2 million cells total)
23. Bring the volume in the dish up to 10 ml with pre-warmed media
24. Supplement the media with 20 ng/ml of mouse recombinant GM-CSF
   a. I usually like to keep the GM-CSF at 10 μg/ml stock (I will at 20 μl of this stock directly to the dish)
   b. This is Day 0
25. On Day 3, add 10 ml of fresh pre-warmed DC media (now 20 ml total)

    a. Supplement with 10 ng/ml GM-CSF (i.e. 20 µl of 10 µg/ml stock)

26. On Day 6, remove 10 ml from each culture (50% of the media), centrifuge at 300 x g for 5 min, and resuspend the non-adherent cells in 10 ml of pre-warmed DC media
    a. Supplement with 10 ng/ml fresh GM-CSF (i.e. 20 µl of 10 µg/ml stock)
27. Add the non-adherent cells in fresh media back to the culture dishes
28. On Day 8, you should notice that the cells have proliferated quite a bit since Day 0
    a. Harvest the cells by gently pipetting the media against the plate with a 10 ml serological pipette
    b. Do not pipette to aggressively, or you will kill the cells (they are very loosely adherent and come off easily)
29. Centrifuge at 300 x g for 5 min
    a. Count cells during this time
30. Plate the immature BMDCs in whatever plate or at whatever concentration is appropriate for your experiment

A.1.2 Splenocyte Cell Preparation

1. Pre-warm **Full RPMI** (10% FBS, 1% antibiotic/antimycotic) at 37°C.
   Make 1000X βME by adding 3.7 ul of BME to 1 ml of RPMI.
2. Add 50 ul of 1000X BME into 50 mL of Full RPMI to make **Complete RPMI**.
3. Sacrifice mouse and extract spleen and/or lymph nodes, place in 1 mL Complete RPM1.
4. Set up 70 m strainer in a 50 mL tube. Crush spleen and wash with 20 mL RPMI (empty) through strainer.
5. Spin for 5 min on setting 4. Aspirate media.
6. Gently resuspend in 1 mL ACK, then add 4 mL slowly. Incubate for 4 minutes MAX. Quench reaction with 25 mL RPMI (empty). (skip step to step 7 if working with lymph nodes)
7. Spin for 5 min on setting 4. Aspirate media.
8. Resuspend in 10 mL RPMI (empty).
   Optional: Refilter
9. Count cells. 90 µL Trypan blue + 10 µL cells. Stain for 2 minutes. Count cells, calculate the average of 2 quadrants and divide by dilution factor to obtain number of million cells/mL.
10. Dilute cells to desired concentration with Complete RPMI

A.1.3 pmel-1 CFSE Proliferation Assays

1. Prepare splenocytes at 20 milion cells/mL in PBS
    a. Red blood cells lysed with ACK lysing buffer
2. Prepare CFSE (stock solution at 5 mM in DMSO) at 5 μM in PBS
3. Combine equal amounts of splenocytes and CFSE
    a. 10 million cells/mL and 2.5 μM CFSE final
4. Incubate at room temperature in the dark for 10 minutes
5. Quench with 5× volume of warm RPMI + 10% FBS and pellet at 300×g for 5 minutes
6. Wash 1× with 10 mL PBS and pellet at 300×g for 5 minutes
    a. Count cells while spinning down
7. Prepare cells at 2 million/mL in RPMI + 10% FBS, L-glu, Na-Pyruvate, NEAA, P/S, 50 μM –β-ME
8. Add 100 μL of cells per well in 96-well plate (200,000 cells)
9. Prepare antigen at 2× concentration in complete RPMI media
    a. 20 μg/mL for peptides or 2% PHA
10. Add 100 μl antigen to each well
11. Culture at 37°C for 24 hours
12. Centrifuge plate @ 300×g for 3 minutes and aspirate culture media
13. Add 200 μL PBS per well and centrifuge @ 300×g for 3 minutes
    a. Repeat one more time
14. Add 200 μL warm complete RPMI media
15. Culture for an additional 72 hours
16. Harvest cells by pipetting gently
17. Prepare cells in FACS buffer containing anti-mouse-CD8-APC (1:400 dilution)
18. Stain on ice for 30 minutes, wash 2× with FACS buffer
19. Analyze on flow cytometer, gating on CD8 for CFSE analysis

A.1.4 Detailed Example of A Complement Activation Experiment

Reagents:

500ml DGVB (prepared fresh): 0.5g gelatin (dissolve in 100ml heated water)
15g dextrose
40ml 5x VBS
0.5ml Ca 0.15M/1M Mg stock
bring to 500ml

50-100ml GVBE: 5mL 0.2M EDTA + 45ml GVB++
20ul NHS
100ul C4depleted GPS
E2-wt complex = 1.7 mg/ml in low salt PBS (0.1M NaCl)
E3-mut/peg complex = 2 mg/ml , dilute to 1.7mg/ml (12ul protein +2.1ul buffer)
Sheep EA's (1/3200 hemolysin) standardized @ $5x10^8$ cells/ml

Activation of Complement by E2:

2. Dilute NHS 1:2.5 in DGVB, keep on ice
   20ul NHS in 30ul DGVB

3. Prepare sample and control
   12.5ul E2WT + 12.5 ul diluted NHS
   12.5ul E279C-PEG(24) + 12.5 ul diluted NHS
   12.5 ul 50 mM Potassium Phosphate pH 7.4 + 12.5 ul diluted NHS

4. Incubate 30oC, 30 mins

5. Dilute sample and control each to 1/200, by adding 975ul DGVB, keep on ice.

Measurement of C4 depletion :

1. Make serial dilutions of sample or control into DGVB to 1/1638,400 (14 dilutions)

1. 1:200 -
2. 1:400 - 300 µl of 1:200 + 300 µl DGVB++
3. 1:800 - 300 µl of 1:400 + 300 µl DGVB++
4. 1:1,600 - 300 µl of 1:800 + 300 µl DGVB++
5. 1:3,200 - 300 µl of 1:1,600 + 300 µl DGVB++
6. 1:6,400 - 300 µl of 1:3,200 + 300 µl DGVB++
7. 1:12,800 - 300 µl of 1:6,400 + 300 µl DGVB++
8. 1:25,600 - 300 µl of 1:12,800 + 300 µl DGVB++
9. 1:51,200 - 300 µl of 1:25,600 + 300 µl DGVB++
10. 1:102,400 - 300 µl of 1:51,200 + 300 µl DGVB++

11. 1:204,800 - 300 µl of 1:102,400 + 300 µl DGVB++
12. 1:409,600 - 300 µl of 1:204,800 + 300 µl DGVB++
13. 1:819,200 - 300 µl of 1:409,600 + 300 µl DGVB++
14. 1:1,638,400 - 300 µl of 1:819,200 + 300 µl DGVB++

2. Prepare 1/100 C4D-GPS (C4depleted Guinea Pig Serum)
100ul C4D-GPS in 9900 ul DGVB

3. Prepare EA's at $1x10^8$/ml.
2 ml EA's at $5x10^8$/ml and 8 ml DGVB++ **Keep this on ice.**

4. Prepare assay tubes (in duplicate). **These should also be on ice.** There must be two tubes for <u>every</u> dilution of <u>every</u> sample in step 1, in addition to two tubes for the water control and two for the buffer control. Also, the order in which the components are added is very important:

a) First add the diluted samples to appropriate tubes. Add water to the water control and DGVB++ to the buffer control.
b) Add diluted EA's to all tubes. Swirl to mix.
c) Add diluted C4DGPS to all tubes except the water control. Swirl to mix.

<u>Samples</u>:	100 µl diluted sample
	100 µl diluted EA's
	100 µl diluted C4DGPS
<u>Water control</u>:	200 µl water
	100 µl diluted EA's
<u>Buffer control</u>:	100 µl diluted DGVB++
	100 µl diluted EA's
	100 µl C4DGPS

5. Cover the tubes with a sheet of parafilm and incubate in a 37°C water bath for 60 min. Shake the rack periodically to keep the cells in suspension.
6. Add 0.5 ml of water to the water control. Add 0.5 ml GVBE to all other tubes.
7. Pellet remaining EA's 2000rpm, 4°C for 5 min.
8. Pipet 250 µl of the supernatant from each tube into a microtiter plate (be sure not to disrupt the pellets) and take an endpoint reading at 412 nm

A.1.5 PEGylation of E2 Surface Amines

1. Reagents
    a. E2 (D381C) – molecular weight 28105 Da (per monomer)
        i. 60 monomers per nanoparticle
        ii. For cell studies, will want to have cysteines fluorescently labeled
    b. NHS-PEG2000-maleimide – molecular weight 2000 Da
    c. Potassium Phosphate Buffer
        i. 50 mM potassium phosphate pH 7.4
        ii. 100 mM NaCl
    d. DMSO
    e. L-cysteine @ 10 mM in MilliQ H_2O
        i. Optional – Also dissolve 10 mM TCEP to keep thiols reduced
2. Procedure:
    a. Determine concentration of the E2 protein
        i. If unknown, need to run a BCA assay
        ii. Typically at ~ 1 mg/ml → 1 / 28105 = ~ 36 μM (with respect to E2 monomer)
    b. Want to react the PEG reagent with the E2 protein at 30 molar excess of NHS to the E2 monomer
        i. 1 mg/ml E2 example → 36 * 30 = 1 mM
        ii. PEG stock at 10 mM (maleimide-PEG2000-NSH) or 100 mM (mPEG2000-NHS) in DMSO
    c. Add PEG to E2, mix, and keep at room temperature for 1-2 hour
    d. Apply the reaction to a 40 kDa cutoff Zeba spin desalting column
        i. From Pierce – follow the manufacturer's instructions
    e. Options for reacting with free maleimide group:
        i. Add L-cysteine at ~ 20-fold molar excess to E2 monomer
        ii. Add cysteine containing peptide at 5-10 molar excess to E2 monomer
    f. React thiol containing compound with maleimide for 2 hr at room temperature
    g. Remove excess unreacted cysteine or peptide with desalting column
    h. Measure protein concentration with BCA

A.1.6 CH12 and B3Z Cell Maintenance

CH12 B cells should be maintained at the density between 50,000 – 200,000 cells/ml (absolutely not over 300,000 cells/ml at any time or 700,000 cells/mL for B3Z) in 5 ml of RPMI plus FBS, antibiotics and β-mercaptoethanol in a T-50 culture flask. It is important to split almost everyday due to the 8 hour-doubling time of this cell line.

CH12 only: To expand cells for biochemical analysis (less than 24 hr of stimulation), a larger volume and a higher density are needed. For CSR analysis, which requires 48 hr of stimulation, optimal seeding density is 200,000 cells/ml.

For maintenance:

1. Transfer cells into a 15 mL conical Falcon tube.
2. Spin for 4 minutes on setting 3 in a clinical centrifuge. Meanwhile, wash the T-50 culture flask with 6 mL of PBS or use a new flask, and set up the hemocytometer.
3. Wash cell pellet with 2 mL of PBS, aspirate. Resuspend cells in 2 mL of fresh full medium.
4. Count cells and split cells to 50,000 cells/mL in 5 ml

CH12 only information:

Maintain below 5% $IgA^{+}IgM^{-}$, check by FACS (see below).

For stimulation to induce CSR from IgM to IgA (only CSR to IgA is inducible):

1. Wash cells with PBS, seed at 200,000 cells /mL in 24-well plates (2mL/well).
2. Add CIT (CD40 ligand, IL-4, TGF-β, left panel below) or nil (as control, right panel below) and culture for 48 h.

CD40 ligand (CD154): 3 unit/mL (depending on the potency of different batches); this is made in the lab, but should also be commercially available.

Mouse IL-4: 1 μL/mL (4 ng/μL stock, from R&D)

Mouse TGF-β: 1 μL/mL (2 ng/μL stock, from R&D)

3. Stain with 7-AAD, FITC-conjugated anti-IgA (BD Pharmingen) and PE-conjugated anti-IgM (BD Pharmingen) and analyze by FACS. A representative plot below shows 46.5% of B cells are $IgA^{+}IgM^{-}$.

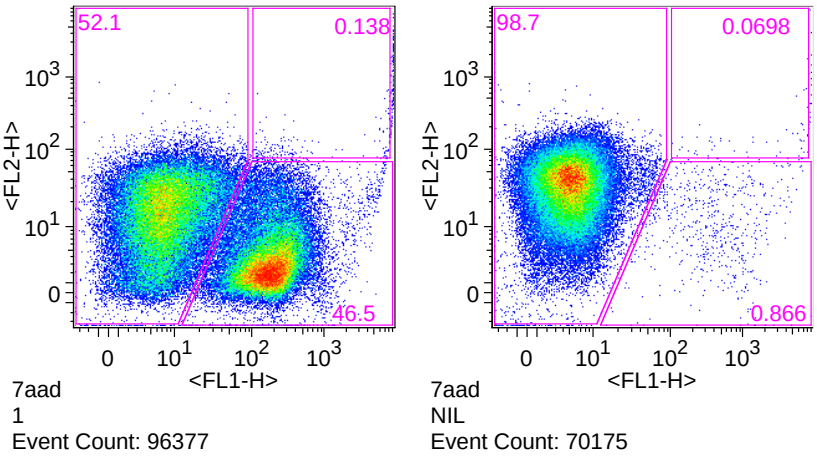

Figure A.1.1. CH12 B cell information

A.1.7 poly(I:C) Conjugation to E2 Surface Amines

Briefly, the reaction scheme begins by purifying only shorter chain poly(I:C) molecules (< 500 bp) using size exclusion chromatography with Superose 6, then phosphorylating the 5' ends with T4 polynucleotide kinase, followed by 1-Ethyl-3-[3-dimethylaminopropyl]carbodiimide Hydrochloride (EDC) activation in 0.1 M imidazole buffer and 150 mM NaCl at pH 6.0, and finally conjugation to cysteamine through a phosphoramidate linkgage, leaving free 5' thiol groups. The bifunctional linker Sulfosuccinimidyl 4-(N-maleimidomethyl)cyclohexane-1-carboxylate (Sulo-SMCC) is reacted with the external lysines (amide bond) of the E2 nanosapsule and subsequently incubated with the thiol-functionalized poly(I:C) (thioether bond), forming a covalent linkage between the nanocapsules and the polymers. The reaction scheme is depicted in **Figure A.1.2**. The conjugates were purified from unreacted poly(I:C) by size exclusion chromatography. Characterization of the poly(I:C)-conjugated E2 particles included 0.6% agarose gel analysis (determination of successful conjugation qualitatively), spectroscopic absorbance measurements (230 and 260 nm in order to quantify poly(I:C) conjugation ratios), and DLS to determine particle sizes.

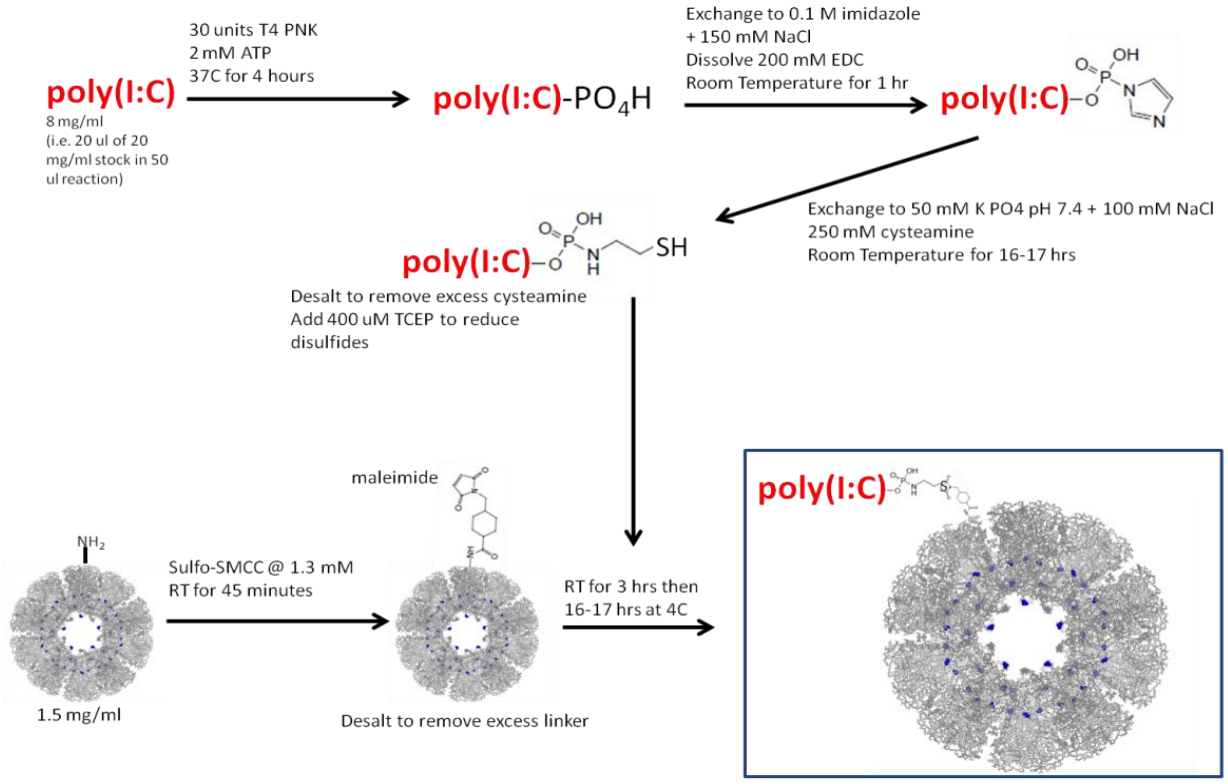

FIGURE A.1.2. Depicted is a schematic showing the conjugation scheme of poly(I:C) to the D381C nanocapsule. The EDC linker forms a phosphoramidate linkage between the poly(I:C) and cysteamine, reported to be acid-labile at endosomal pH's. [1] The thiol-activated poly(I:C) is then conjugated to the D381C nanocapsule through a 2-step reaction with the bifunctional linker Sulfo-SMCC, forming an amide bond (D381C external lysines) and a thioether bond (5' thiol-terminated poly(I:C)). The final conjugate is depicted in the blue box, with only one poly(I:C) molecule attached, for simplicity.

A.1.8 Developing E2 Mutants for N-terminal Peptide Additions

The following is an example of one of the mutants generated, called E2-158. The E2 scaffold containing a flexible linker region for the presentation of peptides was created. The gene for this scaffold was based on a previously-published plasmid pE2, which encodes for the E2 structural core protein in a pET-11a expression vector. Silent mutations were made in the E2 gene to introduce an *Xma1* restriction site at base pairs 13-18 (CCCGGG). To incorporate the native linker region, the N-terminus was extended from proline-175 to valine-158 (with numbering corresponding to amino acid location from NCBI, accession number P11961). Valine-158 lies in a loop region near the N-terminus of an α-helix that extends away from the structural E2 core, allowing for insertion of fusions with reduced steric interactions. The forward and reverse primers for creating this extended N-terminus region were 5'-GATATACATATGGCTAGCGTGCTGAAAGAAGACATTGATGCGTTTCTGGCG-3' and 5'-CCCTTTCCCGGGTTTCGCGCCGCCCGCCAGAAACGCATCAATGTC-3', respectively. Primers were heated to 90°C for 5 min, slowly cooled to 4°C to allow annealing, extended at 37°C for 2 hours with 20 U/mL T4 polymerase (New England Biolabs) and dNTP (0.5 mM each nucleotide; New England Biolabs), and brought to 75°C for enzyme inactivation. This product was then digested with *Nde1* and *Xma1* and ligated into the corresponding endonuclease sites of the pE2 plasmid [E2(158)]. The expression and solubility of this resulting protein was confirmed. The full DNA sequences for the various E2 mutants generated in this same way can be found below. Information on the primers used to generate the mutants is following the DNA sequences.

DNA Sequences:

pE2-WT

ATGCTGTCTGTTCCTGGTCCCGCTGCTGCAGAGGAAAAGGCTGCTCCAGCGGCTGCGAAACCGGCTACTAC
TGAAGGTGAATTCCCTGAAACCCGTGAAAAAATGTCTGGTATCCGTCGTGCAATCGCGAAAGCCATGGTTC
ACTCTAAACACACCGCGCCACACGTTACCCTGATGGATGAAGCAGACGTTACCAAACTGGTTGCGCACCGT
AAAAAATTCAAGGCGATTGCGGCGGAAAAAGGTATCAAACTGACCTTCCTGCCGTACGTTGTTAAAGCTC
TGGTTTCGGCTCTGCGTGAATACCCGGTTCTGAACACCTCTATTGACGACGAGACCGAAGAAATCATCCAG
AAACACTACTACAACATCGGTATCGCTGCGGACACTGATCGTGGTCTGCTGGTTCCTGTGATTAAACACGC
GGACCGTAAACCGATCTTCGCGCTCGCTCAGGAAATCAACGAACTGGCTGAGAAAGCTCGTGACGGTAAAC
TGACTCCTGGTGAAATGAAAGGCGCGTCTTGCACTATTACCAACATCGGCTCTGCAGGTGGTCAGTGGTTC
ACCCCAGTTATCAACCACCCGGAAGTTGCGATCCTGGGTATTGGTCGTATAGCCGAAAAGCCGATCGTTCG
TGACGGTGAAATCGTTGCTGCTCCGATGCTGGCCCTGTCTCTGTCTTTCGATCATCGTATGATTGATGGCG
CGACCGCACAGAAAGCCCTGAACCACATCAAACGTCTGCTGTCCGACCCGGAACTGCTGCTGATGGAAGCT
taa

E2-152

ATGGCTAGCACCGGCAAAAATGGTCGTGTGCTGAAAGAAGACATTGATGCGTTTCTGGCGGGCGGCGCGA
AACCCGGGCCCGCTGCTGCAGAGGAAAAGGCTGCTCCAGCGGCTGCGAAACCGGCTACTACTGAAGGTGAA
TTCCCTGAAACCCGTGAAAAAATGTCTGGTATCCGTCGTGCAATCGCGAAAGCCATGGTTCACTCTAAACA
CACCGCGCCACACGTTACCCTGATGGATGAAGCAGACGTTACCAAACTGGTTGCGCACCGTAAAAAATTCA
AGGCGATTGCGGCGGAAAAAGGTATCAAACTGACCTTCCTGCCGTACGTTGTTAAAGCTCTGGTTTCGGCT
CTGCGTGAATACCCGGTTCTGAACACCTCTATTGACGACGAGACCGAAGAAATCATCCAGAAACACTACTA
CAACATCGGTATCGCTGCGGACACTGATCGTGGTCTGCTGGTTCCTGTGATTAAACACGCGGACCGTAAAC
CGATCTTCGCGCTCGCTCAGGAAATCAACGAACTGGCTGAGAAAGCTCGTGACGGTAAACTGACTCCTGGT
GAAATGAAAGGCGCGTCTTGCACTATTACCAACATCGGCTCTGCAGGTGGTCAGTGGTTCACCCCAGTTAT
CAACCACCCGGAAGTTGCGATCCTGGGTATTGGTCGTATAGCCGAAAAGCCGATCGTTCGTGACGGTGAAA
TCGTTGCTGCTCCGATGCTGGCCCTGTCTCTGTCTTTCGATCATCGTATGATTGATGGCGCGACCGCACAG
AAAGCCCTGAACCACATCAAACGTCTGCTGTCCGACCCGGAACTGCTGCTGATGGAAGCTTAA

E2-158

ATGGCTAGCGTGCTGAAAGAAGACATTGATGCGTTTCTGGCGGGCGGCGCGAAACCCGGGCCCGCTGCTGC
AGAGGAAAAGGCTGCTCCAGCGGCTGCGAAACCGGCTACTACTGAAGGTGAATTCCCTGAAACCCGTGAA
AAAATGTCTGGTATCCGTCGTGCAATCGCGAAAGCCATGGTTCACTCTAAACACACCGCGCCACACGTTAC
CCTGATGGATGAAGCAGACGTTACCAAACTGGTTGCGCACCGTAAAAAATTCAAGGCGATTGCGGCGGAA
AAAGGTATCAAACTGACCTTCCTGCCGTACGTTGTTAAAGCTCTGGTTTCGGCTCTGCGTGAATACCCGGT
TCTGAACACCTCTATTGACGACGAGACCGAAGAAATCATCCAGAAACACTACTACAACATCGGTATCGCTG
CGGACACTGATCGTGGTCTGCTGGTTCCTGTGATTAAACACGCGGACCGTAAACCGATCTTCGCGCTCGCT
CAGGAAATCAACGAACTGGCTGAGAAAGCTCGTGACGGTAAACTGACTCCTGGTGAAATGAAAGGCGCGT
CTTGCACTATTACCAACATCGGCTCTGCAGGTGGTCAGTGGTTCACCCCAGTTATCAACCACCCGGAAGTT
GCGATCCTGGGTATTGGTCGTATAGCCGAAAAGCCGATCGTTCGTGACGGTGAAATCGTTGCTGCTCCGAT
GCTGGCCCTGTCTCTGTCTTTCGATCATCGTATGATTGATGGCGCGACCGCACAGAAAGCCCTGAACCACA
TCAAACGTCTGCTGTCCGACCCGGAACTGCTGCTGATGGAAGCTTAA

E2-167

ATGGCTAGCCTGGCGGGCGGCGCGAAACCCGGGCCCGCTGCTGCAGAGGAAAAGGCTGCTCCAGCGGCTGC
GAAACCGGCTACTACTGAAGGTGAATTCCCTGAAACCCGTGAAAAAATGTCTGGTATCCGTCGTGCAATCG
CGAAAGCCATGGTTCACTCTAAACACACCGCGCCACACGTTACCCTGATGGATGAAGCAGACGTTACCAAA
CTGGTTGCGCACCGTAAAAAATTCAAGGCGATTGCGGCGGAAAAAGGTATCAAACTGACCTTCCTGCCGTA
CGTTGTTAAAGCTCTGGTTTCGGCTCTGCGTGAATACCCGGTTCTGAACACCTCTATTGACGACGAGACCG
AAGAAATCATCCAGAAACACTACTACAACATCGGTATCGCTGCGGACACTGATCGTGGTCTGCTGGTTCCT
GTGATTAAACACGCGGACCGTAAACCGATCTTCGCGCTCGCTCAGGAAATCAACGAACTGGCTGAGAAAGC
TCGTGACGGTAAACTGACTCCTGGTGAAATGAAAGGCGCGTCTTGCACTATTACCAACATCGGCTCTGCAG
GTGGTCAGTGGTTCACCCCAGTTATCAACCACCCGGAAGTTGCGATCCTGGGTATTGGTCGTATAGCCGAA
AAGCCGATCGTTCGTGACGGTGAAATCGTTGCTGCTCCGATGCTGGCCCTGTCTCTGTCTTTCGATCATCG
TATGATTGATGGCGCGACCGCACAGAAAGCCCTGAACCACATCAAACGTCTGCTGTCCGACCCGGAACTGC
TGCTGATGGAAGCTTAA

E2-173 (This is E2-WT with the silent mutation included for peptide insertion)

ATGGCTAGCGTTCCCGGGCCCGCTGCTGCAGAGGAAAAGGCTGCTCCAGCGGCTGCGAAACCGGCTACTAC
TGAAGGTGAATTCCCTGAAACCCGTGAAAAAATGTCTGGTATCCGTCGTGCAATCGCGAAAGCCATGGTTC
ACTCTAAACACACCGCGCCACACGTTACCCTGATGGATGAAGCAGACGTTACCAAACTGGTTGCGCACCGT
AAAAAATTCAAGGCGATTGCGGCGGAAAAAGGTATCAAACTGACCTTCCTGCCGTACGTTGTTAAAGCTC
TGGTTTCGGCTCTGCGTGAATACCCGGTTCTGAACACCTCTATTGACGACGAGACCGAAGAAATCATCCAG
AAACACTACTACAACATCGGTATCGCTGCGGACACTGATCGTGGTCTGCTGGTTCCTGTGATTAAACACGC
GGACCGTAAACCGATCTTCGCGCTCGCTCAGGAAATCAACGAACTGGCTGAGAAAGCTCGTGACGGTAAAC
TGACTCCTGGTGAAATGAAAGGCGCGTCTTGCACTATTACCAACATCGGCTCTGCAGGTGGTCAGTGGTTC
ACCCCAGTTATCAACCACCCGGAAGTTGCGATCCTGGGTATTGGTCGTATAGCCGAAAAGCCGATCGTTCG
TGACGGTGAAATCGTTGCTGCTCCGATGCTGGCCCTGTCTCTGTCTTTCGATCATCGTATGATTGATGGCG
CGACCGCACAGAAAGCCCTGAACCACATCAAACGTCTGCTGTCCGACCCGGAACTGCTGCTGATGGAAGCT
TAA

E2-179

ATGGCTAGCGGCGGCAGCGAGGAAAAGGCTGCTCCAGCGGCTGCGAAACCGGCTACTACTGAAGGTGAAT
TCCCTGAAACCCGTGAAAAAATGTCTGGTATCCGTCGTGCAATCGCGAAAGCCATGGTTCACTCTAAACAC
ACCGCGCCACACGTTACCCTGATGGATGAAGCAGACGTTACCAAACTGGTTGCGCACCGTAAAAAATTCAA
GGCGATTGCGGCGGAAAAAGGTATCAAACTGACCTTCCTGCCGTACGTTGTTAAAGCTCTGGTTTCGGCTC
TGCGTGAATACCCGGTTCTGAACACCTCTATTGACGACGAGACCGAAGAAATCATCCAGAAACACTACTAC
AACATCGGTATCGCTGCGGACACTGATCGTGGTCTGCTGGTTCCTGTGATTAAACACGCGGACCGTAAACC
GATCTTCGCGCTCGCTCAGGAAATCAACGAACTGGCTGAGAAAGCTCGTGACGGTAAACTGACTCCTGGTG
AAATGAAAGGCGCGTCTTGCACTATTACCAACATCGGCTCTGCAGGTGGTCAGTGGTTCACCCCAGTTATC
AACCACCCGGAAGTTGCGATCCTGGGTATTGGTCGTATAGCCGAAAAGCCGATCGTTCGTGACGGTGAAAT
CGTTGCTGCTCCGATGCTGGCCCTGTCTCTGTCTTTCGATCATCGTATGATTGATGGCGCGACCGCACAGA
AAGCCCTGAACCACATCAAACGTCTGCTGTCCGACCCGGAACTGCTGCTGATGGAAGCTTAA

Primer Dimer Sequences

I. E2-152

Nhe1

5'-GAT ATA CAT ATG GCT AGC ACC GGC AAA AAT GGT CGT GTG CTG AAA GAA GAC ATT GAT G

3'- GAC TTT CTT CTG TAA CTA CGC AAA GAC CGC CCG CCG CGC TTT GGG CCC TTT CCC**-5'**

Reverse 5'→3' CCC TTT CCC GGG TTT CGC GCC GCC CGC CAG AAA CGC ATC AAT GTC TTC TTT CAG

T_M= 45.9°C
Dimerization deltaG= -31 kcal/mol
Self Dimer, Hairpin (coding)= -10.44,-1.76 kcal/mol @37°C
Self Dimer, Hairpin (template)= -15.89, -1.76 kcal/mol @ 37°C

II. E2-158

Nhe1

5'-GAT ATA CAT ATG GCT AGC GTG CTG AAA GAA GAC ATT GAT GCG TTT CTG GCG

3'- CTG TAA CTA CGC AAA GAC CGC CCG CCG CGC TTT GGG CCC TTT CCC**-5'**

Reverse 5'→3' CCC TTT CCC GGG TTT CGC GCC GCC CGC CAG AAA CGC ATC AAT GTC

T_M= 57.2°C
Dimerization deltaG= -42 kcal/mol
Self Dimer, Hairpin (coding)= -10
Self DImer, Hairpin (template)= -16

III. E2-167

Nhe1

5'-GAT ATA CAT ATG GCT AGC CTG GCG GGC GGC GCG AAA CCC GGG AAA GGG **-3'**

3'-CTA TAT GTA TAC CGA TCG GAC CGC CCG CCG CGC TTT GGG CCC TTT CCC **-5'**

Reverse 5'→3' CCC TTT CCC GGG TTT CGC GCC GCC CGC CAG GCT AGC CAT ATG TAT ATC

T_M=73.5°C
Dimerization deltaG= -110 kcal/mol
Self Dimer, Hairpin (coding)= -16, -2
Self DImer, Hairpin (template)=-16, -2

Primer Sequence for E2-179 (this is not an N-terminal extension, it is a deletion, and therefor only a forward primer was used)

Forward

5'-GAT ATA CAT ATG GCT AGC GGG GGG AGC GAG GAA AAG GCT GCT CCA GCG-3'

T_M= 60.9°C
Dimerization = -44
Self Dimer, Hairpin= -10, -3

A.1.9 References.

1. Jeong JH, Kim SW, Park TG: Novel intracellular delivery system of antisense oligonucleotide by self-assembled hybrid micelles composed of DNA/PEG conjugate and cationic fusogenic peptide. *Bioconjug Chem* 2003, 14:473-479.

APPENDIX A.2

Appendix A.2 Additional Results

A.2.1 Characterization of poly(I:C) Conjugation to E2

The widely used synthetic double stranded RNA known as polyinosinic:polycytidylic acid (poly(I:C)) was chosen as a secondary activator for study. This activator binds TLR3, which, like TLR9, is present in the endosome. Due to the physical size of commercial poly(I:C) (100-1000 basepairs), we are restricted to external conjugation, due to geometric constraints. The synthetic dsRNA poly(I:C) molecules were purified by FPLC and attached to the E2 nanocapsule external surface by the multistep conjugation scheme outlined in **Figure A.1.2**. The conjugate was purified from the Superose 6 10/300 size exclusion column by collecting the elute from 0.3-0.4 cv and successful conjugation determined qualitatively with non-denaturing 0.6% agarose gel analysis (**Figure A.2.1**). The conjugate was also subject to DLS analysis to determine any changes to particle size due to the attachment of the large nucleic acid polymers (**Figure A.2.1**). The observed particle size was 35.5 ± 2.3 nm (n=3), an increase in diameter relative to the published E2-WT diameter of 26.6 ± 0.6 nm.

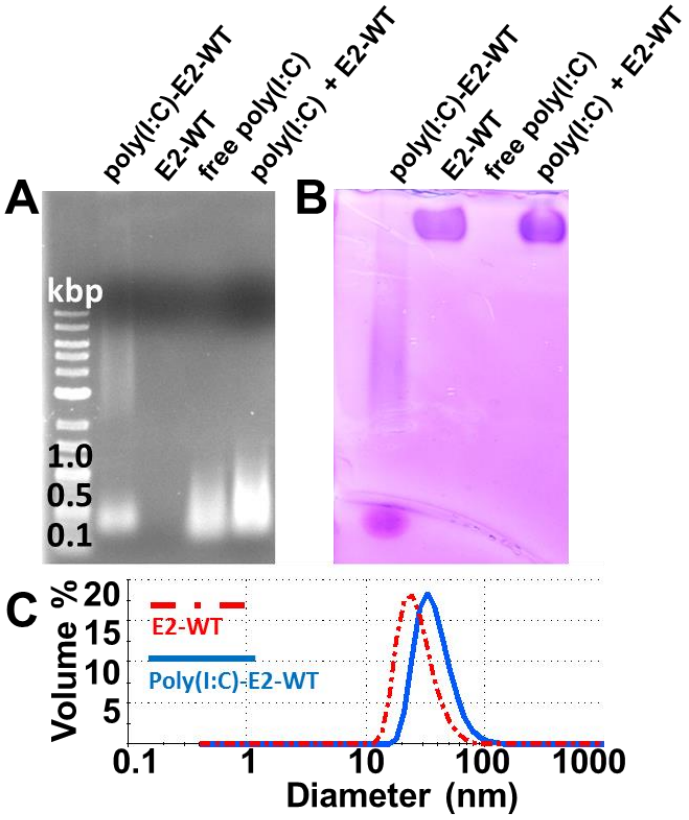

FIGURE A.2.1. Non-denaturing agarose gel (0.6%) analysis of the poly(I:C)-conjugated E2 proteins shows indication of protein and poly(I:C) co-migration following conjugation, as evidenced by A) ethidium bromide staining (nucleic acid) and B) protein stain. The right-most lane in the gel is a mixture of soluble protein and soluble nucleic acid and shows that the co-migration of the E2 protein and the poly(I:C) is not due to non-specific interaction.

The agarose gel allows for tracking of both protein and poly(I:C) by using protein stain and ethidium bromide, respectively. **Figure A.2.1** shows that the poly(I:C)-E2 conjugate exhibits increased electrophoretic mobility, relative to the E2 protein alone, and that the protein stain and ethidium bromide stain indicate a co-migration of the protein and nucleic acid. In order to quantify the amount of poly(I:C) attachment to the E2 particles, a standard curve was generated measuring the absorbance ratio of A_{260}/A_{230} of varying poly(I:C) to E2 mass percentages in a fixed volume and protein concentration. The E2 protein absorbs strongly at 230 nm and the poly(I:C) absorbs strongly at 260 nm, and therefore the relative mass amounts can be determined by taking the ratios of these two

measurements and comparing to the standard curve. The amount of poly(I:C) attachment to the E2 particle was determined to be 26 ± 13% (n=5). Previous literature has shown that by electrostatically coating cationic microparticles with poly(I:C), a mass ratio of ~ 16 μg poly(I:C)/mg microparticle (1.6% w/w) can be achieved, with subsequent demonstration of the ability to induce human peripheral blood DC maturation *in vitro* [1]. Here, we have covalently attached the poly(I:C) molecules to the E2 surface and have achieved a ~ 15-fold higher mass ratio than that observed for the aforementioned study. Therefore, based on this previous research, we would anticipate the ability to activate BMDCs via TLR3 with our functionalized E2 nanocapsule. The phosphoramidate bond formed between the poly(I:C) 5' phosphate group and cysteamine is reported to be acid-labile at endosomal pH [2]. We will test the acid-hydrolysis of our conjugate, which can be followed by agarose gel analysis just as in **Figure A.2.1**, and we would expect the poly(I:C) and E2 protein to no longer co-migrate if hydrolyzed and to display a profile similar to that of free protein and free poly(I:C). Quantification of the hydrolysis can be measured by purifying the protein with size exclusion chromatography to remove hydrolyzed poly(I:C) molecules and taking absorbance ratio measurements.

A.2.2 N-terminal E2 mutants and Recombinant Peptide Display

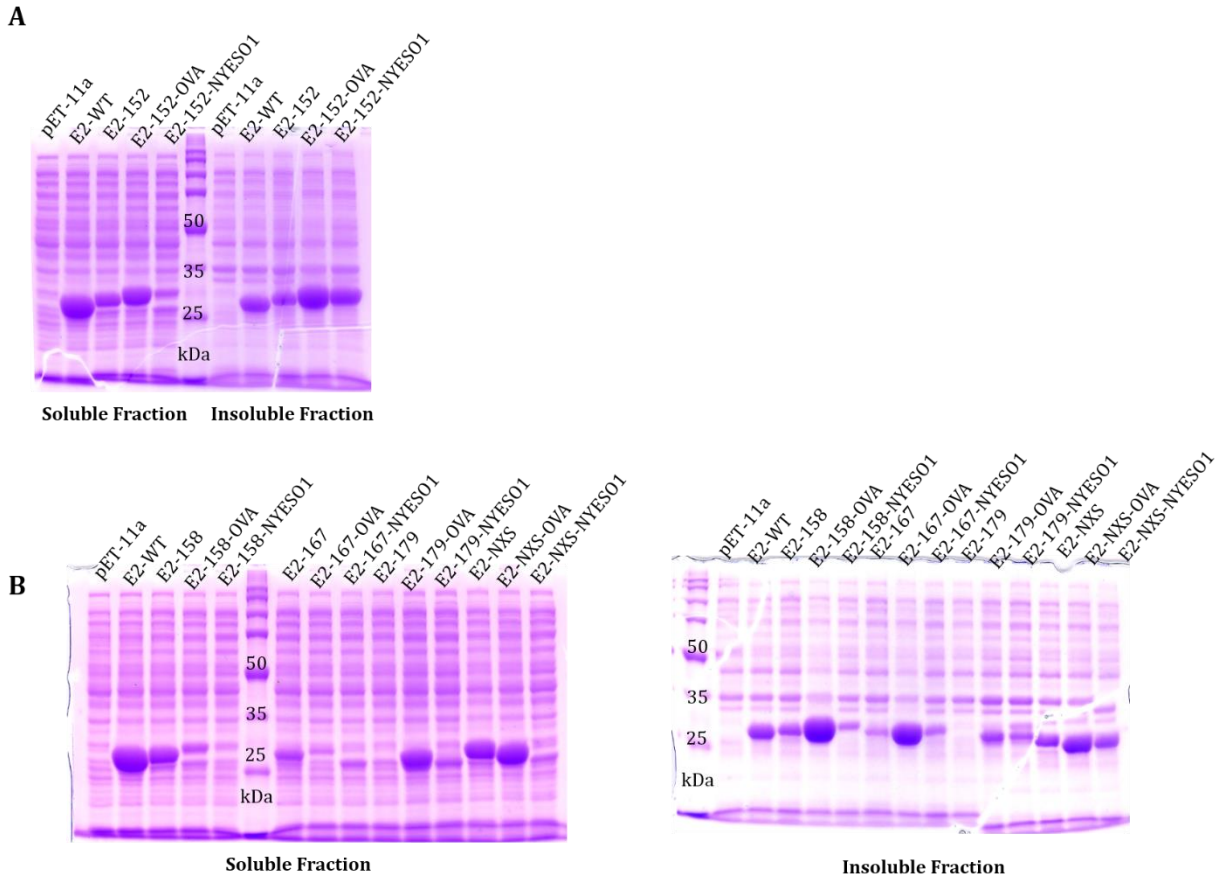

Figure A.2.2. SDS-PAGE of E2 N-terminal mutants to peptide recombinant insertion along with 2 mutants containing peptides. The number following E2 indicates the amino acid the N-terminus begins at, relative to wild-type sequence from the NCBI website. The suffix NXS refers to an E2-WT sequence beginning with the amino acids MAS, as opposed to the MLS for E2-WT, and contain Xma1 and Nhe1 restriction sites tandem to each other. OVA is the peptide sequence SIINFEKLTEWT from the chicken ovalbumin protein and NYESO1 is the sequecen SLLMWITQVFLPV from the NY-ESO-1 cancer/testis antigen. Both of these peptide sequences are CTL-restricted epitopes (SIINEKL for H-2Kb in mice and SLLMWITQV for HLA-A2 in humans). **A)** Soluble and insoluble fractions of BL21(DE3) *E. coli* transformed with the plasmid encoding the E2-152 gene in a pET-11a plasmid. **B)** The soluble (left gel) and insoluble (right gel) fractions of BL21(DE3) with the genes encoding for the E2-158, E2-167, E2-179, and E2-NXS plasmids with or without peptides inserted. Primers for the flagellin peptide SANSTNSQSDLDSIQAEITQGSGSGS were designed but never successfully cloned in to the plasmids.

A.2.3 HPLC Analysis of Peptide and CpG Conjugation to E2

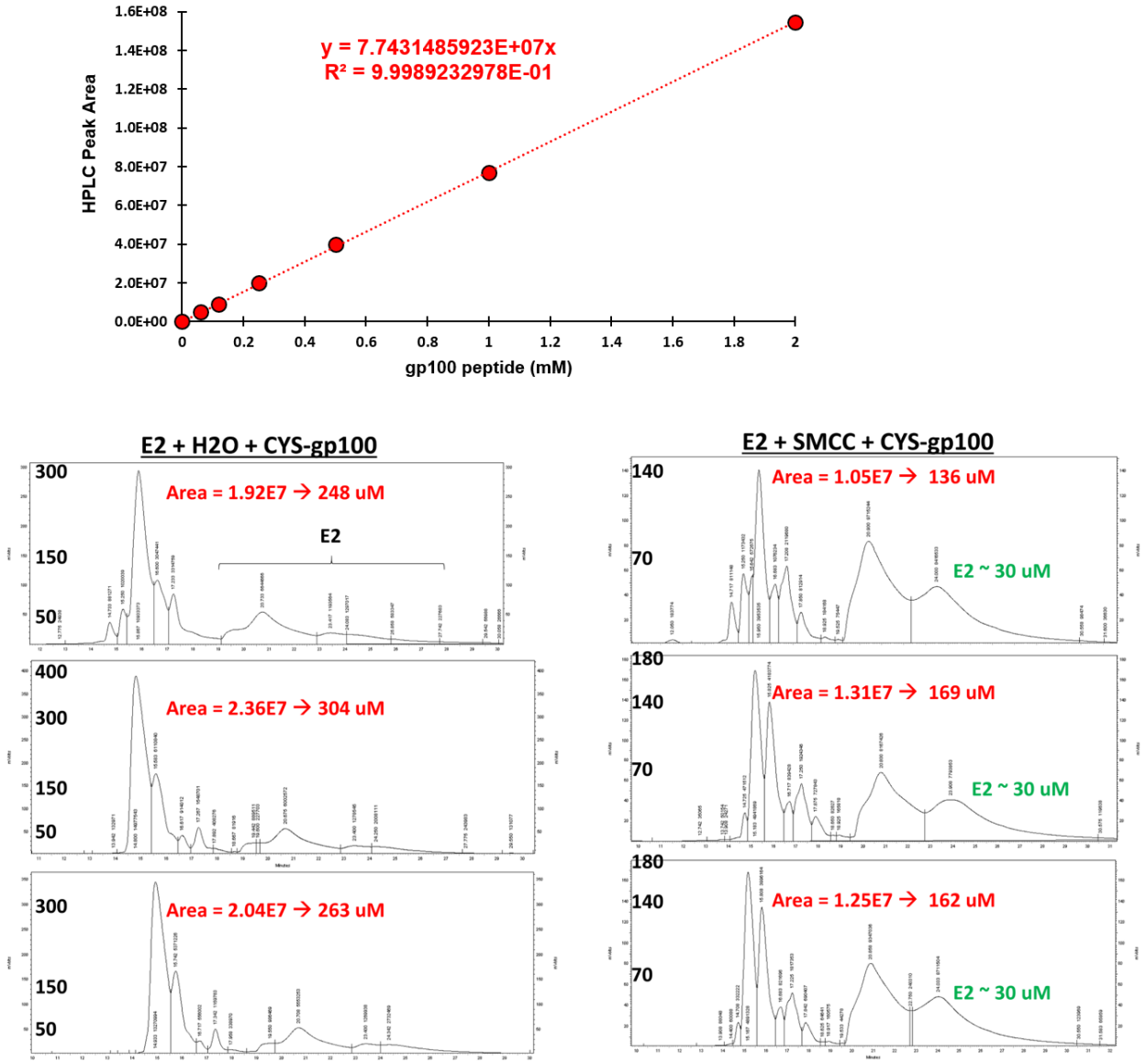

Figure A.2.3. Standard curve generated from free CKVPRNQDWL (CYS-gp100) peptide using HPLC analysis (Upper Panel). Peptides were reduced with TCEP before analysis, and all injections were 100 µL to a C18 reverse phase column, with water and acetonitrile as the elution buffers (both with 0.1% acetic acid). Lower panels represent the analysis of gp100 peptide conjugation to the E2 protein nanoparticle. The three charts on the left represent mock reactions where water was used in place of the SMCC cross-linker and the panels on the right represent the peptide conjugation reactions. The red areas labeled correspond to the area under the curve for free peptide only, which elutes before the E2 protein. The concentration of E2 (green) was determined with BCA analysis.

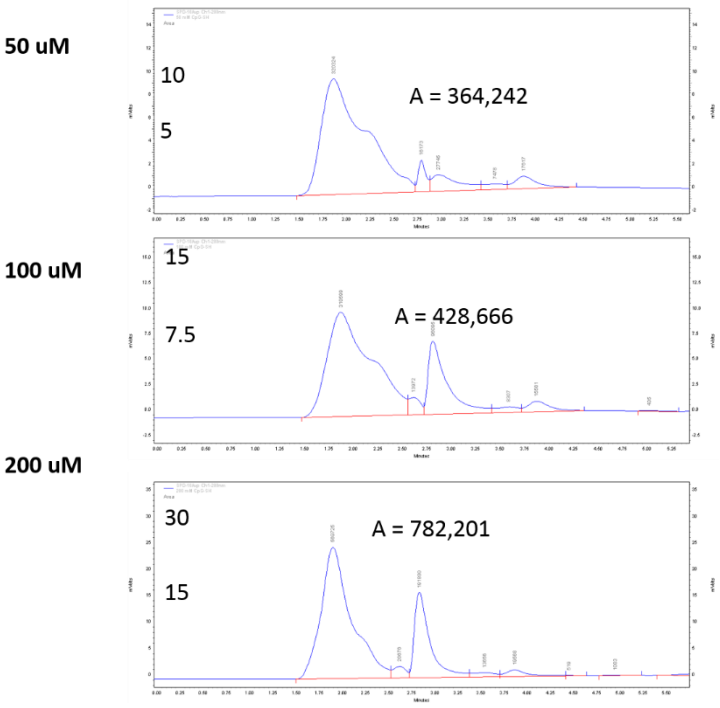

Figure A.2.4. HPLC analysis of TCEP-reduced CpG oligos used for surface conjugation to the E2 nanoparticle. The CpG's contain a 5' thiol for conjugation.

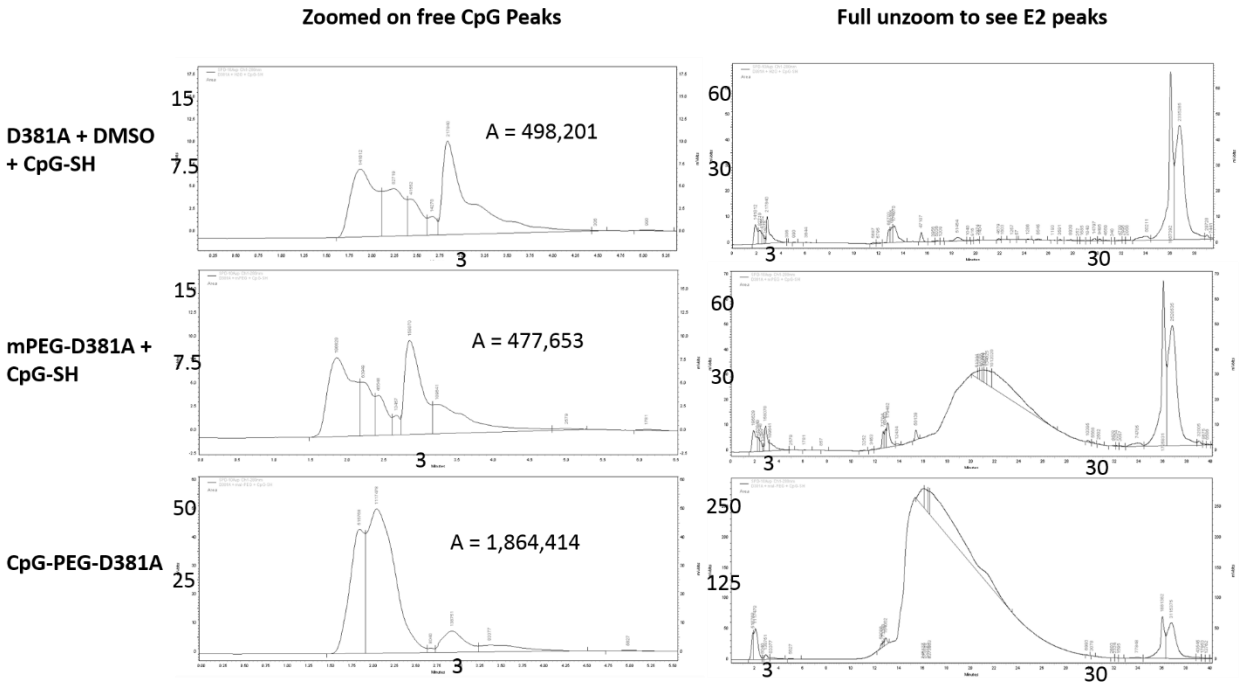

Figure A.2.5. HPLC Analysis of E2 (D381A mutant) conjugation to the CpG-SH. The in the left and right columns are the same graph for a particular row, with different zoom levels. The first row represents E2 mixed with CpG-SH, without any PEG linker (DMSO was added as a vehicle control). The second row represents mPEG-E2 mixed with CpG-SH (to observe any non-specific interaction between PEG and CpG). The third row represent the CpG-PEG-E2 nanoparticle conjugate. The third row demonstrates that the peaks corresponding to fre CpG (~ 3 minutes, see first column), appear to partially co-elute with the CpG-PEG-E2, or some other interaction is occurring to affect absorbance levels (a large increase in absorbance, even though there should theoretically be less free CpG-SH in solution).

A.2.4 PEGylation and Cross-Presentation of SIINFEKL-Conjugated E2

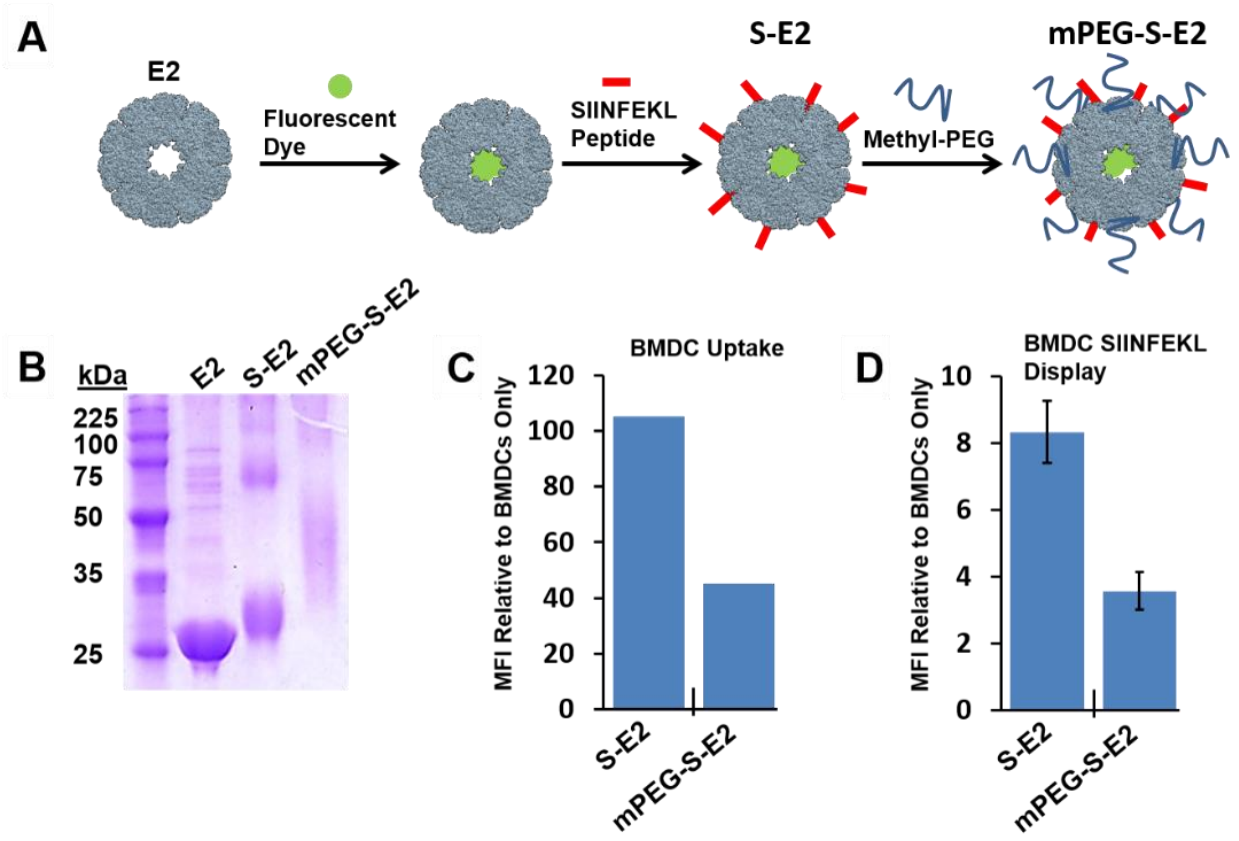

Figure A.2.6. PEGylation does not inhibit cross-presentation of conjugated epitopes. **A)** General reaction scheme for fabrication of the mPEG-S-E2 nanoparticle. **B)** SDS-PAGE analysis shows successful conjugation of mPEG to the S-E2 nanoparticle. **C)** BMDC uptake was measured over 18 hours (the length of time for cross-presentation assays) in the presence of S-E2 and mPEG-S-E2 (both with AF488-C5-maleimide conjugated internally). There is ~ 50% uptake of the PEGylated vs. non-PEGylated E2 nanoparticle. **D)** BMDCs are able to process and display the SIINFEKL peptides from the mPEG-S-E2 nanoparticle. Display was measured by flow cytometry (antibody against SIINFEKL bound to H-2Kb mouse MHC I). The decrease in antigen display is roughly equivalent to the decrease in uptake.

A.2.5 BMDC Targeting and Biodistribution with Peptide Aptamers

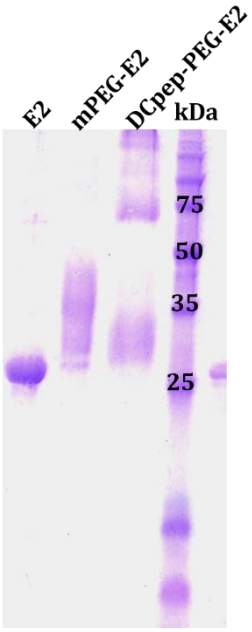

Figure A.2.7. SDS-PAGE analysis of E2, mPEG-E2, and DCpep-PEG-E2. DCpep is the FYPSYHSTPRPGGGSC peptide reported to target DCs. DCpep was conjugated to the E2 nanoparticle surface cysteines in the same exact method as for CpG-SH (See Chapter 5). The broad band in the 30-35 kDA is an indication of successful peptide conjugation with the maleimide-PEG-NHS linker.

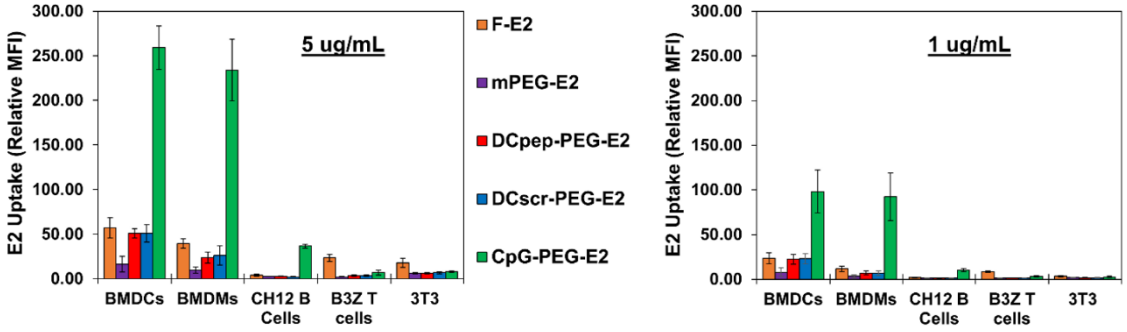

Figure A.2.8. DCpep-PEG-E2 shows similar cellular uptake compared to AF-E2 for bone marrow-derive dendritic cells (BMDCs), bone marrow-derive macrophages (BMDMs), CH12 B cells, B3Z T cells, and NIH3T3 mouse fibroblasts, while CpG-PEG-E2 shows enhanced uptake in antigen presenting cells (BMDCs, BMDMs, and CH12 B cells), compared to both AF-E2 and mPEG-E2. Cellular association was measured by recording the MFI of cells incubated with **A)** 5 μg/mL or **B)** 1 μg/mL of the E2 nanoparticle for 1 hour at 37°C. Data is reported as average ± S.D. DCpep: FYPSYHSTPQRPGGGSC (underlined portion reported to target DCs). DCscr: scrambled sequence of DCpep to serve as negative control.

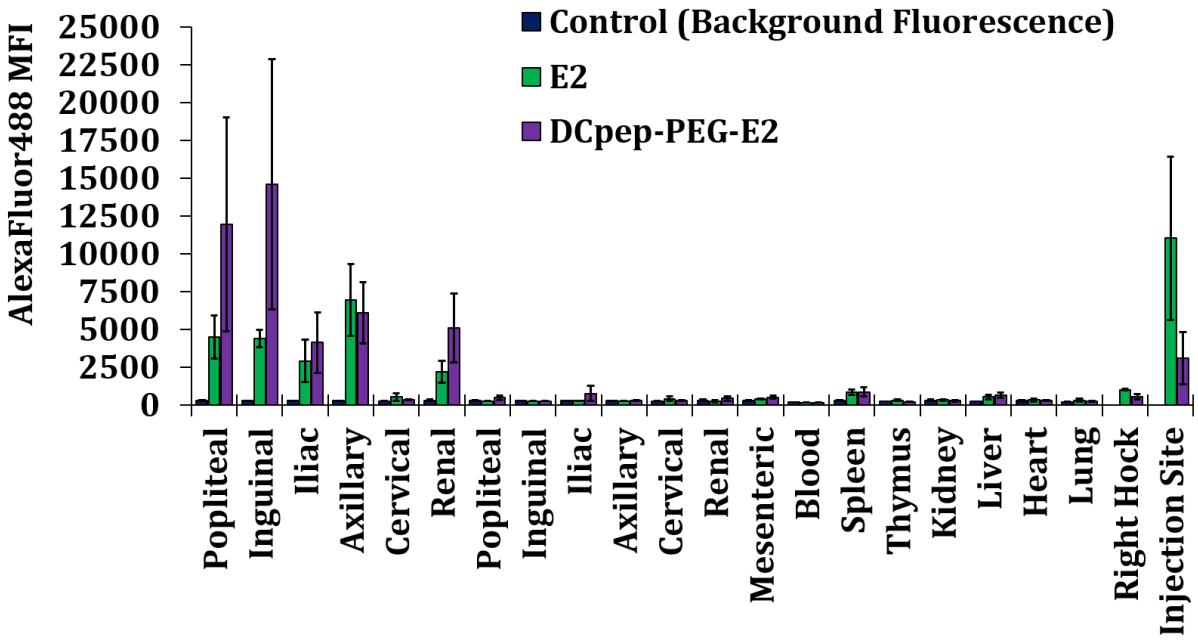

Figure A.2.9. Measured fluorescence in secondary lymphoid organs and other blood draining organs following 6 hours after subcutaneous administration the E2 or DCpep-PEG-E2 nanoparticle. MFI was measured by flow cytometry of cells from the lymph nodes ipsilateral to the left hock injection site (first six bars), contralateral lymph nodes (bars 7-12), mesenteric lymph node (bar 13), blood draining organs (including blood), and the injection site. Data is presented as average ± S.E.M. of cellular MFI of 3 independent experiments.

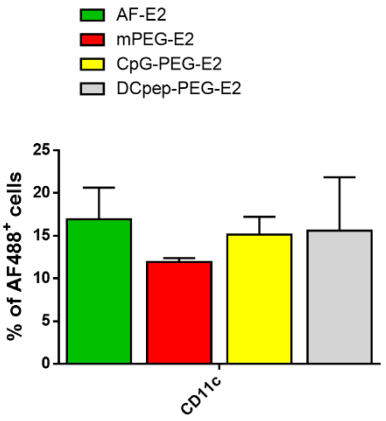

Figure A.2.10. The percentage of Alexa Fluor 488 positive (AF488+) cells that were DCs was determine at 6 hours following subcutaneous administration. Data is reported as average ± S.E.M. of percentage of cells positive for AF488 of 3 independent experiments.

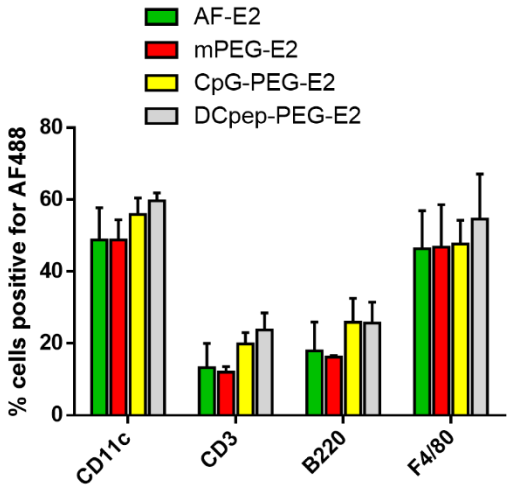

Figure A.2.11. The percentage of a cellular population within the lymph node that are Alexa Fluor 488 positive (AF488+) cells was determined by flow cytometry after 6 hours following subcutaneous administration. Cells tested for AF488 were dendritic cells (CD11c), T cells (CD3), B cells (B220), and macrophages (F4/80). Data is reported as average ± S.E.M. of percentage of cells positive for AF488 of 3 independent experiments.

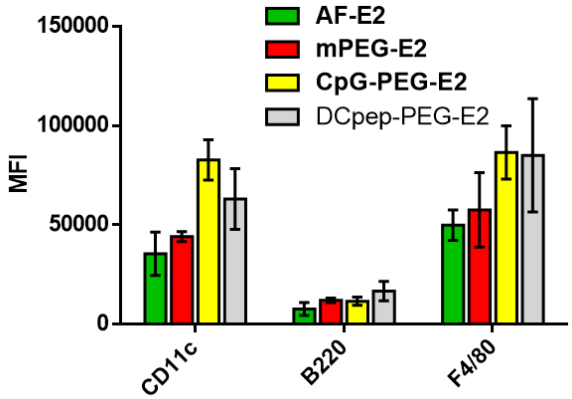

Figure A.2.12. The MFI (E2 uptake extent on a single cell level) of Alexa Fluor 488 positive cells was determined by flow cytometry after 6 hours following subcutaneous administration. Cells tested for AF488 were dendritic cells (CD11c), B cells (B220), and macrophages (F4/80). Data is reported as average ± S.E.M. MFI of 3 independent experiments.

A.2.5 References

1. Wischke C, Zimmermann J, Wessinger B, Schendler A, Borchert HH, Peters JH, Nesselhut T, Lorenzen DR: Poly(I:C) coated PLGA microparticles induce dendritic cell maturation. *Int J Pharm* 2009, 365:61-68.
2. Jeong JH, Kim SW, Park TG: Novel intracellular delivery system of antisense oligonucleotide by self-assembled hybrid micelles composed of DNA/PEG conjugate and cationic fusogenic peptide. *Bioconjugate Chemistry* 2003, 14:473-479.